FLUCTUATING MEMBRANES

RENORMALIZATION GROUP APPROACHES TO FREESTANDING TWO-DIMENSIONAL MATERIALS

Fluctuating membranes: Renormalization group approaches to freestanding two-dimensional materials
PhD thesis, Radboud University

ix + 186 pages; illustrated, with bibliographic references and summary in English and Dutch

ISBN 978-94-6419-602-3

Printed in the Netherlands by Ipskamp Printing

This work has been financially supported by the Dutch Research Council (NWO) via the Spinoza Prize of Professor M.I. Katsnelson.

FLUCTUATING MEMBRANES

RENORMALIZATION GROUP APPROACHES TO FREESTANDING TWO-DIMENSIONAL MATERIALS

PROEFSCHRIFT

ter verkrijging van de graad van doctor
aan de Radboud Universiteit Nijmegen
op gezag van de rector magnificus prof. dr. J.H.J.M. van Krieken,
volgens besluit van het college voor promoties
in het openbaar te verdedigen op

donderdag 3 november 2022
om 10.30 uur precies

door

ACHILLE MAURI

geboren op 22 maart 1994
te Milaan (Italië)

PROMOTOR	Prof. dr. M.I. Katsnelson
MANUSCRIPTCOMMISSIE	Prof. dr. H.M. Cuppen Dr. F.S. Saueressig Prof. dr. V. Rychkov (IHES, Frankrijk)

To my family

CONTENTS

1

INTRODUCTION

Examples of thin membranes are very numerous and diverse, from amphiphilic bilayers to polymerized sheets, biological cell membranes and atomically-thin two-dimensional materials [1–5]. Although these systems are very different microscopically, they have in common that, in a coarse-grained continuum picture, they can be represented as two-dimensional (2D) media able to deform and fluctuate in three-dimensional space. After the progress of renormalization, scaling, and universality concepts in the theory of critical phenomena, the possibilty to identify universal properties in the physics of membranes has been the focus of an intense theoretical research. Already in the 1980s, it was realized that the structural behavior of 2D continuum media cannot be completely universal, because it depends crucially on the degree of internal order, fluid, crystalline, or hexatic, of the matter composing the system [1, 2]. Fluid layers—such as, for example, non-polymerized lipid bilayers—were predicted to be always in a highly-entropic "crumpled phase" [1, 4, 5]. The pioneering work of Nelson and Peliti [6] has shown instead that *solid membranes*, with a nonzero shear modulus, can remain macroscopically flat, even in absence of a supporting substrate and of an applied tension, provided that the temperature is not too large. This crucial theoretical prediction, strikingly in contrast with a naive application of the Mermin-Wagner theorem [7, 8], can be traced to a strong suppression of out-of-plane thermal fluctuations induced by a geometric "frustration" effect: fluctuations with a nonzero Gaussian curvature generate inevitably a nonzero shear strain and are suppressed by an energy-costly elastic stress. As a result, for temperatures lower than a crumpling transition temperature T_c, thermal fluctuations induce a random distribution of ripples, but do not destroy the macroscopic orientational order of the system [6]. The properties of the "flat phase", at the same time, are strikingly determined by the presence of thermal ripples. As it was soon realized, already in the first investigations in the field, the nonlinear mechanical effects drive the distribution of thermal fluctuations to a strongly-interacting renormalization-group (RG) fixed point [9–12]. Similarly to order-parameter fluctuations at a second-order phase transition [13–16], correlation functions of elastic degrees of freedom (the long-wavelength phonon modes) exhibit a scale-invariant distribution, controlled by universal non-integer exponents. The scaling phenomenon translates into singular power-laws in all response functions. For example, when the system is subject to a small externally applied stress, the response is not linear: the stress-strain relation is governed by an *anomalous*

Hooke's law $\epsilon(\sigma) \propto \sigma^{\alpha}$ [11, 17, 18], governed by an universal noninteger exponent α.

Following the first pioneering predictions, the anomalous elasticity of freestanding crystalline membranes has attracted a vast research effort for more than four decades. The picture of a scale-invariant flat phase, the existence of a RG fixed point, and the quantitative calculation of critical exponents have been addressed by complementary field-theoretical techniques (the ε-expansion [10, 19–21], the large-d_c expansion [9, 12, 22], the self-consistent screening approximation [23–25], and the nonperturbative renormalization group [26–28]) and by numerical simulations (see, for example, Refs. [4, 25, 29–38]), leading, over the years, to a growing control over theoretical predictions.

Motivated by phenomenological applications to graphene and other laboratory realizations of crystalline membranes, numerous analyses have addressed extensions of the theory including effects of disorder [17, 25, 39–44], a quenched preferred metric [45, 46], long-range interactions [47, 48], elastic anisotropy [25, 49, 50], finite-size effects [18, 51–53], fluctuating charge degrees of freedom [54, 55], and other[1].

From the experimental side, an evidence in support of the existence of the flat phase and the corresponding scaling behavior has been reported in Ref. [56], which analyzed scattering of light and x rays from an ensemble of spectrin networks extracted from the membrane of red blood cells. In the context of inorganic surfaces and two-dimensional materials, some experiments conducted in the 1990s explored the conformations of an ensemble of graphite oxide (GO) membranes in suspension [57–59]. The membranes observed in Ref. [57] had sizes of the order of microns and estimated thicknesses between 50 and 100 Å. The scattering structure facture exhibited scale invariance over an order of magnitude of length scales (between 500 and 5000 Å), but the scaling exponent could not be interpreted via the roughness exponent expected for the flat phase. In contrast, the data were interpreted as resulting from a collection of crumpled membranes or a polydisperse mixture between flat and crumpled membranes. The possibility that the membranes were frozen into non-equilibrium conformations was also not ruled out. The observation of micrometer sized GO membranes in Ref. [58] indicated evidence of a crumpled state and a transition to a more compact collapsed structure triggered by a change of solvent concentrations. The analysis of Ref. [59], however, revisited measurements of GO by a freeze-fracture method and found, in the non-collapsed phase, a structure factor with an exponent more close to that expected for a flat phase. The small interval of wavevector probed in the experiment, however, was not sufficient to establish the presence of a flat phase in a conclusive way. Other early-investigated crystalline membranes are for example molybdenum disulfide (MoS_2) and polymerized lipid bilayers (see Refs. [1, 4, 5] for references). In the case

1 The list of contributions in this chapter is very far from being complete.

of partially-polymerized bilayers, the experiments in Ref. [60] provided evidence of a low-temperature wrinkled phase, which may be induced by quenched disorder (see also Ref. [19, 43]).

After the isolation of graphene by Geim and Novoselov in 2004, the progress in fabricating and controlling individual atomically-thin two-dimensional crystals has offered new opportunities to study anomalous elasticity and scaling phenomena. Since the binding forces of a substrate and strong external stresses suppress out-of-plane fluctuations, the critical behavior is expected to be observable in free-standing or suspended graphene subject to a weak tension. Quantitative estimates and numerical simulations show that a clean free-standing graphene membrane at room temperature should exhibit the critical flat phase behavior at all scales larger than a few nanometers [3, 38, 51, 61, 62] and for tensions smaller than tenths of N/m [17]. Experimentally, the existence of out-of-plane random deformations in suspended graphene samples has been widely documented [63–74]. The random deformations, in general, are not only induced by thermal fluctuations, but depending on the sample preparation and the experiment geometry, can be induced for example by defects, inhomogeneous stress, and boundary forces. These different effects can give rise to distorsions with very different wavelengths and aspect ratios. Despite these difficulties, some experiments have reported on observations of anomalous effects. For example, Ref. [69] measured the bending rigidity of a micrometer-sized polycrystalline graphene sample immersed in water at room temperature. The resulting value was found to be more than 1000 times larger than the microscopic rigidity of graphene. This strong enhancement of rigidity may be a signature of nonlinear renormalization effects—the frustration of out-of-plane motion due to shear elasticity. The renormalization in this case, may not be triggered by temperature effects, but rather by large static ripples present in the sample, evidenced by interferometric measurements. Refs. [69, 72] reported on experimental signatures of an anomalous Hooke's law in suspended graphene samples subject to small stress. Evidence of strong fluctuation effects have also been identified in Refs. [74–77], which explored mechanical and thermodynamic properties of suspended graphene membranes made defective by controllable ion bombardment. The experimental reports [69, 72, 74] have indicated that interpretation of data require an account of static ripples.

In addition to providing new experimental platforms for testing predictions, two-dimensional materials have opened the way to atomistic numerical simulations. This approach is made possible by the simple structure of these materials which, in contrast with a lipid bilayer or a thick graphite oxide system, have a simple unit cell composed of just a few atoms. Fluctuations of clean graphene samples have been simulated by complementary techniques, from classical Monte Carlo and molecular dynamics methods [62, 78] to quantum path approaches [36, 38]. A

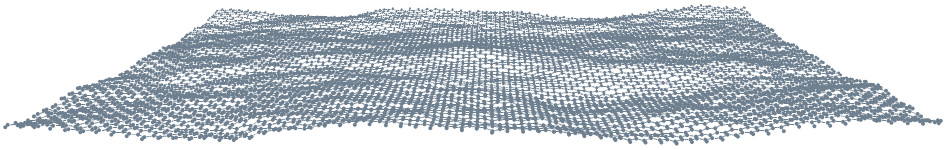

Figure 1.1: Snapshot from a molecular dynamics simulation of graphene (Courtesy of Jan Los).

snapshot of a fluctuating graphene membrane simulated by a molecular dynamics method is shown in Fig. 1.1.

The contributions presented in this thesis focus mostly on renormalization group and field theory methods in disorder-free membranes. Chapter 3 presents a calculation of the fixed point and the scaling indices at second order in the ε-expansion. At the moment in which the work was completed, the result was the first calculation beyond leading order in ε. During the last two years, analyses developed by other authors have pushed calculations to three- [19, 20] and four-loop orders in the expansion [21], leading to an improved quantitative control. Chapter 4 investigates a fundamental question: whether the scale invariance emerging at the fixed point is enhanced to a full conformal invariance. The analysis is performed to all orders in the ε-expansion and is worked out considering two alternative dimensional continuations of membrane theory. For both models, the theory is shown to be scale-invariant but not conformal. This implies that the recently developed bootstrap methods [79, 80] cannot be straightforwardly applied to membrane theory. At the same time, the result sheds light in the search for general connections between scale and conformal symmetries. Chapter 5 presents an analysis on how quantum mechanical effects affect the low-temperature thermodynamic of crystalline membrane. Finally, chapter 6, illustrates a theory of fluctuations in bilayer graphene, obtained by combining a phenomenological model, an *ab-initio* calculation of model parameters, and a numerical solution of Dyson equations within the self-consistent screening approximation. All chapters have been written by modifying and extending the text of published articles (see page 181 for a list of publications).

In order to make the reading of the thesis more self-contained, chapter 2 provides an introduction to the statistical mechanics of thermally-fluctuating membranes.

2

STATISTICAL MECHANICS OF MEMBRANES

This chapter provides brief introduction to the statistical mechanics of fluctuating membranes, focused on the physics of the flat phase and, in particular, on the effects of thermal fluctuations in homogeneous crystalline layers (without defects and disorder). After discussing the elasticity theory of solid membranes, this chapter introduces two crucial theoretical predictions, already derived in the first investigations on the field: the stability of the flat state and the existence of anomalous scaling behavior. We then review field-theoretical methods for the description of scaling behavior and the analogies between flexible membranes and critical phenomena. The quick introduction presented here does not attempt to provide a complete review of the vast field of fluctuating membranes. The objective is instead to give a summary of conceptual and methodological aspects used in the research works of this thesis, which are presented in the succeeding chapters.

Some parts of this chapter have been derived from the article:
Achille Mauri and Mikhail I. Katsnelson, "Scale without conformal invariance in membrane theory", Nucl. Phys. B **969**, 115482 (2021); preprint: arXiv:2104.06859 (2021)

2.1 CONTINUUM ELASTICITY THEORY

In the theory of phase transition and critical phenomena, a crucial phenomenon is the *universality* of scaling behavior. Systems with very different microscopic constituents near a critical point can exhibit identical scaling properties, provided that they have the same symmetries and dimensionality [14, 81, 82]. For example, the behavior of an Ising ferromagnet at the Curie point is identical, when looked upon from a sufficiently large distance, to the critical opalescence of a liquid-vapor mixture. From a fundamental point of view, universality derives from the fact that the scaling behavior is induced by thermal fluctuations which have a wavelength much larger than the atomic scales. The behavior of diverse systems can be thus analyzed in terms of similar continuum field theories, despite having very different models at an atomistic scale.

In the theory of fluctuating membranes, similarly, it is useful to analyze a continuum-medium description, which is simpler than a microscopic dynamical theory, but still captures the physics of long-wavelength fluctuations [1, 3, 4, 6, 10–12, 19, 22, 25]. For a 2D solid which is able to deform into the three-dimensional space, the natural continuum-medium model is provided by elasticity theory [1, 6, 83]. In this framework, the kinematic description of the configurations of the membrane can be given by introducing a continuous 2D coordinate $\mathbf{x} \in \mathbb{R}^2$, which acts as a label distinguishing different infinitesimal area elements, and a 3D coordinate $\mathbf{r}(\mathbf{x})$ specifying the location of area elements in 3D space (see Fig. 2.1). A given function $\mathbf{r}(\mathbf{x})$ fixes a specific 'snapshot' of the system, by assigning the coordinates of all infinitesimal elements. Although the coordinate $\mathbf{x}$ on the manifold could be chosen arbitrarily [11], for solid surfaces the crystalline structure singles out a natural choice: the identification of $\mathbf{x}$ with the rest coordinates of the atoms in an undeformed structure. With this convention, $\mathbf{x}$ is defined in such way that $\mathbf{r}(\mathbf{x}) = \mathbf{x}$ when the medium assumes a planar and undeformed configuration. To describe deformations it is then convenient to parametrize $\mathbf{r}(\mathbf{x}) = (x_\alpha + u_\alpha(\mathbf{x}), h(\mathbf{x}))$, where the Greek index $\alpha = 1, 2$ runs over 2D cartesian components, u_α is the component of the displacement $\mathbf{r}(\mathbf{x}) - \mathbf{x}$ in the direction parallel to the plane, and $h(\mathbf{x})$ the out-of-plane displacement (see Fig. 2.1). According to elasticity theory, the Hamiltonian of the deformed medium can be assumed to take the form[1]:

$$H = H_{\text{curv}} + \int \mathrm{d}^2x \Big[c^{(1)}_{\alpha_1\beta_1} U_{\alpha_1\beta_1} + c^{(2)}_{\alpha_1\beta_1,\alpha_2\beta_2} U_{\alpha_1\beta_1} U_{\alpha_2\beta_2} + c^{(3)}_{\alpha_1\beta_1,\alpha_2\beta_2,\alpha_3\beta_3} U_{\alpha_1\beta_1} U_{\alpha_2\beta_2} U_{\alpha_3\beta_3} + \ldots \Big] , \tag{2.1}$$

1 More exactly, H could be interpreted as a free energy functional obtained by a partial trace over microscopic degrees of freedom at fixed $h(\mathbf{x})$ and $u_\alpha(\mathbf{x})$. To simplify the notation, the elastic free energy will be referred to as a Hamiltonian since as usual the partial free energy plays the same role of an effective Hamiltonian in the Gibbs distribution $\mathcal{Z}^{-1} \exp[-H/(k_{\text{B}}T)]$ [1, 6, 84].

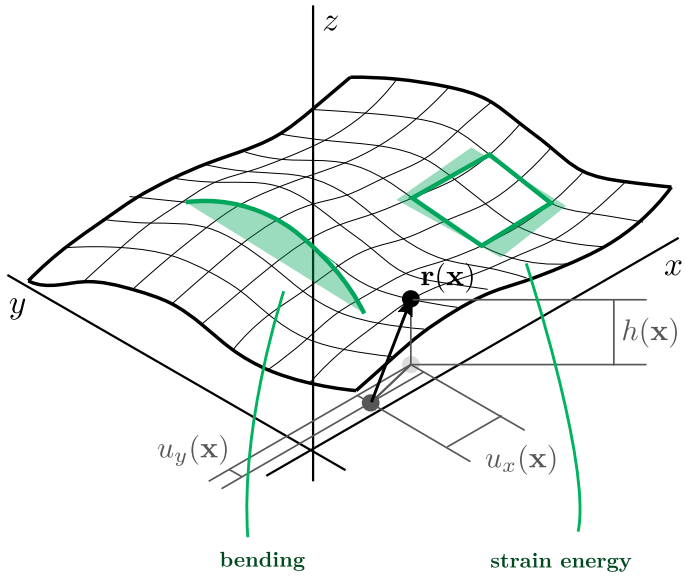

Figure 2.1: Schematic representation of a deformed crystalline membrane.

where

$$U_{\alpha\beta} = \frac{1}{2}(\partial_\alpha \mathbf{r} \cdot \partial_\beta \mathbf{r} - \delta_{\alpha\beta}) = \frac{1}{2}(\partial_\alpha u_\beta + \partial_\beta u_\alpha + \partial_\alpha h \partial_\beta h + \partial_\alpha u_\gamma \partial_\beta u_\gamma) \qquad (2.2)$$

is the strain tensor[2], and H_{curv} denotes contributions to the free energy involving higher derivatives $\partial^2\mathbf{r}$, $\partial^3\mathbf{r}$, ... The underlying assumption is that the Hamiltonian can be written as a *local* functional of strains, which is valid in absence of long-range forces. Assuming locality, Eq. (2.1) is the most general possible form of free energy consistent with homogeneity and isotropy of the 3D space.

The conventional choice that $\mathbf{r}(\mathbf{x}) = \mathbf{x}$ in the 'ground state' at zero temperature implies that the linear coefficient $c^{(1)}_{\alpha_1\beta_1}$ must be equal to zero[3]. The coefficients $c^{(2)}$, $c^{(3)}$, ... in Eq. (2.1), then play the role of linear and nonlinear elastic moduli, and encode anharmonic elasticity at arbitrarily high order. For small fluctuations near a quasi-planar configuration, the dominant effect is due to the leading term of second order with respect to strain, which is controlled by the coefficient $c^{(2)}$. The matrix $c^{(2)}$ must transform as an invariant tensor with respect to the discrete symmetries of the crystal. For hexagonal lattices, this forces the elastic constants

2 The Einstein summation convention is assumed throughout the thesis, and the notation ∂_α is used as a short-hand for $\partial/\partial x_\alpha$.

3 Other conventions are possible and often used in the literature (see, for example, Refs. [11, 12, 26, 41]). For example, a choice could be to define the reference point in such way that $\mathbf{r}(\mathbf{x}) = \mathbf{x}$ at a given temperature T. Any choice of parametrization gives the same physical results.

to be actually fully isotropic under all continuous rotations[4] [83]. As a result, in the Hamiltonian $H = H_{\text{curv}} + H_{\text{el}}$, the elastic contribution can be approximated as

$$H_{\text{el}} = \frac{1}{2}\int \mathrm{d}^2x\big[\lambda(U_{\alpha\alpha})^2 + 2\mu U_{\alpha\beta}U_{\alpha\beta}\big] \ . \tag{2.3}$$

The coefficients λ and μ are, respectively, the first Lamé modulus and the shear modulus.

For 2D membranes which are able to deform into three-dimensional space it is essential to take into account not only the elastic energy but also a stiffness to extrinsic curvature [1, 10]. An energy term describing resistance to curvature can be written as [1, 10]

$$H_{\text{curv}} = \frac{\kappa}{2}\int \mathrm{d}^2x(\partial_\alpha \mathbf{n}\cdot\partial_\alpha \mathbf{n}) \ , \tag{2.4}$$

where κ is the bending rigidity and $\mathbf{n}(\mathbf{x})$ is, for each point of the membrane, the local normal to the surface. The specific form of curvature energy is not unique. Another form which is often considered in the literature is [22, 26]

$$H'_{\text{curv}} = \frac{\kappa}{2}\int \mathrm{d}^2x(\partial^2\mathbf{r})^2 \ . \tag{2.5}$$

For small deformations, both H_{curv} and H'_{curv} reduce to the same expression, $\kappa(\partial^2 h)/2$. The difference between the two terms, thus, is unimportant, at least when the membrane is in its low-temperature "flat phase" (see Sec. 2.2), characterized by small deformations with respect to a planar state.

When the membrane is not free but subject to an externally-imposed in-plane tension σ, the free-energy includes an additional term coupling tension with the in-plane displacement [18, 41, 52, 85]. For small in-plane strain and within an "isotensional ensemble" this term can be written as[5]

$$H_\sigma = -\sigma\int \mathrm{d}^2x \ \partial_\alpha u_\alpha \ . \tag{2.6}$$

For small deformation H_σ can be equivalently interpreted as a coupling of the form $-\sigma(A_\parallel - A)$, where A is the rest area of the membrane and $A_\parallel$ the area of the projection of the membrane on the xy plane.

The overall energy can thus be modelled, collecting elastic, tension, and curvature terms as

$$H = \frac{1}{2}\int \mathrm{d}^2x\big[\kappa(\partial^2\mathbf{r})^2 + \lambda(U_{\alpha\alpha})^2 + 2\mu U_{\alpha\beta}U_{\alpha\beta} - 2\sigma\partial_\alpha u_\alpha\big] \ . \tag{2.7}$$

4 See Ref. [49, 53] for theories of anisotropic crystalline membranes.

5 The "isotensional ensemble" is the 2D analogue of the conventional fixed-pressure, fixed-temperature ensemble in three-dimensions: the tension is fixed and the area is allowed to fluctuate. Most analyses in this thesis focus on membranes subject to a vanishing tension and with free boundaries, which are expected to be captured by an isotensional ensemble with $\sigma = 0$. For an analysis of the complementary "isometric" ensemble see Ref. [18].

An essential property of H is that, after expansion in terms of u_α and h it is *nonlinear*: the strain elasticity terms give rise to terms of the type $\partial u(\partial h)^2$ and $(\partial h)^4$. These nonlinearities arise even if, as in Eq. (2.7), the energy is expanded only up to the Hookean order. The reason is that the very definition of the strain tensor $U_{\alpha\beta}$, which is dictated by rotational invariance, is a nonlinear expression when expanded in terms of u_α and h. These nonlinearities of purely geometric origin are responsible for driving some of the most important phenomena in membrane: the stability of a flat phase and scaling behavior.

2.2 FLAT PHASE AND CRUMPLING TRANSITION

At finite temperature, the partition function $\mathcal{Z}$ and the thermal averages can be computed by using the free energy (2.7) as an effective Hamiltonian in the Gibbs probability distribution $P = \mathcal{Z}^{-1} \exp[-H/(k_B T)]$. The statistical mechanical behavior of this model has been investigated extensively for more than three decades[6], and is briefly introduced in this chapter.

A crucial prediction, already derived in the first theoretical investigations [1, 6, 9, 10], is that 2D crystalline membrane can exist, even for vanishing external tension $\sigma = 0$, in a thermodynamically-stable "flat phase", characterized by an extended, macroscopically planar, state. This strikingly contrasts with one-dimensional polymers and two-dimensional fluid membranes [1, 4, 23], which for zero tension are always "crumpled" manifolds, even at an arbitrary low temperature (see Fig. 2.2). The very nontrivial character of this prediction can be appreciated by noticing the following analogy [1]. After identification of the local normal vector $\mathbf{n}(\mathbf{x})$ with a Heisenberg spin, the bending rigidity term $\kappa(\partial_\alpha \mathbf{n})^2/2$ plays a role analogue to an exchange stiffness tending to align the spins. Since for $\sigma = 0$ the membrane model is completely isotropic, we can thus make a parallelism with a fully-symmetric Heisenberg model without an applied magnetic field. It is well known that the Heisenberg model in two dimensions remains paramagnetic at arbitrarily low temperature: in the thermodynamic limit, the spins are disordered and the average magnetization in vanishing field is zero for any $T > 0$ [15]. The phase structure of membranes, instead, includes a flat phase and a crumpled phase and thus realizes the analogues of ferromagnetic order and a paramagnetic state.

Why crystalline membranes behave so differently from the 2D Heisenberg model can be explained by two different reasons. First, the local normal $\mathbf{n}(\mathbf{x})$ cannot fluctuate arbitrarily as if it was a localized spin, because the condition that $\mathbf{n}(\mathbf{x})$ is orthogonal to the surface imposes additional constraints [1, 86]. Secondly, the out-of-plane fluctuations which tend to disorder the flat phase are suppressed not only by the bending stiffness but also by elastic strain energy, an effect which has no

6 See, for example, Refs. [1, 3, 4, 6, 9–12, 18, 19, 22, 23, 25–28].

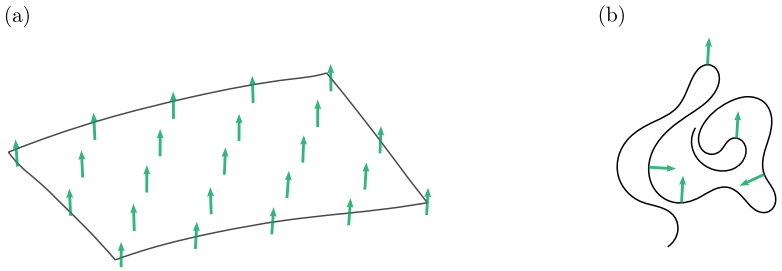

Figure 2.2: Qualitative structural behavior of crystalline membranes in the flat phase (a) and in the crumpled phase (b). The arrows represent unit vectors normal to the surface. In the flat phase, the vectors are 'ferromagnetically' ordered, while in the crumpled phase they are decorrelated beyond a coherence length. Membrane theory predicts that the flat phase is stable below a finite transition temperature T_c. Above T_c, the system behaves as a crumpled manifold. (Figure redrawn from [4]).

analogue in the spin model. The suppression of out-of-plane modes derives from the fact that most curved configurations must inevitably induce a local elastic strain. If we imagine to consider a fixed profile of out-of-plane displacement, specified by a function $h(\mathbf{x})$, it is in general impossible to choose in-plane displacements $u_\alpha(\mathbf{x})$ in such way that the total deformation has zero strain at each point. This follows directly from the fact that $u_\alpha(\mathbf{x})$ provides two degrees of freedom while $U_{\alpha\beta}(\mathbf{x}) = 0$ requires the solution of three constraints (one for each independent components of the symmetric 2×2 matrix $U_{\alpha\beta}$) [1]. This results in a frustration of thermal out-of-plane fluctuations and a suppression of their amplitude [1, 6]. A mathematical basis for describing this frustration effect is provided by the Gauss's *Theorema Egregium*, which relates components of extrinsic and intrinsic curvatures. As a consequence of the theorem, deformations for which the Gaussian curvature $K(\mathbf{x}) = \det\left[(\mathbf{n}\cdot\partial_\alpha\partial_\beta\mathbf{r})\right]$ is nonzero must inevitably present a position-dependent strain field and, thus, a nonzero elastic energy[7] [6, 87].

The elastic strain fields induced by out-of-plane deformations propagate at a distance, leading to effective long-range forces. For this reason, the theory of crystalline membranes does not fulfill the assumptions of the Mermin-Wagner theorem [7, 8, 11, 25, 88]. Despite being two-dimensional, the membrane exhibits at low-temperatures, extended orientational order.

To make the discussion quantitative, it is necessary to solve the statistical mechanical problem explicitly. As in many field-theoretical calculations, it is useful to consider, instead of the physical case of 2D membranes in three-dimensions, the more general problem of a D-dimensional manifold embedded in d-dimensional

7 For an introduction to differential geometry methods in membranes see for example Chap. 7 of Ref. [1].

space. The derivation of the Hamiltonian for arbitrary dimensionalities remains almost identical to that in Sec. 2.1. The in-plane displacement field $u_\alpha(\mathbf{x})$, however, becomes a D-dimensional vector and similarly all Greek indices become D-dimensional cartesian components. The out-of-plane field $h(\mathbf{x})$, which is a scalar in the physical case, becomes promoted to a vector $\mathbf{h}(\mathbf{x}) \in \mathbb{R}^{d_c}$ with $d_c = d - D$ components. The free energy (2.7) remains then valid, with $\mathbf{r}(\mathbf{x}) = (x_\alpha + u_\alpha(\mathbf{x}), \mathbf{h}(\mathbf{x}))$, and $U_{\alpha\beta}(\mathbf{x}) = (\partial_\alpha u_\beta + \partial_\beta u_\alpha + \partial_\alpha \mathbf{h} \cdot \partial_\beta \mathbf{h} + \partial_\alpha u_\gamma \partial_\beta u_\gamma)/2$, where $\partial_\alpha \mathbf{h} \cdot \partial_\beta \mathbf{h}$ denotes the scalar product in d_c-dimensional space[8].

2.3 HARMONIC APPROXIMATION

For a system with finite size in the limit of very low temperatures, the amplitudes of fluctuations are small and the anharmonic effects are suppressed. In this case, the theory can be well described by a harmonic approximation. In the framework of the isotensional ensemble [18], we assume that the tension σ is fixed while the total projected area of the system is free to fluctuate. The harmonic fluctuation theory is then derived by expanding the Hamiltonian H at quadratic order near its minimum. Explicit calculation shows that the minimum occurs at $\mathbf{h} = 0$, $u_\alpha(\mathbf{x}) = (\xi^{(0)} - 1)x_\alpha$. The extension factor $\xi^{(0)}$ describes the macroscopic stretching of the membrane in the zero-temperature limit of the model (2.7), and is fixed, for small strain, by the zero-temperature equation of state

$$(D\lambda + 2\mu)(\xi^{(0)} - 1) = \sigma \ , \tag{2.8}$$

which is the linear Hooke's law. Expansion of the free energy at the minimum then gives, at quadratic order and for $\xi^{(0)} \simeq 1$, the Hamiltonian

$$\begin{aligned} H^{(2)} = \frac{1}{2} \int \mathrm{d}^D x \big[& \kappa(\partial^2 \mathbf{h})^2 + \sigma(\partial_\alpha \mathbf{h} \cdot \partial_\alpha \mathbf{h}) + \kappa(\partial^2 u_\gamma)^2 \\ & + (\lambda + \mu)(\partial_\alpha u_\alpha)^2 + \mu(\partial_\alpha u_\beta)(\partial_\alpha u_\beta) \big] \ , \end{aligned} \tag{2.9}$$

which describes, at linearized level, the fluctuations of non-uniform modes of $u_\alpha(\mathbf{x})$ and $\mathbf{h}(\mathbf{x})$. The equipartition theorem then shows that, at finite temperature T, the amplitude of in-plane and out-of-plane fluctuations in Fourier space are, respectively[9,10]:

8 A less straightfoward adaptation is needed if the bending rigidity is described by a term $\kappa(\partial_\alpha \mathbf{n} \cdot \partial_\alpha \mathbf{n})^2/2$ because the unit vector normal to the surface $\mathbf{n}(\mathbf{x})$ loses meaning in general dimension $D \neq 2$, $d \neq 3$. However, as shown in Ref. [10], the product $\partial_\alpha \mathbf{n} \cdot \partial_\alpha \mathbf{n}$ can be rewritten in terms of the components of the curvature tensor. The expression in terms of curvature has a natural extension to generic dimensionality.

9 The Latin indices i and j run over Cartesian components of d_c-dimensional space.

10 In a model in which the bending rigidity is not represented as $\kappa(\partial^2 \mathbf{r})^2/2$ but modeled via a term involving the square of the extrinsic curvature tensor [10], the fluctuation spectrum of in-plane modes does not contain the contribution κq^4, but only the elastic stiffness terms.

$$\begin{aligned}
\langle u_\alpha(\mathbf{q})u_\alpha(-\mathbf{q}')\rangle &= (2\pi)^2\delta(\mathbf{q}-\mathbf{q}')D^{(0)}_{\alpha\beta}(\mathbf{q}) \ , \\
\langle h_i(\mathbf{q})h_j(-\mathbf{q}')\rangle &= (2\pi)^2\delta(\mathbf{q}-\mathbf{q}')G^{(0)}_{ij}(\mathbf{q}) \ , \\
D^{(0)}_{\alpha\beta}(\mathbf{q}) &= \frac{k_{\rm B}TP^L_{\alpha\beta}(\mathbf{q})}{\kappa q^4+(\lambda+2\mu)q^2} + \frac{k_{\rm B}TP^T_{\alpha\beta}(\mathbf{q})}{\kappa q^4+\mu q^2} \ , \\
G^{(0)}_{ij}(\mathbf{q}) &= \frac{k_{\rm B}T\delta_{ij}}{\kappa q^4+\sigma q^2} \ .
\end{aligned} \tag{2.10}$$

In Eq. (2.10), $P^L_{\alpha\beta}(\mathbf{q}) = q_\alpha q_\beta/q^2$ and $P^T_{\alpha\beta}(\mathbf{q}) = \delta_{\alpha\beta} - P^L_{\alpha\beta}(\mathbf{q})$ are longitudinal and transverse projectors. The fact that both amplitudes diverge for $\mathbf{q}\to 0$ reflects the gapless nature of acoustic phonons, which play the role of Goldstone modes associated with the spontaneously-broken translational invariance (the energy does not depend on $\mathbf{h}$ and u_α but only on their derivatives). The fluctuation spectrum of the $\mathbf{h}$ field, furthermore, shows that when $\sigma = 0$, the dispersion of out-of-plane modes becomes *doubly* soft [11, 25, 61, 88–90]: it diverges as q^{-4} and not as q^{-2}. This stronger divergence can be traced to the fact that when $\sigma = 0$ the system presents, in addition to translational invariance, also rotational symmetry in the d-dimensional ambient space. This symmetry is spontenaously broken by the flat phase, which develops long-range orientational order. The out-of-plane phonon field $\mathbf{h}$ then plays the role of a Goldstone fluctuation associated not only with translational symmetry but also with the broken rotations. As it was already noticed by Lifshitz in 1952 [89] the broken rotational symmetry forces the dispersion to be doubly soft.

Although the harmonic approximation could be a valid description for finite size systems at small T, the strong infrared (IR) singularities generated by the small $\mathbf{q}$ behaviors in Eq. (2.10) destroy its validity in the thermodynamic limit. The failure of the linearized theory becomes evident, for example, if we try to use the Hamiltonian (2.9) to estimate the value of the projected area $A_\parallel$ at finite temperatures. Using the thermodynamic relations of the fixed-tension ensemble $A_\parallel/A \simeq 1 - \partial\mathcal{G}/\partial\sigma$ and the harmonic approximation to the Gibbs free energy density $\mathcal{G} = -A^{-1}k_{\rm B}T\ln\mathcal{Z}$ gives [18]

$$\frac{A_\parallel}{A} \simeq 1 + \frac{\sigma}{\lambda+2\mu/D} - \frac{d_c}{2}\int\frac{{\rm d}^Dq}{(2\pi)^D}\,\frac{k_{\rm B}T}{\kappa q^2+\sigma} \ . \tag{2.11}$$

For zero applied tension, the reduction of the projected area [11, 18, 72, 85, 91]

$$\frac{A_\parallel}{A} = 1 - \frac{d_c}{2}\int\frac{{\rm d}^Dq}{(2\pi)^D}\frac{k_{\rm B}T}{\kappa q^2} \tag{2.12}$$

reflects physically the fact that out-of-plane undulations tend to shrink the average size of the membrane in the planar directions (see Fig. 2.3).

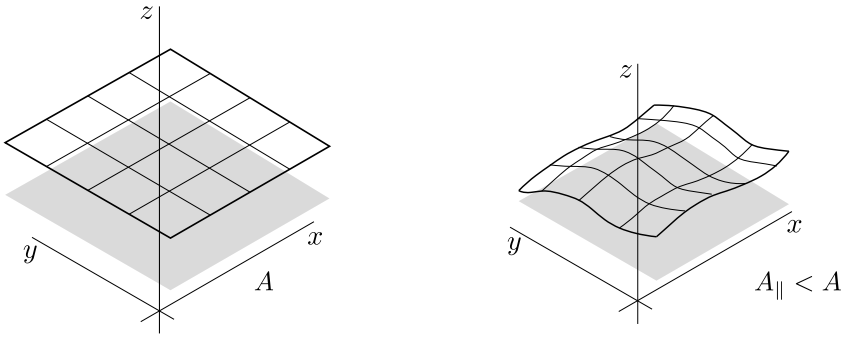

Figure 2.3: Schematic representation of the contraction of the area: at finite T, the thermally excited out-of-plane undulations reduce the projected extension in the xy plane [11, 18, 72, 85, 91].

The difficulty with this harmonic theory is that in the physical dimension $D = 2$, the integral (2.12) is infrared divergent. This seems to indicate that the flat phase is unstable at arbitrarily small T, similarly to systems obeying the Mermin-Wagner theorem. In fact, as it has long been realized [1, 6, 12], the flat phase is physically stable, but can only be described by a theory which goes beyond the harmonic approximation.

2.4 MOMENTUM-SHELL RENORMALIZATION GROUP

The effect of anharmonic interactions can be understood by using an analysis based on Wilson's momentum-shell renormalization group [18, 51]. At low temperatures, the smallness of undulations allows us to approximate [1, 6, 10–12, 41]

$$\begin{aligned} (\partial^2\mathbf{r})^2 &\simeq (\partial^2\mathbf{h})^2 \ , \\ U_{\alpha\beta} \simeq u_{\alpha\beta} &= \frac{1}{2}(\partial_\alpha u_\beta + \partial_\beta u_\alpha + \partial_\alpha \mathbf{h}\cdot\partial_\beta \mathbf{h}) \end{aligned} \tag{2.13}$$

and, thus, to replace the full model (2.7) with the Hamiltonian

$$H = \frac{1}{2}\int \mathrm{d}^2x \big[\kappa(\partial^2\mathbf{h})^2 + \lambda(u_{\alpha\alpha})^2 + 2\mu u_{\alpha\beta}u_{\alpha\beta} - 2\sigma\partial_\alpha u_\alpha\big] \ . \tag{2.14}$$

The neglected terms can be shown, in fact, to be irrelevant in the flat phase, in the sense of the perturbative renormalization group and within an ε-expansion[11] [10–12].

The Hamiltonian (2.14) contains anharmonic interactions of order h^4 and uh^2, but is a quadratic function with respect to the in-plane displacement field $u_\alpha(\mathbf{x})$.

11 See Sec. 2.5 and chapter 3 for a discussion on the ε-expansion.

It is thus convenient to integrate out explicitly the fluctuations of $u_\alpha(\mathbf{x})$, which can be done exactly via the calculation of a Gaussian functional integral. Similarly to the theory of compressible magnets, the Gaussian integration over u_α requires a careful separation between uniform modes of $\partial_\alpha u_\alpha$ (with momentum $\mathbf{q} = 0$) and non-uniform fluctuation parts (with Fourier components at non-zero momentum $\mathbf{q} \neq 0$) [1, 18, 85]. In the isotensional ensemble, the zero mode $u^{0\|}_{\alpha\beta}$ of the strain tensor $(\partial_\alpha u_\beta + \partial_\beta u_\alpha)/2$ is integrated out without constraints and the integral over its components has the effect to remove all interactions with zero momentum transfer [1, 18]. The remaining integral over the nonuniform in-plane displacement fields gives rise, instead, to an effective quartic interaction for out-of-plane undulations. After integration, the effective field theory for $\mathbf{h}$ fields reads [6, 10, 23, 25]

$$\begin{aligned} H_{\text{eff}} &= -\frac{A\sigma^2}{2(\lambda + 2\mu/D)} + \frac{1}{2}\int_{\mathbf{q}} (\kappa q^4 + \sigma q^2)|\mathbf{h}(\mathbf{q})|^2 \\ &+ \frac{1}{4}\int_{\mathbf{k}_1,\mathbf{k}_2,\mathbf{k}_3} R_{\alpha\beta,\gamma\delta}(\mathbf{q}) k_{1\alpha} k_{2\beta} k_{3\gamma} k_{4\delta} \big(\mathbf{h}(\mathbf{k}_1)\cdot\mathbf{h}(\mathbf{k}_2)\big)\big(\mathbf{h}(\mathbf{k}_3)\cdot\mathbf{h}(\mathbf{k}_4)\big) \ , \end{aligned} \tag{2.15}$$

where $\mathbf{h}(\mathbf{k})$ are Fourier components of $\mathbf{h}$, $\mathbf{k}_4 = -\mathbf{k}_1 - \mathbf{k}_2 - \mathbf{k}_3$, $\int_{\mathbf{k}} = \int \mathrm{d}^D k/(2\pi)^D$ denotes momentum integration, and A is the total area (in D dimensions, the total D-dimensional volume). The bare vertex function $R_{\alpha\beta,\gamma\delta}(\mathbf{q})$ depends only on the momentum transfer $\mathbf{q} = \mathbf{k}_1 + \mathbf{k}_2 = -\mathbf{k}_3 - \mathbf{k}_4$ and is given by $R_{\alpha\beta,\gamma\delta} = bN_{\alpha\beta,\gamma\delta} + \mu M_{\alpha\beta,\gamma\delta}$, with $b = \mu(D\lambda + 2\mu)/(\lambda + 2\mu)$,

$$N_{\alpha\beta,\gamma\delta}(\mathbf{q}) = \frac{1}{D-1} P^T_{\alpha\beta}(\mathbf{q}) P^T_{\gamma\delta}(\mathbf{q}) \ , \tag{2.16}$$

$$M_{\alpha\beta,\gamma\delta}(\mathbf{q}) = \frac{1}{2}(P^T_{\alpha\gamma}(\mathbf{q})P^T_{\beta\delta}(\mathbf{q}) + P^T_{\alpha\delta}(\mathbf{q})P^T_{\beta\gamma}(\mathbf{q})) - N_{\alpha\beta,\gamma\delta}(\mathbf{q}) \ . \tag{2.17}$$

The effective interaction (2.15) describes quantitatively the geometric frustration effect described in Sec. 2.2. After fixing a given configuration of the out-of-plane displacement field $\mathbf{h}(\mathbf{x})$, it is impossible in general to adjust the in-plane displacement field $u_\alpha(\mathbf{x})$ in such way to make the strain $u_{\alpha\beta}(\mathbf{x})$ vanish at all points. The non-vanishing strain induced by out-of-plane fluctuations results in the nonlinear interaction, quartic in $\mathbf{h}(\mathbf{x})$, expressed in the second line of Eq. (2.15).

The solution of the nonlinear model by renormalization group methods presents a close analogy to the theory of critical phenomena [13–16, 81]. The RG equation can be derived by the following sequence of steps[12]. (i) Integrating out modes within a momentum shell $\mathrm{e}^{-\ell}\Lambda < |\mathbf{k}| < \Lambda$, where Λ is the maximum wavenumber in the system (of the order of the inverse of the lattice spacing). After integration, the initial microscopic Hamiltonian is mapped to an effective theory for slowly

12 More generally, the RG transformation could be defined as a combination of a scale transformation and a general nonlinear change of field variables [92].

varying modes with momenta $|\mathbf{k}| < \mathrm{e}^{-\ell}\Lambda$, where the effects of short-wavelength modes are encoded in a renormalization of effective interactions. Following step (i), the renormalization group transformation is defined by two additional steps: (ii) rescaling momenta as $\mathbf{q} = \mathrm{e}^{-\ell}\mathbf{q}'$, and (iii) rescaling the field as $\mathbf{h}(\mathbf{q}) = \mathrm{e}^{\ell(D-\Delta)}\mathbf{h}'(\mathbf{q}')$ [13, 14]. After steps (i), (ii), and (iii), the microscopic Hamiltonian is mapped to an effective Hamiltonian $H_{\mathrm{eff}}(\ell)$, dependent on the scale factor ℓ, which lives in the same space of the initial Hamiltonian (it has the same cutoff Λ and the same number of degrees of freedom) [93], but which physically describes the system when regarded with a resolution and a magnification lowered by a factor e^{ℓ}.

Similarly to the theory of critical phenomena, it is sufficient to consider simple truncated forms of the Hamiltonian $H_{\mathrm{eff}}(\ell)$ to obtain a qualitatively correct solution of the theory. In the simplest approximation, it can be assumed that $H_{\mathrm{eff}}(\ell)$ has the same functional form of Eq. (2.15), but with renormalized, ℓ-dependent, parameters $\kappa(\ell)$, $b(\ell)$, $\mu(\ell)$, $\sigma(\ell)$. With this assumption, it can be shown that renormalized parameters evolve with scale according to the differential RG equations[13,14]

$$\begin{aligned}
\frac{\mathrm{d}\kappa}{\mathrm{d}\ell} &= -\eta\kappa + \frac{2a_D k_{\mathrm{B}} T(b+(D-2)\mu)\Lambda^{D-2}}{\kappa\Lambda^2+\sigma} \ , \\
\frac{\mathrm{d}\sigma}{\mathrm{d}\ell} &= (2-\eta)\sigma \ , \\
\frac{\mathrm{d}b}{\mathrm{d}\ell} &= (4-D-2\eta)b - \frac{a_D d_c k_{\mathrm{B}} T b^2 \Lambda^D}{(\kappa\Lambda^2+\sigma)^2} \ , \\
\frac{\mathrm{d}\mu}{\mathrm{d}\ell} &= (4-D-2\eta)\mu - \frac{2a_D d_c k_{\mathrm{B}} T \mu^2 \Lambda^D}{(D+1)(\kappa\Lambda^2+\sigma)^2} \ .
\end{aligned} \tag{2.18}$$

where $\eta = 4 - D + 2\Delta$ is the anomalous dimension, and

$$a_D = \frac{2(D+1)}{D(D+2)} \frac{\Gamma(D/2)}{(4\pi)^{D/2}} \ . \tag{2.19}$$

The structure of Eqs. (2.18) can be understood as follows. The first terms on the right hand side of Eqs. (2.18), which do not depend explicitly on T, describe simply the effect of rescaling lengths and field amplitudes. The anomalous dimension η can be chosen arbitrarily without changing physical predictions of the theory but, as in

13 For derivations (in different notations and field-theoretical schemes) see Refs. [18–20, 51].

14 Eqs. (2.18) are derived by computing one-loop Feynman diagrams illustrated in Fig. 2.4, assuming that internal lines are confined to the momentum shell $\mathrm{e}^{-\ell}\Lambda < |\mathbf{k}| < \Lambda$. Since in the differential form of the RG flow the width of the momentum shell is infinitesimal, the one-loop calculation is in fact exact within the framework of perturbation theory. Indeed, each loop in a Feynman diagram corresponds to a free momentum integration. Thus diagrams with $L \geq 2$ loops are suppressed by powers of $(\mathrm{d}\ell)^L$ and do not contribute to the differential equation. Eqs. (2.18) are however approximate due to the truncation of the action. The one-loop structure is a general property of momentum-shell implementations of the RG and also emerges in exact formulations of the renormalization group such as the Wegner-Houghton RG [94] and the Wetterich equation [95].

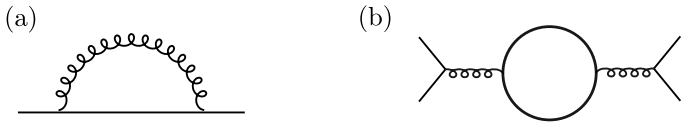

Figure 2.4: Feynman graphs determining the renormalizations of the bending rigidity and elastic constants expressed in Eqs. (2.18). The solid line represents the propagator of flexural fields $G^{(0)}_{ij}(\mathbf{k}) = k_{\rm B}T/(\kappa k^4 + \sigma k^2)$, the curly line the nonlinear interaction $(k_{\rm B}T)^{-1}R_{\alpha\beta,\gamma\delta}(\mathbf{q})k_{1\alpha}k_{2\beta}k_{3\gamma}k_{4\delta}$.

the theory of critical phenomena, needs to be set to a special value in order for the RG to exhibit fixed points. The terms proportional to $k_{\rm B}T$ on the right-hand side of Eqs. (2.18) describe, instead, renormalizations induced by the interplay between anharmonic effects and thermal fluctuations and can be explicitly calculated by evaluating the Feynman diagrams in Fig. 2.4. The equations show that, due to the interaction of fluctuations, the bending rigidity κ becomes *enhanced* by nonlinear effects, while the elastic moduli, represented by b and μ become *softened*. The direction of these renormalization can be intuitively understood by an analogy with the familiar properties of a sheet of paper [1, 74]. Compared to a perfectly flat sheet, a corrugated sheet of paper which is on average flat but presents random buckles is much easier to stretch: pulling the system from one side generates a dilatation of the in-plane projected area by "ironing" the ripples rather than by stretching the molecular bonds. At the same time, a buckled sheet of paper presents an enhanced stiffness to curvature, and for strong buckling can hold its own gravitational weigth [1, 74]. The same occurs in corrugated iron roofs [1], which receive a strong enhancement of the effective bending rigidity from the interplay between elasticity and their geometrical shape.

Differently from κ, b, and μ, the external in-plane tension σ does not receive corrections from fluctuations: the self-energy diagram (a) in Fig. 2.4 vanishes as q^4 where $\mathbf{q}$ is the momentum, and does not contain a term proportional to q^2 corresponding to a tension renormalization. This property can be traced to rotational invariance and the related Ward identities [11, 12, 18] (see Sec. 2.5).

To solve the RG equations, it is convenient to introduce the couplings

$$\hat{b} = \frac{k_{\rm B}Tb\Lambda^{D-4}}{\kappa^2} \ , \qquad \hat{\mu} = \frac{k_{\rm B}T\mu\Lambda^{D-4}}{\kappa^2} \ , \qquad \hat{\sigma} = \frac{\sigma}{\kappa\Lambda^2} \tag{2.20}$$

which are dimensionless quantities for any D. The anomalous dimension η can be chosen in any conventional way without modifying the physics of the system [14]. To study membranes with small external tension, it is convenient to choose

$$\eta = \frac{2a_D(\hat{b} + (D-2)\hat{\mu})}{1+\hat{\sigma}} \ , \tag{2.21}$$

in such way that, by Eq. (2.18), $\mathrm{d}\kappa/\mathrm{d}\ell = 0$. The RG flow can thus be rewritten as

$$\begin{aligned}
\frac{\mathrm{d}\hat{\sigma}}{\mathrm{d}\ell} &= (2-\eta)\hat{\sigma} \ , \\
\frac{\mathrm{d}\hat{b}}{\mathrm{d}\ell} &= (4-D-2\eta)\hat{b} - \frac{a_D d_c \hat{b}^2}{(1+\hat{\sigma})^2} \ , \\
\frac{\mathrm{d}\hat{\mu}}{\mathrm{d}\ell} &= (4-D-2\eta)\hat{\mu} - \frac{2a_D d_c \hat{\mu}^2}{(D+1)(1+\hat{\sigma})^2} \ ,
\end{aligned} \tag{2.22}$$

where η is fixed by Eq. (2.21).

Eq. (2.22) shows immediately that the surface $\sigma_0 = 0$ is invariant under the RG flow. This is a consequence of the fact that for zero external in-plane tension, the system is symmetric under rotations in d-dimensional space[15]. Since symmetries are preserved under renormalization, if $\sigma_0 = 0$ initially, it must remain zero at each step of the RG trajectory.

When restricted to the surface of rotationally-invariant theories, the RG flow takes, for $D < 4$, the form illustrated in Fig. 2.5. There are four fixed points, denoted as P_1', P_2', P_3', P_4' at which the renormalization group flow stops [18–20, 51]. At these points, the theory becomes scale-invariant: it remains equal to itself under a change of length scale. The coordinates and anomalous dimensions at the four fixed points are listed in table 2.1.

	$\hat{b}$	$\hat{\mu}$	η
P_1'	0	0	0
P_2'	$\frac{4-D}{(d_c+4)a_D}$	0	$\frac{2(4-D)}{d_c+4}$
P_3'	0	$\frac{(D+1)(4-D)}{(4(D^2-D-2)+2d_c)a_D}$	$\frac{2(D-2)(D+1)(4-D)}{4(D^2-D-2)+2d_c}$
P_4'	$\frac{4-D}{(2D^2-2D+d_c)a_D}$	$\frac{(D+1)(4-D)}{2(2D^2-2D+d_c)a_D}$	$\frac{D(D-1)(4-D)}{(2D^2-2D+d_c)}$

Table 2.1: Coordinates of fixed points and corresponding anomalous dimensions. The values of the anomalous dimensions are exact at first order in $\varepsilon = 4 - D$ [19, 20]. For $D = 2$ and $d_c = 1$, P_2' and P_4' have, in this approximation, $\eta = 4/5$ [18, 51].

A generic solid membrane with nonzero shear modulus is described by an initial theory having $b \neq 0$ and $\mu \neq 0$. If the temperature T is small, the model is very close to the "Gaussian fixed point" P_1', which is the harmonic approximation.

15 More precisely, after taking the small-undulation approximation, the theory is invariant under the transformations $\mathbf{h} \to \mathbf{h} + \mathbf{A}_\alpha x_\alpha$, $u_\alpha \to u_\alpha - \mathbf{A}_\alpha x_\alpha$, which are linearized versions of rotations in the d-dimensional embedding space [1, 10, 11]. See Sec. 2.5 for a discussion of the symmetries of the small-undulation approximation.

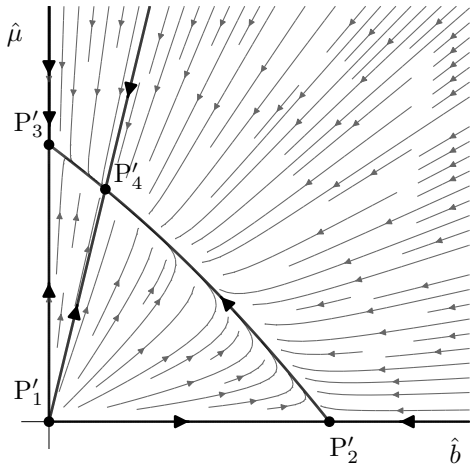

Figure 2.5: RG flow for tensionless membranes ($\sigma_0 = 0$). The figure represents the flow functions (2.22) in the case $D = 3.99$, $d_c = 1$.

However, after many iterations of the RG transformations, the effective theory flows, independently of the initial conditions, to the fixed point P'_4. As a result, in the limit of large length scales and small wavevectors, thermal ripples are governed by an effective theory which is universal, independent on the temperature and the material parameters [1, 6, 9–11, 26]. Furthermore, being a fixed point, the model described by P'_4 is scale-invariant[16]. Scaling arguments can be used to show that correlation and response functions behave in the limit of long wavelengths and small tension, as power laws with universal non-integer exponents. In particular, the correlation function $\langle h_i(\mathbf{q}) h_j(-\mathbf{q}')\rangle = (2\pi)^D \delta(\mathbf{q}-\mathbf{q}') G_{ij}(\mathbf{q})$ behaves, for zero applied tension and $\mathbf{q} \to 0$, as $G_{ij}(\mathbf{q}) \propto \delta_{ij}/|\mathbf{q}|^{4-\eta_*}$ where η_* is the anomalous dimension at the fixed point. Higher-order correlations are also scale-invariant in the long-wavelength limit: the n-point function $\langle h_{i_1}(\mathbf{q}_1) h_{i_2}(\mathbf{q}_2) ... h_{i_n}(\mathbf{q}_n)\rangle = (2\pi)^D \delta(\mathbf{q}_1+\mathbf{q}_2+...+\mathbf{q}_n) G^{(n)}_{i_1 i_2 ... i_n}(\mathbf{q}_1, \mathbf{q}_2, ..., \mathbf{q}_n)$ satisfies the self-similarity relation

$$\begin{aligned} G^{(n)}_{i_1 i_2 ... i_n}(\rho\mathbf{q}_1, \rho\mathbf{q}_2, ..., \rho\mathbf{q}_n) &= \rho^{D-n(D-\Delta)} G^{(n)}_{i_1 i_2 ... i_n}(\mathbf{q}_1, \mathbf{q}_2, ..., \mathbf{q}_n) \\ &= \rho^{D-\frac{n}{2}(D+4-\eta_*)} G^{(n)}_{i_1 i_2 ... i_n}(\mathbf{q}_1, \mathbf{q}_2, ..., \mathbf{q}_n) \ . \end{aligned} \tag{2.23}$$

16 In the physical case $D = 2$, the tensor $M_{\alpha\beta,\gamma\delta}(\mathbf{q})$ vanishes identically and thus the coupling constant μ becomes redundant. In the limit $D \to 2$, the two fixed points P'_2 and P'_4 remain formally distinct, but their anomalous dimensions approach the same limiting value. The coalescence of the two fixed points implies that both P'_2 and P'_4 can be regarded as alternative continuations of the theory from dimension $D = 2$ to a general dimensionality. The use of P'_2 as a dimensional continuation is discussed in detail in chapter 3.

As mentioned in Sec. 2.2, an essential consequence of scaling behavior is that, differently from the harmonic model, the full nonlinear theory admits a stable flat phase in the thermodynamic limit, which spontaneously breaks rotational symmetry and which exhibits long-range orientational order [1, 6, 10, 12]. This can be seen by noticing that, within the small undulation theory (2.14), the average projected area is given by the relation [11, 12, 18, 22, 41, 51, 85, 91]

$$\frac{A_\parallel}{A} = 1 + \frac{\sigma}{\lambda + 2\mu/D} - \frac{1}{2}\langle(\partial_\alpha \mathbf{h} \cdot \partial_\alpha \mathbf{h})\rangle = 1 + \frac{\sigma}{\lambda + 2\mu/D} - \frac{1}{2}\int_{\mathbf{q}} q^2 G_{ii}(\mathbf{q}) \ . \quad (2.24)$$

This expression can be derived, for example, by applying the Hellmann-Feynman theorem $A\partial\mathcal{G}/\partial\sigma\big|_T = \langle \partial H/\partial\sigma\rangle$ to the Hamiltonian (2.15). For zero tension $\sigma = 0$, the anomalous dimension $\eta_* > 0$ makes the integral $\int_{\mathbf{q}} q^2 G_{ii}(\mathbf{q})$ convergent in the thermodynamic limit, even in dimension $D = 2$. This ensures the stability of a flat phase at sufficiently low temperatures [11, 12, 18, 25, 41, 85, 96].

Since renormalization softens the elastic constants b and μ, the effect on in-plane translational order is opposite: rather than stabilizing the crystalline order, they lead to an enhancement of the amplitude of fluctuations. Eq. (2.18) implies in particular that the physical elastic constants $b_{\mathrm{R}}(\mathbf{q})$ and $\mu_{\mathrm{R}}(\mathbf{q})$ (coarse-grained but expressed in standard units of measurements, without rescaling) vanish as $b_{\mathrm{R}}(\mathbf{q}) \propto q^{4-D-2\eta_*}$, $\mu_{\mathrm{R}}(\mathbf{q}) \propto q^{4-D-2\eta_*}$ where q is the momentum scale [10, 11]. As a result, the propagator of in-plane displacement fields $D_{\alpha\beta}(\mathbf{q})$ scales as $1/q^{6-D-2\eta_*}$, which is more infrared-singular than in the harmonic approximation $D^{(0)}_{\alpha\beta} \propto 1/q^2$ (see Eq. (2.10)).

Scale invariance and the existence of a fixed point also imply that the response functions are governed by universal power law. An important example is the stress-strain relation, which can be accessed by experiments on suspended graphene [69, 72]. It can be shown that in the limit of a very small external stress $\sigma \to 0$, the ordinary linear relation becomes replaced by an *anomalous Hooke's law*: the strain $\epsilon(\sigma)$ scales for $\sigma \to 0$ as $\epsilon(\sigma) \propto \sigma^{1/\gamma}$ where $\gamma = (2 - \eta_*)/(D - 2 + \eta_*)$ [11, 12, 18, 41, 51, 85].

2.4.1 *External tension*

The RG equations (2.18), (2.22) show that the external tension σ is a relevant perturbation: a deviation from the "critical surface" $\sigma = 0$ grows under scaling. This reflects the fact that a membrane under stress behaves in the long-wavelength limit in a very different way from a tensionless membrane. In the case of tensile stress, $\sigma > 0$, tension has the effect to suppress the amplitude of out-of-plane fluctuations by introducing the "mass" term σk^2 in the dispersion $G^{-1}_{ij}(\mathbf{k}) = \delta_{ij}(\kappa k^4 + \sigma k^2)$. For $\sigma < 0$, instead, the applied stress is compressive and tends to buckle the membrane out of plane. For this reason the equilibrium phase of tensionless membranes can

also be interpreted as the critical state associated with a "buckling transition" [11, 18, 52] separating the regimes $\sigma > 0$ and $\sigma < 0$. The role played by tension in the phase diagram has some analogy with the role of an applied magnetic field in a spin system below the Curie point [11]. The buckled state with $\sigma < 0$ (a 2D solid subject to lateral compression) however is much more complex [11] that a spin system with negative magnetic field, which is just the mirror image of a system with positive field[17].

2.4.2 *Remarks*

In most applications of RG approaches, locality plays an essential role [14–16, 81]. Since the effective Hamiltonian (2.15) is not local, the applicability of RG theory may appear problematic. Actually, the effective interaction $R_{\alpha\beta,\gamma\delta}(\mathbf{q})k_{1\alpha}k_{2\beta}k_{3\gamma}k_{4\delta}$ $\times(\mathbf{h}(\mathbf{k}_1)\cdot\mathbf{h}(\mathbf{k}_2))(\mathbf{h}(\mathbf{k}_3)\cdot\mathbf{h}(\mathbf{k}_4))$ is not a generic fourth order coupling: in real space, it corresponds to a long-range interaction between two local composite operators. By using a Hubbard-Stratonovich (HS) transformation, the model can thus be expressed by an effective theory having only local vertices. A more explicit derivation will be described in chapter 3, where it is shown that the line of theories with $\mu = 0$ and $b \neq 0$ can be represented by a quasi-local model, involving an auxiliary scalar field χ, proportional to the Airy stress function. A similar derivation could be used in the case $\mu \neq 0$, $b \neq 0$. In this case, the HS transformation could be achieved by introducing an auxiliary tensor field. After HS transformation, standard RG methods can be applied[18].

As a second remark, note that the integration over the field u_α is a simple step only due to the small-undulation approximation 2.13. In the full theory (2.7), integration over u_α would generate instead a complex model, with infinitely many non-local vertices. The analysis in Sec. 2.5 shows that terms beyond the small-undulation approximation are in fact irrelevant in the ε-expansion. This justifies the application of standard RG methods to the non-local model[19].

17 See, for example, Refs. [18, 83, 97–99] for discussions of buckling, wrinkling, and other elastic instabilities.

18 The coupling matrix $R_{\alpha\beta,\gamma\delta}(\mathbf{q})$ has a non-analytic dependence on $\mathbf{q}$ proportional to q^{-4}. Thus, after Hubbard-Stratonovich transformation, the kinetic term ($\propto q^4$) of auxiliary fields is local (see Chap. 3). Note, however, that in the framework of perturbation theory, standard RG methods can be applied even to theories in which *propagators* are non-local but interaction *vertices* are local (see for example Refs. [15, 100] for a discussion in the context of magnetic phase transitions).

19 A systematic analysis of the full theory (2.7) is a complex task. This problem has been addressed, for example, by a large-d method in Ref. [9] and by non-perturbative renormalization group approaches in Refs. [26–28].

2.5 PERTURBATION THEORY AND THE ε-EXPANSION

The picture of a scale-invariant flat phase has been corroborated by numerous field theoretical techniques, such as the ε-expansion [10–12, 19, 20, 96], the large-d expansion [9, 22, 96], the self-consistent screening approximation [23–25], and the nonperturbative renormalization group [26–28]. These techniques are closely analogue to similar methods in the theory of critical phenomena and provide a basis for a systematic expansion of the scaling index η. The next sections summarize the main results obtained in the literature by these complementary techniques, starting from the ε-expansion method.

As in the case of second-order phase transitions [14–16, 81, 101] the ε-expansion is based on the fact that the critical fixed point approaches the Gaussian fixed point at a certain dimension $D_{\rm uc}$ (the upper critical dimension). The scaling index η is thus small near $D_{\rm uc}$ and can be expanded in powers of $\varepsilon = D_{\rm uc} - D$. The upper critical dimension $D_{\rm uc}$ is determined by a stability analysis of the Gaussian fixed point: for $D > D_{\rm uc}$ the harmonic approximation is stable and anharmonic effects are irrelevant while for $D < D_{\rm uc}$ anharmonic effects become relevant and drive the RG flow away from the Gaussian fixed point.

In the case of the flat phase of crystalline membrane, the scaling behavior of propagators implies that the canonical dimensionalities [15] of in-plane and out-of-plane displacement field are respectively $\{u_\alpha\} = (D-2)/2$ and $\{\mathbf{h}\} = (D-4)/2$. It is then simple to check that for $D > 4$ all anharmonic interactions consistent with translational and rotational invariance are irrelevant. For $D < 4$, instead, the anharmonic interaction $(\partial_\alpha \mathbf{h} \cdot \partial_\alpha \mathbf{h})^2$ and other are relevant at the Gaussian fixed point. The upper critical dimension[20] is, therefore, $D_{\rm uc} = 4$ [10] and the ε-expansion is a series expansion of $\eta(D)$ in powers of $\varepsilon = 4 - D$.

Similarly to the Ginzburg-Landau theory [101], the series coefficients $\eta(D) = \eta_1\varepsilon + \eta_2\varepsilon^2 + \ldots$ can be computed from a Feynman graph expansion of any theory in the universality class of the flat phase fixed point. In order to discuss the perturbative series, it is useful to start from the model membrane Hamiltonian (2.7) (adapted to general $D = 4 - \varepsilon$ and $d_c \neq 1$). After the field rescalings $\mathbf{h} \to \bar{\mathbf{h}} = (\sqrt{\kappa/(k_{\rm B}T)})\mathbf{h}$, $u_\alpha \to \bar{u}_\alpha = \kappa/(k_{\rm B}T)u_\alpha$, the reduced Hamiltonian $\mathcal{H} = H/(k_{\rm B}T)$ reads, in the case of zero external stress

$$\mathcal{H} = \frac{1}{2}\int \mathrm{d}^D x \left[(\partial^2 \bar{\mathbf{h}})^2 + \alpha_0 (\partial^2 \bar{u}_\alpha)^2 + \lambda_0 (\bar{U}_{\alpha\alpha})^2 + 2\mu_0 \bar{U}_{\alpha\beta}\bar{U}_{\alpha\beta} \right] , \tag{2.25}$$

where $\lambda_0 = k_{\rm B}T\lambda/\kappa^2$, $\mu_0 = k_{\rm B}T/\kappa^2$, $\alpha_0 = k_{\rm B}T/\kappa$ and

$$\bar{U}_{\alpha\beta} = \frac{1}{2}\left(\partial_\alpha \bar{u}_\beta + \partial_\beta \bar{u}_\alpha + \partial_\alpha \bar{\mathbf{h}} \cdot \partial_\beta \bar{\mathbf{h}} + \alpha_0 \partial_\alpha \bar{u}_\gamma \partial_\beta \bar{u}_\gamma \right) . \tag{2.26}$$

20 That $D_{\rm uc} = 4$ is evident in the RG flow expressed in Eq. (2.18) and in the coordinates of the fixed points in table 2.1.

A simple dimensional analysis shows that $\bar{\mathbf{h}}$ has the units of $q^{(D-4)/2}$ while $\bar{u}_\alpha$ has units q^{D-3}, where q is a wavevector scale[21]. Since $\mathcal{H}$, appears in the exponential of the partition function $\mathrm{e}^{-\mathcal{H}}$, it must be dimensionless. Matching dimensionalities shows that λ_0 and μ_0 have dimension q^{4-D}, while α_0 has dimension q^{2-D}.

As a result, near four dimensions, λ_0 and μ_0 are weakly relevant while α_0 has a negative canonical dimension ≈ -2 and, thus, is irrelevant. According to the general theory of the field-theoretical ε-expansion [15], the canonically-irrelevant interactions are not essential for the calculation of the exponents and can be set equal to zero without changing the structure of universality classes near $D = 4$ and the values of the exponents to all orders in powers of ε.

It is thus possible to set $\alpha_0 = 0$ and to analyze the effective model

$$\mathcal{H} = \frac{1}{2}\int \mathrm{d}^D x \left[(\partial^2 \bar{\mathbf{h}})^2 + \lambda_0 (\bar{u}_{\alpha\alpha})^2 + 2\mu_0 \bar{u}_{\alpha\beta}\bar{u}_{\alpha\beta} \right] , \tag{2.27}$$

with $\bar{u}_{\alpha\beta} = (\partial_\alpha \bar{u}_\beta + \partial_\beta \bar{u}_\alpha + \partial_\alpha \bar{\mathbf{h}} \cdot \partial_\beta \bar{\mathbf{h}})/2$. This effective theory is identical to the small-undulation Hamiltonian introduced in section 2.4, which contains only the relevant and marginal part of propagators and interactions. The irrelevance of α_0 near four dimension thus shows that the small-undulation theory actually remains to all orders in the ε-expansion [10–12].

2.5.1 *Symmetries of the effective Hamiltonian*

The neglection of the irrelevant parameter α_0 induces a "deformation" of the symmetries of the Hamiltonian [10, 11]. The full model (2.25), before neglection of α_0, is symmetric under translations and rotations of the membrane in d-dimensional space. The corresponding infinitesimal transformations read, in terms of rescaled fields $\bar{\mathbf{h}}$ and $\bar{u}$,

$$\begin{aligned}
&\bar{\mathbf{h}}'(\mathbf{x}) = \bar{\mathbf{h}}(\mathbf{x}) + \mathbf{B}^\perp , && \text{(translations in } \perp \text{ space)} \\
&\bar{u}'_\alpha(\mathbf{x}) = \bar{u}_\alpha(\mathbf{x}) + B^\parallel_\alpha , && \text{(translations in } \parallel \text{ space)} \\
&\bar{\mathbf{h}}'_l = \bar{\mathbf{h}}_l + E^\perp_{lm}\bar{\mathbf{h}}_m , && \text{(rotations in } \perp \text{ space)} \\
&\bar{u}'_\alpha = \bar{u}_\alpha + E^\parallel_{\alpha\beta}(x_\beta + \alpha_0 \bar{u}_\beta) , && \text{(rotations in } \parallel \text{ space)} \\
&\begin{cases} \bar{\mathbf{h}}'(\mathbf{x}) = \bar{\mathbf{h}}(\mathbf{x}) + \mathbf{A}_\alpha (x_\alpha + \alpha_0 \bar{u}_\alpha(\mathbf{x})) \\ \bar{u}'_\alpha(\mathbf{x}) = \bar{u}_\alpha - \mathbf{A}_\alpha \cdot \bar{\mathbf{h}}(\mathbf{x}) \end{cases} . && \text{(mixed rotations)}
\end{aligned} \tag{2.28}$$

In Eqs. (2.28), $\mathbf{B}^\perp$, $B^\parallel_\alpha$, and $\mathbf{A}_\alpha$ are fixed, space-independent, vectors and $E^{(\perp)}_{lm} = -E^\perp_{ml}$, $E^\parallel_{\alpha\beta} = -E^\parallel_{\beta\alpha}$ fixed antisymmetric matrices.

21 The unit of the in-plane field, q^{D-3}, differs from the power-counting dimension $q^{(D-2)/2}$ because in the Hamiltonian (2.25) the propagator of $\bar{u}_\alpha$ is not canonically normalized: the part of the action quadratic in $\bar{u}_\alpha$ is multiplied by factors λ_0 and μ_0 which are not dimensionless.

The effective Hamiltonian (2.27) obtained by neglecting irrelevant operators is instead invariant under

$$\begin{cases} \bar{\mathbf{h}}'(\mathbf{x}) = \bar{\mathbf{h}}(\mathbf{x}) + \mathbf{B}^{\perp} + \bar{E}^{\perp} \cdot \bar{\mathbf{h}} + \mathbf{A}_{\alpha} x_{\alpha} \\ \bar{u}'_{\alpha}(\mathbf{x}) = \bar{u}_{\alpha}(\mathbf{x}) + B^{\parallel}_{\alpha} + E^{\parallel}_{\alpha\beta} x_{\beta} - \mathbf{A}_{\alpha} \cdot \bar{\mathbf{h}}(\mathbf{x}) \end{cases} , \tag{2.29}$$

which is the $\alpha_0 \to 0$ limit of (2.28)[22,23].

The Ward identities [10, 11, 15] imply that order by order in the perturbative expansion (2.27), the effective action $\Gamma[\bar{\mathbf{h}}(\mathbf{x}), \bar{u}_{\alpha}(\mathbf{x})]$, generating functional of one-particle irreducible correlation functions, is also invariant under the transformations (2.29).

2.5.2 *Diagrammatic rules, Ward identities, and infrared divergences*

The elasticity theory defined in Eq. (2.27) has a perturbative expansion described by the Feynman rules illustrated in Fig. 2.6.

$$\underset{i \qquad\qquad j}{\overset{\mathbf{k}}{\longrightarrow}} = \frac{\delta_{ij}}{k^4} \qquad\qquad \underset{\alpha \qquad\qquad \beta}{\overset{\mathbf{q}}{\sim\sim\sim}} = \frac{P^L_{\alpha\beta}(\mathbf{q})}{(\lambda_0 + 2\mu_0) q^2} + \frac{P^T_{\alpha\beta}(\mathbf{q})}{\mu_0 q^2}$$

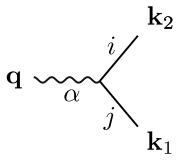

$$= -i\delta_{ij} \left(\lambda_0 q_{\alpha} (\mathbf{k}_1 \cdot \mathbf{k}_2) + \mu_0 (\mathbf{q} \cdot \mathbf{k}_2) k_{1\alpha} + \mu_0 (\mathbf{q} \cdot \mathbf{k}_1) k_{2\alpha} \right)$$

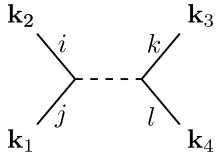

$$\begin{aligned} &= -\delta_{ij}\delta_{kl} \left(\lambda_0 (\mathbf{k}_1 \cdot \mathbf{k}_2)(\mathbf{k}_3 \cdot \mathbf{k}_4) \right. \\ &\quad \left. + \mu_0 (\mathbf{k}_1 \cdot \mathbf{k}_3)(\mathbf{k}_2 \cdot \mathbf{k}_4) + \mu_0 (\mathbf{k}_1 \cdot \mathbf{k}_4)(\mathbf{k}_2 \cdot \mathbf{k}_3) \right) \end{aligned}$$

Figure 2.6: Feynman rules for the elasticity theory of crystalline membranes. Solid and wiggly lines represent propagators of the $\bar{\mathbf{h}}$ and of the $\bar{u}_{\alpha}$ field respectively. The model has a three-leg vertex, corresponding to interactions of the form $(\partial \bar{u})(\partial \bar{\mathbf{h}})^2$ and a four-leg vertex corresponding to $(\partial \bar{\mathbf{h}})^4$.

22 For compactness, Eq. (2.29) is expressed by collecting together the action of independent generators. The notation $\bar{E} \cdot \mathbf{h}$ stands for the vector $E^{\perp}_{lm} h_m$.

23 The invariance of the effective Hamiltonian under the transformation (2.29) was derived in Refs. [10, 11].

Some of the most crucial properties of the perturbative series can be understood by explicit inspection of diagrams after calculating the fundamental "building block"

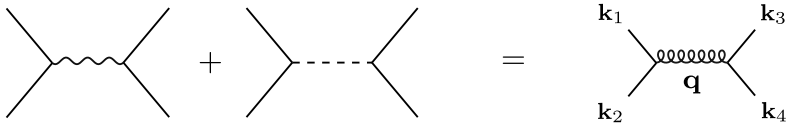

(2.30)

$$= -(b_0 N_{\alpha\beta,\gamma\delta}(\mathbf{q}) + \mu_0 M_{\alpha\beta,\gamma\delta}(\mathbf{q}))k_{1\alpha}k_{2\beta}k_{3\gamma}k_{4\delta} \ ,$$

which is identical to the effective interaction obtained by integrating out the in-plane displacement fields (see Eqs. (2.16), (2.17)). The tensors $N_{\alpha\beta,\gamma\delta}$ and $M_{\alpha\beta,\gamma\delta}$, being constructed from transverse projectors, annihilate the component of $\mathbf{k}_1$, $\mathbf{k}_2$, $\mathbf{k}_3$, and $\mathbf{k}_4$ which is longitudinal to the momentum transfer $\mathbf{q}$. Since, by momentum conservation, $\mathbf{k}_1 + \mathbf{k}_2 = -\mathbf{k}_3 - \mathbf{k}_4 = \mathbf{q}$, it follows that the vertex (2.30) vanishes as k_i^2 when one of the momenta $\mathbf{k}_i$ $(i = 1, ..., 4)$ tends to zero at fixed $\mathbf{q}$.

This simple property provides the basis of how the Ward identity is realized diagrammatically. In any one-particle irreducible (1PI) diagram [15], each external solid line which is attached to an internal curly line comes with a factor k_i^2 of its momentum. The substitution (2.30) can be applied to all internal dashed and wiggly lines a part from those internal dashed lines which, when cut, disconnect the diagram (see Fig. 2.7). As a result, it can be checked by inspection of diagrams that the effective 1PI action[24] must take the form $\Gamma[\bar{\mathbf{h}}(\mathbf{x}), \bar{u}_\alpha(\mathbf{x})] = \Gamma[\partial_\alpha\partial_\beta\bar{\mathbf{h}}(\mathbf{x}), \bar{u}_{\alpha\beta}(\mathbf{x})]$. In other words, Γ is a (generally nonlocal) functional of the strain tensor $\bar{u}_{\alpha\beta}(\mathbf{x})$ and of the curvature tensor. This ensures consistency with the Ward identities associated with the transformations (2.29).

A particular case of the Ward identities is an analogue of the Goldstone theorem ensuring that the ultrasoft behavior of flexural phonons is preserved to all orders in perturbation theory [11, 25, 85, 88]. The exact propagator of out-of-plane phonons, including all diagrammatic corrections, is determined by expanding the effective action Γ at second order in $\bar{\mathbf{h}}$ at its minimum. The minimum occurs for $\bar{\mathbf{h}} = 0$, $\bar{u}_\alpha = (\xi - 1)x_\alpha$ or any other configuration obtained by application of the symmetries (2.29). After setting the value of ξ by the condition $\partial\Gamma/\partial\xi = 0$, the expansion of the effective action cannot contain terms linear in $\bar{u}_{\alpha\beta}$. As a result, the fluctuation free energy at quadratic order in $\bar{\mathbf{h}}(\mathbf{x})$ receives contributions only from curvature terms and is suppressed by four gradients. In Fourier space $\bar{G}_{ij}^{-1}(\mathbf{q}) = \delta_{ij}q^4 g^{-1}(\mathbf{q})$, where $g^{-1}(\mathbf{q})$ is a non-analytic function of $\mathbf{q}$.

24 The 1PI effective action is the generating functional of one-particle irreducible correlation functions (self-energies and proper vertices) [15]. It can be defined as the action which, when used at tree level (without loop diagrams), effectively gives the full correlation functions of the bare theory including all loop corrections.

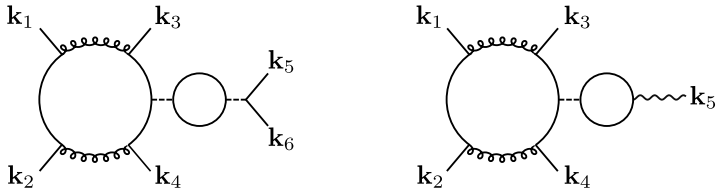

Figure 2.7: Examples of one-particle irreducible diagrams. The diagrams are suppressed by *two* powers of $\mathbf{k}_1$, $\mathbf{k}_2$, $\mathbf{k}_3$, $\mathbf{k}_4$ whenever one of these momenta tends to zero. The dashed lines on the right side of the diagrams cannot be combined according to the substitution (2.30) because the corresponding diagrams with wiggly lines would not be one-particle irreducible. The sum of the two diagrams gives a contribution to the effective action at first order in the strain $\bar{u}_{\alpha\beta}$ and fourth order in the curvature $\partial_\alpha \partial_\beta \bar{\mathbf{h}}$.

The massless character of flexural phonons gives rise to infrared divergences which destroy the perturbative expansion for any $\varepsilon > 0$, similarly to the case of critical phenomena [16]. For example, the self-energy diagram at one-loop order evaluates to [25]

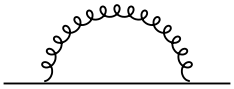

$$= \frac{2(D+1)(b_0+(D-2)\mu_0)}{(D-1)} \frac{\Gamma(2-D/2)\Gamma^2(D/2)}{4(4\pi)^{D/2}\Gamma(D)} q^{4-\varepsilon} \tag{2.31}$$

The flexural propagator obtained by N insertions of this self-energy diagram scales as $q^{-4-N\varepsilon}$ and, for N large, becomes more and more singular. As a result, at order $\approx 2/\varepsilon$ in perturbation theory, insertion of the dressed propagator as a subdiagram generates divergences in all correlation functions[25].

Within the ε-expansion, however, correlation functions can be defined via a double series, expanding not only in coupling constants but also in powers of ε [15]. In the double series, $q^{-\varepsilon} \approx 1 - \varepsilon \ln q + \varepsilon^2 \ln^2 q/2 - ..$ is replaced by powers of logarithms and the infrared singularities disappear.

2.5.3 *Renormalization within the dimensional regularization scheme*

For $\varepsilon \to 0$ the theory behaves as a renormalizable model with dimensionless coupling constants, which can be studied by renormalization theory. The RG equations were first derived by Aronovitz and Lubensky using dimensional regularization and minimal subtraction [10]. As in any renormalizable field theory, divergences can be removed by adding one counterterm for each local interaction which (i) is consistent with symmetries and (ii) is relevant or marginal according to power counting [15].

25 The same phenomenon occurs in the theory of phase transitions [16].

In the case of membranes, the Ward identities associated with the spontaneously-broken symmetries (2.29) imply that the model can be renormalized by considering the renormalized Hamiltonian [11, 96]

$$\begin{aligned}\tilde{\mathcal{H}}[\tilde{\mathbf{h}},\tilde{u}_\alpha] = \frac{1}{2}\int \mathrm{d}^D x \big[Z(\partial^2\tilde{\mathbf{h}})^2 + M^\varepsilon g_\lambda (\tilde{u}_{\alpha\alpha})^2 \\ + 2M^\varepsilon g_\mu \tilde{u}_{\alpha\beta}\tilde{u}_{\alpha\beta} + 2r_0\tilde{u}_{\alpha\alpha}\big] \ .\end{aligned} \tag{2.32}$$

In Eq. (2.32), M is an arbitrary wavevector scale, Z, G_λ, G_μ, and r_0 are functions of the dimensionless renormalized coupling constants $\tilde{\lambda}$, $\tilde{\mu}$, and $\tilde{u}_{\alpha\beta} = (\partial_\alpha\tilde{u}_\beta + \partial_\beta\tilde{u}_\alpha + \partial_\alpha\tilde{\mathbf{h}}\cdot\partial_\beta\tilde{\mathbf{h}})/2$ is the renormalized strain tensor. The counterterm $r_0\tilde{u}_{\alpha\alpha}$ encodes the change of average area induced in the membrane by thermal fluctuations. For membranes with free boundaries, it is always possible to remove the contribution $\int \mathrm{d}^D x r_0 u_{\alpha\alpha}$ from the Hamiltonian by a change of variables of the form $\tilde{u}_\alpha \to \tilde{u}_\alpha + \epsilon x_\alpha$ [11]. This shows that the value of r_0 has no effect on correlation functions but only on the value of the average area. Furthermore, power-counting shows that r_0 diverges quadratically, in contrast with Z, G_λ, and G_μ, which diverge logarithmically. Within dimensional regularization, therefore, it can be taken formally equal to zero [11, 15, 81].

The renormalized Hamiltonian is therefore

$$\tilde{\mathcal{H}}[\tilde{\mathbf{h}},\tilde{u}_\alpha] = \frac{1}{2}\int \mathrm{d}^D x \big[Z(\partial^2\tilde{\mathbf{h}})^2 + M^\varepsilon g_\lambda (\tilde{u}_{\alpha\alpha})^2 + 2M^\varepsilon g_\mu \tilde{u}_{\alpha\beta}\tilde{u}_{\alpha\beta}\big] \ . \tag{2.33}$$

Correlation functions calculated with the Hamiltonian (2.32) are finite for $\varepsilon \to 0$ when expanded in powers of the renormalized coupling constants $\tilde{\lambda}$ and $\tilde{\mu}$. Comparing Eq. (2.27) with (2.33) shows that bare and renormalized quantities are related as [10, 11]:

$$\begin{aligned}&\bar{\mathbf{h}} = \sqrt{Z}\tilde{\mathbf{h}} \ , \qquad \bar{u}_\alpha = Z\tilde{u}_\alpha \ , \qquad \lambda_0 = \frac{M^\varepsilon g_\lambda}{Z^2} \ , \\ &\mu_0 = \frac{M^\varepsilon g_\mu}{Z^2} \ , \qquad \tilde{\mathcal{H}}[\tilde{\mathbf{h}},\tilde{u}_\alpha] = \mathcal{H}[\bar{\mathbf{h}},\bar{u}_\alpha] \ .\end{aligned} \tag{2.34}$$

Renormalization group equations follow, as usual, from the fact that bare correlation functions are independent of M [10, 11]. After introduction of the RG functions

$$\eta = \frac{\partial \ln Z}{\partial \ln M}\Big|_{\lambda_0,\mu_0} \ , \qquad \beta_\lambda = \frac{\partial\tilde{\lambda}}{\partial \ln M}\Big|_{\lambda_0,\mu_0} \ , \qquad \beta_\mu = \frac{\partial\tilde{\mu}}{\partial \ln M}\Big|_{\lambda_0,\mu_0} \ , \tag{2.35}$$

the RG equations read

$$\begin{aligned}\Big[\frac{\partial}{\partial \ln M}\Big|_{\tilde{\lambda},\tilde{\mu}} + \beta_\lambda \frac{\partial}{\partial\tilde{\lambda}}\Big|_{M,\tilde{\mu}} + \beta_\mu \frac{\partial}{\partial\tilde{\mu}}\Big|_{M,\tilde{\lambda}} \\ + \Big(\frac{n}{2}+\ell\Big)\eta\Big]\tilde{G}^{(n,\ell)}_{i_1..i_n;\alpha_1\ldots\alpha_\ell}(\mathbf{k}_1,..,\mathbf{k}_n;\mathbf{q}_1,..,\mathbf{q}_\ell) = 0 \ .\end{aligned} \tag{2.36}$$

In Eq. (2.36), $\tilde{G}^{(n,\ell)}_{i_1..i_n;\alpha_1...\alpha_\ell}(\mathbf{k}_1,..,\mathbf{k}_n;\mathbf{q}_1,..,\mathbf{q}_\ell)$ denotes the renormalized correlation function with n external $\mathbf{h}$ lines and ℓ external u_α lines.

The RG coefficient functions η, β_λ and β_μ are, by definition, dimensionless and thus can only depend on $\tilde{\lambda}$, $\tilde{\mu}$, and ε, but not on the scale parameter M. In addition, the coefficient functions can be extracted, via the RG equation (2.36), from the knowledge of renormalized correlation functions, which are finite. As a result, η, β_λ, and β_μ must also be finite[26] when $\varepsilon \to 0$.

The RG functions, the fixed points, and the corresponding anomalous dimensions have been calculated at one-loop order in Refs. [10, 11]. Over the last two years, the calculation has been extended to two [19], three [20], and four [21] loops. The flow of coupling constants in the one-loop approximation reads

$$\begin{aligned}
\beta_\lambda &= -\varepsilon\tilde{\lambda} + \frac{d_c}{16\pi^2}\left(\tilde{\lambda}^2 + \tilde{\lambda}\tilde{\mu} + \frac{1}{6}\tilde{\mu}^2\right) + \frac{5}{8\pi^2}\frac{\tilde{\lambda}\tilde{\mu}(\tilde{\lambda}+\tilde{\mu})}{\tilde{\lambda}+2\tilde{\mu}} \ , \\
\beta_\mu &= -\varepsilon\tilde{\mu} + \frac{d_c}{96\pi^2}\tilde{\mu}^2 + \frac{5}{8\pi^2}\frac{\tilde{\mu}^2(\tilde{\lambda}+\tilde{\mu})}{\tilde{\lambda}+2\tilde{\mu}} \ , \\
\eta &= \frac{5}{16\pi^2}\frac{\tilde{\mu}(\tilde{\lambda}+\tilde{\mu})}{\tilde{\lambda}+2\tilde{\mu}} \ ,
\end{aligned} \tag{2.37}$$

and is illustrated in Fig. 2.8.

For membranes with generic elastic constants, RG trajectories connect the Gaussian fixed point P_1 to an infrared-attractive interacting fixed point P_4 [10, 12].

A different behavior emerges on the lines $\mu_0 = 0$ and $B_0 = \lambda_0 + 2\mu_0/D = 0$, which describe, respectively, membranes with zero shear modulus and zero compression modulus. For these special values of the bare elastic constants, the theory presents additional symmetries [11]. When $\mu_0 = 0$, the model is invariant under the shift $u_\alpha \to u_\alpha + s_{\alpha\beta}x_\beta$ for any traceless matrix $s_{\alpha\beta}$. For vanishing bulk modulus $B_0 = 0$, the theory is instead invariant under uniform compression ($u_\alpha \to u_\alpha + \ell x_\alpha$) or, more, generally under the transformation $u_\alpha \to u_\alpha + \tau_\alpha$ for any vector field τ_α satifsying the conformal Killing equation $\partial_\alpha\tau_\beta + \partial_\beta\tau_\alpha = 2\delta_{\alpha\beta}(\partial_\gamma\tau_\gamma)/D$ [11, 102][27]. The flows restricted to these lines terminate at two different fixed points, P_2 and P_3[28]. Physically, the line $\mu_0 = 0$ and the fixed point P_2 have been associated to

26 The finiteness of RG functions is a general property of all renormalizable field theories (see, for example, Refs. [15, 81]).

27 This symmetry is not equivalent to the usual notion of conformal invariance intended in CFT: the conformal transformation, here, does not act on the coordinates $\mathbf{x}$, but, rather, acts as a shift of the field itself. In two dimensions with $\lambda_0 + \mu_0 = 0$, the linear model of in-plane displacement fields is also conformal in the standard CFT sense if u_α is regarded as a collection of scalars (see Ref. [103]).

28 The line $\mu_0 = 0$ corresponds, to all orders in perturbation theory, to the line $\tilde{\mu} = 0$, as it can be verified by inspecting the structure of Feynman diagrams. The curve in the $(\tilde{\lambda}, \tilde{\mu})$ plane

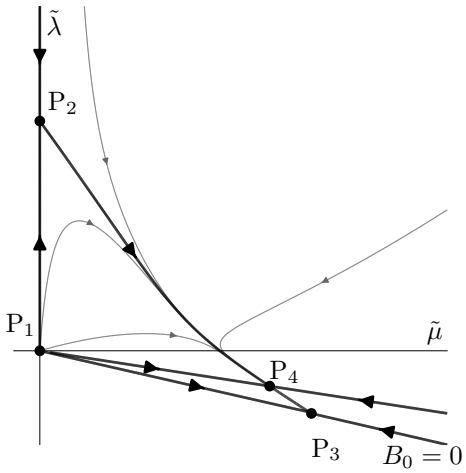

Figure 2.8: Renormalization group flow for the flat phase of crystalline membranes at one-loop order [10].

fluid membranes[29] [10, 11]. The line $B_0 = 0$, instead, has a physical counterpart, for example, in two-dimensional twisted kagome lattices [102].

Coordinates of fixed points at one-loop order are reported in table 2.2, together with the more recent four-loop result obtained in Ref. [21].

When the renormalized couplings are fixed to the coordinates $(\tilde{\lambda}_*, \tilde{\mu}_*)$ of the infrared-stable fixed point P_4, the RG equations (2.36) imply that correlation functions exhibit scaling behavior. In particular the flexural Green function behaves as $G_{ij}(\mathbf{q}) \propto \delta_{ij} q^{-4+\eta_*}$ [11]. The in-plane Green function, instead, exhibits the power-law behavior $D_{\alpha\beta}(\mathbf{q}) \propto q^{-6+D+2\eta_*}$. Consistently with the discussion in Sec. 2.4, these results ban be interpreted as a power-law divergence of the scale-dependent bending rigidity $\kappa_{\mathrm{R}}(q) \propto q^{-\eta_*}$, and as a power-law softening of elastic constants $\lambda_{\mathrm{R}}(q) \propto q^{4-D-2\eta_*}$, $\mu_{\mathrm{R}}(q) \propto q^{4-D-2\eta_*}$.

corresponding to $B_0 = 0$, instead, is less straightforward to express explicitly. In Ref. [11], which used a renormalized bulk modulus as fundamental coupling constant, this line corresponds simply to $\tilde{B} = 0$. However, defining minimal subtraction with $\tilde{\lambda}$ and $\tilde{\mu}$ as couplings reshuffles the parametrization of renormalization constants in a non-trivial way. At leading order in perturbation theory the curve $B_0 = 0$ corresponds to the line $\tilde{\lambda} + \tilde{\mu}/2 = 0$. Already at two loop order, however, the coordinates of the fixed point P$_3$ can be seen to lie outside of this line. In Ref. [19], this was interpreted as an artifact of the renormalization scheme. It is likely in fact that the RG-invariant manifold $B_0 = 0$ is not a straight line, but, rather, a curve $(\tilde{\lambda}, \tilde{\mu})$ plane.

29 A difficulty in this interpretation, however, is that the elastic energy associated with transverse waves is exactly zero for vanishing shear modulus, and higher-derivative terms of the form $(\partial^2 u)^2$, neglected in the theory, could play a role [104].

	$\tilde{\lambda}_*$	$\tilde{\mu}_*$	η_*	η_*(order ε^4)
P_1	0	0	0	0
P_2	$\frac{16\pi^2\varepsilon}{d_c}$	0	0	0
P_3	$-\frac{48\pi^2\varepsilon}{d_c+20}$	$\frac{96\pi^2\varepsilon}{d_c+20}$	$\frac{10\varepsilon}{d_c+20}$	$\frac{0.952\varepsilon}{2} - \frac{0.071\varepsilon^2}{4} - \frac{0.069\varepsilon^3}{8} - \frac{0.075\varepsilon^4}{16}$
P_4	$-\frac{32\pi^2\varepsilon}{d_c+24}$	$\frac{96\pi^2\varepsilon}{d_c+24}$	$\frac{12\varepsilon}{d_c+24}$	$\frac{0.96\varepsilon}{2} - \frac{0.0461\varepsilon^2}{4} - \frac{0.00267\varepsilon^3}{8} - \frac{0.002\varepsilon^4}{16}$

Table 2.2: Coordinates of fixed points and corresponding anomalous dimensions at leading order in the ε-expansion. The last column shows the value of the exponents at four-loop orders for $d_c = 1$ [21].

Before concluding this section, let us comment on the relation between the fixed points P_1, P_2, P_3, P_4 in the $(\tilde{\lambda}, \tilde{\mu})$ plane and the fixed points in the (b, μ) plane derived in Sec. 2.4. The infrared-stable fixed point P_4, which has a nonzero shear and bulk modulus, is equivalent to the fixed point P_4' in the (b, μ) plane of the effective theory (2.15), discussed in Sec. 2.4. Similarly, the fixed points P_3 and P_3' can be viewed as equivalent representations of the same theory: the model of a membrane with zero bulk modulus and finite shear modulus.

The fixed points P_2, instead, has no counterpart in the effective field theory (2.15). It only appears in a model describing both in-plane and out-of-plane fields explicitly [19]. Indeed, P_2 lives on the line $\mu = 0$, which is mapped to an effective theory in which both b and μ are equal to zero. Conversely, the fixed point P_2' which emerged in the analysis of Sec. 2.4 has no analogue in the space of elasticity theories, and only exists in the space of effective theories.

In the physical dimension $D = 2$, however, the theories P_2' and P_4 become identically equivalent and, thus, P_2' can be used as an alternative dimensional continuation providing the basis of an ε-expansion (see chapter 3).

2.6 LARGE-d EXPANSION

In full analogy with the large-N expansion in the theory of phase transitions [15, 16, 105], the exponents of crystalline membranes can be computed systematically in the limit in which the fluctuating fields have a large number of components, that is, when the dimension d of the embedding space tends to infinity [9, 11, 22, 23, 25, 41, 96]. It is usually assumed that the expansion parameter playing the role of $1/N$ in the usual large-N expansion is $1/d_c$, since $d_c = d - D$ is the number of components of the $\mathbf{h}$ field. The value of η_* within the large-d_c theory for the physical internal dimension $D = 2$ has been determined at first order already in the early investigations on

crystalline membranes [9, 12], and has been extended to second order in a recent analysis [22], which lead to $\eta_* = 2/d_c + (78 - 68\zeta(3))/(27 d_c^2) \approx 2/d_c - 0.32/d_c^2$.

Differently from the ε-expansion, which starts from a quasi-harmonic theory, the large-d_c expansion has as a starting point a zero-order theory in which interactions are already screened by fluctuations via diagrams of the form

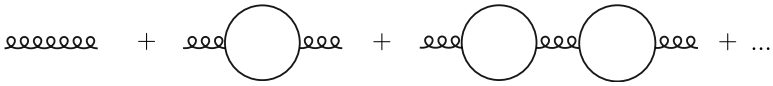

After screening, the coupling constants become momentum-dependent and behave as

$$b_{\mathrm{R}}(\mathbf{q}) = \frac{b_0}{1 + c_1(D) b_0 q^{D-4}} \ , \qquad \mu_{\mathrm{R}}(\mathbf{q}) = \frac{\mu_0}{1 + c_2(D) \mu_0 q^{D-4}} \ , \tag{2.38}$$

where $c_1(D)$ and $c_2(D)$ are positive constants dependent on the dimension [12, 22, 25, 41]. For $q \to 0$, or equivalently for infinite elastic constants, the screened interactions become independent on parameters and scale-invariant with exponent q^{4-D}. As a result, in analogy with other applications of large-N techniques [15, 105], the $1/d_c$ expansion becomes free of infrared divergences and renormalizable in any dimension, including the physical dimensionality $D = 2$. In this renormalization, the finite value of the coupling constants plays the role of an ultraviolet cutoff, which sets the starting point of the renormalization group [41].

Besides providing a tool for the computation of η_*, the large-d_c expansion has been used in Refs. [17, 22, 41] to describe mechanical nonlinearities induced by fluctuations, the anomalous Hooke's law, and the response to anisotropic external stress.

In Ref. [9], a first-order large-d technique has been used to investigate the theory of membranes in a formalism which does not involve the small-undulation approximation[30]. By considering the limit of infinitely large elastic constants, in analogy with the nonlinear sigma model, the authors derived a RG flow exhibiting for large κ the divergence $\kappa_{\mathrm{R}}(q) \approx q^{-\eta_*}$ characteristic of the flat phase, and for a critical value $\kappa = \kappa_c$ a fixed point corresponding to the crumpling transition.

2.7 SELF-CONSISTENT SCREENING APPROXIMATION

By adapting a method introduced by Bray in the theory of magnetic transitions [106], Le Doussal and Radzihovsky have proposed an approximate theory based on a set of truncated Dyson equations in which screened interactions and self-energy corrections are determined self-consistently [23, 25]. In diagrammatic language, the "self-consistent screening approximation" (SCSA) consists in the

30 In this case, the expansion parameter was considered to be $1/d$ and not $1/d_c$.

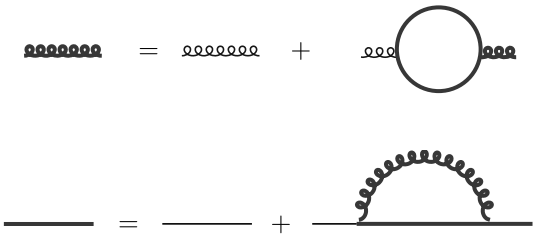

Figure 2.9: Diagrams defining the self-consistent screening approximation.

resummation of Feynman graphs illustrated in Fig. 2.9, which are akin to the GW diagrams in electronic structure theory. Explicitly, the summation of diagrams gives (in standard units of measurement and for zero applied tension), the following set of equations [25]

$$G_{ij}(\mathbf{q}) = \frac{k_{\rm B}T\delta_{ij}}{\kappa_{\rm R}(\mathbf{q})q^4} \ , \tag{2.39}$$

$$b_{\rm R}(\mathbf{q}) = \frac{b}{1+(D+1)bk_{\rm B}TI(\mathbf{q})} \ , \qquad \mu_{\rm R}(\mathbf{q}) = \frac{\mu}{1+2\mu k_{\rm B}TI(\mathbf{q})} \tag{2.40}$$

$$\kappa_{\rm R}(\mathbf{q}) = \kappa + \frac{2k_{\rm B}T}{q^4}\int_{\mathbf{k}} \frac{(b_{\rm R}(\mathbf{k})+(D-2)\mu_{\rm R}(\mathbf{k}))}{(D-1)} \frac{(P^T_{\alpha\beta}(\mathbf{k})q_\alpha q_\beta)^2}{|\mathbf{k}-\mathbf{q}|^4\kappa_{\rm R}(\mathbf{k}-\mathbf{q})} \ , \tag{2.41}$$

$$I(\mathbf{q}) = \frac{d_c}{(D^2-1)}\int_{\mathbf{k}} \frac{(P^T_{\alpha\beta}(\mathbf{q})k_\alpha k_\beta)^2}{k^4|\mathbf{k}-\mathbf{q}|^4\kappa_{\rm R}(\mathbf{k})\kappa_{\rm R}(\mathbf{k}-\mathbf{q})} \ . \tag{2.42}$$

In the long-wavelength limit $\mathbf{q}\to 0$, the zero-order terms become negligible with respect to the self-energy corrections and Eqs. (2.40), (2.41) can be approximated as

$$b_{\rm R}(\mathbf{q}) = \frac{1}{(D+1)k_{\rm B}TI(\mathbf{q})} \ , \qquad \mu_{\rm R}(\mathbf{q}) = \frac{1}{2k_{\rm B}TI(\mathbf{q})} \ , \tag{2.43}$$

$$\begin{aligned}\kappa_{\rm R}(\mathbf{q}) &= \frac{2k_{\rm B}T}{q^4}\int_{\mathbf{k}} \frac{(b_{\rm R}(\mathbf{k})+(D-2)\mu_{\rm R}(\mathbf{k}))}{(D-1)} \frac{(P^T_{\alpha\beta}(\mathbf{k})q_\alpha q_\beta)^2}{|\mathbf{k}-\mathbf{q}|^4\kappa_{\rm R}(\mathbf{k}-\mathbf{q})} \\ &= \frac{D}{(D+1)q^4}\int_{\mathbf{k}} \frac{(P^T_{\alpha\beta}(\mathbf{k})q_\alpha q_\beta)^2}{|\mathbf{k}-\mathbf{q}|^4\kappa_{\rm R}(\mathbf{k}-\mathbf{q})I(\mathbf{k})}\end{aligned} \tag{2.44}$$

Eqs. (2.42) and (2.44) admit a power-law solution $\kappa_{\rm R}(\mathbf{q}) = z_1 q^{-\eta_*}$, $I(\mathbf{q}) = 1/(z_2 q^{4-D-2\eta_*})$, where z_1 and z_2 are constants, and the exponent is fixed by the relation [25]

$$d_c = \frac{D(D-1)\Gamma(2-\eta_*)\Gamma(2-\eta_*/2)\Gamma(\eta_*/2)\Gamma(D+\eta_*)}{\Gamma(2-D/2-\eta_*)\Gamma((D+4-\eta_*)/2)\Gamma(D/2+\eta_*)\Gamma((D+\eta_*)/2)} \ . \tag{2.45}$$

In dimension $D = 2$, the equation is exactly solvable and gives a value of the scaling exponent

$$\eta_*(D = 2, d_c) = \frac{4}{d_c + \sqrt{16 - 2d_c + d_c^2}} , \tag{2.46}$$

which reduces, for the physical dimensionality $d_c = 1$, to $\eta_* = 4/(1 + \sqrt{15}) \simeq 0.821$.

If the bare elastic moduli are not generic but, instead, $b = 0$ or $\mu = 0$, the equation (2.45) for the exponent acquires a different prefactor and gives different solutions corresponding the the dimensions of the fixed points P_2' and P_3' [25]. The SCSA equations for the fixed point P_2' will be discussed in more detail in chapter 3.

In Ref. [24], the SCSA method was been pushed one step further by including the leading vertex corrections. By a numerical solution of the integral equation, the value of the exponent for physical dimensionality $D = 2$, $d_c = 1$ was determined to be, at the next SCSA order, $\eta_* \simeq 0.789$.

2.8 NONPERTURBATIVE RG APPROACHES AND NUMERICAL SIMULATIONS

The problem of determining quantitatively the value of the exponent η_* has also been addressed by nonperturbative RG techniques [26–28, 42, 50, 107]. In particular, Ref. [26] analyzed nonperturbatively the renormalization of an elastic membrane described by a Hamiltonian

$$H = \int \mathrm{d}^D x \left[\frac{Z}{2} (\partial^2 \mathbf{r})^2 + u(\partial_\alpha \mathbf{r} \cdot \partial_\beta \mathbf{r} - \xi^2 \delta_{\alpha\beta})^2 + v(\partial_\alpha \mathbf{r} \cdot \partial_\alpha \mathbf{r} - D\xi^2)^2 \right] . \tag{2.47}$$

Assuming as an approximation that the effective average action remains of the form at each step of the RG flow (2.47), the theory allowed to describe, within a single space of coupling constants, the flat phase and the crumpling transition. For the flat phase and in the physical case $D = 2$, $d_c = 1$, the resulting exponent was found to be $\eta_* \simeq 0.85$. The analysis has been extended by considering more general forms for the effective average action, including a non-locality of elastic couplings [27, 28]. The flat-phase exponent was found to remain close to $\eta_* \simeq 0.85$, indicating the stability of the nonperturbative RG results with respect to the truncation of the action. However Ref. [35] predicted, by a combination of numerical simulations and momentum-shell RG, a value of the exponent $\eta_* \simeq 0.793$, with a small estimated error bar.

Besides RG methods, another important tool to access scaling behavior is provided by direct numerical simulations of correlation functions [25, 29–32, 34, 35, 37, 38, 78, 108, 109]. Investigations of fluctuating membranes by computer simulations have been ongoing for several decades. Several works [29, 30, 108] have analyzed network models mathematically designed to provide a discretization of

the continuum theory. In more recent years, the discovery of graphene and other 2D materials has raised an extensive interest in simulating atomically-thin membranes within realistic microscopic models [31, 34, 37, 38, 78].

Results of computer methods provide full information on momentum-dependent correlation functions, and can be used in particular to extract the exponent η_* controlling the long-wavelength scaling regime in the flat phase. The values $\eta_* \simeq 0.750$ [4], 0.81 [29, 30], 0.85 [31, 34], 0.66 [37], 0.85–0.88 [38] have been reported by different works in the literature. In Ref. [32] a Fourier Monte Carlo method lead to the prediction $\eta_* = 0.795(10)$.

Within analytical field-theoretical methods, a 'high-precision' determination of scaling indices remains an open problem. In the framework of the NPRG, a systematic derivation could be given by extending the derivative expansion to higher and higher order [19][31]. Calculations within the derivative expansion, are however, more technically complex than ε-expansion and large-d_c computations. For this reason, it is interesting to get access to values of the exponents at higher order in the ε-expansion. This direction will be discussed in more details in Chap. 3.

2.9 WEAK TO STRONG-COUPLING CROSSOVER

It is physically intuitive that lowering the temperatures T has the effect to reduce the amplitude of thermal fluctuations and, thus, the strength of anharmonic effects. The scaling phenomenon, however, implies that the low-temperature limit is realized in a very nontrivial way. As T approaches 0 for fixed material parameters, the bare theory, initial point of the RG flow, becomes closer and closer to the Gaussian fixed point. However, even for an infinitesimal T, the flow is eventually repulsive and drives the system to the strongly-coupled infrared fixed point, which is dominated by anharmonic effects.

The characteristic wavelength at which the behavior crosses over from weak to strong coupling can be estimated by calculating the first-order self-energy in perturbation theory [3, 12, 61]. Using Eq. (2.31) shows that in two dimensions and in conventional units of measurements, the inverse Green function at first order is:

$$G_{ij}^{-1}(\mathbf{q}) = \frac{\kappa\delta_{ij}q^4}{k_{\mathrm{B}}T}\left[1 + \frac{3b_0}{8\pi q^2}\right] . \tag{2.48}$$

For $|\mathbf{q}| \gg q_{\mathrm{G}} = \sqrt{3b_0/8\pi}$, the anharmonic correction is much smaller than the leading-order term, while for $|\mathbf{q}| \ll q_{\mathrm{G}}$, the self-energy correction becomes larger

31 By analogy with other field theory problems, Ref. [19] suggested that the derivative expansion could give a *convergent* series for the exponent η_*, as opposed to perturbative series, which are more likely only asymptotic.

than the leading term. When the simple first order calculation is replaced with a full solution of the model, the interacting Green function behaves as

$$G_{ij}^{-1}(\mathbf{q}) = \begin{cases} \frac{\kappa\delta_{ij}q^4}{k_{\mathrm{B}}T} & q \gg q_{\mathrm{G}} \\ \frac{c\kappa\delta_{ij}q^{4-\eta_*}q_{\mathrm{G}}^{\eta_*}}{k_{\mathrm{B}}T} & q \ll q_{\mathrm{G}} \end{cases} , \tag{2.49}$$

where c is a dimensionless coefficient of the order of 1 [3, 17, 41, 51, 85]. The scale q_{G} thus plays a role analogue to the Ginzburg criterion in critical phenomena [84]. Using the explicit expression for b_0 shows that the characteristic crossover scale is

$$q_{\mathrm{G}} = \sqrt{\frac{3k_{\mathrm{B}}TY}{16\pi\kappa^2}} , \tag{2.50}$$

where $Y = 4\mu(\lambda+\mu)/(\lambda+2\mu)$ is the two-dimensional Young modulus [3, 61]. The fact that $q_{\mathrm{G}} \to 0$ as $T \to 0$ reflects the fact that the theory spends a long RG time near the Gaussian fixed point. In the case of graphene at $T = 300$ K, the Ginzburg wavelength $\lambda_{\mathrm{G}} = 2\pi/q_{\mathrm{G}}$ is approximately 4 nm [3, 31, 61].

The amplitude z can be approximately estimated by matching the two limiting behaviors at $q \approx q_{\mathrm{G}}$.

In presence of a weak external stress, the system exhibits a further crossover between a tensionless and a tension-dominated regime. In the long-wavelength stress-dominated region, nonlinearities drive a singular logarithmic renormalization of the bending rigidity (a much weaker effect than the power-law renormalization in the tension-free case). The behavior of the Green function becomes [17, 41, 51, 85]

$$G_{ij}^{-1}(\mathbf{q}) = \begin{cases} \frac{\kappa\delta_{ij}q^4}{k_{\mathrm{B}}T} & q \gg q_{\mathrm{G}} \\ \frac{c\kappa\delta_{ij}q^{4-\eta_*}q_{\mathrm{G}}^{\eta_*}}{k_{\mathrm{B}}T} & q_\sigma \ll q \ll q_{\mathrm{G}} \\ \frac{\sigma q^2 + d\kappa q^4 (q_\sigma/q_{\mathrm{G}})^{\eta_*}\ln(q_\sigma/q)}{k_{\mathrm{B}}T} & q \ll q_\sigma \end{cases} , \tag{2.51}$$

where d is a numerical coefficient and q_σ is the momentum scale at which $\sigma q_\sigma^2 \approx \kappa q_\sigma^4 (q_\sigma/q_{\mathrm{G}})^{\eta_*}$ [17].

If the applied tension is sufficiently strong ($\sigma \gtrapprox \kappa q_{\mathrm{G}}^2$), propagators become dominated by stress before the onset of scaling behavior. In this case, the strongly-anharmonic region is completely suppressed [62, 85, 110]. The anomalous stress-strain relation is then replaced by a regular, linear Hooke's law [17, 62].

In the case of graphene, the value of q_G at room temperature is of the order of 4 nm [61], implying that the strongly-anharmonic scaling behavior sets in already at the nanoscale [25, 51].

2.10 ANOMALOUS HOOKE'S LAW AND UNIVERSAL POISSON RATIO

The anomalous scale invariance of fluctuations translates also in an anomalous behavior of response functions. The same phenomenon occurs for example in

second-order magnetic transitions, where the scaling behavior determines power-law divergences of the field susceptibility [13–15]. In the case of membranes, a striking manifestation is the anomalous Hooke's law: for small applied stress σ, the induced strain $\varepsilon(\sigma)$ is not proportional to σ but, rather, proportional to σ^α with $\alpha = (D+\eta_*-2)/(2-\eta_*)$. This phenomenon has been analyzed in detail, for example, in Refs. [11, 17, 18, 52, 85][32]. The essence of the derivation can be understood by combining the explicit formula (2.24) for the projected area and a reasoning on the Ward identities. The diagrammatic analysis of Ward identities given in Sec. 2.5.2 can be applied without variation also in presence of an external stress: the only difference is that the bare propagator k^{-4} becomes replaced by $(\sigma_0 k^2 + k^4)^{-1}$. It remains true, however, that anharmonic interactions contribute only self-energy terms which vanish as k^4. As a result, the tension is unrenormalized: even after inclusion of perturbative corrections of arbitrary order, the inverse interacting propagator still vanishes as $\sigma_0 k^2$ with the same prefactor σ_0 which appears in the bare propagator (see Ref. [85] for a more detailed derivation). Due to this property, we can assume that the unrenormalized Green function behaves as described in Sec. 2.9. Using this form of the Green function in Eq. (2.24) we get approximately

$$\begin{aligned}\frac{A_\parallel}{A} &\approx 1 + \frac{\sigma}{\lambda+2\mu/D} - \frac{d_c k_{\rm B} T}{2}\Bigg\{ \int_{|\mathbf{q}|<q_\sigma} \frac{1}{\sigma} + \int_{q_\sigma<|\mathbf{q}|<q_G} \frac{1}{\kappa q^{2-\eta_*} q_G^{\eta_*}} \\ &\quad + \int_{q_G<|\mathbf{q}|<\Lambda} \frac{1}{\kappa q^2}\Bigg\} \\ &= 1 + \frac{\sigma}{\lambda+2\mu/D} - \frac{d_c k_{\rm B} T}{2(4\pi)^{D/2}\Gamma(D/2)}\left[\frac{q_\sigma^D}{D\sigma} + \frac{q_G^{D-2+\eta_*} - q_\sigma^{D-2+\eta_*}}{(D-2+\eta_*)\kappa q_G^{\eta_*}}\right] \\ &\quad - \frac{d_c k_{\rm B} T}{2}\int_{q_\sigma<|\mathbf{q}|<q_G} \frac{1}{\kappa q^{2-\eta_*} q_G^{\eta_*}}\ ,\end{aligned} \tag{2.52}$$

where Λ is the ultraviolet cutoff (of the order of the inverse lattice spacing). The last term is independent of stress. It contributes to the average "hidden area" but not to its variation with an externally-imposed tension. Using $\sigma q_\sigma^2 \approx \kappa q_\sigma^{4-\eta_*} q_G^{\eta_*}$ and assuming that $\eta_* < 2$ (this is the case for physical membranes) shows that the leading contribution to the strain for small external stress is positive and proportional to $\sigma^{(D-2+\eta_*)/(2-\eta_*)}$. Physically, this nonlinear positive strain can be traced to the suppression of out-of-plane fluctuations. The applied stress prevents long-wavelength modes to fluctuate strongly and "irons" the hidden area, leading to an increased projected size.

For sufficiently large stress, the anomalous Hooke's law becomes replaced by a regular, linear response. In order for the anomalous response to dominate, the

32 Ref. [17] analyzed the anomalous Hooke's law for a disordered membrane. In this section we discuss the case of a disorder-free membrane. The effects of tension on a finite-size graphene drum subject to a transverse pressure has been studied in Ref. [78].

stress must be sufficiently small to ensure that (i) $q_\sigma < q_G$, and (ii) the amplitude of the anomalous contribution is larger than the Hookean term $\sigma/(\lambda + 2\mu/D)$. The condition $q_\sigma < q_G$ translates approximately into $\sigma < \kappa q_G^2$, which, in the physical case $D = 2$, $d_c = 1$ corresponds to

$$\sigma \lesssim \sigma_G = \frac{3k_{\rm B}TY}{16\pi\kappa} \ . \tag{2.53}$$

Using as parameters characteristic for a graphene membrane $\lambda \simeq 3.8$ eV Å^{-2}, $\mu \simeq 9.3$ eV Å^{-2} [111], and $\kappa \simeq 1$ eV [31, 112], leads to an estimate[33] $\sigma_G \approx 0.5$ N/m. When the condition $\sigma \lesssim \sigma_G$ is satisfied, it can be checked that the nonlinear response is larger than the Hookean term: the conditions (i) and (ii) have approximately the same boundaries of validity, as order of magnitude.

Another striking prediction is that fluctuating membranes present an universal auxetic effect. Most materials, when subject to uniaxial extension tend to respond by compressing in the orthogonal directions. However, in presence of out-of-plane fluctuations, the applied stress has the effect to "flatten" the random distribution of flexural deformations. This flattening induces in turn an *extension* in both longitudinal and transverse directions. For weak applied stress, the resulting extension dominates over the conventional Hookean behavior and leads to a auxetic behavior.

Within linear elasticity theory, the response to uniaxial stresses is quantified by a dimensionless "Poisson ratio" ν, defined as the negative ratio $-\epsilon_y/\epsilon_x$ between the strain ϵ_y induced in transverse directions and the strain ϵ_x in the direction of the applied unidirectional forces. The value of ν is simply related to the elastic Lamé coefficients λ, and μ of the material. In two dimensions, the condition of vanishing transverse stress $\sigma_{yy} = 0$ implies in particular that $\nu = \lambda/(\lambda + 2\mu)$ [3, 83]. Due to the stability conditions $\mu > 0$, $\lambda + \mu > 0$, the Poisson ratio in 2D must be within the range of values $-1 < \nu < 1$. "Normal" response corresponds to positive values of the Poisson ratio, while auxetic behavior is described by $\nu < 0$.

The auxetic effect due to fluctuations has been investigated from a theoretical point of view for several decades [1, 2, 22, 25, 26, 52, 85]. Several approaches have lead to the prediction of an *universal* negative Poisson ratio $\nu = -1/3$. A detailed analysis actually shows that the value $-1/3$ emerges only as a consequence of a special tensorial symmetry of the leading order bubble diagram [85] (see also Ref. [20] for a related comment). Vertex corrections lead instead to a value which differs from $-1/3$ [22].

In contrast with Hookean elasticity theory, the auxetic response induced by fluctuations is highly nonlinear with respect to the applied stress. As a result, a precise

33 This estimate is valid in order of magnitude, up to a factor of order unity. Ref. [17] has considered a stress-strain relation proportional to $\sigma/\sigma_* + \alpha(\sigma/\sigma_*)^\alpha$ with $\alpha = 2/(2 - \eta_*)$. By a fitting to numerical simulation data of Ref. [78], the crossover tension σ_* was estimated to be $\sigma_* \simeq 0.1$ N/m.

definition of the Poisson requires a distinction between absolute and differential Poisson ratios [85]. Furthermore, finite size effects and boundary conditions have been predicted to play an important role [52].

3

SCALING AND RENORMALIZATION: SECOND-ORDER ε-EXPANSION

In this chapter we develop a theory of scaling behavior at second order in the ε-expansion. Generalization of the problem from the physical dimensionality $D = 2$ to arbitrary non-integer dimensions, necessary to control the ε-expansion, is achieved by dimensional continuation of the fixed point P_2', as opposed to the elasticity theory fixed point P_4. Although the dimensions of the two fixed points coalesce to a single value in the physical dimension $D = 2$, the effective theories differ in general dimensions. Physically, the fixed point P_2' describes a well-known effective theory involving out-of-plane fluctuations coupled via a long-range interaction controlled by the Gaussian curvatures. After a Hubbard-Stratonovich decoupling, the "Gaussian-curvature interactions" (GCI) model can be reduced to a quasi-local field theory and can be analyzed by standard field-theoretical renormalization group methods. The RG functions at two-loop orders and the corresponding fixed point allow to calculate the scaling index η_* at order ε^2 in the $\varepsilon = (4 - D)$ expansion. A direct extrapolation of the $\mathrm{O}(\varepsilon)$ and $\mathrm{O}(\varepsilon^2)$ results to dimension $D = 2$ gives $\eta = 0.8$ and $\eta \simeq 0.795$, values which are surprisingly close to earlier predictions by the self-consistent screening approximation (SCSA), the non-perturbative renormalization group, and other analytical and numerical methods. In addition, it is shown that the value of η at order ε^2 is insensitive to Feynman diagrams involving vertex corrections. As a consequence, the self-consistent screening approximation for the GCI model is shown to be exact to $\mathrm{O}(\varepsilon^2)$.

This chapter is based on the article:
Achille Mauri and Mikhail I. Katsnelson, "Scaling behavior of crystalline membranes: an ε-expansion approach", Nucl. Phys. B **956**, 115040 (2020); preprint: arXiv:2003.04043 (2020)

3.1 INTRODUCTION

As it was discussed in Chapter 2, the quantitative description of scaling behavior in flat membranes has been addressed by several approaches, from the large-d_c expansion [9, 11, 12, 41, 96], to the ε-expansion [4, 10, 11, 96], the self-consistent screening approximation [23–25], the nonperturbative renormalization group [26–28, 35, 42, 50], and numerical simulations [25, 29–32, 34, 35, 37, 38, 78, 108].

In several field-theoretical methods [6, 12, 17, 22–25, 41, 51, 85] the starting point consists in the elimination of in-plane displacements in favor of an effective theory describing out-of-plane fluctuations with long-range phonon-mediated interactions. This step can be performed exactly by a simple Gaussian integration because, after neglection of nonlinearities which are irrelevant near the upper critical dimension $D = 4$ [10], elasticity theory is quadratic with respect to the in-plane displacements. The mediated long-range interactions are quartic in the out-of-plane displacement field $\mathbf{h}$ and have been discussed in Chap. (2). In short, the effective field theory for zero external tension reads [6, 10, 23, 25]

$$\begin{aligned} H_{\text{eff}} = \frac{1}{2}\int_{\mathbf{q}} \kappa q^4 + \frac{1}{4}\int_{\mathbf{k}_1,\mathbf{k}_2,\mathbf{k}_3} \big[R_{\alpha\beta,\gamma\delta}(\mathbf{q}) \\ \times k_{1\alpha}k_{2\beta}k_{3\gamma}k_{4\delta}\big(\mathbf{h}(\mathbf{k}_1)\cdot\mathbf{h}(\mathbf{k}_2)\big)\big(\mathbf{h}(\mathbf{k}_3)\cdot\mathbf{h}(\mathbf{k}_4)\big)\big] \ , \end{aligned} \tag{3.1}$$

where $\mathbf{q} = \mathbf{k}_1 + \mathbf{k}_2 = -\mathbf{k}_3 - \mathbf{k}_4$ is the momentum transfer $R_{\alpha\beta,\gamma\delta}(\mathbf{q}) = bN_{\alpha\beta,\gamma\delta} + \mu M_{\alpha\beta,\gamma\delta}$, $b = \mu(D\lambda + 2\mu)/(\lambda + 2\mu)$, and

$$\begin{aligned} N_{\alpha\beta,\gamma\delta}(\mathbf{q}) &= \frac{1}{D-1}P^T_{\alpha\beta}(\mathbf{q})P^T_{\gamma\delta}(\mathbf{q}) \ , \\ M_{\alpha\beta,\gamma\delta}(\mathbf{q}) &= \frac{1}{2}(P^T_{\alpha\gamma}(\mathbf{q})P^T_{\beta\delta}(\mathbf{q}) + P^T_{\alpha\delta}(\mathbf{q})P^T_{\beta\gamma}(\mathbf{q})) - N_{\alpha\beta,\gamma\delta}(\mathbf{q}) \ . \end{aligned} \tag{3.2}$$

In general dimension $D \neq 2$, a membrane with generic elastic couplings is described by a theory in which both b and μ are nonzero. Under renormalization, the coupling constants b and μ flow to the infrared stable fixed point P'_4 described in Sec. 2.4, which is equivalent, in a different representation, to the fixed point P_4 in the space of renormalized elasticity theories [23, 25]. The special lines, $b = 0$ and $\mu = 0$, which lie at the boundary of the stability region of the Hamiltonian (3.1), belong instead to different universality classes[1], and flow to two distinct fixed points P'_2 and P'_3 (see Fig. 2.5). The point P'_3 describes membranes with zero bulk modulus and nonzero shear modulus. A realization could be provided by twisted kagome lattices [102].

1 Diagrammatically this can be proven by noticing that, by the orthogonality relations $N_{\alpha\beta,\mu\nu}N_{\mu\nu,\gamma\delta} = N_{\alpha\beta,\gamma\delta}$, $M_{\alpha\beta,\mu\nu}N_{\mu\nu,\gamma\delta} = 0$, $M_{\alpha\beta,\mu\nu}M_{\mu\nu,\gamma\delta} = M_{\alpha\beta,\gamma\delta}$, the lines $b = 0$ and $\mu = 0$ are preserved under renormalization [25]. A theory which has initially $b = 0$ or $\mu = 0$ cannot flow to the fixed point P'_4 where both b and μ are nonzero.

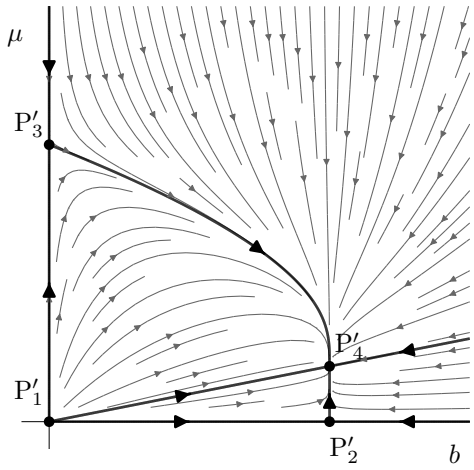

Figure 3.1: RG flow of the coupling constants (b, μ) for physical dimensionality $D = 2$, $d_c = 1$. The flow in the figure is calculated using the momentum-shell RG equations (2.22) for $\sigma = 0$.

The fixed point P_2', instead, has coordinates $\mu = 0$, $b \neq 0$ and thus has no counterpart in the space of elasticity theories (the definition $b = \mu(D\lambda + 2\mu)/(\lambda + 2\mu)$ makes it impossible, among elasticity theories, to have $\mu = 0$ and $b \neq 0$ simultaneously). Nevertheless, it is still provides a well-defined interacting scale-invariant model.

In $D = 2$, the theory simplifies considerably [1, 24, 51, 113], because the tensor $M_{\alpha\beta,\gamma\delta}(\mathbf{q})$ is exactly equal to zero. As a result, the coupling constant μ becomes redundant. Furthermore, the effective quartic interaction reduces to [1, 3, 6, 23, 24, 41, 51]

$$b \int_{\mathbf{q}} \frac{K(\mathbf{q})K(-\mathbf{q})}{q^4} \ , \tag{3.3}$$

where $K(\mathbf{q})$ is the Fourier transform of

$$K(\mathbf{x}) = -\frac{1}{2}(\delta_{\alpha\beta}\partial^2 - \partial_\alpha\partial_\beta)(\partial_\alpha \mathbf{h} \cdot \partial_\beta \mathbf{h}) = \frac{1}{2}[(\partial^2 \mathbf{h} \cdot \partial^2 \mathbf{h}) - (\partial_\alpha\partial_\beta \mathbf{h} \cdot \partial_\alpha\partial_\beta \mathbf{h})] \ . \tag{3.4}$$

The composite field $K(\mathbf{x})$ is, at leading order for small undulations, the Gaussian curvature of the membrane [6]. The coupling constant b, in two dimensions becomes equal to $Y/2$ where $Y = 4\mu(\lambda + \mu)/(\lambda + 2\mu)$ is the Young modulus.

This chapter describes a calculation of the scaling index ε based on the dimensional continuation of the "Gaussian curvature interaction" (GCI) model, defined

as the sum of bending energy and the quartic term (3.3). The same model has been investigated in Refs. [18, 51, 113] using a momentum-shell technique. The analysis presented here uses instead a field-theoretical perturbative RG, which is technically more convenient for the calculation of η_* within a systematic ε-expansion[2].

Implementing the dimensional continuation via the GCI model instead of the elasticity theory is equivalent to considering the fixed point P_2' instead of P_4'. The fixed points P_4' and P_2' approach different limits as $D \to 2$ (see Fig. 3.1), but the anomalous dimensions collapse to a single value, since μ becomes redundant in two dimensions.

3.2 HUBBARD-STRATONOVICH TRANSFORMATION

The starting point of our analysis is the "GCI model"

$$H_{\text{eff}} = \frac{1}{2}\int_{\mathbf{q}} \kappa |\mathbf{h}(\mathbf{q})|^2 + \frac{Y}{2}\int_{\mathbf{q}}{}' \frac{|K(\mathbf{q})|^2}{q^4} \ , \tag{3.5}$$

in $D = 4 - \varepsilon$ dimensions[3] To analyze the GCI model, it is convenient to decouple interactions by a Hubbard-Stratonovich transformation:

$$\mathrm{e}^{-H_{\text{eff}}[\mathbf{h}(\mathbf{x})]/(k_{\mathrm{B}}T)} = \int [\mathrm{d}\chi(\mathbf{x})]\, \mathrm{e}^{-H[\mathbf{h}(\mathbf{x}),\chi(\mathbf{x})]/(k_{\mathrm{B}}T)} \ , \tag{3.6}$$

where $\int[\mathrm{d}\chi(\mathbf{x})]$ denotes functional integration over an auxiliary real field $\chi(\mathbf{x})$ coupled to curvature $K(\mathbf{x})$. After the field rescaling $\mathbf{h} \to \bar{\mathbf{h}} = (\sqrt{\kappa/(k_{\mathrm{B}}T)})\mathbf{h}$, the reduced Hamiltonian $\mathcal{H} = H/(k_{\mathrm{B}}T)$ reads:

$$\mathcal{H} = \int \mathrm{d}^D x \left[\frac{1}{2}(\partial^2 \bar{\mathbf{h}})^2 + \frac{1}{2Y_0}(\partial^2\chi)^2 + i\chi\bar{K}\right] , \tag{3.7}$$

2 Momentum-shell techniques and nonperturbative RG techniques organize the theory in a different way than the perturbative field-theoretical method. In the momentum-shell method, the fixed point lives inevitably in an infinitely-dimensional space of theories and has infinitely many nonzero coupling constants [14]. To derive the exact exponent systematically within the ε expansion, it is necessary to extend the Hamiltonian beyond the truncated form which appears at tree level. The field theoretical method, instead, extracts the exponent by matching the explicit solution of a given model with the scaling laws. The universality hypothesis implies that any model, including one with just a few coupling constants, will "know" the exact value of the exponent η_*.

3 In the integration over in-plane displacement vectors $\mathbf{u}$, zero modes of the strain tensor require a separate analysis (see Chap. 2 and Refs. [1, 18]). Functional integration involves, besides finite-wavelength phonon deformations, a sum over macroscopic in-plane deformations of the crystal. This leads to a prescription on the momentum integral defining the effective Hamiltonian: the $\mathbf{q} = 0$ contribution must be omitted from integration in Eq. (3.5) (see also Refs. [12, 25]). The primed integral $\int_{\mathbf{q}}'$ denotes integration with the zero mode $\mathbf{q} = 0$ omitted. The prescription $\mathbf{q} \neq 0$ is non-local. However, it has the only effect to suppress tadpole diagrams (see below). Thus, the standard methods of local field theories remain valid.

where $Y_0 = TY/\kappa^2$, and $\bar{K}(\mathbf{x}) = [(\partial^2\bar{\mathbf{h}} \cdot \partial^2\bar{\mathbf{h}}) - (\partial_\alpha\partial_\beta\bar{\mathbf{h}} \cdot \partial_\alpha\partial_\beta\bar{\mathbf{h}})]/2$. The field $\chi(\mathbf{x})$ plays the role of the Airy stress function [1]. The Hubbard-Stratonovich transformation (3.6) consists in the replacement of the "instantaneous" Airy stress with an independently-fluctuating quantity.

The perturbative expansion in powers of Y_0 is generated by the propagators and the vertex illustrated in Fig. 3.2. The vertex presents a simple geometric structure. From the definition of the curvature $\bar{K}(\mathbf{x})$ and momentum conservation, $\mathbf{k}_1 + \mathbf{k}_2 + \mathbf{k}_3 = 0$, it can be verified that:

$$\bar{\gamma}(\mathbf{k}_1, \mathbf{k}_2, \mathbf{k}_3) = k_1^2 k_2^2 - (\mathbf{k}_1 \cdot \mathbf{k}_2)^2 = k_2^2 k_3^2 - (\mathbf{k}_2 \cdot \mathbf{k}_3)^2 = k_3^2 k_1^2 - (\mathbf{k}_3 \cdot \mathbf{k}_1)^2 \ . \quad (3.8)$$

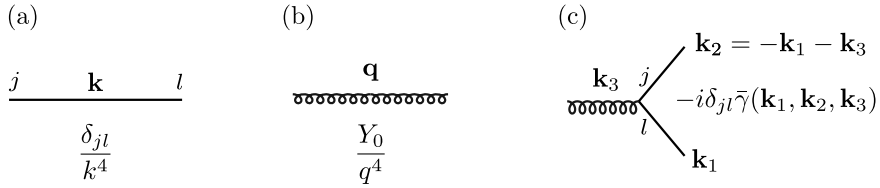

Figure 3.2: Bare propagators and vertex of the model. (a) $\mathbf{h}$-field propagator, (b) χ-field propagator, (c) interaction vertex.

3.3 RENORMALIZATION GROUP EQUATIONS

Representation of the GCI model by Hubbard-Stratonovich transformation gives access to the methods of perturbative renormalization of local field theories [15, 16, 81]. This section presents a derivation of renormalization group equations for the theory in the representation expressed by Eq. (3.7).

Power counting shows that the coupling constant Y_0 has dimension $\varepsilon = (4 - D)$. The GCI theory has therefore the same upper critical dimension $D_{\mathrm{uc}} = 4$ as the conventional model of D-dimensional elastic membranes [10]. For $D < 4$ the perturbative expansion breaks down at sufficiently large order because of infrared divergences, similarly to the theory of critical behavior [15, 16]. In analogy with earlier approaches to crystalline membranes [10, 11, 96] and critical phenomena, the massless perturbation theory is however well-defined within the ε-expansion, since perturbative corrections modify the propagators and vertices only by logarithmic functions.

A power counting analysis of one-particle irreducible (1PI) correlation functions shows that the $\bar{\mathbf{h}}$ and χ field self-energies and the χ one-point function are the only superficial ultraviolet divergences [15] in four dimensions. The structure of the vertex, Eq. (3.8), implies that in any diagram two powers of momentum can be

attached to each external leg and factorized from the loop momentum integration[4]. For any 1PI diagram Δ with L loops, V vertices, I internal and E external lines (of either solid or wiggly type), the degree of superficial divergence [15] is therefore

$$\delta_\Delta = DL + 4V - 4I - 2E \ , \tag{3.9}$$

or equivalently, using the topological relations $L = 2V - I - E + 1$ and $2I + E = 3V$,

$$\delta_\Delta = D - \frac{D}{2}E - \frac{1}{2}(4-D)V \ . \tag{3.10}$$

For $D = 4$ the degree of divergence is independent on the number of vertices and the model is renormalizable by power counting. The only superficially divergent 1PI functions, characterized by $\delta_\Delta > 0$, are two-point functions in Fig. 3.3(a) and 3.3(b), which diverge logarithmically, and 3.3(c), which diverges quadratically. The three-point vertex function is, instead, convergent and it does not require the introduction of an independent renormalization constant[5].

The one-point function (Fig. 3.3c) vanishes at nonzero momentum. On the other hand, the field χ was introduced to mediate the non-local interaction of Eq. (3.3), in which the $\mathbf{q} = 0$ mode is excluded. We thus assume that functional integration runs only over finite-momentum Fourier components of the χ field. Diagrams for the one-point function can then be dropped, consistently with the elimination of tadpole diagrams in earlier approaches to crystalline membranes [1, 12, 25].

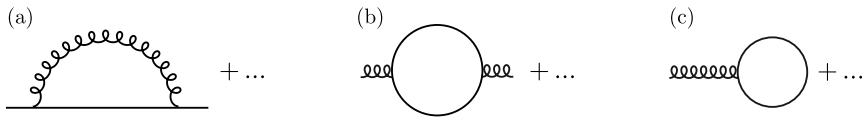

Figure 3.3: Superficially divergent 1PI correlation functions.

Ultraviolet divergences are therefore removed by the introduction of two renormalization constants, corresponding to the superficial divergences in the two-point

4 This property was suggested in Ref. [23], and reflects the symmetry of the theory under the shifts $\bar{\mathbf{h}}(\mathbf{x}) \to \bar{\mathbf{h}}(\mathbf{x}) + \mathbf{A}_\alpha x_\alpha + \mathbf{B}$ and $\chi(\mathbf{x}) \to \chi(\mathbf{x}) + A'_\alpha x_\alpha + B'$, which leave the Hamiltonian (3.7) invariant up to boundary terms. Shifts of $\bar{\mathbf{h}}(\mathbf{x})$ by a first order polynomial in the coordinates correspond to translations and rotations of the membrane in the d-dimensional embedding space. Invariance of the theory is therefore related to the Goldstone-mode character of the out-of-plane fluctuation fields and to Ward identities of embedding space rotational invariance. The analysis is consistent with Refs. [12, 23, 25].

5 The convergence of the vertex function and the subsequent absence of vertex renormalization in a Hubbard-Stratonovich representation was recognized in Refs. [23, 25]. It was related to Ward identities and it was proven to imply the exactness of the self-consistent screening approximation to $\mathrm{O}(\varepsilon)$ in the ε-expansion for D-dimensional elastic membranes [23, 25]. Refs. [23, 25], however, focused mostly on the fixed point P'_4 and did not analyze in detail the field theory after Huubard-Stratonovich transformation.

functions [23, 25]. Within dimensional regularization and the minimal subtraction scheme [15, 81], the renormalized Hamiltonian equipped with necessary counterterms reads:

$$\tilde{\mathcal{H}}[\bar{\mathbf{h}},\chi] = \int \mathrm{d}^D x \left[\frac{Z}{2}(\partial^2 \bar{\mathbf{h}})^2 + \frac{s_D}{2M^\varepsilon Z_y y}(\partial^2\chi)^2 + i\chi\bar{K} \right] , \tag{3.11}$$

where M is an arbitrary wavevector scale and $\tilde{y}$ is a dimensionless renormalized coupling. For later convenience in explicit calculations, we have redefined the coupling constant by introducing $y_0 = s_D Y_0$, with

$$s_D = \frac{(D^2-1)\Gamma^2(D/2)\Gamma(3-D/2)}{4(4\pi)^{D/2}\Gamma(D)} , \tag{3.12}$$

because a geometric factor similar to s_D is generated in the one-loop Feynman diagrams [23, 25]. In the renormalization of the theory, this parametrization converts minimal subtraction into an analogue of the modified minimal subtraction scheme [15]. The amplitudes Z and Z_y are double series in $\tilde{y}$ and $1/\varepsilon$ and, being dimensionless, do not depend explicitly on M. Comparison of Eq. (3.7) and Eq. (3.11) gives the following relations between bare and renormalized quantities:

$$\begin{aligned} \bar{\mathbf{h}}(\mathbf{x}) &= \sqrt{Z}\,\tilde{\mathbf{h}}(\mathbf{x}) , \qquad \chi(\mathbf{x}) = \frac{1}{Z}\tilde{\chi}(\mathbf{x}) , \\ y_0 &= \frac{M^\varepsilon Z_y}{Z^2}\tilde{y} , \qquad \mathcal{H}[\bar{\mathbf{h}}(\mathbf{x}),\chi(\mathbf{x})] = \tilde{\mathcal{H}}[\tilde{\mathbf{h}}(\mathbf{x}),\tilde{\chi}(\mathbf{x})] . \end{aligned} \tag{3.13}$$

The renormalization of 1PI correlation functions with n external $\mathbf{h}$ lines and ℓ external χ lines reads:

$$\Gamma^{(n,\ell)}_{i_1..i_n}(\mathbf{k}_1,..,\mathbf{k}_n;\mathbf{q}_1,..,\mathbf{q}_\ell;y_0) = Z^{\ell-\frac{n}{2}}\tilde{\Gamma}^{(n,\ell)}_{i_1..i_n}(\mathbf{k}_1,..,\mathbf{k}_n;\mathbf{q}_1,..,\mathbf{q}_\ell;M,\tilde{y}) . \tag{3.14}$$

Renormalization group equations follow, in a standard way [15, 81], from the independence of the bare functions $\Gamma^{(n,\ell)}$ on the wavevector scale M. Introducing

$$\beta(\tilde{y}) = \left.\frac{\partial\tilde{y}}{\partial \ln M}\right|_{y_0} , \qquad \eta(\tilde{y}) = \left.\frac{\partial \ln Z}{\partial \ln M}\right|_{y_0} , \tag{3.15}$$

the RG equations for one-particle irreducible correlation functions read:

$$\left[M\frac{\partial}{\partial M} + \beta(\tilde{y})\frac{\partial}{\partial\tilde{y}} - \left(\frac{n}{2}-\ell\right)\eta(\tilde{y})\right]\tilde{\Gamma}^{(n,\ell)}_{i_1..i_n}(\mathbf{k}_1,..,\mathbf{k}_n;\mathbf{q}_1,..,\mathbf{q}_\ell;M,\tilde{y}) = 0 . \tag{3.16}$$

As a consequence of dimensional regularization and the minimal subtraction prescription [15], $\eta(\tilde{y})$ does not depend explicitly on ε and $\beta(\tilde{y}) = -\varepsilon\tilde{y} + b(\tilde{y})$ where $b(\tilde{y})$ is ε-independent. Being dimensionless, $\beta(\tilde{y})$ and $\eta(\tilde{y})$ are independent of the renormalization scale M.

In the long wavelength limit, the running coupling approaches an infrared-attractive fixed point $\tilde{y} = \tilde{y}_*$, determined by the condition $\beta(\tilde{y}_*) = 0$ [15, 81]. At the fixed point, a combination of RG equations and dimensional analysis shows that correlation functions[6] scale according to:

$$\begin{aligned}\tilde{\Gamma}^{(n,\ell)}_{i_1..i_n}(\rho\mathbf{k}_1,..,\rho\mathbf{k}_n;\rho\mathbf{q}_1,..,\rho\mathbf{q}_\ell;M,\tilde{y}_*) \\ = \rho^{D+\frac{n}{2}(4-D-\eta)+\eta\ell}\tilde{\Gamma}^{(n,\ell)}_{i_1..i_n}(\mathbf{k}_1,..,\mathbf{k}_n;\mathbf{q}_1,..,\mathbf{q}_\ell;M,\tilde{y}_*)\ ,\end{aligned} \tag{3.17}$$

where the scaling exponent is $\eta_* = \eta(\tilde{y}_*)$. In particular two-point functions satisfy the scaling relations:

$$\tilde{\Gamma}^{(2,0)}_{ij}(\mathbf{k}) \propto \delta_{ij}|\mathbf{k}|^{4-\eta_*}\ , \qquad \tilde{\Gamma}^{(0,2)}(\mathbf{q}) \propto |\mathbf{q}|^{D+2\eta_*}\ . \tag{3.18}$$

We can interpret Eq. (3.18) by recognizing a power law divergence of the effective bending rigidity $\kappa_{\rm R}(q)$ and a suppression of the effective Young modulus $Y_{\rm R}(q)$. Defining $\kappa_{\rm R}(q)$ and $Y_{\rm R}(q)$ by the identifications

$$\Gamma^{(2,0)}_{ij}(\mathbf{q}) = \delta_{ij}\frac{\kappa_{\rm R}(q)q^4}{\kappa}\ , \qquad \Gamma^{(0,2)}(\mathbf{q}) = \frac{\kappa^2 q^4}{TY_{\rm R}(q)}\ , \tag{3.19}$$

implies, since bare and renormalized correlation functions are proportional, that $\kappa_{\rm R}(q) \propto q^{-\eta_*}$ and $Y_{\rm R}(q) \propto q^{\eta_u}$ with $\eta_u = 4 - D - 2\eta_*$. The relation between η_u and η_* is consistent with the theory of D-dimensional membranes, for which a well-known analogue exponent identity holds in arbitrary dimension [10, 12, 23–25, 96].

3.4 SCALING EXPONENT

This section reports explicit results for the scaling exponent η_* to order ε^2 in the ε-expansion. As it will be verified, the coupling strength $\tilde{y}_*$ at the fixed point is of order ε near dimension four. Determination of η_* with accuracy ε^2, therefore, requires the knowledge of $\beta(\tilde{y})$ and $\eta(\tilde{y})$ to order $\tilde{y}^3$ and $\tilde{y}^2$ respectively. RG functions at this order can be calculated by computing the renormalization constants Z and Z_y at two-loop level.

The bare one-particle irreducible two-point functions are given, in second order perturbation theory, by the sum of Feynman diagrams in Fig. 3.4.

Perturbative calculations are extensively simplified by the similarity between $\bar{\mathbf{h}}$- and χ-field propagators, both scaling with momentum $\mathbf{k}$ as k^{-4}, and the permutation-invariance of the vertex function expressed by Eq. (3.8). These properties imply that, up to a prefactor, the loop integral corresponding to a Feynman

6 In Eq. (3.17), 1PI correlation functions in momentum space are defined after factorization and cancellation of the momentum-conservation factor $(2\pi)^D\delta\big(\sum_i \mathbf{k}_i + \sum_j \mathbf{q}_j\big)$.

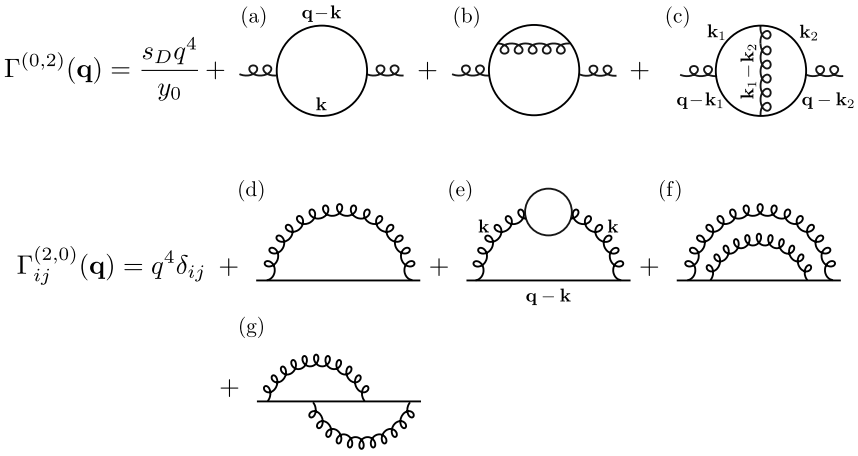

Figure 3.4: Feynman diagrams for the one-particle irreducible two-point functions at order two-loops. The values of diagrams (a), (b) and (c) are denoted as $D_a(\mathbf{q})$, $D_{\rm b}(\mathbf{q})$ and $D_{\rm c}(\mathbf{q})$ respectively. Diagrams (d), (e), (f) and (g) are proportional to the identity in d_c-dimensional space and, therefore, are denoted as $\delta_{ij}D_l(\mathbf{q})$, where l = d, .., g.

diagram does not depend on the type (solid or wavy) of its lines, but only on its overall connectivity. Denoting as $D_l(\mathbf{q})$ (l = a, .., c) and $\delta_{ij}D_l(\mathbf{q})$ (l=d, .. , g) the values of the l-th Feynman diagram in Fig. 3.4, the following relations hold[7]:

$$\begin{aligned} &\frac{y_0}{s_D}D_{\rm a}(\mathbf{q}) = \frac{d_c}{2}D_{\rm d}(\mathbf{q}) \ , \qquad D_{\rm e}(\mathbf{q}) = \frac{y_0}{2s_D}D_{\rm b}(\mathbf{q}) = \frac{d_c}{2}D_{\rm f}(\mathbf{q}) \ , \\ &\frac{y_0}{s_D}D_{\rm c}(\mathbf{q}) = \frac{d_c}{2}D_{\rm g}(\mathbf{q}) \ . \end{aligned} \tag{3.20}$$

Calculation of the seven diagrams thus reduces to the computation of three independent integrals. Explicit expressions for diagrams (a), (e) and (c) are:

$$\begin{aligned} D_{\rm a}(\mathbf{q}) &= \frac{d_c}{2}\int_{\mathbf{k}} \frac{(q^2k^2 - (\mathbf{q}\cdot\mathbf{k})^2)^2}{|\mathbf{k}|^4|\mathbf{q}-\mathbf{k}|^4} \ , \\ D_{\rm e}(\mathbf{q}) &= -\int_{\mathbf{k}} \frac{(q^2k^2 - (\mathbf{q}\cdot\mathbf{k})^2)^2}{|\mathbf{q}-\mathbf{k}|^4}\left[\frac{y_0}{s_Dk^4}D_{\rm a}(\mathbf{k})\frac{y_0}{s_Dk^4}\right] \ , \\ D_{\rm c}(\mathbf{q}) &= -\frac{d_cy_0}{2s_D}\int_{\mathbf{k}_1}\int_{\mathbf{k}_2} \frac{\gamma(\mathbf{q},\mathbf{k}_1)\gamma(\mathbf{k}_1,\mathbf{k}_2)\gamma(\mathbf{q},\mathbf{k}_2)\gamma(\mathbf{q}-\mathbf{k}_1,\mathbf{q}-\mathbf{k}_2)}{|\mathbf{k}_1|^4|\mathbf{k}_2|^4|\mathbf{q}-\mathbf{k}_2|^4|\mathbf{q}-\mathbf{k}_1|^4|\mathbf{k}_1-\mathbf{k}_2|^4} \ , \end{aligned} \tag{3.21}$$

7 In Eqs. (3.20) and (3.21), combinatorial factors 1/2 appear in presence of closed solid-line loops with flip symmetry. An analogue Feynman rule applies to the the Ginzburg-Landau model in a Hubbard-Stratonovich representation [14].

where $\gamma(\mathbf{k}_1,\mathbf{k}_2) = k_1^2 k_2^2 - (\mathbf{k}_1\cdot\mathbf{k}_2)^2$. The diagrams D_a and D_e can be deduced from the general integral [25]

$$\begin{aligned}\Pi(\eta,\eta',D) &= \int \frac{\mathrm{d}^D k}{(2\pi)^D}\frac{(k^2-(\hat{\mathbf{q}}\cdot\mathbf{k})^2)^2}{|\mathbf{k}|^{4-\eta}|\mathbf{k}+\hat{\mathbf{q}}|^{4-\eta'}} \\ &= (D^2-1)\frac{\Gamma(2-\frac{\eta+\eta'}{2}-\frac{D}{2})\Gamma(\frac{D}{2}+\frac{\eta}{2})\Gamma(\frac{D}{2}+\frac{\eta'}{2})}{4(4\pi)^{D/2}\Gamma(2-\frac{\eta}{2})\Gamma(2-\frac{\eta'}{2})\Gamma(D+\frac{\eta+\eta'}{2})}\ ,\end{aligned} \tag{3.22}$$

where $\hat{\mathbf{q}} = \mathbf{q}/|\mathbf{q}|$ is an unit vector. Using Eq. (3.22) repeatedly gives the expressions for the diagrams

$$\begin{aligned}D_\mathrm{a}(\mathbf{q}) &= \frac{d_c}{2}\Pi(0,0,D)q^{4-\varepsilon} = \frac{d_c s_D}{\varepsilon}q^{4-\varepsilon}\ , \\ D_\mathrm{e}(\mathbf{q}) &= -\frac{d_c}{2}\Pi(0,0,D)\Pi(-\varepsilon,0,D)\frac{y_0^2 q^{4-2\varepsilon}}{s_D^2}\ .\end{aligned} \tag{3.23}$$

Near $D=4$, $D_\mathrm{e}(\mathbf{q})$ has the expansion:

$$D_\mathrm{e}(\mathbf{q}) = -d_c\left(\frac{1}{\varepsilon^2}-\frac{1}{12\varepsilon}+\mathrm{O}(1)\right)y_0^2 q^{4-2\varepsilon}\ , \tag{3.24}$$

where O(1) denotes the finite part of $D_\mathrm{e}(\mathbf{q})$ for $\varepsilon\to 0$. The remaining independent diagram $D_\mathrm{c}(\mathbf{q})$ gives, by dimensional analysis:

$$D_\mathrm{c}(\mathbf{q}) = -\frac{d_c s_D a_D}{2}y_0 q^{4-2\varepsilon}\ , \tag{3.25}$$

where a_D is a function of internal dimension D. As it is shown in 3.A, a_D presents a first-order pole at $D=4$

$$a_D = \frac{A}{\varepsilon}+\mathrm{O}\left(1\right)\ , \tag{3.26}$$

with residue $A = 121/90$, corresponding to the UV divergence of $D_\mathrm{c}(\mathbf{q})$ in four dimensions. The bare two-point functions can therefore be written as:

$$\begin{aligned}\Gamma^{(0,2)}(\mathbf{q}) &= \frac{s_D q^4}{y_0} + D_\mathrm{a}(\mathbf{q}) + D_\mathrm{b}(\mathbf{q}) + D_\mathrm{c}(\mathbf{q}) \\ &= \frac{s_D q^4}{y_0}\left[1+\frac{d_c}{\varepsilon}\frac{y_0}{q^\varepsilon} - d_c\left(\frac{2}{\varepsilon^2}-\frac{1}{6\varepsilon}+\frac{A}{2\varepsilon}+\mathrm{O}(1)\right)\frac{y_0^2}{q^{2\varepsilon}}+\mathrm{O}\left(y_0^3\right)\right]\ ,\end{aligned} \tag{3.27}$$

$$\begin{aligned}\Gamma^{(2,0)}(\mathbf{q}) &= \delta_{ij}[q^4 + D_\mathrm{d}(\mathbf{q}) + D_\mathrm{e}(\mathbf{q}) + D_\mathrm{f}(\mathbf{q}) + D_\mathrm{g}(\mathbf{q})] \\ &= \delta_{ij}q^4\Bigg[1+\frac{2}{\varepsilon}\frac{y_0}{q^\varepsilon} - \left(1+\frac{d_c}{2}\right)\left(\frac{2}{\varepsilon^2}-\frac{1}{6\varepsilon}+\mathrm{O}(1)\right)\frac{y_0^2}{q^{2\varepsilon}} \\ &\qquad - \left(\frac{A}{\varepsilon}+\mathrm{O}(1)\right)\frac{y_0^2}{q^{2\varepsilon}}+\mathrm{O}\left(y_0^3\right)\Bigg]\ .\end{aligned} \tag{3.28}$$

With the choice of renormalization constants

$$\begin{aligned} Z_y &= 1 + \frac{d_c\tilde{y}}{\varepsilon} + d_c(d_c+2)\frac{\tilde{y}^2}{\varepsilon^2} + \frac{d_c}{2}\left(\frac{1}{3} - A\right)\frac{\tilde{y}^2}{\varepsilon} + \mathrm{O}\left(\tilde{y}^3\right) \ , \\ Z &= 1 - \frac{2\tilde{y}}{\varepsilon} - (d_c+2)\frac{\tilde{y}^2}{\varepsilon^2} - \left(\frac{d_c+2}{12} - A\right)\frac{\tilde{y}^2}{\varepsilon} + \mathrm{O}\left(\tilde{y}^3\right) \ , \end{aligned} \tag{3.29}$$

the renormalized correlation functions $\tilde{\Gamma}^{(0,2)} = Z^{-2}\Gamma^{(0,2)}$ and $\tilde{\Gamma}^{(2,0)} = Z\Gamma^{(2,0)}$ are finite to order $\tilde{y}^2$ after the coupling renormalization $y_0 = M^{\varepsilon}Z_y\tilde{y}/Z^2$. The corresponding RG functions can be determined from the relations [15]

$$\beta(\tilde{y}) = \frac{-\varepsilon\tilde{y}}{1 + \frac{\partial \ln(Z_y/Z^2)}{\partial \ln \tilde{y}}} \ , \qquad \eta(\tilde{y}) = \beta(\tilde{y})\frac{\partial \ln Z}{\partial \tilde{y}} \ , \tag{3.30}$$

which lead to:

$$\beta(\tilde{y}) = -\varepsilon\tilde{y} + (d_c+4)\tilde{y}^2 + \left(\frac{2}{3}(d_c+1) - (d_c+4)A\right)\tilde{y}^3 + \mathrm{O}\left(\tilde{y}^4\right) \ , \tag{3.31}$$

$$\eta(\tilde{y}) = 2\tilde{y} + \left(\frac{d_c+2}{6} - 2A\right)\tilde{y}^2 + \mathrm{O}\left(\tilde{y}^3\right) \ . \tag{3.32}$$

The β function describes, for ε small, a renormalization group flow from the Gaussian fixed point $\tilde{y} = 0$ to a nontrivial infrared stable fixed point $\tilde{y} = \tilde{y}_*$ corresponding to the coupling strength

$$\tilde{y}_* = \frac{\varepsilon}{d_c+4} - \frac{\left(\frac{2}{3}(d_c+1) - (d_c+4)A\right)}{(d_c+4)^3}\varepsilon^2 + \mathrm{O}(\varepsilon^3) \ . \tag{3.33}$$

The anomalous dimension controlling the long-wavelength scaling behavior is therefore

$$\eta_* = \eta(\tilde{y}_*) = \frac{2\varepsilon}{d_c+4} - \frac{d_c(2-d_c)}{6(d_c+4)^3}\varepsilon^2 + \mathrm{O}(\varepsilon^3) \ . \tag{3.34}$$

3.4.1 *Exactness of the self-consistent screening approximation to $O(\varepsilon^2)$.*

As Eq. (3.34) shows, the scaling exponent η is insensitive to the value of the residue A describing the contribution of diagrams (c) and (g) in Fig. 3.4. Only diagrams (a), (b), (d), (e) and (f), representing propagator corrections contribute to the value of η_* to order ε^2. This suggests that the self-consistent screening approximation [23, 25] is exact to $\mathrm{O}(\varepsilon^2)$ for the GCI model.

Within the SCSA, scaling exponents are determined by identifying power-law solutions to truncated Dyson equations for the χ- and $\bar{\mathbf{h}}$- field propagators $D(\mathbf{q})$ and $\bar{G}_{ij}(\mathbf{q})$. In analogy with the theory of D-dimensional membranes [23, 25]

(see also Chap. 2), we define the self-consistent screening approximation by the equations

$$\begin{aligned}\left[\bar{G}^{-1}(\mathbf{q})\right]_{ij} &= \delta_{ij}q^4 + \int \frac{\mathrm{d}^D k}{(2\pi)^D}\left(q^2k^2 - (\mathbf{q}\cdot\mathbf{k})^2\right)^2 \bar{G}_{ij}(\mathbf{k})D(\mathbf{q}-\mathbf{k}) \ , \\ D^{-1}(\mathbf{q}) &= \frac{s_D q^4}{y_0} + \frac{1}{2}\int \frac{\mathrm{d}^D k}{(2\pi)^D}\left(q^2k^2 - (\mathbf{q}\cdot\mathbf{k})^2\right)^2 \bar{G}_{ij}(\mathbf{k})\bar{G}_{ji}(\mathbf{q}-\mathbf{k}) \ ,\end{aligned} \tag{3.35}$$

which correspond to the diagrams in Fig. 3.5.

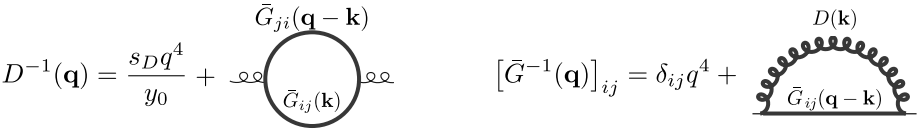

Figure 3.5: Diagrams corresponding to SCSA equations. $D(\mathbf{q})$ and $\bar{G}_{ij}(\mathbf{q})$ denote the χ- and $\bar{\mathbf{h}}$-field propagators respectively.

The inverse two-point functions $[\bar{G}^{-1}_{ij}(\mathbf{q})]$ and $D^{-1}(\mathbf{q})$ approximate, within the SCSA, the interacting 1PI two-point functions $\Gamma^{(2,0)}_{ij}(\mathbf{q})$ and $\Gamma^{(0,2)}(\mathbf{q})$ respectively. In the long-wavelength, strong-coupling limit zero-order propagators are negligible compared to self-energy terms [24]. The SCSA equations admit, in this regime, scaling solutions of the form [23, 25]:

$$\bar{G}_{ij}(\mathbf{q}) = z\delta_{ij}|\mathbf{q}|^{-4+\eta'} \ , \qquad D(\mathbf{q}) = c(\eta, D)z^{-2}|\mathbf{q}|^{-4+\eta'_u} \ , \tag{3.36}$$

where z is a non-universal amplitude. Consistency of the solution with Eq. (3.35) imposes the exponent relation $\eta'_u = 4 - D - 2\eta'$ and an equation determining η':

$$\frac{d_c}{2} = \frac{\Pi(\eta', \eta'_u, D)}{\Pi(\eta', \eta', D)} = \frac{\Gamma(\frac{\eta'}{2})\Gamma(2-\eta')\Gamma(D+\eta')\Gamma(2-\frac{\eta'}{2})}{\Gamma(\frac{D}{2}+\frac{\eta'}{2})\Gamma(2-\eta'-\frac{D}{2})\Gamma(\frac{D}{2}+\eta')\Gamma(\frac{D}{2}+2-\frac{\eta'}{2})} \ . \tag{3.37}$$

The power-law behavior and the relation between η'_u and η' agrees with the scaling form of the effective bending rigidity and Young modulus, Eq. (3.19). Solving Eq. (3.37) order by order in ε, it can be explicitly verified that the SCSA exponent η' agrees with the exact ε-expansion, Eq. (3.34), not only at leading order but also at order ε^2: $\eta' - \eta_* = \mathrm{O}(\varepsilon^3)$. The exactness of the SCSA at leading order in ε is a consequence of the structure of renormalization in the theory. Due to the absence of vertex renormalization, the one-loop RG functions are determined by diagrams without vertex corrections: the same diagrams included in the self-consistent screening approximation. An analogue situation occurs in the theory of D-dimensional crystalline membranes in the conventional dimensional

continuation scheme for which the SCSA approximation yields the exact exponent $\eta_* = \varepsilon/(2 + d_c/12)$ [10] at leading order in the ε-expansion [23, 25].

Exactness of the SCSA at order ε^2 in the ε-expansion, follows instead from Eq. (3.20), which relates the amplitude of diagrams for the $\bar{\mathbf{h}}$- and χ-field correlation functions. These relations can be traced to the permutation invariance of the vertex function, Eq. (3.8), and the identity (up to a factor y_0/s_D and an identity matrix δ_{ij}) of the $\bar{\mathbf{h}}$- and the χ-field non-interacting propagators.

By construction, the SCSA is also exact at leading order in the $1/d_c$ expansion for any dimension D [23, 25].

As a final remark, we note that the SCSA equation for the GCI model, Eq. (3.37), is very similar to the self-consistent screening approximation for a crystalline D-dimensional membrane in the conventional dimensional continuation scheme, which is given by Eq. (2.45) [23, 25]. The two equations differ by a simple factor $D(D-1)/2$, which reduces to unity in the physical case $D = 2$. As expected, in two dimensions the GCI model and the theory of D-dimensional crystalline membranes present the same exponent $\eta' = 4/(d_c + \sqrt{16 - 2d_c + d_c^2})$, approximately equal to 0.821 for $d_c = 1$ [23, 25].

3.4.2 *Extrapolation to the physical dimensionality*

For the physical codimension $d_c = 1$, the ε-expansion of the scaling exponent, Eq. (3.34), reduces to:

$$\eta_* = \frac{2\varepsilon}{5} - \frac{\varepsilon^2}{750} + \mathrm{O}(\varepsilon^3) \ . \tag{3.38}$$

Compared to the leading order result, the $\mathrm{O}(\varepsilon^2)$ correction is strongly suppressed by its small numerical prefactor. Although ε is as large as 2, a direct extrapolation to the physical internal dimension $D = 2$ reveals an unexpectedly small deviation between the first and the second order results, $\eta = 0.8$ and $\eta \simeq 0.795$ respectively.

The first and second-order results, moreover, are close to the non-perturbative RG results $\eta \simeq 0.85$ [26–28], the first and second-order SCSA $\eta \simeq 0.821$ [23, 25], $\simeq 0.789$ [24] and to several numerical simulations, reporting approximately $\eta \simeq 0.750$ [4], 0.81 [29, 30], 0.85 [31, 34], 0.795 [32], 0.793–0.795 [35], 0.66 [37], 0.85–0.88 [38] (see Refs. [25, 29, 30] for results of early simulations). Finally, the leading-order extrapolation $\eta = 0.8$ is in exact agreement with the prediction of Ref. [51], where the exponent was obtained by a one-loop momentum shell renormalization group directly in $D = 2$.

3.4.3 *Extensions and higher-order calculations*

When our calculations were finished, available results were limited to the first order in the ε-expansion [10, 11], and the value (3.34) provided the first result beyond

leading order. Soon after, Coquand, Mouhanna, and Teber [19], extended two-loop calculations to all fixed points, both in the framework of elasticity theory and within the effective field theory for flexural fluctuations. In the recent publication [20], Metayer, Mouhanna, and Teber extended all results to three loops. Finally, in Ref. [21], Pikelner has derived a four-loop result in the framework of elasticity theory. The values of exponents determined by these higher-order calculations are summarized in tables 3.1, 3.2, and 3.3.

	η_*	η_{SCSA}
P_2'	$\frac{2\varepsilon}{d_c+4} - \frac{d_c(2-d_c)\varepsilon^2}{6(d_c+4)^3}$	$\frac{2\varepsilon}{d_c+4} - \frac{d_c(2-d_c)\varepsilon^2}{6(d_c+4)^3}$
P_3	$\frac{10\varepsilon}{20+d_c} - \frac{d_c(37d_c+950)\varepsilon^2}{6(20+d_c)^3}$	$\frac{10\varepsilon}{20+d_c} - \frac{d_c(37d_c+890)\varepsilon^2}{6(20+d_c)^3}$
P_4	$\frac{12\varepsilon}{24+d_c} - \frac{6d_c(d_c+29)\varepsilon^2}{(24+d_c)^3}$	$\frac{12\varepsilon}{24+d_c} - \frac{6d_c(d_c+30)\varepsilon^2}{(24+d_c)^3}$

Table 3.1: Anomalous dimensions at order ε^2 for all independent interacting fixed points [19]. P_2' is the fixed point of the GCI model analyzed in this chapter. P_4 describes the dimensional continuation of elasticity theory. P_3 corresponds instead to a medium with zero bulk modulus and a nonzero shear modulus [19]. The fixed point P_2, corresponding to an elastic medium with zero shear modulus and nonzero bulk modulus is not reported because it has zero anomalous dimension (see, however, Ref. [104]). The last column reports the $\mathrm{O}(\varepsilon^2)$ expansion of the SCSA exponents corresponding to the fixed points [19].

	η_*
P_2'	$\frac{0.8\varepsilon}{2} - \frac{0.005\bar{3}\varepsilon^2}{4} + \frac{0.01104\varepsilon^3}{8}$
P_3	$\frac{0.952\varepsilon}{2} - \frac{0.071\varepsilon^2}{4} - \frac{0.069\varepsilon^3}{8} - \frac{0.075\varepsilon^4}{16}$
P_4	$\frac{0.96\varepsilon}{2} - \frac{0.0461\varepsilon^2}{4} - \frac{0.00267\varepsilon^3}{8} - \frac{0.002\varepsilon^4}{16}$

Table 3.2: Anomalous dimensions at order ε^4 for P_3 and P_4 [21] and at order ε^3 for P_2' [20]. (All results are expressed for the case $d_c = d - D = 1$).

Tab. 3.1 shows that the SCSA is exact at order ε^2 only for the GCI model (the fixed point P_2'). For other fixed points, the SCSA is only exact at first order in ε [19]. The three-loop result of Ref. [20] showed that at order ε^3 there appear corrections beyond SCSA also for the fixed point P_2'.

Analogy with the theory of critical phenomena [15] suggests that the ε-expansion could be asymptotic, with zero radius of convergence [20]. In this case a resummation would be necessary to improve the quantitative accuracy of the results. A rigorous

	$1L$	$2L$	$3L$	$4L$
P_2'	0.8	$0.794\bar{6}$	0.8057	–
P_3	0.9524	0.8813	0.8116	0.7368
P_4	0.96	0.9139	0.8872	0.8670

Table 3.3: Direct extrapolation of one-, two-, three-, and four-loop anomalous dimensions to $D = 2$ and $d_c = 1$ [20, 21].

control over the series and the "error bars" in the ε-expansion calculation remains an open question.

The explicit values of the exponents at the lowest orders indicate that the ε expansion based on the fixed point P_4 may be less divergent than the expansion based on P_2'. For example, in the series for $\eta_2' = \eta_*(P_2')$, the three-loop contribution is larger than the two-loop one when $\varepsilon = 2$, which might be an indication of the asymptotic nature of the expansion [20]. For $\eta_4 = \eta_*(P_4)$ the relative strength of two-, three-, and four-loop contributions is instead decreasing. At the same time, the special permutation symmetry of the vertex and the identical behavior of $\bar{\mathbf{h}}$ and χ propagators implies that the expansion of the GCI model can be extended to high order by computation of a smaller number of Feynman diagrams. Therefore, it may be an useful tool in high order computations.

Before concluding this chapter, it is interesting to note that models almost identical to the GCI theory (3.7) emerge in the context of Galileon theories, which are relevant in high-energy physics (see, for example, Ref. [114]). A close analogy, for example, is the absence of vertex renormalization, which is at the basis of the calculations presented in this chapter and which also emerges in Galileon models [114]. It would be interesting to investigate in more detail the connections between the two theories.

ACKNOWLEDGEMENTS

This work was supported by the Dutch Research Council (NWO) via the Spinoza Prize of Professor M.I. Katsnelson.

APPENDIX 3

3.A TWO-LOOP SELF-ENERGY DIAGRAM

Diagrams (c) and (g) in Fig. 3.4 lead to the two-loop integral:

$$a_D = \frac{1}{s_D^2}\int\frac{\mathrm{d}^D k_1}{(2\pi)^D}\int\frac{\mathrm{d}^D k_2}{(2\pi)^D}\frac{\gamma(\hat{\mathbf{q}},\mathbf{k}_1)\gamma(\mathbf{k}_1,\mathbf{k}_2)\gamma(\hat{\mathbf{q}},\mathbf{k}_2)\gamma(\hat{\mathbf{q}}-\mathbf{k}_1,\hat{\mathbf{q}}-\mathbf{k}_2)}{|\mathbf{k}_1|^4|\mathbf{k}_2|^4|\hat{\mathbf{q}}-\mathbf{k}_2|^4|\hat{\mathbf{q}}-\mathbf{k}_1|^4|\mathbf{k}_1-\mathbf{k}_2|^4}\ , \quad (3.39)$$

where $\gamma(\mathbf{k}_1,\mathbf{k}_2) = k_1^2k_2^2-(\mathbf{k}_1\cdot\mathbf{k}_2)^2$, $\hat{\mathbf{q}} = \mathbf{q}/|\mathbf{q}|$ is an unit vector and integration runs over dimensionless momenta $\mathbf{k}_1$ and $\mathbf{k}_2$. The diagram presents a logarithmic UV divergence in four dimensions. Because of the finiteness of the $\chi\mathbf{h}^2$ three-point vertex function, all subdiagrams are finite. The UV divergence is thus of global type: it is generated by the region of integration in which $\mathbf{k}_1$ and $\mathbf{k}_2$ are both simultaneously large. As any global UV divergence, the divergence in $D_c(\mathbf{q})$ corresponds to a first order pole in dimensional regularization. Following a standard strategy, it is possible to extract the singularity by replacing the integrand in Eq. (3.39) by any simpler expression which presents the same large-momentum behavior. A convenient choice consists in the replacement $a_D \to \bar{a}_D$, with:

$$\bar{a}_D = \frac{1}{s_D^2}\int\frac{\mathrm{d}^D k_1}{(2\pi)^D}\int\frac{\mathrm{d}^D k_2}{(2\pi)^D}\frac{\gamma(\hat{\mathbf{q}},\mathbf{k}_1)\gamma(\hat{\mathbf{q}},\mathbf{k}_2)\gamma^2(\mathbf{k}_1,\mathbf{k}_2)}{\left(|\mathbf{k}_1|^4+\sigma_0k_1^2\right)^2\left(|\mathbf{k}_2|^4+\sigma_0k_2^2\right)^2|\mathbf{k}_1-\mathbf{k}_2|^4}\ . \quad (3.40)$$

In this expression σ_0 plays the role of an external tension [11, 52, 85], modifying the $\bar{\mathbf{h}}$ field propagator from $1/k^4$ to $1/(k^4+\sigma_0k^2)$. Imposing a finite σ_0 in Eq. (3.40) is necessary in order to avoid infrared divergence of the integral. The dependence of $\bar{a}_D$ on the external momentum $\hat{\mathbf{q}}$ can now be factorized. The integral takes the form:

$$\bar{a}_D = P^T_{\alpha\beta}(\hat{\mathbf{q}})P^T_{\gamma\delta}(\hat{\mathbf{q}})\int_{\mathbf{k}_1}\int_{\mathbf{k}_2} f(k_1^2,k_2^2,\mathbf{k}_1\cdot\mathbf{k}_2)k_{1\alpha}k_{1\beta}k_{2\gamma}k_{2\delta}\ , \quad (3.41)$$

where $P^T_{\alpha\beta}(\mathbf{q}) = \delta_{\alpha\beta}-\hat{q}_\alpha\hat{q}_\beta$ is the transverse projector and $\int_{\mathbf{k}} = \int\mathrm{d}^Dk/(2\pi)^D$ denotes momentum integration. It is then convenient to average over angles [25]. By using the relation [15]

$$\begin{aligned}&\int_{\mathbf{k}_2} f(k_1^2,k_2^2,\mathbf{k}_1\cdot\mathbf{k}_2)k_{2\gamma}k_{2\delta}\\ &= \int_{\mathbf{k}_2}\frac{f(k_1^2,k_2^2,\mathbf{k}_1\cdot\mathbf{k}_2)}{(D-1)k_1^2}\left[\gamma(\mathbf{k}_1,\mathbf{k}_2)\delta_{\gamma\delta}+\left(D(\mathbf{k}_1\cdot\mathbf{k}_2)^2-k_1^2k_2^2\right)\frac{k_{1\gamma}k_{1\delta}}{k_1^2}\right]\end{aligned} \quad (3.42)$$

and the spherical averages [25]

$$\begin{aligned}\int_{\mathbf{k}_1} g(k_1^2)k_{1\alpha}k_{1\beta} &= \frac{\delta_{\alpha\beta}}{D}\int_{\mathbf{k}_1} g(k_1^2)k_1^2\ ,\\ \int_{\mathbf{k}_1} g(k_1^2)k_{1\alpha}k_{1\beta}k_{1\gamma}k_{1\delta} &= \frac{\delta_{\alpha\beta}\delta_{\gamma\delta}+\delta_{\alpha\gamma}\delta_{\beta\delta}+\delta_{\alpha\delta}\delta_{\beta\gamma}}{D(D+2)}\int_{\mathbf{k}_1} g(k_1^2)k_1^4\ ,\end{aligned} \quad (3.43)$$

we obtain:

$$\begin{aligned}\bar{a}_D &= \frac{1}{D(D+2)}\int_{\mathbf{k}_1}\int_{\mathbf{k}_2} f(k_1^2,k_2^2,\mathbf{k}_1\cdot\mathbf{k}_2)[(D^2-1)k_1^2k_2^2-2\gamma(\mathbf{k}_1,\mathbf{k}_2)] \\ &= \frac{1}{D(D+2)s_D^2}\int_{\mathbf{k}_1}\int_{\mathbf{k}_2}\frac{\gamma^2(\mathbf{k}_1,\mathbf{k}_2)[(D^2-1)k_1^2k_2^2-2\gamma(\mathbf{k}_1,\mathbf{k}_2)]}{(|\mathbf{k}_1|^4+\sigma_0k_1^2)^2(|\mathbf{k}_2|^4+\sigma_0k_2^2)^2|\mathbf{k}_1-\mathbf{k}_2|^4}\ .\end{aligned} \tag{3.44}$$

By introducing integration over five Schwinger-type parameters t_i $(i=1,..,5)$, the expression for $\bar{a}_D$ can be represented as

$$\begin{aligned}\bar{a}_D &= \frac{1}{D(D+2)s_D^2}\int_0^\infty \mathrm{d}t_1\mathrm{d}t_2\mathrm{d}t_3\mathrm{d}t_4\mathrm{d}t_5\Big(\prod_{i=1}^5 t_i\Big)\int_{\mathbf{k}_1}\int_{\mathbf{k}_2}\Big\{\gamma^2(\mathbf{k}_1,\mathbf{k}_2) \\ &\times[(D^2-1)k_1^2k_2^2-2\gamma(\mathbf{k}_1,\mathbf{k}_2)]\exp\Big[-\sum_{a,b=1}^2 M_{ab}(\mathbf{k}_a\cdot\mathbf{k}_b)-(t_2+t_4)\sigma_0\Big]\Big\}\ ,\end{aligned} \tag{3.45}$$

where M is the 2×2 matrix:

$$M=\begin{bmatrix}t_1+t_2+t_5 & -t_5\\ -t_5 & t_3+t_4+t_5\end{bmatrix} \tag{3.46}$$

and integrals over all five variables t_i $(i=1,..,5)$ run from 0 to ∞. Momentum integrals in Eq. (3.45) are determined by moments of a Gaussian distribution. It is convenient to express moments by differentiation with respects to the matrix elements M_{ab}. This leads to the representation

$$\begin{aligned}\bar{a}_D &= \frac{1}{D(D+2)s_D^2}\int_0^\infty \mathrm{d}t_1\mathrm{d}t_2\mathrm{d}t_3\mathrm{d}t_4\mathrm{d}t_5\Big(\prod_{i=1}^5 t_i\Big)\int_{\mathbf{k}_1}\int_{\mathbf{k}_2}\Big\{\mathrm{e}^{-(t_2+t_4)\sigma_0} \\ &\times\Big[(D^2-1)\frac{\partial^2}{\partial M_{11}\partial M_{22}}-2\Big(\frac{\partial^2}{\partial M_{11}\partial M_{22}}-\frac{1}{4}\frac{\partial^2}{\partial M_{12}^2}\Big)\Big] \\ &\Big[\frac{\partial^2}{\partial M_{11}\partial M_{22}}-\frac{1}{4}\frac{\partial^2}{\partial M_{12}^2}\Big]^2\mathrm{e}^{-\sum_{a,b}M_{ab}(\mathbf{k}_a\cdot\mathbf{k}_b)}\Big\}\ ,\end{aligned} \tag{3.47}$$

where $M_{12}=M_{21}$ is considered as a single independent variable. By using the relation

$$\Big[\frac{\partial^2}{\partial M_{11}\partial M_{22}}-\frac{1}{4}\frac{\partial^2}{\partial M_{12}^2}\Big](\det M)^{-\omega}=\frac{\omega(2\omega-1)}{2}(\det M)^{-\omega-1} \tag{3.48}$$

after momentum integration, we obtain:

$$\begin{aligned}\bar{a}_D &= \frac{(D^2-1)(D+4)}{64(4\pi)^D s_D^2}\int_0^\infty \mathrm{d}t_1\mathrm{d}t_2\mathrm{d}t_3\mathrm{d}t_4\mathrm{d}t_5\Big\{\Big(\prod_{i=1}^5 t_i\Big)\frac{\mathrm{e}^{-(t_2+t_4)\sigma_0}}{(\det M)^{\frac{D+6}{2}}} \\ &\times\Big[(D^2-1)(D+6)\frac{M_{12}^2}{\det M}+(D^2-1)(D+4)-2(D+3)\Big]\Big\}\ .\end{aligned} \tag{3.49}$$

Near $D = 4$ regular functions of D can be replaced by their four dimensional value. Using the explicit form of the matrix M, Eq. (3.46), and integrating over t_5 gives:

$$\bar{a}_D \approx 4 \int_0^\infty \mathrm{d}t_1 \mathrm{d}t_2 \mathrm{d}t_3 \mathrm{d}t_4 \Big\{ \Big(\prod_{i=1}^4 t_i \Big) \Big(9 + \frac{53}{5} \frac{s^2}{(t_1+t_2)(t_3+t_4)} \Big) \times \frac{\mathrm{e}^{-(t_2+t_4)\sigma_0}}{s^4 (t_1+t_2)^{D/2} (t_3+t_4)^{D/2}} \Big\} , \tag{3.50}$$

where $s = t_1 + t_2 + t_3 + t_4$. By the change of variables

$$\begin{aligned} t_1 &= (1-x_1)ys \ , \qquad & t_2 &= x_1 y s \ , \\ t_3 &= (1-x_2)(1-y)s \ , \qquad & t_4 &= x_2(1-y)s \ , \end{aligned} \tag{3.51}$$

the integral can be rewritten in a Feynman-type parametrization:

$$\bar{a}_D \approx 4 \int_0^1 \mathrm{d}x_1 \int_0^1 \mathrm{d}x_2 \int_0^1 \mathrm{d}y \int_0^\infty \mathrm{d}s \, \big\{ x_1(1-x_1)x_2(1-x_2) y^{3-\frac{D}{2}} (1-y)^{3-\frac{D}{2}} s^{3-D} \Big(9 + \frac{53}{5y(1-y)} \Big) \exp\big[-(x_1 y + x_2(1-y)) s\sigma_0 \big] \big\} \ . \tag{3.52}$$

Integration over s generates a first order pole at $D = 4$. The remaining integrals, being finite, can be calculated by replacing $D = 4$ in the integrand function. The result is:

$$\bar{a}_D \approx 4\Gamma(4-D) \int_0^1 \mathrm{d}x_1 \int_0^1 \mathrm{d}x_2 \int_0^1 \mathrm{d}y \, \Big[x_1(1-x_1)x_2(1-x_2) \Big(9y(1-y) + \frac{53}{5} \Big) \Big] \approx \frac{121}{90(4-D)} \ . \tag{3.53}$$

The two-loop integral a_D, therefore, behaves near four dimensions as:

$$a_D = \frac{121}{90\varepsilon} + \mathrm{O}(1) \ . \tag{3.54}$$

4

SCALE WITHOUT CONFORMAL INVARIANCE

Field theories at renormalization-group fixed points exhibit an emergent symmetry: the invariance under dilatation of length scales. In several field theories with rotation and translation symmetries, the appearance of scale invariance triggers the emergence of an even larger symmetry: conformal invariance. When this symmetry enhancement occurs, powerful conformal field theory (CFT) methods can often be used to derive very accurate numerical calculations of universal quantities and, in several 2D models, even exact solutions. In this chapter, we investigate the relation between dilatation and conformal symmetries in the statistical mechanics of flexible crystalline membranes. We argue that, in the elasticity theory representation, the ultraviolet and the infrared fixed points of the RG flow exhibit scale invariance but not the conformal symmetry. In the GCI representation, instead, the RG flow connects a conformal ultraviolet fixed point to a scale-invariant but nonconformal infrared fixed point. The analysis is based on an inspection of the corresponding energy-momentum tensors to all order in the ε-expansion.

This chapter is based on the publication:
Achille Mauri and Mikhail I. Katsnelson, "Scale without conformal invariance in membrane theory", Nucl. Phys. B **969**, 115482 (2021); preprint: arXiv:2104.06859 (2021)

4.1 INTRODUCTION

Asymptotic scale invariance plays a crucial role in quantum field theory, from statistical mechanics to models of fundamental interactions. In several cases, the asymptotically-emergent scaling symmetry is enlarged to full conformal invariance, which opens the way to powerful techniques such as bootstrap equations [79, 80] or, in two dimensions, methods based on the infinite Virasoro algebra [115]. These approaches give access to high-precision non-perturbative calculations and, in some cases, even to exact solutions. Understanding the conditions under which conformal symmetry arises is thus of great importance, and has motivated extensive investigations [116].

Particularly general results were established for two- and four-dimensional field theories assuming unitarity, or, in Euclidean space, the corresponding property of reflection positivity [79, 117–119]. In the two-dimensional case, Zamolodchikov and Polchinski proved that unitary scale-invariant field theories are always conformal under two mild assumptions: the existence of a well-defined energy-momentum tensor and the discreteness of the spectrum of operator dimensions [117, 118]. In four-dimensional space, a similar result is expected to hold [116], as indicated by perturbative proofs to all orders [120–122] and corroborated by non-perturbative evidences [116, 121, 123–125]. Some analogue derivations were argued to be applicable to unitary theories in any even dimension $D = 2n$ [126].

These arguments, however, cannot be extended straightforwardly to arbitrary dimensions (possibly odd or non-integer) or to models lacking unitarity or reflection positivity. In addition, several derivations break down when the energy-momentum tensor and its two-point function are not well defined, which can happen in sigma models relevant for string theories [118, 127, 128]. Models with scale but without conformal invariance, in fact, exist and have been explicitly identified [103, 116, 118, 127–133], or indirectly conjectured based on holographic analyses [134–136]. Although unphysical in the context of fundamental interactions, models defined in general dimension D and without unitarity or reflection positivity are recurrent in statistical mechanics. Analyses of the relation between scale and conformal invariance in more general classes of theories are thus crucial for several physical applications (see Refs. [79, 118, 137–142] for some of the results and methods).

If we try to consider, roughly speaking, how likely it is for a scale-invariant model to exhibit conformal symmetry, we can often run into a dilemma. On the one hand, dilatation invariance is not a sufficient condition for the extended conformal invariance and, therefore, a generic scale-invariant theory can be expected to lack conformal symmetry. On the other hand, there exist arguments suggesting that, for *interacting* field theories, scale invariance should imply conformal invariance generically [79, 130, 132, 142]. A formulation of this reasoning starts from the structure of the energy-momentum tensor $T_{\alpha\beta}$ and its trace T^{α}_{α}. In local and scale-

invariant theories, dilatation symmetry implies that $T^{\alpha}_{\alpha} = \partial_{\alpha} V^{\alpha}$, where V^{α} is a local field, the "virial current". Conformal invariance arises instead whenever $V^{\alpha} = j^{\alpha} + \partial_{\beta} L^{\alpha\beta}$ where j^{α} is conserved ($\partial_{\alpha} j^{\alpha} = 0$) and $L^{\alpha\beta}$ is a tensor field [118]. Although the requirements for conformal symmetry are stronger and not automatically satisfied a priori, possible candidates for the virial current are constrained, because V^{α} must have a scaling dimension exactly equal to $\{V^{\alpha}\} = D - 1$ in order to match the dimensions of the energy-momentum tensor $\{T_{\alpha\beta}\} = D$ [79, 130, 132, 142] [1]. All vector currents are usually expected to acquire anomalous dimensions in presence of interactions, unless they are conserved. Consistent candidates for V^{α} in a generic theory can thus be expected to be conserved currents, which implies conformal invariance [79, 130, 132, 142].

A basis from which we can formulate similar arguments is provided by the results of Refs. [137, 140, 141] which, instead of analyzing the energy-momentum tensor, used non-perturbative renormalization group techniques. Refs. [140, 141] showed that, for critical scalar and O(N) models, scale implies conformal invariance if no vector eigenoperator with scaling dimension -1 exists [2]. This vector quantity plays a role analogue to the space integral of the virial current. Ref. [137], instead, used a generalization of Wilson's renormalization group to argue that, for a general fixed point theory, two- and three-point functions are consistent with the constraints imposed by conformal invariance provided that (i) there exists no vector eigenoperator with dimension -1, (ii) interactions are sufficiently local, (iii) the real parts of operator dimensions are bounded from below, and (iv) some surface effects are negligible[3]. With the same logic used for the virial current, the existence of vectors with dimension tuned to -1 appears to be unlikely in generic

1 More precisely, the change of a symmetric energy-momentum tensor under infinitesimal dilatations reads $i[S, T_{\alpha\beta}] = x^{\rho}\partial_{\rho} T_{\alpha\beta} + D T_{\alpha\beta} + \partial^{\sigma}\partial^{\rho} Y_{\alpha\sigma\beta\rho}$ where $Y_{\alpha\sigma\beta\rho} = -Y_{\sigma\alpha\beta\rho} = Y_{\beta\rho\alpha\sigma}$ [118, 123]. The first two terms, $x^{\rho}\partial_{\rho} T_{\alpha\beta} + D T_{\alpha\beta}$ describe the scaling law of an eigenoperator with dimension D, while the third, inhomogeneous term is generated by renormalization. In scale-invariant theories, where $T^{\alpha}_{\alpha} = \partial_{\alpha} V^{\alpha}$, the scaling law for the virial current must read, therefore, $i[S, V^{\alpha}] = x^{\rho}\partial_{\rho} V^{\alpha} + (D-1)V^{\alpha} + l^{\alpha} + \partial^{\rho} Y^{\sigma\alpha}{}_{\sigma\rho}$, with $\partial_{\alpha} l^{\alpha} = 0$ (see also Ref. [123]). The inhomogeneous terms $l^{\alpha} + \partial^{\rho} Y^{\sigma\alpha}{}_{\sigma\rho}$ have precisely the form of the combination of a conserved current and a total divergence, which are irrelevant to the discussion of scale and conformal invariance. This justifies considering V^{α} as a scaling operator of dimension $D - 1$. It is usually possible to choose an improved energy-momentum tensor in such way that $Y_{\alpha\sigma\beta\rho} = 0$ and the canonical scaling laws holds (see however Ref. [123] for a more detailed discussion).

2 Redundant operators, whose insertion is equivalent to an infinitesimal change of variables, are allowed: even if their dimension is exactly equal to -1, they do not destroy conformal invariance but, rather, modify the transformation of fields under the elements of the conformal group [141]. This is consistent with the fact that the scaling dimension of redundant operators can actually be chosen at will, by suitable design of the specific renormalization group transformation [143]. The dimensions of non-redundant operators are, instead, intrinsic quantities, invariant under redefinitions of the RG.

3 In Ref. [137] the vector operator dimension is reported as $+1$, because length units are used instead of inverse-length units. Similarly, the lower bound in the real part of operator dimensions is expressed there as an upper bound.

interacting field theories, suggesting that scale implies conformal invariance in a broad class of models. The argument can actually be extended by a reasoning based on continuity: even if a vector happens by coincidence to have scaling dimension -1 in D-dimensional space, conformal invariance can still be inferred by continuation from neighbouring dimensions $D + \delta D$. A scenario without conformal invariance thus requires the existence of a vector presenting dilatation eigenvalue exactly equal to -1 throughout a continuous interval of dimensions in the neighbourhood of D, which seems even more unlikely [140].

Although genericity arguments hint at a general explanation of conformal invariance, they cannot set a fully definite answer. The same reasonings, for example, could be read from a different point of view: it might be the case that scale without conformal invariance is recurrent in several field theories, and vectors with dimension -1 or currents with dimension $D - 1$ are not unlikely as a first expectation suggests. With this reversed perspective, the arguments could be regarded as proofs that these vectors are common even in interacting theories[4].

For given field theories, it is usually not necessary to argue from genericity. For example, in the Ising and in the O(N) model, the presence of conformal invariance can be argued by setting bounds on the dilatation spectrum[5] [140–142]. Also, powerful tools are available to analyze perturbative theories explicitly [116, 118, 120, 121, 138, 139, 145].

It is interesting, however, to explore the genericity arguments in more depth. In this direction, Ref. [132] identified and analyzed an interacting scale invariant model which is not conformal: the theory of SU(N) gauge fields coupled to massless fermions at the Banks-Zaks fixed point. As it was shown, the model is conformal when regarded as a gauge theory, but presents a nontrivial virial current V^α when gauge fixed. The scaling dimension of V^α was shown to be exactly equal to $\{V^\alpha\} = D - 1$, to all orders in perturbation theory, which was traced to BRST invariance of the theory. Other scale-invariant but nonconformal theories were identified in the context of turbulence [133], sigma models [118, 127–129], topologically-twisted theories [134, 135], Wess-Zumino models with scale-invariant renormalization-group trajectories [131], or were recognized by holographic analysis [116, 134–136]. Finally, we note that Ref. [146] recognized the presence of scale-invariance without conformal

4 A critical examination of the genericity argument was given in Ref. [144]. A more detailed elaboration on this question, in the framework of perturbative renormalization and the ε-expansion, will be presented in Sec. 4.5.3.

5 Ref. [140] proposed a proof implying that all local vector fields in the critical Ising model have dimension larger than $D - 1 + \eta$, where η is the field anomalous dimension, unless they are total derivatives. The validity of the proof was later criticized [142] and has been a subject of debate [141, 142]. The final result that vectors with dimension $D - 1$ do not exist in the critical Ising model, is however, corroborated by the complementary analysis of Ref. [142], which investigated the dimension of scaling operators by Monte Carlo simulations.

symmetry in an analysis at classical level of symmetric superfluids characterized by shift-invariant actions.

In this chapter, we analyze the relation between scale and conformal symmetry in the statistical mechanics of fluctuating crystalline membranes. We verify that, in the ε-expansion, the theory generates a virial current V^α which cannot be reduced to a combination of a conserved current and a total derivative. Despite being non-conserved, the V^α is shown to have scaling eigenvalue $\{V^\alpha\} = D-1$ to all orders in perturbation theory, without anomalous dimensions. This absence of renormalization is traced to the fact that V^α is not invariant under the spontaneously-broken embedding-space translations and rotations, which are realized as shifts of the phonon fields. A similar result is found for the GCI model in dimension $D = 4 - \varepsilon$. Even for this alternative theory, the infrared behavior is shown to be scale invariant but nonconformal. A consequence of our analysis is that methods of conformal field theory (CFT), such as the conformal bootstrap, cannot be straightforwardly applied to the flat phase of crystalline membranes.

The membrane models analyzed in this work can be viewed as a generalization of the linearized theory of elasticity, a model which was identified by Riva and Cardy as an example of scale-invariant but non-conformal field theory [103, 130, 147]. The main difference is that the Riva-Cardy model describes an elastic medium confined in D dimensions, while solid membranes are allowed to fluctuate in an embedding space with higher dimension $d > D$. While linearized elasticity is a Gaussian, non-interacting theory, transverse fluctuations in the additional $d - D$ space dimensions make membrane theory an anharmonic model, which realizes scale invariance via an interacting RG fixed point. The presence of interactions makes membrane theory an interesting platform to test the genericity arguments on scale and conformal invariance.

By analyzing molecular dynamics simulations of fluctuating graphene, Giordanelli *et al.* [148] reported that the contour lines of equal heigth at the percolation threshold exhibit properties consistent with Schramm-Loewner evolution (SLE) curves [149]. The SLE equation is invariant under the infinite-dimensional 2D conformal group and thus this finding provided numerical evidence on a manifestation of conformal symmetry in thermally-fluctuating graphene. The analysis presented in this chapter is not necessarily in contradiction, because we did not consider the statistical properties of iso-height lines but rather field correlations as a function of the internal coordinate. The difference between the results presented here and the numerical findings of Ref. [148] calls however for a further investigation[6].

6 Note also that the analysis presented in this chapter is constructed in the framework of the ε-expansion. The absence of conformal invariance is proven for $D < 4$ only in the sense of this expansion (to all orders in ε). We expect however that the analysis should remain the same in $D = 2$. The problem could be revisited directly in two dimensions for example in the framework of the large-d_c expansion. Another possibility consists in defining perturbation theory directly

4.2 CONFORMAL INVARIANCE

Conformal transformations can be defined as those changes of coordinates which, at each point, appear *locally* like the combination of a translation, a rotation, and a dilatation. In other words, conformal transformations preserve all angles: if two curves cross at a point $\mathbf{x}$ with a relative angle $\Delta\theta$, the image of the two curves after conformal transformations will cross at the image point $\mathbf{x}'$ with the same relative angle $\Delta\theta' = \Delta\theta$.

Mathematically, the properties of conformal transformations can be expressed by the condition that the transformed metric

$$h'_{\mu\nu}(\mathbf{x}') = \frac{\partial x^\rho}{\partial x'^\mu}\frac{\partial x^\sigma}{\partial x'^\nu} h_{\rho\sigma}(\mathbf{x}) \tag{4.1}$$

after the change of coordinate $\mathbf{x} \to \mathbf{x}(\mathbf{x}')$ remains proportional to the non-transformed metric $h_{\mu\nu}(\mathbf{x})$ up to a scalar factor:

$$h'_{\mu\nu}(\mathbf{x}') = \mathrm{e}^{\lambda(\mathbf{x})} h_{\mu\nu}(\mathbf{x}) \ . \tag{4.2}$$

For a space with Euclidean geometry, $h_{\mu\nu}(\mathbf{x}) = \delta_{\mu\nu}$, this implies

$$h'_{\mu\nu}(\mathbf{x}') = \frac{\partial x^\rho}{\partial x'^\mu}\frac{\partial x^\sigma}{\partial x'^\nu}\delta_{\rho\sigma} = \mathrm{e}^{\lambda(\mathbf{x})}\delta_{\mu\nu} \ . \tag{4.3}$$

For infinitesimal transformations $x'^\mu = x^\mu + \epsilon^\mu$, the conformality conditions reduce to the "Killing equations"

$$\partial_\mu \epsilon_\nu + \partial_\nu \epsilon_\mu = \frac{1}{D}(\partial_\rho \epsilon_\rho)\delta_{\mu\nu} \ , \tag{4.4}$$

where D is the space dimension. For $D > 2$ the solutions are translations ($\epsilon_\mu(\mathbf{x}) = t_\mu$), rotations ($\epsilon_\mu(\mathbf{x}) = \omega_{\mu\nu}x_\nu$ with $\omega_{\mu\nu} = -\omega_{\nu\mu}$), dilatations ($\epsilon_\mu = \lambda x_\mu$) and *special conformal transformations*

$$\epsilon_\mu(\mathbf{x}) = 2(\mathbf{b}\cdot\mathbf{x})x_\mu - b_\mu x^2 \ , \tag{4.5}$$

which together form a group with $(D+1)(D+2)/2$ independent generators [115, 116, 151].

For finite parameters the special conformal transformation reads [7]

$$x'_\mu = \frac{x_\mu - b_\mu x^2}{1 + b^2x^2 - 2(\mathbf{b}\cdot\mathbf{x})} \tag{4.6}$$

in $D = 2$ after regularizing divergences via an infrared cutoff (see for example Ref. [16, 150] for analogue methods in the theory of phase transitions).

7 Eq. (4.6) can be derived by performing a sequence of three steps: an inversion $x_\mu \to x_\mu/x^2$, a translation $x_\mu \to x_\mu + b_\mu$, and a subsequent inversion $x_\mu \to x_\mu/x^2$ [115, 116, 119]. The inversion is a conformal transformation, but it belongs to a component of the group which is not continuously connected to the identity. The special conformal transformation instead reduces to the identity when $b_\mu \to 0$. This construction also makes it clear that the special conformal transformations form a D-dimensional commutative subgroup [115].

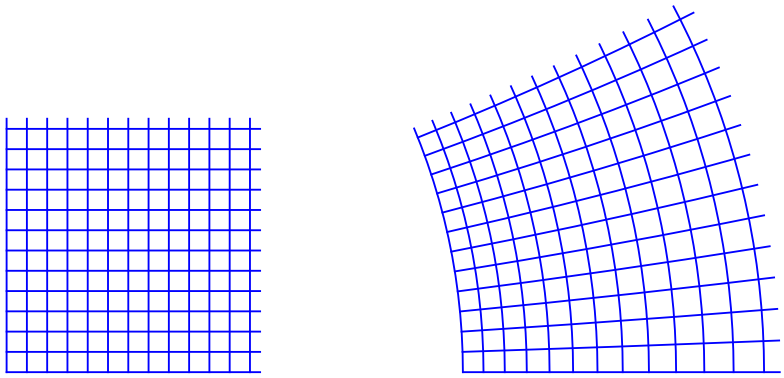

Figure 4.1: Image of a square net after a conformal map. The net gets locally rotated and dilated by inhomogeneous, space-dependent amounts, but the angles between all lines remains 90° and infinitesimal squares are mapped to infinitesimal squares (not to rectangles).

The effect of this mapping on a square net is illustrated graphically in Fig. 4.1. All angles between lines are preserved and locally the transformation looks like a combination of a translation, a rotation, and a dilatation. However, the amount of rotation and dilatation differs from point to point.

In two dimensional space, the conformal group is, instead, infinite dimensional. The Killing equation (4.4) can be showed to be equivalent to the Cauchy-Riemann conditions [115, 151], which have as a solution all holomorphic mappings of the complex plane. The group of translations, rotations, dilatations, and special conformal transformations of the form (4.6) can be collectively represented in complex coordinates as mappings of the form

$$z' = \frac{az + b}{cz + d} \ , \tag{4.7}$$

with complex coefficients a, b, c, d satisfying $ad - bc \neq 0$ [115]. The mappings (4.7) are known as Möbius transformations and form a subgroup of the holomorphic functions.

Systems tuned at the critical temperature of a second-order phase transition are often described by continuum field theories invariant under conformal transformations [13, 79, 115, 119]. The presence of rotational and translational symmetries is a consequence of the existence of a continuum limit. At the critical point, the divergence of the correlation length implies the emergence of fluctuations at arbitry large wavelengths [13–16, 81, 84], and the discrete nature of the microscopic lattice,

which breaks continuum space symmetries, becomes irrelevant. The appearance of scale invariance is a further consequence of the continuum limit, and arises when the only large length scale in the problem (the correlation length) becomes strictly infinite. A priori, there is no group theoretical reason why a model invariant under rotations, translations, and dilatations should exhibit the extended conformal symmetry. However, field theories relevant in high energy physics and in several statistical mechanical problems are local, involving only short range interactions [14, 15]. In this case, the enhancement to conformal invariance becomes more likely, since in the neighbourhood of each point, a conformal mapping behaves approximately as a combination of an isometry and a scale transformation. The symmetry enhancement, however, is still not guaranteed, because the local values of the rotation angles and dilatation factors change from point to point. Since field theories always contain gradient terms, this inhomogeneity can destroy the conformal invariance even in a local model symmetric under rigid, space-independent isometries and dilatations [116, 118]. As discussed in Sec. 4.1, in the case of unitary or reflection positive theories, it is possible to prove that the conformal invariance always emerges [117, 118, 152]. In this chapter, we argue that this, instead, does not happen in the case of thermal ripples in membranes within the ε-expansion: despite having isometric and dilatation symmetries, the statistical distribution of ripples is not enhanced to the full conformal symmetry.

Before starting the discussion, it is useful to emphasize the possibility of very different notions of conformal invariance in the case of membranes. In high-energy physics and in the statistical mechanics of critical phenomena, the continuum field theories usually have as degrees of freedom quantized matter fields, gauge fields, or order parameters (a local magnetization in the case of ferromagnetic transitions). For membranes, instead, the fluctuating fields $\mathbf{h}(\mathbf{x})$ and $u_\alpha(\mathbf{x})$ are themselves spacial coordinates. In addition to coordinate transformations of $\mathbf{x}$, analogue to transformations in any other field theory, it is thus possible to apply space transformations to $\mathbf{h}(\mathbf{x})$ and $u_\alpha(\mathbf{x})$.

Membranes with a vanishing bulk modulus, realized for example by twisted Kagome lattices, present a form of "embedding-space" conformal invariance [102]. Since they present a finite resistance to shear but not to compression, they can be deformed without any elastic energy cost provided that at each point in the medium, the deformation is free of shearing distortions. Shearless deformations are realized by any configuration of the in-plane displacement fields for which u_α satisfies the conformal Killing equation. In two dimensions, all deformations for which $u_x + iu_y$ is a holomorphic function of $x + iy$ are shear-free and correspond to states with zero elastic energy [102]. In this form of embedding-space invariance, the conformal transformations leave $\mathbf{x}$ invariant and act on u_α.

In this chapter, we analyze instead the existence of "internal-space" conformal invariance: invariance under conformal transformations of the D-dimensional

coordinate $\mathbf{x}$. This notion mirrors the usual realizations of conformal invariance in quantum field theory. It represents the group theoretical extension of scale invariance in the sense of the RG fixed point: the existence of inhomogeneous ripples at all wavelengths.

4.3 ENERGY-MOMENTUM TENSOR

The response to translations, rotations, scale, and conformal transformations can be described in an unified language in terms of special structural properties of the energy-momentum tensor [15, 115, 118, 153].

In any local and translationally invariant field theory, the energy-momentum tensor $T_{\mu\nu}$ is defined as the conserved Noether current associated with translational symmetry. In a model involving a collection of fields $\Phi_a(\mathbf{x})$ as degrees of freedom, $T_{\mu\nu}$ can be calculated by measuring the change of the action $S[\Phi_a(\mathbf{x})]$ under the change of variables $\Phi_a(\mathbf{x}) \to \Phi'_a(\mathbf{x}) = \Phi_a(\mathbf{x} + \epsilon(\mathbf{x}))$, where ϵ is an infinitesimal space-dependent vector field. Due to locality and translational symmetry the variation of the action must take the form[8]

$$\delta S = S[\Phi'_a(\mathbf{x})] - S[\Phi_a(\mathbf{x})] = \int \mathrm{d}^D x \; T_{\alpha\beta} \partial_\alpha \epsilon_\beta \; , \tag{4.8}$$

in such way that it vanishes when ϵ_β is space-independent. Eq. (4.8) defines the energy-momentum tensor $T_{\alpha\beta}$. Due to the least action principle, δS is always equal to zero when $\Phi_a(\mathbf{x})$ are solutions of the equations of motion. Since this is valid for any ϵ_β this implies that $\partial_\alpha T_{\alpha\beta} = 0$: the energy-momentum tensor is locally conserved [115, 118, 154].

Although $T_{\alpha\beta}$ is designed as a current associated with translations, Eq. (4.8) in fact encodes the response to *any* coordinate change, because the space-dependent translation $\epsilon(\mathbf{x})$ is in fact a general transformation of coordinates [15]. Therefore, the conserved currents associated with rotations, dilatations, and conformal transformation can all be related to the energy momentum tensor.

If the action is invariant not only under translations, but also under rotations, the angular momentum current

$$M_{\alpha,\beta\gamma} = x_\gamma T_{\alpha\beta} - x_\beta T_{\alpha\gamma} + s_{\alpha,\beta\gamma} \tag{4.9}$$

is conserved [115, 153]. In Eq. (4.9), $s_{\mu,\nu\rho}$ is a local tensor, antisymmetric for $\nu \leftrightarrow \rho$, which does not depend explicitly on the coordinates. The conservation law $\partial_\mu M_{\mu,\nu\rho} = 0$ implies that

$$T_{\alpha\beta} - T_{\beta\alpha} = -\partial_\gamma s_{\gamma,\beta\alpha} \; . \tag{4.10}$$

8 Since in this work we consider Euclidean geometries it is not necessary to distinguish covariant and contravariant indices. We thus drop upper indices and write all tensors with lower indices only.

In this case it is possible to introduce an "improved" energy-momentum tensor [115]

$$\theta_{\alpha\beta} = T_{\alpha\beta} + \frac{1}{2}\partial_\gamma \left(s_{\beta,\alpha\gamma} + s_{\alpha,\beta\gamma} - s_{\gamma,\beta\alpha}\right) \tag{4.11}$$

which has the same divergence of the canonical energy-momentum tensor, $\partial_\alpha T_{\alpha\beta} = \partial_\alpha \theta_{\alpha\beta}$, and which is symmetric ($\theta_{\alpha\beta} = \theta_{\beta\alpha}$ when evaluated for fields $\Phi_a(\mathbf{x})$ which solve the equations of motion $\delta S/\delta\Phi_a(\mathbf{x}) = 0$.

The improved energy-momentum tensor $\theta_{\alpha\beta}$ is not uniquely specified by the symmetry $\theta_{\alpha\beta} = \theta_{\beta\alpha}$ and the conservation law $\partial_\alpha\theta_{\alpha\beta}$, but has a residual "gauge freedom". All equivalent energy-momentum tensors can be shown to be identical up to the addition of a symmetric improvement term of the form $\partial_\rho\partial_\sigma Y_{\alpha\sigma\beta\rho}$, where $Y_{\alpha\sigma\beta\rho}$ has the symmetries of the Riemann tensor $Y_{\alpha\sigma\beta\rho} = -Y_{\sigma\alpha\beta\rho} = Y_{\beta\rho\alpha\sigma}$ [118]

It the action is invariant under translations, rotations, and dilatations, the system presents a conserved dilatation current [115, 116, 118, 153] of the form

$$S_\alpha = x_\beta\theta_{\alpha\beta} - V_\alpha \ , \tag{4.12}$$

where V_α, the "virial current", has no explicit coordinate dependence. Scale invariance is equivalent to the current conservation $\partial_\alpha S_\alpha = 0$ and thus requires $\theta_{\alpha\alpha} = \partial_\alpha V_\alpha$. This condition is invariant for any "gauge choice" of the symmetric energy momentum tensor, because, if $\theta_{\alpha\beta}$ is replaced with $\theta'_{\alpha\beta} = \theta_{\alpha\beta} + \partial_\rho\partial_\sigma Y_{\alpha\sigma\beta\rho}$ then the equation $\theta'_{\alpha\alpha} = \partial_\alpha V'_\alpha$ remains valid with $V'_\alpha = V_\alpha + \partial_\rho Y_{\mu\rho\mu\alpha}$ [118].

Group theoretical relations imply that the general form of the special conformal current is [118, 153]

$$C_{\alpha\beta} = (2x_\beta x_\nu - x^2\delta_{\beta\nu})\theta_{\alpha\nu} - 2x_\beta(V_\alpha - j_\alpha) + 2L_{\alpha\beta} \ , \tag{4.13}$$

where j_α is a conserved current, satisfying $\partial_\alpha j_\alpha = 0$. Conformal invariance requires $\partial_\alpha C_{\alpha\beta} = 0$ and, therefore,

$$\theta_{\alpha\alpha} = \partial_\alpha V_\alpha \quad \text{and} \qquad V_\alpha = j_\alpha + \partial_\beta L_{\alpha\beta} \ . \tag{4.14}$$

Eq. (4.14) is again invariant under the choice of a different improved energy-momentum tensors, because the redefinition $\theta_{\alpha\beta} \to \theta_{\alpha\beta} + \partial_\rho\partial_\sigma Y_{\sigma\alpha\rho\beta}$ can be absorbed by redefining $V_\alpha \to V'_\alpha$ and $L_{\alpha\beta} \to L'_{\alpha\beta} = L_{\alpha\beta} + Y_{\mu\alpha\mu\beta}$ [118]. If all conditions for conformal invariance are satisfied, it is possible to choose an improved energy-momentum tensor which is traceless, by choosing [118]

$$\begin{aligned} Y_{\sigma\alpha\rho\beta} = {} & \frac{1}{D-2}\left(L_{\alpha\rho}\delta_{\sigma\beta} + L_{\sigma\beta}\delta_{\alpha\rho} - L_{\sigma\rho}\delta_{\alpha\beta} - L_{\alpha\beta}\delta_{\sigma\rho}\right) \\ & + \frac{1}{(D-1)(D-2)}(\delta_{\sigma\rho}\delta_{\alpha\beta} - \delta_{\alpha\rho}\delta_{\sigma\beta})L_{\gamma\gamma} \ . \end{aligned} \tag{4.15}$$

For $D = 2$, the expression (4.15) is not valid. If $L_{\alpha\beta}$ is proportional to the identity matrix, $L_{\alpha\beta} = L\delta_{\alpha\beta}$, it is possible to recover a traceless improved energy-momentum tensor by choosing $Y_{\sigma\alpha\rho\beta} = -(\delta_{\sigma\rho}\delta_{\alpha\beta} - \delta_{\alpha\rho}\delta_{\sigma\beta})L$. If this is the case, it

can be shown that the theory is invariant under the infinite-dimensional group of holomorphic functions in the complex plane [117, 118, 147]. If, instead, $L_{\alpha\beta}$ cannot be written as $L\delta_{\alpha\beta}$, the energy-momentum tensor cannot be made traceless. In this case, the model is invariant only under Möbius transformations: despite being two-dimensional it behaves, from the point of view of the conformal symmetry, as a higher-dimensional system [118, 147].

The conditions relating symmetries to the structure of the energy-momentum tensor can be understood more intuitively by returning to the definition (4.8) [15, 79, 151]. The expression for the variation of the action remains valid if we replace $T_{\alpha\beta}$ with any improved energy-momentum tensor, because after integration by parts $-\int \mathrm{d}^D \partial_\alpha T_{\alpha\beta}\epsilon_\beta$, the improvement terms drop from $\partial_\alpha T_{\alpha\beta}$, even when the equations of motion are not satisfied. If $\theta_{\alpha\beta}$ is symmetric, the variation of the action vanishes when $\partial_\alpha \epsilon_\beta$ is antisymmetric. This corresponds to rotational invariance. If $\theta_{\alpha\alpha} = \partial_\alpha V_\alpha$ is a total first derivative, then $\delta S = 0$ for $\epsilon_\alpha = \epsilon x_\alpha$. This leads to scale invariance. Conformal invariance requires $\theta_{\alpha\beta}$ to be symmetric and the trace $\theta_{\alpha\alpha}$ to be a total *second* derivative $\theta_{\alpha\alpha} = \partial_\alpha \partial_\beta L_{\alpha\beta}$. If this is the case, the action remains invariant under an infinitesimal transformation with $\epsilon_\alpha = 2x_\alpha x_\beta - x^2\delta_{\alpha\beta}$, as it can be checked by direct calculation.

4.4 SCALE VS. CONFORMAL INVARIANCE IN LINEAR ELASTICITY THEORIES

Before examining the interacting fixed points of membrane theory, it is interesting to examine the membrane and the GCI model at the level of a linearized free-field approximation. For membrane theory, the harmonic approximation to the Hamiltonian (2.27) reads[9]:

$$\mathcal{H}^{(2)} = \frac{1}{2}\int \mathrm{d}^D x \left[(\partial^2 \mathbf{h})^2 + (\lambda_0 + \mu_0)(\partial_\alpha u_\alpha)^2 + \mu_0 \partial_\alpha u_\beta \partial_\alpha u_\beta\right] \ . \tag{4.16}$$

Fluctuations of $\mathbf{h}$ are thus described by the free bi-harmonic model $H^{(\mathbf{h})} = \int \mathrm{d}^D x (\partial^2 \mathbf{h})^2/2$. It can be shown that this model is conformally-invariant in general dimension[10]. An explicit calculation, in fact, shows that the theory admits a symmetric energy-momentum tensor with trace

$$\theta^{(\mathbf{h})}_{\alpha\alpha} = \frac{1}{2}(4-D)(\partial^2 \mathbf{h})^2 = \frac{1}{2}(4-D)\left[\mathbf{h}\cdot\partial^2\partial^2\mathbf{h} + \partial_\alpha\partial_\beta L_{\alpha\beta}\right] \ , \tag{4.17}$$

and $L_{\alpha\beta} = 2(\partial_\alpha \mathbf{h}\cdot\partial_\beta\mathbf{h}) - \delta_{\alpha\beta}(\partial_\gamma\mathbf{h}\cdot\partial_\gamma\mathbf{h}) - \delta_{\alpha\beta}(\mathbf{h}\cdot\partial^2\mathbf{h})$. This form is consistent with that expected for a conformal theory [147]: the trace can be reduced to a

9 In order to simplify the notation, we drop the bar symbols in $\bar{\mathbf{h}}$ and $\bar{u}$. Throughout the exposition, $\mathbf{h}$ and u_α denote fields after the rescalings $\mathbf{h} \to \sqrt{T/\kappa}\mathbf{h}$, $u_\alpha \to T/\kappa u_\alpha$.

10 See Ref. [155] for a detailed analysis of the biharmonic theory in integer dimensions and Ref. [147] for an application to 2D elasticity theory.

total second derivative, up to the term $\mathbf{h}\cdot\partial^2\partial^2\mathbf{h}$, which vanishes with the equation of motion $\partial^2\partial^2\mathbf{h}=0$ and can be identified as the generator of local field rescaling. Since $L_{\alpha\beta}\neq\delta_{\alpha\beta}L$, the biharmonic theory in dimension $D=2$ is invariant under the global conformal group but not under the infinite Virasoro symmetry [147].

The theory for u_α fluctuations,

$$\mathcal{H}^{(u)}=\frac{1}{2}\int \mathrm{d}^D x[(\lambda_0+\mu_0)(\partial_\alpha u_\alpha)^2+\mu_0\partial_\alpha u_\beta\partial_\alpha u_\beta] \tag{4.18}$$

is the well-known theory of linear isotropic elastic media. As it was shown in Refs. [103, 130], this model provides a physical realization of a scale-invariant but nonconformal field theory.

An explicit calculation shows the improved symmetric energy-momentum tensor $\theta_{\alpha\beta}$ has trace $\theta_{\alpha\alpha}=\partial_\alpha V_\alpha$,

$$V_\alpha=\frac{1}{2}(D\lambda_0+(D+2)\mu_0)u_\alpha\partial_\gamma u_\gamma-\frac{1}{2}(D-2)\mu_0 u_\gamma\partial_\alpha u_\gamma-\mu_0 u_\gamma\partial_\gamma u_\alpha\ , \tag{4.19}$$

up to terms which vanish when the equation of motion $-(\lambda_0+\mu_0)\partial_\alpha\partial_\beta u_\beta-\mu_0\partial^2 u_\alpha=0$ is satisfied. For generic λ_0 and μ_0, the virial current cannot be reduced to the form $V_\alpha=j_\alpha+\partial_\beta L_{\alpha\beta}$, with $\partial_\alpha j_\alpha=0$, implying the absence of conformal invariance. This lack of symmetry manifests itself in a the form of correlation functions, which, despite being scale-invariant, violate the more restrictive conformal selection rules [103, 130].

Conformal symmetry is however recovered when elastic constants are adjusted to special values. If $D\lambda_0+(D+4)\mu_0=0$, the virial current reduces to the form $V_\alpha=\partial_\beta L_{\alpha\beta}$, and the model becomes conformal. The corresponding model is unphysical as an elasticity theory, being outside of the stability region $\mu_0\geq 0$, $B_0=\lambda_0+2\mu_0/D\geq 0$, but it is relevant as a gauge-fixed electrodynamics [130].

For $\lambda_0+\mu_0=0$ another, "twisted", form of conformal invariance appears. In this case, the symmetry of the theory is enhanced from O(D) to O(D)×O(D), and we can choose to regard u_α as a set of scalar fields rather than a vector field [103, 132]. The Hamiltonian then describes D copies of a free scalar field, and can be shown to be conformal in arbitrary dimension[11,12]. For $D=2$, the condition $\lambda_0+\mu_0=0$ also corresponds to a vanishing physical bulk modulus $\lambda_0+2\mu_0/D$. Thus, the model exhibits in addition to the twisted invariance, also the embedding-space conformal invariance discussed in Sec. 4.2.

11 The virial current in Eq. (4.19) is not valid for the twisted model. In fact, Eq. (4.19) was derived by including improvement terms needed to make $\theta_{\alpha\beta}$ symmetric. If $\lambda_0+\mu_0=0$ and u_μ is assumed to transform as a scalar, $\theta_{\alpha\beta}$ is already symmetric and the improvement must not be performed [103].

12 The possibility to promote u_α to a collection of scalars is destroyed in the nonlinear membrane model since the form of the strain tensor $(\partial_\alpha u_\beta+\partial_\beta u_\alpha+\partial_\alpha\mathbf{h}\cdot\partial_\beta\mathbf{h})/2$ forces the components of u_α to transform as a vector field.

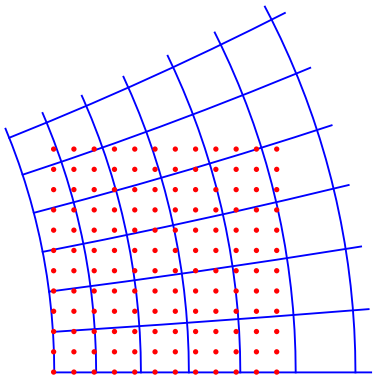

Figure 4.2: Generalization of a Kadanoff-Wilson spin-block renormalization group to a nonuniform coordinate transformation. (Figure adapted from Ref. [79].)

Finally, Ref. [147] showed that in two dimensions the elasticity model for *any* choice of λ_0 and μ_0 presents a hidden conformal symmetry which emerges when displacement fields are represented as gradients of scalar potentials: $u_\alpha = \partial_\alpha \phi + \epsilon_{\alpha\beta}\partial_\beta \omega$, where ϕ and ω are respectively a scalar and a pseudoscalar field. This representation maps Eq. (4.18) to two copies of the biharmonic theory, which is conformal in general dimension. The GCI model analyzed in chapter 3, similarly, reduces to two decoupled biharmonic theories in the non-interacting limit $Y_0 \to 0$.

4.5 SCALE VS. CONFORMAL INVARIANCE IN NONLINEAR MEMBRANE THEORY

The analysis of scale and conformal invariance in interacting quantum field theories and statistical models is made complex by the very nontrivial way in which these symmetries are realized. Within a Wilson scaling picture [13, 14, 16], scale invariance emerges when the process of coarse graining degrees of freedom reaches a fixed point. An adaptation of the same method to the case of conformal invariance consists in a generalization of the Kadanoff block method to a nonuniform renormalization group transformation [79, 119]. Considering the example of the Ising model at the critical point, a non-uniform RG scaling can be visualized similarly to Fig. 4.2 [79, 119]. The procedure of considering groups of spins forming collective block variables is generalized to blocks of nonequal size, following the coordinate transformation encoded in a conformal map.

Direct implementations of nonuniform RG transformations have been studied extensively using nonperturbative techniques [137, 140, 156], although usually via methods which employ a smooth cutoff instead of a block scaling approach. Nonuni-

form renormalization group equations have also been explored in perturbative settings [157], by analyzing field theories with space-dependent coupling constants.

In this work we use, in analogy with other quantum field theory and statistical mechanics problems [138, 139, 145], a method based on the analysis of Ward identities in perturbation theory, which has the technical advantage of acting directly in a continuum space.

4.5.1 *Energy-momentum tensor and bare Ward identities*

The improved energy-momentum tensor, calculated directly from the Hamiltonian (2.27) reads[13,14]

$$\begin{aligned}\theta_{\alpha\beta} = &-\frac{1}{2}\delta_{\alpha\beta}\left[(\partial^2\mathbf{h})^2 + \lambda_0(u_{\gamma\gamma})^2 + 2\mu_0 u_{\gamma\delta}u_{\gamma\delta}\right] \\ &+ 2\partial_\alpha\partial_\beta\mathbf{h}\cdot\partial^2\mathbf{h} - \partial_\alpha\mathbf{h}\cdot\partial_\beta\partial^2\mathbf{h} - \partial_\beta\mathbf{h}\cdot\partial_\alpha\partial^2\mathbf{h} \\ &+ \frac{1}{D-1}\left[\delta_{\alpha\beta}\partial_\gamma\mathbf{h}\cdot\partial_\gamma\partial^2\mathbf{h} + \delta_{\alpha\beta}\partial_\gamma\partial_\delta\mathbf{h}\cdot\partial_\gamma\partial_\delta\mathbf{h}\right. \\ &\left.+ (D-2)\partial_\gamma\mathbf{h}\cdot\partial_\alpha\partial_\beta\partial_\gamma\mathbf{h} - D\partial_\alpha\partial_\gamma\mathbf{h}\cdot\partial_\beta\partial_\gamma\mathbf{h}\right] \\ &+ 2\lambda_0 u_{\gamma\gamma}u_{\alpha\beta} + 4\mu_0 u_{\alpha\gamma}u_{\beta\gamma} - \frac{1}{2}(E_\alpha u_\beta + E_\beta u_\alpha) \\ &+ \lambda_0\partial_\gamma\left[(\delta_{\alpha\beta}u_\gamma - \delta_{\beta\gamma}u_\alpha - \delta_{\alpha\gamma}u_\beta)u_{\delta\delta}\right] \\ &+ 2\mu_0\partial_\gamma\left[u_\gamma u_{\alpha\beta} - u_\alpha u_{\beta\gamma} - u_\beta u_{\alpha\gamma}\right] \ .\end{aligned} \tag{4.20}$$

It is symmetric and locally conserved reflecting the rotational and translational invariance of the continuum medium. The conservation law for $\theta_{\alpha\beta}$ reads

$$\partial_\alpha\theta_{\alpha\beta} = -\mathbf{E}\cdot\partial_\beta\mathbf{h} - E_\alpha\partial_\beta u_\alpha - \frac{1}{2}\partial_\alpha(E_\beta u_\alpha - E_\alpha u_\beta) \tag{4.21}$$

13 In order to obtain an improved energy-momentum tensor which is symmetric for any values of the fields, also off-shell (without the use of equations of motion), we define $\theta_{\alpha\beta}$ as the response of the Hamiltonian to the infinitesimal transformation $\mathbf{h}(\mathbf{x}) \to \mathbf{h}'(\mathbf{x}) = \mathbf{h}(\mathbf{x}')$, $u_\alpha(\mathbf{x}) \to u'_\alpha(\mathbf{x}) = \left(\delta_{\alpha\beta} + (\partial_\alpha\epsilon_\beta - \partial_\beta\epsilon_\alpha)/2\right) u_\beta(\mathbf{x}')$, $x_\alpha \to x'_\alpha = x_\alpha + \epsilon_\alpha$, including a local rotation of u_α in reaction to the antisymmetric part of $\partial_\alpha\epsilon_\beta$. For this reason the conservation law, Eq. (4.21), includes the term $-\partial_\alpha(E_\beta u_\alpha - E_\alpha u_\beta)/2$, an operator which, inserted in correlation functions, acts as a generator for local rotations of the u_α field (see Eqs. (4.27), (4.28)).

14 The Hamiltonian $\mathcal{H}$ plays in the statistical mechanical problem the role of the action in quantum field theory. The energy-momentum tensor of quantum field theory becomes the generator of local translations with respect to the internal coordinate $\mathbf{x}$. Using a standard terminology, we refer to $\theta_{\alpha\beta}$ as the "energy-momentum tensor" although it does not describe the densities and current of mechanical energy and momentum in the membrane but, rather, the conserved current associated with the symmetry under translations $\mathbf{x} \to \mathbf{x} + \mathbf{a}$ in the internal space.

where

$$\begin{aligned}\mathbf{E} &= \frac{\delta\mathcal{H}}{\delta\mathbf{h}} = \partial^2\partial^2\mathbf{h} - \partial_\alpha(\lambda_0 u_{\beta\beta}\partial_\alpha\mathbf{h} + 2\mu_0 u_{\alpha\beta}\partial_\beta\mathbf{h}) \ , \\ E_\alpha &= \frac{\delta\mathcal{H}}{\delta u_\alpha} = -\lambda_0\partial_\alpha u_{\beta\beta} - 2\mu_0\partial_\beta u_{\alpha\beta} \ ,\end{aligned} \tag{4.22}$$

are the equations of motion of the $\mathbf{h}$ and the u_α field. (Using a terminology of quantum field theory we refer to the functional derivatives $\mathbf{E}$ and E_α as "equations of motion" meaning that $\mathbf{E} = 0$ and $E_\alpha = 0$ would be the equations of motion in a classical setting, governed by the principle of least action. In this case $\mathbf{E} = 0$ and $E_\alpha = 0$ are the mechanical Föppl-von Karman equations giving the conditions of energy minimization).

At finite temperature, due to statistical fluctuations, $\mathbf{E}$ and E_α cannot be set to zero, because the system explores the entire phase space, not only the minimum energy state. The operators $\mathbf{E} = \delta\mathcal{H}/\delta\mathbf{h}$ and $E_\alpha = \delta\mathcal{H}/\delta u_\alpha$ however become promoted to differential operators generating the Dyson-Schwinger equations of motion[15] [15]

$$\left[\mathbf{J}(\mathbf{x}) - \frac{\delta\mathcal{H}}{\delta\mathbf{h}(\mathbf{x})}\left(\frac{\delta}{\delta\mathbf{J}}, \frac{\delta}{\delta j_\alpha}\right)\right]\mathcal{Z}[\mathbf{J}(\mathbf{x}), j_\alpha(\mathbf{x})] = 0 \ , \tag{4.23}$$

$$\left[j_\alpha(\mathbf{x}) - \frac{\delta\mathcal{H}}{\delta u_\alpha(\mathbf{x})}\left(\frac{\delta}{\delta\mathbf{J}}, \frac{\delta}{\delta j_\alpha}\right)\right]\mathcal{Z}[\mathbf{J}(\mathbf{x}), j_\alpha(\mathbf{x})] = 0 \ , \tag{4.24}$$

for the generalized partition function

$$\mathcal{Z}[\mathbf{J}(\mathbf{x}), j_\alpha(\mathbf{x})] = \int [\mathrm{d}\mathbf{h}(\mathbf{x})][\mathrm{d}u_\alpha(\mathbf{x})] \exp\left[-\mathcal{H} + \int \mathrm{d}^D\big(\mathbf{J}\cdot\mathbf{h} + j_\alpha u_\alpha\big)\right] \ , \tag{4.25}$$

which generates correlation functions

$$\begin{aligned}&\langle h_{i_1}(\mathbf{x}_1)..h_{i_n}(\mathbf{x}_n)u_{\alpha_1}(\mathbf{x}'_1)..u_{\alpha_\ell}(\mathbf{x}'_\ell)\rangle \\ &= \frac{\delta}{\delta J_{i_1}(\mathbf{x}_1)}..\frac{\delta}{\delta J_{i_1}(\mathbf{x}_n)}\frac{\delta}{\delta j_{\alpha_1}(\mathbf{x}'_1)}..\frac{\delta}{\delta j_{\alpha_\ell}(\mathbf{x}'_\ell)}\mathcal{Z}[\mathbf{J}(\mathbf{x}), j_\alpha(\mathbf{x})]\Big|_{\mathbf{J}=0, j_\alpha=0} \ .\end{aligned} \tag{4.26}$$

15 As a remark, note that the expressions (4.23)–(4.31) are only formal, because the correlation functions of $\mathbf{h}(\mathbf{x})$ and $u_\alpha(\mathbf{x})$ in real space does not exist for $D < 4$. However, the expressions become defined if we consider correlation functions of gradients $\partial_\alpha\mathbf{h}$ and $\partial_\alpha u_\beta$.

Adapting standard field theoretical methods [15, 138, 139] it can then be shown that the connected correlation functions with insertions of the composite operators $\mathbf{E}\cdot\partial_\beta\mathbf{h}$, $E_\alpha\partial_\beta u_\alpha$, $E_\beta u_\alpha$, and $\mathbf{E}\cdot\mathbf{h}$ are respectively given by[16]

$$\begin{aligned} G_{\mathbf{E}(\mathbf{x})\cdot\partial_\beta\mathbf{h}(\mathbf{x})} &= \langle\langle h_{i_1}(\mathbf{x}_1)...h_{i_n}(\mathbf{x}_n)u_{\alpha_1}(\mathbf{x}'_1)...u_{\alpha_2}(\mathbf{x}'_\ell)\mathbf{E}(\mathbf{x})\cdot\partial_\beta\mathbf{h}(\mathbf{x})\rangle\rangle = \\ &= \sum_{a=1}^{n}\delta(\mathbf{x}-\mathbf{x}_a)\frac{\partial}{\partial x_{a\beta}}\langle\langle h_{i_1}(\mathbf{x}_1)...h_{i_n}(\mathbf{x}_n)u_{\alpha_1}(\mathbf{x}'_1)...u_{\alpha_2}(\mathbf{x}'_\ell)\rangle\rangle\ , \\ G_{E_\alpha(\mathbf{x})\partial_\beta u_\alpha(\mathbf{x})} &= \langle\langle h_{i_1}(\mathbf{x}_1)...h_{i_n}(\mathbf{x}_n)u_{\alpha_1}(\mathbf{x}'_1)...u_{\alpha_2}(\mathbf{x}'_\ell)E_\alpha(\mathbf{x})\partial_\beta u_\alpha(\mathbf{x})\rangle\rangle = \\ &= \sum_{b=1}^{\ell}\delta(\mathbf{x}-\mathbf{x}'_b)\frac{\partial}{\partial x'_{b\beta}}\langle\langle h_{i_1}(\mathbf{x}_1)...h_{i_n}(\mathbf{x}_n)u_{\alpha_1}(\mathbf{x}'_1)...u_{\alpha_2}(\mathbf{x}'_\ell)\rangle\rangle\ , \end{aligned} \tag{4.27}$$

$$\begin{aligned} &G_{E_\beta(\mathbf{x})u_\alpha(\mathbf{x})i_1..i_n\alpha_1..\alpha_\ell}(\mathbf{x}_1..\mathbf{x}_n\mathbf{x}'_1..\mathbf{x}'_\ell) \\ &= \sum_{b=1}^{\ell}\delta(\mathbf{x}-\mathbf{x}'_b)\delta_{\beta\alpha_b}G_{i_1..i_n\alpha_1..\alpha_{b-1}\alpha\alpha_{b+1}..\alpha_\ell}(\mathbf{x}_1..\mathbf{x}_n\mathbf{x}'_1..\mathbf{x}'_\ell)\ , \end{aligned} \tag{4.28}$$

$$\begin{aligned} &G_{\mathbf{E}(\mathbf{x})\cdot\mathbf{h}(\mathbf{x})i_1..i_n\alpha_1..\alpha_\ell}(\mathbf{x}_1..\mathbf{x}_n\mathbf{x}'_1..\mathbf{x}'_\ell) \\ &\qquad = \sum_{a=1}^{n}\delta(\mathbf{x}-\mathbf{x}_a)G_{i_1..i_n\alpha_1..\alpha_\ell}(\mathbf{x}_1..\mathbf{x}_n\mathbf{x}'_1..\mathbf{x}'_\ell)\ . \end{aligned} \tag{4.29}$$

Using these relations, the conservation laws of the energy-momentum tensor $\partial_\alpha\theta_{\alpha\beta}$ and of the angular momentum current $M_{\alpha,\beta\gamma} = x_\gamma\theta_{\alpha\beta} - x_\beta\theta_{\alpha\gamma}$ become Ward identities expressing the translational and rotational invariance of all correlation functions.

The dilatation Ward identity [138] can be expressed by inserting the divergence $\partial_\alpha S_\alpha$ of the scale current $S_\alpha = x_\beta\theta_{\alpha\beta} - V_\alpha$ in correlation functions and by integrating over all space. Dropping boundary terms and using Eqs. (4.27) gives

$$\begin{aligned} 0 &= \int \mathrm{d}^D x\ G_{\partial_\alpha S_\alpha(\mathbf{x})i_1..i_n\alpha_1..\alpha_\ell}(\mathbf{x}_1..\mathbf{x}_n\mathbf{x}'_1..\mathbf{x}'_\ell) \\ &= \int \mathrm{d}^D x\ G_{\theta_{\alpha\alpha}(\mathbf{x})i_1..i_n\alpha_1..\alpha_\ell}(\mathbf{x}_1..\mathbf{x}_n\mathbf{x}'_1..\mathbf{x}'_\ell) \\ &- \left[\sum_{a=1}^{n}x_{a\beta}\frac{\partial}{\partial x_{a\beta}} + \sum_{b=1}^{\ell}x_{b\beta}\frac{\partial}{\partial x_{b\beta}}\right]G_{i_1..i_n\alpha_1..\alpha_\ell}(\mathbf{x}_1..\mathbf{x}_n\mathbf{x}'_1..\mathbf{x}'_\ell)\ . \end{aligned} \tag{4.30}$$

16 To shorten the notation, we introduced the connected Green function $G_{i_1..i_n\alpha_1...\alpha_\ell}(\mathbf{x}_1..\mathbf{x}_n,\mathbf{x}'_1..\mathbf{x}'_\ell) = \langle\langle h_{i_1}(\mathbf{x}_1)..\mathbf{h}_{i_n}(\mathbf{x}_n)u_{\alpha_1}(\mathbf{x}'_1)..u_{\alpha_\ell}(\mathbf{x}'_\ell)\rangle\rangle$. The Green functions with operator insertions $G_{\mathcal{O}(\mathbf{x})i_1..i_n\alpha_1..\alpha_\ell}(\mathbf{x}_1..\mathbf{x}_n\mathbf{x}'_1..\mathbf{x}'_\ell)$ are written shortly as $G_\mathcal{O}$ suppressing the index and coordinate dependences.

A similar identity can be derived using the space part $C'_{\alpha\beta} = (2x_\beta x_\nu - x^2\delta_{\beta\nu})\theta_{\alpha\nu}$ of the conformal current $C_{\alpha\beta}$. Inserting $\partial_\alpha C'_{\alpha\beta}$ in correlation functions, dropping boundary terms, and using Eqs. (4.27) gives

$$\begin{aligned}
&\int \mathrm{d}^D x \; 2x_\beta G_{\theta_{\alpha\alpha}(\mathbf{x})i_1..i_n\alpha_1..\alpha_\ell}(\mathbf{x}_1..\mathbf{x}_n\mathbf{x}'_1..\mathbf{x}'_\ell) \\
&- \Bigg[\sum_{a=1}^{n}(2x_{a\nu}x_{a\beta} - \delta_{\nu\beta}x_a^2)\frac{\partial}{\partial x_{a\nu}} \\
&+ \sum_{b=1}^{\ell}(2x_{b\nu}x_{b\beta} - \delta_{\nu\beta}x_b^2)\frac{\partial}{\partial x_{b\nu}}\Bigg] G_{i_1..i_n\alpha_1..\alpha_\ell}(\mathbf{x}_1..\mathbf{x}_n\mathbf{x}'_1..\mathbf{x}'_\ell) = 0 \ ,
\end{aligned} \tag{4.31}$$

relation which describes the response to a conformal change of coordinates [138, 139]. If the terms $G_{\theta_{\alpha\alpha}}$ and $G_{x_\beta\theta_{\alpha\alpha}}$ vanish up to equations of motion, the Ward identities (4.30) and (4.31) express scale and conformal invariance respectively. The terms proportional to equations of motion then act as generators specifying the way in which fields transform under conformal transformations[17].

4.5.2 *Renormalization*

The model for finite values of the coupling constants λ_0 and μ_0 cannot be neither conformal nor scale invariant. The reason is that the coupling constants are dimensionful, with dimension $\{\lambda_0\} = \{\mu_0\} = \varepsilon$ and thus introduce a characteristic length in the problem. This length is the Ginzburg scale discussed in Sec. 2.9. For $q \gg q_G \approx \mu_0^{1/\varepsilon}$ the correlation functions are approximately given by the harmonic approximation. For $q \ll q_G$, instead, the anomalous power-law behaviors emerge. Exact scale invariance thus emerges in the limit $q \to 0$ or equivalently in the limit of infinitely large elastic constants[18]. This creates difficulties in interpreting the Ward identities order by order in an expansion which uses λ_0 and μ_0 as small coupling constants.

A further difficulty is that the perturbative expansion in powers of λ_0 and μ_0 is infrared divergent and thus is only defined in an infinitesimal neighbourhood of

17 In scalar field theory, for example, $\theta_{\alpha\alpha}$ contains a term proportional to $\eta\phi\delta S/\delta\phi$ which acts as the generator of a field rescaling [138]. This term shows that the field transforms with an anomalous dimension under scale and conformal transformations.

18 In presence of an ultraviolet cutoff Λ we expect, in analogy with critical phenomena [14, 15, 101, 105, 158], that scale invariance emerges when λ_0 and μ_0 are of order Λ^ε, with numerical prefactors of order ε fine-tuned in such way to cancel the leading corrections to scaling. Since we consider a theory without a cutoff, scale invariance requires instead λ_0, $\mu_0 \to \infty$. This limiting procedure (working without a cutoff and taking the infinite coupling limit) corresponds to a model with $\lambda_0^{1/\varepsilon}, \mu_0^{1/\varepsilon} \ll \Lambda$, observed at scales $|\mathbf{k}| \ll \lambda_0^{1/\varepsilon}, \mu_0^{1/\varepsilon}$ much smaller than the Ginzburg wavevector. For discussions on this limit in the massive scalar field theory and its relation to the critical Ginzburg-Landau theory see for example Refs. [15, 16, 150].

$D = 4$. The IR divergences disappear in the ε-expansion, where they are replaced by logarithmic corrections [15]. However, the limit $D \to 4$ generates ultraviolet divergences which appear as poles in $1/\varepsilon$ [15, 81].

The energy-momentum tensor $\theta_{\alpha\beta}$ is almost free of ultraviolet infinities because its divergence $\partial_\alpha \theta_{\alpha\beta}$, Eq. (4.21), is proportional to the equations of motion and can be shown to remain finite also as $D \to 4$. The only counterterm needed to make $\theta_{\alpha\beta}$ finite takes the form of a symmetric improvement term $\partial_\rho \partial_\rho Y_{\alpha\sigma\beta\rho}$, which has an identically zero derivative [15, 118, 123, 159]. This term does not affect conservation laws and Ward identities, and thus is unimportant for the analysis of scale and conformal invariance. However, although the expression (4.20) is a priori finite, its building blocks are unrenormalized coupling constants and unrenormalized operators, both of which are divergent for $\varepsilon \to 0$.

Following Refs. [120, 121, 138, 139], we thus re-express the energy-momentum tensor (4.20) in terms of renormalized composite fields defined by subtracting ultraviolet divergences (poles in ε). Since we are interested only in scale and conformal invariance, which are encoded in the trace $\theta_{\alpha\alpha}$, it is sufficient to renormalize scalar composite fields. The renormalization procedure results in an expansion of $\theta_{\alpha\alpha}$ in a basis of renormalized operators, $[(u_{\alpha\alpha})^2]$, $[u_{\alpha\beta}u_{\alpha\beta}]$, $[u_\alpha u_{\beta\beta}]$, and $[u_\beta u_{\alpha\beta}]$.

As shown in appendices 4.A and 4.B the relation between the bare fields $u_{\alpha\beta}$, $u_{\alpha\alpha}$, $(\partial^2\mathbf{h})^2$, $u_\alpha u_{\beta\beta}$, $u_\beta u_{\alpha\beta}$ and the corresponding renormalized operators is almost completely determined by the RG functions β_λ, β_μ, η, and by amplitude and coupling renormalizations (Z, g_λ and g_μ) which can be calculated from correlation functions *without* operator insertions[19].

In particular, we can obtain relations for two distinct types of operators. A first type is the group of composite fields $\mathcal{O}_1 = (\partial^2\mathbf{h})^2/2 + \lambda_0(u_{\alpha\alpha})^2 + 2\mu_0 u_{\alpha\beta}u_{\alpha\beta}$, $\mathcal{O}_2 = \lambda_0(u_{\alpha\alpha})^2/2$, $\mathcal{O}_3 = \mu_0 u_{\alpha\beta}u_{\alpha\beta}$, $\mathcal{O}_4 = \partial^2 u_{\alpha\alpha}$, $\mathcal{O}_5 = \partial_\alpha\partial_\beta u_{\alpha\beta}$, $\mathcal{O}_6 = u_{\alpha\alpha}$, which are invariant under all symmetries of the Hamiltonian. For these operators, the analysis is closely analogue to derivations in Ref. [138] (see appendix 4.A) and shows that the bulk part of the trace $\theta_{\alpha\alpha}$ is proportional to the RG beta functions.

A second type is constituted by the operators $u_\alpha u_{\beta\beta}$ and $u_\beta u_{\alpha\beta}$, which break the shift symmetry $u_\alpha \to u_\alpha + B_\alpha$ and the invariance under the approximate embedding-space rotations defined in Eq. (2.29). As shown in appendix 4.B, their explicit renormalization relation reads (in a non-minimal scheme):

$$\begin{aligned} u_\alpha u_{\beta\beta} = {} & \frac{M^\varepsilon(D\tilde{\lambda} + 2\tilde{\mu})}{D\lambda_0 + 2\mu_0}[u_\alpha u_{\beta\beta}] \\ & + b_1\partial_\alpha[\partial_\beta\mathbf{h}\cdot\partial_\beta\mathbf{h}] + b_2\partial_\beta[\partial_\alpha\mathbf{h}\cdot\partial_\beta\mathbf{h}] + b_3\partial^2[u_\alpha] + b_4\partial_\alpha\partial_\beta[u_\beta] \ , \end{aligned} \tag{4.32}$$

19 These renormalizations have been discussed in Sec. 2.5.3.

$$u_\beta u_{\alpha\beta} - \frac{1}{D} u_\alpha u_{\beta\beta} = \frac{M^\varepsilon \tilde{\mu}}{\mu_0} \left\{ [u_\beta u_{\alpha\beta}] - \frac{1}{D} [u_\alpha u_{\beta\beta}] \right\} + b_1' \partial_\alpha [\partial_\beta \mathbf{h} \cdot \partial_\beta \mathbf{h}] + b_2' \partial_\beta [\partial_\alpha \mathbf{h} \cdot \partial_\beta \mathbf{h}] + b_3' \partial^2 [u_\alpha] + b_4' \partial_\alpha \partial_\beta [u_\beta] \ . \tag{4.33}$$

where b_k and b_k', $k = 1, .., 4$ are ultraviolet divergent coefficients. These relations can be interpreted as 'non-renormalizations', in the sense that the product of bare couplings with bare operators is equal to the product of renormalized couplings and renormalized operators. Eqs. (4.32) and (4.33) are much simpler than the general relations expected by symmetry and power counting: counterterms with the schematic form u^3 are absent and mixing of operators of the type $u(\partial \mathbf{h} \cdot \partial \mathbf{h})$ and $u \partial u$ is exactly determined in terms of the elementary renormalization constants Z, g_λ, and g_μ. Although appendix 4.B presents a more complete proof, the particular simplicity of the renormalization relations can be directly understood from the structure of Feynman rules: in almost any diagram, we can factorize a power of the momentum of each external line. Diagrammatic corrections, therefore, tend to be shift-symmetric even if the inserted operators $u_\alpha u_{\beta\beta}$ and $u_\beta u_{\alpha\beta}$ are not. This, in particular, protects the 'diagonal' renormalization (the generation of counterterms proportional to the inserted composite fields $u_\alpha u_{\beta\beta}$ and $u_\beta u_{\alpha\beta}$) and implies the simple normalization formulas (4.32) and (4.33). A similar non-renormalization property associated with shift invariance occurs in Galileon theories [114].

For the following analysis, it is also useful to note that the composite operator $E_\alpha h^2$ is not renormalized: $[E_\alpha h^2] = E_\alpha h^2$. In fact, power counting shows that the product $(\mathbf{h}(\mathbf{x}) \cdot \mathbf{h}(\mathbf{x}))$ at coincident points does not generate UV divergences. As a result $[h^2] = \tilde{\mathbf{h}} \cdot \tilde{\mathbf{h}} = Z^{-1} h^2$, where Z is the field-amplitude renormalization. On the other hand, $E_\alpha(\mathbf{x}') h^2(\mathbf{x}')$ is a redundant operator which vanishes with equations of motion and acts as the infinitesimal generator of the field redefinition $u_\beta(\mathbf{x}) \to u_\beta(\mathbf{x}) - \epsilon \delta_{\alpha\beta} \delta(\mathbf{x} - \mathbf{x}') h^2(\mathbf{x})$. Since u_α renormalizes as $\tilde{u}_\alpha = Z^{-1} u_\alpha$, insertion of $E_\alpha(\mathbf{x}') h^2(\mathbf{x}')$ can be equivalently represented as the generator of the infinitesimal transformation $\tilde{u}_\alpha(\mathbf{x}) \to \tilde{u}_\alpha(\mathbf{x}) - \epsilon \delta_{\alpha\beta} \delta(\mathbf{x} - \mathbf{x}') [h^2(\mathbf{x})]$, which is finite and, thus, does not require subtractions.

Collecting results, we obtain the following equivalent expressions for the trace $\theta_{\alpha\alpha}$:

$$\begin{aligned} \theta_{\alpha\alpha} &= (\varepsilon - \eta) \left(\frac{1}{2} (\partial^2 \mathbf{h})^2 + \lambda_0 (u_{\alpha\alpha})^2 + \mu_0 u_{\alpha\beta} u_{\alpha\beta} \right) - E_\alpha u_\alpha \\ &\quad + \frac{1}{2} \beta_\lambda M^\varepsilon \left[(u_{\alpha\alpha})^2 \right] + \beta_\mu M^\varepsilon [u_{\alpha\beta} u_{\alpha\beta}] + ((D-2)\lambda_0 + 2\mu_0) \partial_\alpha (u_\alpha u_{\beta\beta}) \\ &\quad - 4\mu_0 \partial_\alpha (u_\beta u_{\alpha\beta}) + a_1 \partial^2 u_{\alpha\alpha} + a_2 \partial_\alpha \partial_\beta u_{\alpha\beta} \\ &= -\frac{(\eta - \varepsilon)}{2} \mathbf{E} \cdot \mathbf{h} - (1 + \eta - \varepsilon) E_\alpha u_\alpha \\ &\quad + \frac{1}{2} \beta_\lambda M^\varepsilon [(u_{\alpha\alpha})^2] + \beta_\mu M^\varepsilon [u_{\alpha\beta} u_{\alpha\beta}] + \partial_\alpha V_\alpha \ , \end{aligned} \tag{4.34}$$

with

$$V_\alpha = -\frac{1}{4}(\eta-\varepsilon)E_\alpha h^2 + ((2-\eta)\lambda_0 + 2\mu_0)u_\alpha u_{\beta\beta} - 2(2+\eta-\varepsilon)\mu_0 u_\beta u_{\alpha\beta} + \frac{1}{2}(\varepsilon-\eta)\partial_\beta\left(-\delta_{\alpha\beta}(\mathbf{h}\cdot\partial^2\mathbf{h}) + \frac{\lambda_0}{2}\delta_{\alpha\beta}h^2 u_{\gamma\gamma} + \mu_0 h^2 u_{\alpha\beta}\right) + a_1\partial_\alpha u_{\beta\beta} + a_2\partial_\beta u_{\alpha\beta} \tag{4.35}$$

or, after expansion in the basis of renormalized operators $[u_\alpha u_{\beta\beta}]$, $[u_\beta u_{\alpha\beta}]$,

$$\begin{aligned} V_\alpha &= -\frac{1}{4}(\eta-\varepsilon)E_\alpha h^2 + ((2-\eta)\tilde{\lambda} + 2\tilde{\mu})M^\varepsilon[u_\alpha u_{\beta\beta}] \\ &\quad - 2(2+\eta-\varepsilon)\tilde{\mu}M^\varepsilon[u_\beta u_{\alpha\beta}] + \partial_\beta L_{\alpha\beta}\ , \\ L_{\alpha\beta} &= \frac{1}{2}(\varepsilon-\eta)\left[-\delta_{\alpha\beta}\mathbf{h}\cdot\partial^2\mathbf{h} + \frac{1}{2}\lambda_0\delta_{\alpha\beta}h^2 u_{\gamma\gamma} + \mu_0 h^2 u_{\alpha\beta}\right] \\ &\quad + b_1\delta_{\alpha\beta}(\partial_\gamma u_\gamma) + b_2(\partial_\alpha u_\beta + \partial_\beta u_\alpha) + b_3\delta_{\alpha\beta}(\partial_\gamma\mathbf{h}\cdot\partial_\gamma\mathbf{h}) \\ &\quad + b_4(\partial_\alpha\mathbf{h}\cdot\partial_\beta\mathbf{h})\ . \end{aligned} \tag{4.36}$$

In Eqs. (4.34), (4.35), and (4.36), a_1, a_2, and b_i, $(i = 1,..,4)$ are UV-divergent coefficients generated by renormalization[20].

When λ_0 and μ_0 tend to infinity, the renormalized couplings $\tilde{\lambda}$ and $\tilde{\mu}$ remain finite and approach the infrared stable fixed point P_4 (see Sec. 2.5.3). Assuming that in this limit the insertions of renormalized operators remain finite, the terms $\beta_\lambda[(u_{\alpha\alpha})^2]$ and $\beta_\mu[u_{\alpha\beta}u_{\alpha\beta}]$ disappear because the RG flow velocities are equal to zero at the fixed point ($\beta_\lambda = \beta_\mu = 0$).

In this case, the scaling symmetry of the theory, known from RG arguments, becomes manifest and the trace $\theta_{\alpha\alpha}$ becomes a total derivative up to equations of motion. In particular, the dilatation current $S_\alpha = x_\beta\theta_{\alpha\beta} - V_\alpha$ [118] becomes locally conserved, with a conservation law

$$\partial_\alpha S_\alpha = -x_\beta\left(\mathbf{E}\cdot\partial_\beta\mathbf{h} + E_\alpha\partial_\beta u_\alpha\right) - \frac{(\eta_*-\varepsilon)}{2}\mathbf{E}\cdot\mathbf{h} - (1+\eta_*-\varepsilon)E_\alpha u_\alpha\ , \tag{4.37}$$

consistent with the form expected for fields of dimension[21] $\Delta_{\mathbf{h}} = (\eta_*-\varepsilon)/2$ and $\Delta_u = 1+\eta_*-\varepsilon$. More generally it is possible to show that, for general $\tilde{\lambda}$ and $\tilde{\mu}$, the

20 As expected, all renormalization coefficients in Eqs. (4.34) and (4.36) are finite a part from those appearing in $L_{\alpha\beta}$. The reason is that the conservation of the energy-momentum tensor imposes its finiteness up to symmetric improvement terms. These improvement terms are total second derivatives and can be absorbed in $L_{\alpha\beta}$.

21 The dimensionality of a field $\varphi(\mathbf{x})$ is defined as the exponent Δ governing the power-law dependence of the two-point function $\langle\varphi(\mathbf{x})\varphi(\mathbf{x}')\rangle \propto |\mathbf{x}|^{-2\Delta}$. If the two-point function in Fourier space behaves as $\langle\varphi(\mathbf{k})\varphi(-\mathbf{k})\rangle \propto k^{-\sigma}$, the dimension is $\Delta = (D-\sigma)/2$. The renormalization of the bending rigidity $\kappa \to \kappa_{\mathrm{r}}(\mathbf{k}) \propto |\mathbf{k}|^{-\eta_*}$ and of the elastic constants $\lambda, \mu \to \lambda_{\mathrm{r}}(\mathbf{k}), \mu_{\mathrm{r}}(\mathbf{k}) \propto |\mathbf{k}|^{4-D-2\eta_*}$ imply that the the two-point functions of $\mathbf{h}$ and u_α scale in Fourier space with $\sigma_{\mathbf{h}} = 4-\eta_*$ and $\sigma_u = 6-D-2\eta_*$. Thus $\Delta_{\mathbf{h}} = (\eta_*-\varepsilon)/2$ and $\Delta_u = 1+\eta_*-\varepsilon$. Note that $\mathbf{h}$ has negative dimension

Ward identity generated by the dilatation current is equivalent to the RG equation (see appendix 4.A), similarly to the case of other field theories [138, 145].

The vanishing of β functions, however, is not sufficient to imply the conformal invariance of the model due to the presence of the non-zero virial current V_α. An algebraic analysis of terms in Eq. (4.35) shows that V_α cannot be written as the total derivative $V_\alpha = \partial_\beta l_{\alpha\beta}$ of a local operator $l_{\alpha\beta}$. This remains true even in the scale-invariant limit because, as Eq. (4.36) shows, contributions proportional to $[u_\alpha u_{\beta\beta}]$, $[u_\beta u_{\alpha\beta}]$ do not vanish as $\tilde{\lambda}$ and $\tilde{\mu}$ approach their fixed point value. It is also impossible to reduce V_α to the form $j_\alpha + \partial_\beta l_{\alpha\beta}$ where j_α is a conserved current. If $V_\alpha = j_\alpha + \partial_\beta l_{\alpha\beta}$ was true, the total derivative $\partial_\alpha V_\alpha$ should reduce to a combination $\mathcal{O}_{\rm red} + \partial_\alpha \partial_\beta l_{\alpha\beta}$, where $\mathcal{O}_{\rm red}$ is a redundant operator, removable by field redefinition. Working within dimensional regularization, we can assume that the $\mathcal{O}_{\rm red}$ has the form $E_\alpha \chi_\alpha + \mathbf{E}\cdot\mathbf{F}$, where χ_α and $\mathbf{F}$ are local functionals of the field, and we can neglect contributions arising from the Jacobian of the transformation. The only candidates for $\mathcal{O}_{\rm red}$ with power-counting dimension 4 near $D = 4$ are then linear combinations of the form $f_1(h^2)\mathbf{E}\cdot\mathbf{h} + f_2(h^2)E_\alpha u_\alpha + f_3(h^2)E_\alpha(\mathbf{h}\cdot\partial_\alpha\mathbf{h})$, where $f_1(h^2)$, $f_2(h^2)$, $f_3(h^2)$ are functions of h^2. We checked by explicit calculation that $\partial_\alpha V_\alpha$ cannot be reduced to such a combination up to a total second derivative $\partial_\alpha\partial_\beta l_{\alpha\beta}$. It follows that it is impossible to construct a conserved conformal current.

We can thus conclude that the form of the virial current is inconsistent with the structure expected in a conformal theory. Therefore, the theory must exhibit only scale invariance and not the enhanced conformal symmetry.

Before concluding the discussion, let us comment on the role of renormalization in the analysis. Within the framework considered here (the perturbative expansion without ultraviolet and infrared cutoffs), the subtraction of dimensional poles $1/\varepsilon^k$ is a mathematical necessity. Without renormalization, the ε-expansion cannot be defined due to the divergences as $D \to 4$. However, from a physical point of view, the system of interest has a finite $\varepsilon > 0$. The divergences are, rather, generated by the fact that the coupling constants are infinite in the scaling limit. The difference between the two limits $\varepsilon \to 0$ and $\lambda_0, \mu_0 \to \infty$ could be made more explicit defining the perturbative expansion directly at finite ε, after adding mass terms to regularize infrared divergences. In critical phenomena, it is usually assumed that the same structure of counterterms which remove divergences for $D \to 4$ also makes finite

for $D < 4$. The dimension of u also becomes negative when $\varepsilon - \eta_* > 1$. For example in two dimensions, the value of the exponent $\eta_* \simeq 0.8$ implies a negative dimensionality for both fields. For negative dimension the Fourier transform from momentum to real space $\int_{\mathbf{k}} k^{-\sigma}\exp(i\mathbf{k}\cdot\mathbf{x})$ becomes infrared divergent. The derivatives of the fields $\partial_\alpha\mathbf{h}$ and $\partial_\alpha u_\beta$ however have positive dimensions for any $D > 2 - \eta_*(D)$. This ensures that correlation functions of $\partial_\alpha\mathbf{h}$ and $\partial_\alpha u_\beta$ are finite in real space. For $D \le 2 - \eta_*(D)$ the flat phase cannot exist. The equality $D_{\rm lc} = 2 - \eta_*(D_{\rm lc})$ defines the lower critical dimension of the flat phase [12].

correlation functions at $D < 4$ in the limit of infinite coupling constants[22] [15, 16, 150]. In the ε-expansion considered here, we assume that, similarly, the subtraction of dimensional poles $1/\varepsilon^k$ will at the same time make correlation functions finite for $\varepsilon > 0$ and infinite coupling strength[23]. This is confirmed by the fact that the dimensionless renormalized couplings $\tilde{\lambda}$, $\tilde{\mu}$ remain finite when the bare couplings diverge. This finiteness assumption implicitly underlies all applications of dimensional regularization and minimal subtraction methods to critical behavior. We assume that finiteness in the critical limit applies not only to correlation functions but also to renormalized operators. We thus assume that the renormalized expression (4.34) evaluated at the fixed point can be used to directly read the behavior of the model in the scaling limit in which the bare couplings are divergent.

This assumption seems implicit in the analysis of scalar field theory in Ref. [138], and more generally, in all analyses of the energy momentum tensor in critical theories[24].

4.5.3 *Genericity argument*

The group theoretical relations between dilatations and translations imply that the symmetric energy momentum tensor $\theta_{\alpha\beta}$ must transform under an infinitesimal rescaling of coordinates $\mathbf{x} \to (1+\epsilon)\mathbf{x}$ as $\theta_{\alpha\beta} \to \theta_{\alpha\beta} + \epsilon\Delta\theta_{\alpha\beta}$, where

$$\Delta\theta_{\alpha\beta} = x_\gamma \partial_\gamma \theta_{\alpha\beta} + D\theta_{\alpha\beta} + \partial_\rho\partial_\sigma \Delta Y_{\sigma\alpha\rho\beta} \ , \tag{4.38}$$

and ΔY is an infinitesimal improvement term (with the symmetry properties $\Delta Y_{\sigma\alpha\rho\beta} = -\Delta Y_{\alpha\sigma\rho\beta} = \Delta Y_{\rho\beta\sigma\alpha}$) [118, 123]. This transformation law shows that, up to a total second derivative, the energy-momentum tensor must behave as a field with dimension exactly equal to D. In turn, the virial current must have dimension $D-1$ [79].

This fact has suggested a general argument to link scale and conformal invariance. The argument is based on the concept that it is unlikely to have fields with an exact dimension $D-1$ in an interacting field theory. This indicates that generically the virial current is zero and scale invariance is extended to conformal invariance[25] [79, 130].

Having found a violation of conformal invariance, let us comment on the naturalness of having vector operators with dimension exactly equal to $D-1$. In the

22 The specific values of the counterterms depend on the renormalization scheme, but the number of subtractions and the type of counterterms are the same.

23 Qualitatively, the renormalization procedure makes correlation functions insensitive to the large-momentum region $q \gg q_G$ where the behavior crosses over from critical to Gaussian.

24 In scalar field theory, an analysis of the finiteness of integrated operator insertions $\int \mathrm{d}^D x G_{\theta_{\alpha\alpha}(\mathbf{x})}$ and $\int \mathrm{d}^D x x_\alpha G_{\theta_{\alpha\alpha}(\mathbf{x})}$ at the fixed point was given in Ref. [139].

25 See also Ref. [140] for a similar genericity argument in the framework of the exact renormalization group. For tests of the genericity argument, see for example Ref. [132].

membrane model considered here, the non-renormalization relations (4.32), (4.33) can be used to show that the fields $u_\alpha u_{\beta\beta}$ and $u_\beta u_{\alpha\beta}$ scale at the fixed point with a dimension exactly equal to $D-1$ (up to total derivatives). This dimension can also be interpreted as the sum of the dimensions of u_α, which is $1+\eta_*-\varepsilon$, and $u_{\alpha\beta}$ which, as shown in appendix 4.A has dimension $2-\eta_*$. The existence of non-conserved currents with dimension exactly $D-1$ can thus be traced to the shift symmetry of the theory, which protects the terms in the virial current from getting nontrivial renormalizations.

We note, however, that the existence of an unrenormalized virial current could be guessed more quickly even without an explicit analysis of the individual operators (4.32) and (4.33). The reason is that, due to its conservation law, $\theta_{\alpha\beta}$ must be finite for $\varepsilon \to 0$ a priori (up to improvement terms) [118, 159]. The trace of the energy-momentum tensor, expressed in terms of bare quantities, reads

$$\theta_{\alpha\alpha} = -E_\alpha u_\alpha + \frac{\varepsilon}{2}((\partial^2\mathbf{h})^2 + \lambda_0(u_{\alpha\alpha})^2 + 2\mu_0 u_{\alpha\beta}u_{\alpha\beta}) + \partial_\alpha V_\alpha \ . \tag{4.39}$$

The part $\varepsilon((\partial^2\mathbf{h})^2 + \lambda_0(u_{\alpha\alpha})^2 + 2\mu_0 u_{\alpha\beta}u_{\alpha\beta})/2$ is nontrivially renormalized because the factor ε in front of the expression leaves room for the presence of counterterms diverging as first-order poles in ε. The explicit counterterms in particular are proportional to η/ε, $\beta_\lambda/\varepsilon$ and β_μ/ε and introduce the RG functions into the expression of the energy momentum tensor (see 4.A).

The current V_α, instead, contains terms which are not suppressed by factors of ε. In other words, the model in dimension $D=4$ is scale invariant but not conformal at the classical level (without loop corrections)[26]. Since V_α must be finite (up to total derivatives) and there is no compensating factor of ε, Feynman diagrams with insertion of V_α must be directly convergent, after coupling and amplitude renormalizations. Therefore we see that, even without a detailed calculation, we could have expected a non-renormalization relation and the existence of an unrenormalized vector field having dimension exactly equal to $D-1$.

This reasoning can be applied to any model which is scale-invariant but non-conformal at the classical level in dimension 4 (or, more generally, at the upper critical dimension). For these models, unrenormalized vector fields must always exist and thus the genericity argument breaks down.

4.5.4 *Comment on reflection positivity*

In two-dimensions, scale-invariant models which present unitarity (in spacetime) or reflection positivity (in Euclidean space) can be proven to be always conformal, if some additional technical conditions are satisfied [117, 118].

26 At the classical level, conformal invariance can be analyzed by setting $\mathbf{h}=0$, condition which is preserved by equations of motion. The model then reduces to the Riva-Cardy theory, which is not conformal in four dimensions [103, 130].

Although we could not develop a detailed derivation, we expect that the membrane model discussed in this section is not reflection-positive. In the ultraviolet limit, where interactions can be neglected, the theory reduces to

$$\mathcal{H}_{\rm UV} = \frac{1}{2}\int \mathrm{d}^D x \left[(\partial^2\mathbf{h})^2 + (\lambda_0+\mu_0)(\partial_\alpha u_\alpha)^2 + \mu_0\partial_\alpha u_\beta \partial_\alpha u_\beta\right] \ , \tag{4.40}$$

the combination of d_c copies of a higher-derivative scalar theory and a Gaussian vector model. These non-interacting theories were analyzed in Refs. [103, 130, 160] and were shown to lack reflection positivity or, equivalently, unitarity in Minkowski space. It seems likely, therefore, that the also the full interacting model is not reflection-positive.

4.6 GCI MODEL

Differently from elasticity theory, the GCI model is exactly conformal in the Gaussian approximation, and therefore, in the ultraviolet region. In fact, the Hamiltonian (3.7) reduces in the weak-coupling limit $Y_0 \to 0$ to two copies of the biharmonic theory, which is exactly scale and conformal invariant [147, 155]. In this section we show that, instead, conformal symmetry is broken in the infrared region: the IR fixed point theory is only dilatation-invariant.

With calculations illustrated in appendix 4.C and some further algebraic steps, it can be shown that the model admits a symmetric energy-momentum tensor $\theta_{\alpha\beta}$ with trace

$$\theta_{\alpha\alpha} = -\frac{(\eta-\varepsilon)}{2}\mathbf{E}\cdot\mathbf{h} + \eta E\chi - \frac{\beta(Y)}{2Y^2}M^{-\varepsilon}[(\partial^2\chi)^2] + \partial_\alpha V_\alpha \tag{4.41}$$

where

$$\mathbf{E} = \partial^2\partial^2\mathbf{h} + i(\partial^2\chi\partial^2\mathbf{h} - \partial_\alpha\partial_\beta\chi\partial_\alpha\partial_\beta\mathbf{h}) \ , \qquad E = \frac{1}{Y_0}\partial^2\partial^2\chi + iK \tag{4.42}$$

are, respectively, the equations of motion of the $\mathbf{h}$ and the χ field, and $[(\partial^2\chi)^2]$ denotes the renormalized insertion of $(\partial^2\chi)^2$. The expression for $\theta_{\alpha\alpha}$ includes a non-zero 'virial current'

$$V_\alpha = -\frac{i}{2}\big\{(D-3+2\eta)\partial_\alpha\chi(\partial_\beta\mathbf{h}\cdot\partial_\beta\mathbf{h}) + 2(1-\eta)\partial_\beta\chi(\partial_\beta\mathbf{h}\cdot\partial_\alpha\mathbf{h})\big\} + \partial_\beta L_{\alpha\beta} \ , \tag{4.43}$$

where $L_{\alpha\beta}$ is a local tensor field.

At the IR fixed point $Y = Y_*$, assuming that the renormalized operator $[(\partial^2\chi)^2]$ remains finite, the term $-\beta(Y)M^{-\varepsilon}[(\partial^2\chi)^2]/(2Y^2)$ becomes zero due to the vanishing of the β-function $\beta(Y_*) = 0$. We can thus introduce a dilatation current $S_\alpha = x_\beta\theta_{\alpha\beta} - V_\alpha$ which is locally conserved:

$$\partial_\alpha S_\alpha = -x_\beta(\mathbf{E}\cdot\partial_\beta\mathbf{h} + E\partial_\beta\chi) - \frac{(\eta_*-\varepsilon)}{2}\mathbf{E}\cdot\mathbf{h} + \eta_* E\chi \ . \tag{4.44}$$

Whether the scaling symmetry is enhanced to the full conformal invariance depends on the structure of the virial current. It is useful, therefore, to examine insertions of the composite field $P_{\mu,\alpha\beta} = \partial_\mu\chi(\partial_\alpha\mathbf{h}\cdot\partial_\beta\mathbf{h})$, an elementary building block from which the nontrivial terms in Eq. (4.43) can be constructed. The renormalization of $P_{\mu,\alpha\beta}$ has a particularly simple form. In fact, let us consider an arbitrary diagram γ for a 1PI correlation function with n external $\mathbf{h}$ lines, ℓ external χ lines, and one insertion of $P_{\mu,\alpha\beta}$. The diagram can be of one of the three types illustrated in Fig. 4.3: in diagrams of the groups (a) and (b) one of the elementary fields contained in the composite operator is directly connected with external lines, while in diagrams of type (c) all inserted lines enter as loop propagators.

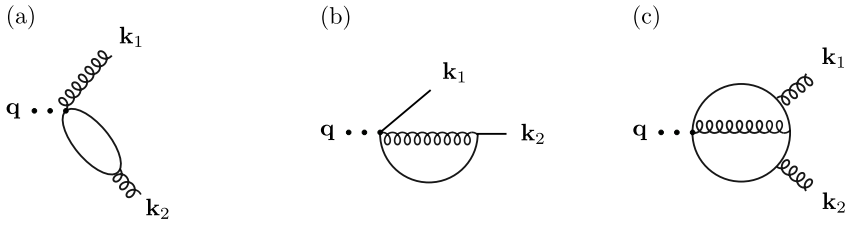

Figure 4.3: Examples of 1PI diagrams of type (a), (b), and (c).

The Feynman rules of the theory imply that the degree of superficial divergence [15] is

$$\delta(\gamma) = 3 + DL - 4I_h - 4I_\chi + 4v - 2n - 2\ell + a_\gamma \ , \tag{4.45}$$

where $I_\mathbf{h}$ and I_χ denote the number of internal $\mathbf{h}$ and χ propagators, v the number of vertices, and L the number of loops. The coefficient a_γ is $a_\gamma = 1$ for diagrams of type (a) and (b) and $a_\gamma = 0$ for type (c). Using the topological relations $L = 3 + 2v - I_\mathbf{h} - I_\chi - n - \ell$, $2I_\mathbf{h} + n = 2v + 2$, and $2I_\chi + \ell = v + 1$, we see that the degree of divergence in the ε expansion is

$$\delta(\gamma) = 3 - 2n - 2\ell + a_\gamma \ . \tag{4.46}$$

It follows that the only counterterms needed for the renormalization of $P_{\mu,\alpha\beta}$ have the schematic form $\partial^3\chi$, $\partial\chi\partial^2\chi$, $\partial\mathbf{h}\cdot\partial^2\mathbf{h}$. These composite operators can always be represented as total derivatives (see Eq. (4.87)).

We can conclude that insertions of the composite fields $\partial_\alpha\chi(\partial_\beta\mathbf{h}\cdot\partial_\beta\mathbf{h})$ and $\partial_\beta\chi(\partial_\alpha\mathbf{h}\cdot\partial_\beta\mathbf{h})$, which contribute to the virial current, are finite up to total-derivative counterterms. Therefore, the "bulk" of the virial current is unrenormalized: we can set $\partial_\alpha\chi_\beta(\partial_\beta\mathbf{h}\cdot\partial_\beta\mathbf{h}) = [\partial_\alpha\chi_\beta(\partial_\beta\mathbf{h}\cdot\partial_\beta\mathbf{h})]$ and $\partial_\beta\chi(\partial_\alpha\mathbf{h}\cdot\partial_\beta\mathbf{h}) = [\partial_\beta\chi(\partial_\alpha\mathbf{h}\cdot\partial_\beta\mathbf{h})]$, up to gradients of the form $\partial_\beta l_{\alpha\beta}$ which do not affect the relation between scale and conformal invariance [118].

Let us check that V_α cannot be reduced completely to the combination $V_\alpha = j_\alpha + \partial_\beta L'_{\alpha\beta}$ of a conserved current j_α and a total derivative. If this was the case, $\partial_\alpha V_\alpha$ should reduce to the combination $\mathcal{O}_{\rm red} + \partial_\alpha\partial_\beta l_{\alpha\beta}$ of a redundant operator $\mathcal{O}_{\rm red}$ and a total second derivative. Within dimensional regularization, candidates for $\mathcal{O}_{\rm red}$ can be taken as linear combinations of operators proportional to the equations of motion $\mathbf{E}$ and E and, in order to match the power-counting dimension of $\partial_\alpha V_\alpha$, must have the form $f_1(h^2,\chi)(\mathbf{E}\cdot\mathbf{h}) + f_2(h^2,\chi)E$, where f_1 and f_2 are functions. We checked from the explicit expression V_α that it is impossible to rewrite $\partial_\alpha V_\alpha$ as a combination of this type up to a total second derivative $\partial_\alpha\partial_\beta l_{\alpha\beta}$. Since contributions to V_α do not renormalize, we expect that this result remains robust at the IR fixed point. We are lead to the conclusion that the GCI model exhibits scale without conformal invariance.

Let us, then, investigate the scaling properties of the operators composing V_α. Since $P_{\mu,\alpha\beta}$ is not renormalized, it does not acquire anomalous exponents. Therefore the naive dimension $\{P_{\mu,\alpha\beta}\} = 3+2\{\mathbf{h}\}+\{\chi\} = 3+2(D-4)/2+0 = D-1$ remains valid at the IR fixed point. This scaling relation can also be understood in terms of the infrared dimensions of fields. The renormalization relations discussed in chapter 3, $\mathbf{h} = \sqrt{Z}\mathbf{h}$, $\chi = Z^{-1}\tilde{\chi}$, imply that $\mathbf{h}$ and χ scale in the long-wavelength limit with dimensionalities $\{\mathbf{h}\} = (D-4+\eta)/2$ and $\{\chi\} = -\eta$. The absence of divergences in the insertion of $P_{\mu,\alpha\beta}$ implies that the naive relation $\{V_\alpha\} = 3 + 2\{\mathbf{h}\} + \{\chi\}$ remains valid in the IR and, in fact, it can be seen that the anomalous exponent η cancels out leaving an exact canonical dimension.

4.7 TWO TESTS ON THE ABSENCE OF CONFORMAL INVARIANCE

Conformal invariance implies a set of constraints and selection rules for correlation functions [79, 115, 119, 137, 151]. Two of the simplest rules are the following[27]:
· The two-point function $\langle\varphi_i(\mathbf{x}_1)\varphi_j(\mathbf{x}_2)\rangle$ of two fields (primary or descendant) must be zero if the difference $\Delta_i - \Delta_j$ of their scaling dimensions is noninteger.
· The two-point function of a quasi-primary vector field $y_\alpha(\mathbf{x})$ must have the form

$$\langle y_\alpha(\mathbf{x}_1) y_\beta(\mathbf{x}_2)\rangle = \frac{A(\delta_{\alpha\beta}x^2 - 2x_\alpha x_\beta)}{|\mathbf{x}|^{2\Delta+2}} \ , \tag{4.47}$$

with $\mathbf{x} = \mathbf{x}_1 - \mathbf{x}_2$. After Fourier transformation, this correspond to a two-point function in momentum space of the form [132]

$$\langle y_\alpha(\mathbf{k}) y_\beta(-\mathbf{k})\rangle = \frac{A'}{k^{2+D-2\Delta}}\left[(\Delta-1)k^2\delta_{\alpha\beta} + (D-2\Delta)k_\alpha k_\beta\right] . \tag{4.48}$$

27 See Refs. [79, 115, 133, 151] for more general constraints on tensorial operators and on n-point correlation functions.

These rules are valid generally in any model with linearly realized conformal symmetry[28].

To directly test the absence of conformal symmetry, let us compare the two-point function $D_{\alpha\beta}(\mathbf{k}) = \langle u_\alpha(\mathbf{k}) u_\beta(-\mathbf{k})\rangle$ with the form expected for a quasi-primary field[29]. To compute $D_{\alpha\beta}(\mathbf{k})$ we can choose a renormalization scale $M \simeq |\mathbf{k}|$. The renormalized propagator $\tilde{D}_{\alpha\beta}(\mathbf{k}) = Z^{-2} D_{\alpha\beta}(\mathbf{k})$ can then be calculated by renormalized perturbation theory and, for ε small, can be approximated by the corresponding tree-level contribution. After calculation at scales $|\mathbf{k}| \simeq M$, the result can be rescaled to any wavelength via scaling relations. Thus the correlation function at an arbitrary $\mathbf{k}$ in the long-wavelength region takes approximately the form

$$\tilde{D}_{\alpha\beta}(\mathbf{k}) \simeq \frac{1}{M^{2\eta_*} k^{6-D-2\eta_*}} \left[\frac{P^L_{\alpha\beta}(\mathbf{k})}{\tilde{\lambda}_* + 2\tilde{\mu}_*} + \frac{P^T_{\alpha\beta}(\mathbf{k})}{\tilde{\mu}_*} \right] . \tag{4.49}$$

Near $D = 4$, the scaling dimension of u_α is $\Delta_u = (1 + \eta_* - \varepsilon) \simeq 1$. Eq. (4.48) shows that if u_α was primary, its two-point function should be almost purely longitudinal. In contrast, the $\mathrm{O}(\varepsilon)$ values of the couplings at the fixed point P_4, $\tilde{\mu}_* = 96\pi^2\varepsilon/(d_c + 24)$, $\tilde{\lambda}_* = -\tilde{\mu}_*/3$, show that longitudinal and transverse components of $\tilde{D}_{\alpha\beta}(\mathbf{k})$ have the same order of magnitude. This simple calculation already shows that the model cannot be conformal, at least in a form in which u_α is a vector primary field (The calculation does not rule out the possibility that u_α is a descendant.)

A drawback in the analysis of $D_{\alpha\beta}$ is that its Fourier transform to real space is only defined when the dimension of u_α, $\Delta_u = 1 + \eta_* - \varepsilon$, is positive. This condition is valid near four dimensions, but breaks down in the physical case $D = 2$, where $\varepsilon = 2$ and $\eta_* \simeq 0.8$.

Although the analysis given here is restricted to the ε-expansion, and thus to D close to four, it is interesting to consider a correlation function which has a direct interpretation in the physical case. As a second test, we can thus consider the two-point function $C(\mathbf{x}_1 - \mathbf{x}_2) = \langle \partial_\alpha u_\beta(\mathbf{x}_1) u_{\gamma\gamma}(\mathbf{x}_2)\rangle$, which is alwas well defined in real space when the flat phase exists[30]. An explicit calculation of the leading order diagram gives

$$\begin{aligned} C(\mathbf{x}) = & \quad \sim\!\sim\!\sim \\ & = \frac{\Gamma(D/2)}{2\pi^{D/2}(\lambda_0 + 2\mu_0)|\mathbf{x}|^{D+2}} (\delta_{\alpha\beta} x^2 - D x_\alpha x_\beta) \end{aligned} \tag{4.50}$$

28 See for example Ref. [161] for a discussion of nonlinearly realized conformal symmetry.

29 Testing conformal invariance via selection rules of two-point functions is a well-known method. See for example Refs. [133, 139].

30 The correlation function is translationally-symmetric and thus only requires the self-consistency of rotational symmetry breaking, which is verified in the flat phase. See also footnote 21.

where $\mathbf{x} = \mathbf{x}_1 - \mathbf{x}_2$. Using the zero-order renormalization $\lambda_0 = M^\varepsilon \tilde{\lambda}$, $\mu_0 = M^\varepsilon \tilde{\mu}$ and setting renormalized couplings to their fixed point values $\tilde{\mu}_* = 96\pi^2\varepsilon/(d_c+24)$, $\tilde{\lambda}_* = -\tilde{\mu}_*/3$, we see that the correlation function is nonzero. Higher order diagrams cannot change this conclusion near four dimensions because after renormalization their contribution is suppressed by powers of ε.

The fact that $C_{\alpha\beta}(\mathbf{x})$ does not vanish is a violation of conformal invariance, because $\partial_\alpha u_\beta$ has dimension $\Delta_1 = 2 + \eta_* - \varepsilon$ while $u_{\gamma\delta}$ is a scaling field with dimension $\Delta_2 = 2 - \eta_*$, as shown in appendix 4.A. Since the difference of their dimension, $\Delta_1 - \Delta_2 = 2\eta_* - \varepsilon$ is noninteger, the conformal selection rule would have required that the two-point function vanishes[31] for any $\mathbf{x} \neq 0$. Instead, we get a correlation function, which is nonzero and decreasing as $|\mathbf{x}|^{-(\Delta_1+\Delta_2)} = |\mathbf{x}|^{-D}$.

It is natural to assume that this test applies also directly in two dimensions.

4.8 GROUP THEORETICAL INTERPRETATION

Another way to understand the absence of conformal invariance can be derived by analyzing how conformal transformations interact with translations and rotations *in the embedding space*.

The embedding-space translations and rotations (see Eq. (2.29)) are symmetries of the model for any values of the coupling constant, and can be represented by the infinitesimal generators

$$t_i = \int \mathrm{d}^D x \frac{\delta}{\delta h_i} , \qquad t_\alpha = \int \mathrm{d}^D x \frac{\delta}{\delta u_\alpha} , \tag{4.51}$$

$$\begin{aligned} R_{\alpha i} &= \int \mathrm{d}^D x \left[x_\alpha \frac{\delta}{\delta h_i} - h_i \frac{\delta}{\delta u_\alpha} \right] , \\ R_{\alpha\beta} &= \int \mathrm{d}^D x \left[x_\alpha \frac{\delta}{\delta u_\beta} - x_\beta \frac{\delta}{\delta u_\alpha} \right] , \\ R_{ij} &= \int \mathrm{d}^D x \left[h_i \frac{\delta}{\delta h_j} - h_j \frac{\delta}{\delta h_i} \right] . \end{aligned} \tag{4.52}$$

The commutators are similar to the Euclidean algebra, but are simpler due to the linearized form of rotations. All commutators are zero a part from $[t_i, R_{\alpha j}] = -\delta_{ij} t_\alpha$, $[R_{\alpha i}, R_{\beta j}] = -\delta_{ij} R_{\alpha\beta}$, $[t_i, R_{jk}] = \delta_{ij} t_k - \delta_{ik} t_j$, $[R_{\alpha i}, R_{jk}] = \delta_{ij} R_{\alpha k} - \delta_{ik} R_{\alpha j}$, $[R_{ij}, R_{kl}] = -(\delta_{ik} R_{jl} + \delta_{jl} R_{ik} - \delta_{il} R_{jk} - \delta_{jk} R_{il})$.

31 We note however that the trace $C_{\alpha\alpha}(\mathbf{x})$ is zero to all orders in the ε-expansion: rotational symmetry and the power-law behavior $C_{\alpha\beta} \approx |\mathbf{x}|^{-D}$ imply that $C_{\alpha\beta}(\mathbf{x})$ must be proportional to $\partial_\alpha(x_\beta/|\mathbf{x}|^D) = (\delta_{\alpha\beta}x^2 - D x_\alpha x_\beta)|\mathbf{x}|^{-D-2}$. In other words, the correlation function at the fixed point remains, to all orders, proportional to the tree-level result (4.50). The trace $C_{\alpha\alpha}(\mathbf{x})$ in particular is always zero. The conformal selection rule nevertheless is violated by the full tensorial correlation function $C_{\alpha\beta}(\mathbf{x})$

Translations and rotations of the internal coordinate $\mathbf{x}$ are also exact symmetries for any values of the coupling constants and are represented by the generators

$$P_\alpha = \int \mathrm{d}^D x \left[\partial_\alpha \mathbf{h} \cdot \frac{\delta}{\delta \mathbf{h}} + \partial_\alpha u_\beta \frac{\delta}{\delta u_\beta} \right] , \tag{4.53}$$

$$\begin{aligned} J_{\alpha\beta} = - \int \mathrm{d}^D x \Big[& (x_\alpha \partial_\beta \mathbf{h} - x_\beta \partial_\alpha \mathbf{h}) \cdot \frac{\delta}{\delta \mathbf{h}} \\ & + (x_\alpha \partial_\beta u_\gamma - x_\beta \partial_\alpha u_\gamma) \frac{\delta}{\delta u_\gamma} + u_\beta \frac{\delta}{\delta u_\alpha} - u_\alpha \frac{\delta}{\delta u_\beta} \Big] , \end{aligned} \tag{4.54}$$

which satisfy the standard commutation relations of the Euclidean algebra:

$$\begin{aligned} [P_\alpha, P_\beta] = 0 \ , \quad [P_\gamma, J_{\alpha\beta}] = \delta_{\alpha\gamma} P_\beta - \delta_{\beta\gamma} P_\alpha \ , \\ [J_{\alpha\beta}, J_{\gamma\delta}] = -(\delta_{\alpha\gamma} J_{\beta\delta} + \delta_{\beta\delta} J_{\alpha\gamma} - \delta_{\alpha\delta} J_{\beta\gamma} - \delta_{\beta\gamma} J_{\alpha\delta}) \ . \end{aligned}$$

The mixed commutators between embedding-space and internal space symmetries are all zero except: $[t_\alpha, J_{\beta\gamma}] = \delta_{\alpha\beta} t_\gamma - \delta_{\alpha\gamma} t_\beta$, $[R_{\alpha i}, P_\beta] = \delta_{\alpha\beta} t_i$, $[R_{\alpha i}, J_{\beta\gamma}] = \delta_{\alpha\beta} R_{\gamma i} - \delta_{\alpha\gamma} R_{\beta i}$, $[R_{\alpha\beta}, P_\gamma] = \delta_{\alpha\gamma} t_\beta - \delta_{\beta\gamma} t_\alpha$, $[R_{\alpha\beta}, J_{\gamma\delta}] = -(\delta_{\alpha\gamma} R_{\beta\delta} + \delta_{\beta\delta} R_{\alpha\gamma} - \delta_{\alpha\delta} R_{\beta\gamma} - \delta_{\beta\gamma} R_{\alpha\delta})$.

At the fixed point, the emergent scaling symmetry is described by a further dilatation operator. The RG equations (2.36) imply that $\mathbf{h}$ and u_α transform linearly under scale transformations: the quantities $\mathbf{h}$ and u_α behave as scaling fields with dimensions $\Delta_h = (\eta_* - \varepsilon)/2$ and $\Delta_u = 1 + \eta_* - \varepsilon$. The dilatation operator is thus represented by a generator

$$T_D = \int \mathrm{d}^D x \left[x_\alpha \partial_\alpha \mathbf{h} \cdot \frac{\delta}{\delta \mathbf{h}} + x_\alpha \partial_\alpha u_\gamma \frac{\delta}{\delta u_\gamma} + \Delta_h \mathbf{h} \cdot \frac{\delta}{\delta \mathbf{h}} + \Delta_u u_\alpha \frac{\delta}{\delta u_\alpha} \right] . \tag{4.55}$$

It can be checked that the algebra remains closed: the commutators of all generators t_i, t_α, $R_{i\alpha}$, $R_{\alpha\beta}$, R_{ij}, P_α, $J_{\alpha\beta}$, and T_D can be expressed as linear combinations of the same generators.

It is interesting to note that the closure of the algebra is only verified when Δ_h and Δ_u are related by $1 + \Delta_h = \Delta_u - \Delta_h$. If this relation was not satisfied, the commutator

$$[T_D, R_{\alpha i}] = - \int \mathrm{d}^D x \left[(1 + \Delta_h) x_\alpha \frac{\delta}{\delta h_i} - (\Delta_u - \Delta_h) h_i \frac{\delta}{\delta u_\alpha} \right] \tag{4.56}$$

would generate a symmetry operation which does not belong to the group. This would mean that the emergence of scale invariance would necessarily trigger the appearance of additional symmetries.

The relation $1 + \Delta_h = \Delta_u - \Delta_h$ is satisfied by the physical values $\Delta_h = (\eta_* - \varepsilon)/2$ and $\Delta_u = 1 + \eta_* - \varepsilon$, which are not independent, but rather related to the same

anomalous dimension η_*. This can be traced to the Ward identities associated with rotational invariance, which forces the fields to renormalize as $\mathbf{h} \to \sqrt{Z}\mathbf{h}$, $u_\alpha \to Z u_\alpha$ in order to preserve the structure of the strain tensor $(\partial_\alpha u_\beta + \partial_\beta u_\alpha + \partial_\alpha \mathbf{h} \cdot \partial_\beta \mathbf{h})/2$ [10–12] (see also Refs. [24, 113] and Sec. 2.5.3). Reversing the point of view, we can however consider Eq. (4.56) as an alternative proof of the Ward identity. Even without a renormalization group calculation, we could have deduced the relation between scaling exponents from closure of the symmetry group.

Let us now consider conformal transformations. By definition, special conformal transformations of the internal $\mathbf{x}$ coordinate must be represented by new generators K_α with the prescribed commutation rules[32] [115]:

$$[K_\alpha, K_\beta] = 0 \ , \quad [T_D, K_\alpha] = -K_\alpha \ , \qquad [K_\gamma, J_{\alpha\beta}] = \delta_{\alpha\gamma} K_\beta - \delta_{\beta\gamma} K_\alpha \ , \tag{4.57}$$

$$[K_\alpha, P_\beta] = 2\delta_{\alpha\beta} T_D - 2 J_{\alpha\beta} \ . \tag{4.58}$$

To study the structure of the extended group, it is useful to analyze Jacobi identities. The relation

$$[[K_\alpha, t_\beta], P_\gamma] + [[t_\beta, P_\gamma], K_\alpha] + [[P_\gamma, K_\alpha], t_\beta] = 0 \ , \tag{4.59}$$

in particular leads after an explicit calculation to

$$[[K_\alpha, t_\beta], P_\gamma] = [[K_\alpha, P_\gamma], t_\beta] = -2\Delta_u \delta_{\alpha\gamma} t_\beta + 2\delta_{\alpha\beta} t_\gamma - 2\delta_{\beta\gamma} t_\alpha \ . \tag{4.60}$$

If the algebra was closed, $[K_\alpha, t_\beta]$ should be expressible as a linear combination of $R_{\alpha\beta}$, $J_{\alpha\beta}$, and $\delta_{\alpha\beta} T_D$. However, it can be seen that there is no linear combination which, commuted with P_γ, gives the right hand side of Eq. (4.60). This shows that any extension to conformal symmetry must inevitably contain new symmetries, one of which described by the generator $[K_\alpha, t_\beta]$.

The general solution of Eq. (4.60) takes the form

$$[K_\alpha, t_\beta] = 2R_{\alpha\beta} + \int \mathrm{d}^D x \left[2\delta_{\alpha\beta} x_\gamma \frac{\delta}{\delta u_\gamma} - 2(1 + \Delta_u) x_\alpha \frac{\delta}{\delta u_\beta} \right] + I_{\alpha\beta} \ , \tag{4.61}$$

where $I_{\alpha\beta}$ commutes with translations: $[I_{\alpha\beta}, P_\gamma] = 0$. Physically, we do not expect that a symmetry of the form (4.61) can appear. The most natural assumption is thus that conformal invariance breaks down.

The derivation requires a separate analysis in the case of the GCI model. The model, in fact, does exhibit conformal symmetry at the harmonic level. For both theories, the direct calculation of the energy-momentum tensor however provides a general derivation on the absence of conformal invariance.

32 Here, we use a normalization of generators which differs from Ref. [115].

ACKNOWLEDGEMENTS

We thank S. Rychkov for stimulating discussions. This work was supported by the Dutch Research Council (NWO) via the Spinoza Prize of Professor M.I. Katsnelson.

APPENDIX 4

4.A INVARIANT COMPOSITE OPERATORS IN MEMBRANE THEORY

This appendix illustrates the renormalization of operators entering the expansion of the trace of the energy-momentum tensor. Let us start by analyzing the set of composite fields

$$\begin{aligned} &\mathcal{O}_1 = \frac{1}{2}(\partial^2\mathbf{h})^2 + \lambda_0(u_{\alpha\alpha})^2 + 2\mu_0 u_{\alpha\beta}u_{\alpha\beta} \ , \qquad \mathcal{O}_2 = \frac{1}{2}\lambda_0(u_{\alpha\alpha})^2 \ , \\ &\mathcal{O}_3 = \mu_0 u_{\alpha\beta}u_{\alpha\beta} \ , \qquad \mathcal{O}_4 = \partial^2 u_{\alpha\alpha} \ , \qquad \mathcal{O}_5 = \partial_\alpha\partial_\beta u_{\alpha\beta} \ , \qquad \mathcal{O}_6 = u_{\alpha\alpha} \ , \end{aligned} \tag{4.62}$$

which are invariant under all symmetries of the theory, including translations in the embedding space $\mathbf{h} \to \mathbf{h} + \mathbf{B}$, $u_\alpha \to u_\alpha + B_\alpha$, and the linearized rotations in Eq. (2.29). According to general renormalization theory [15], the insertion of invariant operators of power-counting dimension Δ is renormalized by a linear combination of operators with the same symmetries and with dimension equal or lower to Δ. From the scaling of $\mathbf{h}$ and u_α tree-level propagator, it follows that the power-counting dimension of a general operator of the schematic form $\partial^k \mathbf{h}^n u^\ell$ is $k + n(D-4)/2 + \ell(D-2)/2$, which reduces to $k+\ell$ in the ε-expansion at $D = 4-\varepsilon$. The composite fields in Eq. (4.62) are a basis for the most general invariant operator with dimension ≤ 4 and are, therefore, closed under renormalization. It is possible to find a matrix Z_{ij} of divergent coefficients such that bare and finite, renormalized operators, are related as $\mathcal{O}_i(\mathbf{x}) = Z_{ij}[\mathcal{O}_j(\mathbf{x})]$.

In analogy with derivations in Ref. [138], it is possible to set strong constraints on renormalization by forming combinations which are a priori known to be finite and free of UV divergences.

The renormalization of $\mathcal{O}_1$ can be fixed by the following argument. The expression for a general correlation function $G^{(n,\ell)}$ in terms of a functional integral over u_α and $\mathbf{h}$,

$$\begin{aligned} &G^{(n,\ell)}_{i_1..i_n\alpha_1..\alpha_\ell}(\mathbf{x}_1,..,\mathbf{x}_n;\mathbf{x}'_1,..,\mathbf{x}'_\ell) = \\ &\qquad \int [\mathrm{d}\mathbf{h}][\mathrm{d}u_\alpha] \left\{ \mathrm{e}^{-\mathcal{H}} h_{i_1}(\mathbf{x}_1)..h_{i_n}(\mathbf{x}_n) u_{\alpha_1}(\mathbf{x}'_1)..u_{\alpha_\ell}(\mathbf{x}'_\ell) \right\} \ , \end{aligned} \tag{4.63}$$

must be invariant under change of variables. If we choose a field redefinition $\mathbf{h} \to (1+\epsilon/2)\mathbf{h}$, $u_\alpha \to (1+\epsilon)u_\alpha$ the Hamiltonian $\mathcal{H}$ changes to first order by

$\epsilon \int \mathrm{d}^D x \mathcal{O}_1(\mathbf{x})$ while the string of fields in the correlator varies by an overall factor $(n/2+\ell)\epsilon$. Invariance of the functional integral then implies

$$\begin{aligned} \int \mathrm{d}^D x G^{(n,\ell)}_{\mathcal{O}_1(\mathbf{x}),i_1..i_n\alpha_1..\alpha_\ell}(\mathbf{x}_1,..,\mathbf{x}_n;\mathbf{x}'_1,..,\mathbf{x}'_\ell) = \\ \left(\frac{n}{2}+\ell\right) G^{(n,\ell)}_{i_1..i_n\alpha_1..\alpha_\ell}(\mathbf{x}_1,..,\mathbf{x}_n;\mathbf{x}'_1,..,\mathbf{x}'_\ell) \ , \end{aligned} \tag{4.64}$$

where

$$\begin{aligned} G^{(n,\ell)}_{\mathcal{O}_1(\mathbf{x}),i_1..i_n\alpha_1..\alpha_\ell}(\mathbf{x}_1,..,\mathbf{x}_n;\mathbf{x}'_1,..,\mathbf{x}'_\ell) = \\ \int [\mathrm{d}\mathbf{h}][\mathrm{d}u_\alpha] \left\{ \mathrm{e}^{-\mathcal{H}} \mathcal{O}_1(\mathbf{x}) h_{i_1}(\mathbf{x}_1)..h_{i_n}(\mathbf{x}_n) u_{\alpha_1}(\mathbf{x}'_1)..u_{\alpha_\ell}(\mathbf{x}'_\ell) \right\} \end{aligned} \tag{4.65}$$

denotes correlation functions with $\mathcal{O}_1(\mathbf{x})$ insertion. From Eq. (4.64), we see that $\int \mathrm{d}^D x G^{(n,\ell)}_{\mathcal{O}_1(\mathbf{x})}$ is already finite after the renormalization of elementary fields, $\mathbf{h} = \sqrt{Z}\tilde{\mathbf{h}}$, $u_\alpha = Z\tilde{u}_\alpha$, without the need of a new operator renormalization. The only divergences in $\mathcal{O}_1$ must be total derivatives, which vanish after space integration. We thus conclude that $\mathcal{O}_1$ can be renormalized as

$$\mathcal{O}_1 = [\mathcal{O}_1] + a_1 \partial^2 [u_{\alpha\alpha}] + b_1 \partial_\alpha \partial_\beta [u_{\alpha\beta}] \ , \tag{4.66}$$

where a_1 and b_1 are divergent coefficients.

We can deduce additional constraints from the fact that derivatives of renormalized correlation functions with respect to $\tilde{\lambda}$ and $\tilde{\mu}$ are finite [138]. Denoting as $G^{(n,\ell)}$ and $\tilde{G}^{(n,\ell)}$ bare and renormalized correlation functions with n external $\mathbf{h}$ fields and ℓ external u_α fields, we find, using Eq. (2.34),

$$\begin{aligned} \frac{\partial \tilde{G}^{(n,\ell)}}{\partial \tilde{\lambda}} &= \frac{\partial}{\partial \tilde{\lambda}} \left(Z^{-\frac{n}{2}-\ell} G^{(n,\ell)} \right) = -\left(\frac{n}{2}+\ell\right) \frac{\partial \ln Z}{\partial \tilde{\lambda}} \tilde{G}^{(n,\ell)} \\ &+ Z^{-\frac{n}{2}-\ell} \left[\frac{\partial \ln \lambda_0}{\partial \tilde{\lambda}}\Big|_{M,\tilde{\mu}} \frac{\partial}{\partial \ln \lambda_0} + \frac{\partial \ln \mu_0}{\partial \tilde{\lambda}}\Big|_{M,\tilde{\mu}} \frac{\partial}{\partial \ln \mu_0} \right] G^{(n,\ell)} \\ &= \text{finite} \ . \end{aligned} \tag{4.67}$$

The derivatives $\partial/\partial \ln \lambda_0$ and $\partial/\partial \ln \mu_0$ generate, respectively, insertions of the integrated operators $-\int \mathrm{d}^D x \mathcal{O}_2(\mathbf{x})$ and $-\int \mathrm{d}^D x \mathcal{O}_3(\mathbf{x})$. Moreover, as shown above, the counting factor $n/2+\ell$ can be written via the insertion of $\int \mathrm{d}^D x \mathcal{O}_1$.

As a result, Eq. (4.67) is equivalent to

$$\begin{aligned} \int \mathrm{d}^D x \left[\frac{\partial \ln Z}{\partial \tilde{\lambda}} \tilde{G}^{(n,\ell)}_{\mathcal{O}_1(\mathbf{x})} + \frac{\partial \ln \lambda_0}{\partial \tilde{\lambda}}\Big|_{M,\tilde{\mu}} \tilde{G}^{(n,\ell)}_{\mathcal{O}_2(\mathbf{x})} + \frac{\partial \ln \mu_0}{\partial \tilde{\lambda}}\Big|_{M,\tilde{\mu}} \tilde{G}^{(n,\ell)}_{\mathcal{O}_3(\mathbf{x})} \right] \\ = \text{finite} \ , \end{aligned} \tag{4.68}$$

where $\tilde{G}^{(n,\ell)}_{\mathcal{O}(\mathbf{x})}$ denotes correlation functions of renormalized fields with an insertion of the bare operator $\mathcal{O}(\mathbf{x})$:

$$\tilde{G}^{(n,\ell)}_{\mathcal{O}(\mathbf{x})} = \langle \mathcal{O}(\mathbf{x}) \tilde{h}_{i_1}(\mathbf{x}_1) .. \tilde{h}_{i_n}(\mathbf{x}_n) \tilde{u}_{\alpha_1}(\mathbf{x}'_1) .. \tilde{u}_{\alpha_\ell}(\mathbf{x}'_\ell) \rangle \ . \tag{4.69}$$

Isolating operators from correlation functions and removing space integration, we can re-express Eq. (4.68) as the statement that the combination

$$\frac{\partial \ln Z}{\partial \tilde{\lambda}}\Big|_{M,\tilde{\mu}} \mathcal{O}_1(\mathbf{x}) + \frac{\partial \ln \lambda_0}{\partial \tilde{\lambda}}\Big|_{M,\tilde{\mu}} \mathcal{O}_2(\mathbf{x}) + \frac{\partial \ln \mu_0}{\partial \tilde{\lambda}}\Big|_{M,\tilde{\mu}} \mathcal{O}_3(\mathbf{x}) \tag{4.70}$$

is finite up to total derivatives. Assuming that amplitude, coupling, and operator renormalizations are all defined within the minimal subtraction scheme [15, 138], this implies

$$\begin{aligned} \frac{\partial \ln Z}{\partial \tilde{\lambda}}\Big|_{M,\tilde{\mu}} \mathcal{O}_1(\mathbf{x}) + \frac{\partial \ln \lambda_0}{\partial \tilde{\lambda}}\Big|_{M,\tilde{\mu}} \mathcal{O}_2(\mathbf{x}) + \frac{\partial \ln \mu_0}{\partial \tilde{\lambda}}\Big|_{M,\tilde{\mu}} \mathcal{O}_3(\mathbf{x}) \\ = \frac{1}{\tilde{\lambda}} [\mathcal{O}_2(\mathbf{x})] + a_\lambda \partial^2 [u_{\alpha\alpha}] + b_\lambda \partial_\alpha \partial_\beta [u_{\alpha\beta}] \ , \end{aligned} \tag{4.71}$$

so that, up to the total-derivative terms, the right-hand side is equal to the tree-level contribution of the left hand side. A consequence of Eq. (4.71) is that

$$\frac{\partial \tilde{G}^{(n,\ell)}}{\partial \ln \tilde{\lambda}}\Big|_{M,\tilde{\mu}} = -\int \mathrm{d}^D x \tilde{G}^{(n,\ell)}_{[\mathcal{O}_2(\mathbf{x})]} \ , \tag{4.72}$$

where $\tilde{G}^{(n,\ell)}_{[\mathcal{O}_2(\mathbf{x})]}$ is the correlation function of renormalized fields with insertion of the renormalized operator $[\mathcal{O}_2(\mathbf{x})]$. An analogue relation was derived for scalar field theory in Ref. [138].

Identical arguments can be used to deduce that

$$\begin{aligned} \frac{\partial \ln Z}{\partial \tilde{\mu}}\Big|_{M,\tilde{\lambda}} \mathcal{O}_1(\mathbf{x}) + \frac{\partial \ln \lambda_0}{\partial \tilde{\mu}}\Big|_{M,\tilde{\lambda}} \mathcal{O}_2(\mathbf{x}) + \frac{\partial \ln \mu_0}{\partial \tilde{\mu}}\Big|_{M,\tilde{\lambda}} \mathcal{O}_3(\mathbf{x}) \\ = \frac{1}{\tilde{\mu}} [\mathcal{O}_3(\mathbf{x})] + a_\mu \partial^2 [u_{\alpha\alpha}] + b_\mu \partial_\alpha \partial_\beta [u_{\alpha\beta}] \ , \end{aligned} \tag{4.73}$$

a relation which follows from the finiteness of $\partial \tilde{G}^{(n,\ell)}/\partial \tilde{\mu}$. A relation similar to Eq. (4.72) holds:

$$\frac{\partial \tilde{G}^{(n,\ell)}}{\partial \ln \tilde{\mu}}\Big|_{M,\tilde{\lambda}} = -\int \mathrm{d}^D x \tilde{G}^{(n,\ell)}_{[\mathcal{O}_3(\mathbf{x})]} \ . \tag{4.74}$$

As a particular case of Eqs. (4.71) and (4.73), let us take the linear combination $\beta_\lambda \times (4.71) + \beta_\mu \times (4.73)$, where β_λ and β_μ are the RG β-functions. Using that [11]

$$\beta_\lambda \frac{\partial \ln Z}{\partial \tilde{\lambda}}\Big|_{M,\tilde{\mu}} + \beta_\mu \frac{\partial \ln Z}{\partial \tilde{\mu}}\Big|_{M,\tilde{\lambda}} = \frac{\partial \ln Z}{\partial \ln M}\Big|_{\lambda_0,\mu_0} = \eta \ , \tag{4.75}$$

$$\beta_\lambda \frac{\partial \ln \lambda_0}{\partial \tilde{\lambda}}\Big|_{M,\tilde{\mu}} + \beta_\mu \frac{\partial \ln \lambda_0}{\partial \tilde{\mu}}\Big|_{M,\tilde{\lambda}} = \frac{\partial \ln(\lambda_0/M^\varepsilon)}{\partial \ln M}\Big|_{\lambda_0,\mu_0} = -\varepsilon \ , \tag{4.76}$$

and

$$\beta_\lambda \frac{\partial \ln \mu_0}{\partial \tilde{\lambda}}\Big|_{M,\tilde{\mu}} + \beta_\mu \frac{\partial \ln \mu_0}{\partial \tilde{\mu}}\Big|_{M,\tilde{\lambda}} = \frac{\partial \ln(\mu_0/M^\varepsilon)}{\partial \ln M}\Big|_{\lambda_0,\mu_0} = -\varepsilon \ , \tag{4.77}$$

we find

$$\varepsilon\mathcal{O}_2 + \varepsilon\mathcal{O}_3 = \eta\mathcal{O}_1 - \beta_\lambda/\tilde{\lambda}[\mathcal{O}_2] - \beta_\mu/\tilde{\mu}[\mathcal{O}_3] + a\partial^2[u_{\alpha\alpha}] + b\partial_\alpha\partial_\beta[u_{\alpha\alpha}] \tag{4.78}$$

with divergent coefficients a and b. This relation can be rewritten in a more explicit notation by setting $[\mathcal{O}_2] = M^\varepsilon\tilde{\lambda}[(u_{\alpha\alpha})^2]/2$, $[\mathcal{O}_3] = M^\varepsilon\tilde{\mu}[u_{\alpha\beta}u_{\alpha\beta}]$. In this basis, Eq. (4.78) becomes

$$\begin{aligned}\frac{\varepsilon}{2}\left(\lambda_0(u_{\alpha\alpha})^2 + 2\mu_0 u_{\alpha\beta}u_{\alpha\beta}\right) = \eta\mathcal{O}_1 - \frac{1}{2}\beta_\lambda M^\varepsilon[(u_{\alpha\alpha})^2] - \beta_\mu M^\varepsilon[u_{\alpha\beta}u_{\alpha\beta}] \\ + a\partial^2[u_{\alpha\alpha}] + b\partial_\alpha\partial_\beta[u_{\alpha\alpha}] \ .\end{aligned} \tag{4.79}$$

As a final remark, we note that Eqs. (4.66), (4.71), and (4.73) imply that the operator $\mathcal{O}_6 = u_{\alpha\alpha}$ does not enter the renormalization of $\mathcal{O}_1$, $\mathcal{O}_2$, and $\mathcal{O}_3$. This is due to the use of dimensional regularization, implicit in the derivations above. This regularization scheme automatically removes ultraviolet divergences of power-law type, implying that operators of dimension 4 do not mix under renormalization with operators of dimension 2.

With results derived above, it is possible to show that the Ward identity for broken dilatation invariance is equivalent to the RG equations (2.36). (An analogue result was derived for scalar field theory in Ref. [138, 139]). Away from fixed points, the dilatation current $S_\alpha = x_\beta\theta_{\alpha\beta} - V_\alpha$ is not conserved: the RG flow functions β_λ and β_μ act as sources for the violation of the conservation law of S_α

$$\begin{aligned}\partial_\alpha S_\alpha = \frac{\beta_\lambda}{2}M^\varepsilon[(u_{\alpha\alpha})^2] + \beta_\mu M^\varepsilon[u_{\alpha\beta}u_{\alpha\beta}] - x_\beta\left(\mathbf{E}\cdot\partial_\beta\mathbf{h} + E_\alpha\partial_\beta u_\alpha\right) \\ - \frac{(\eta-\varepsilon)}{2}\mathbf{E}\cdot\mathbf{h} - (1+\eta-\varepsilon)E_\alpha u_\alpha \ .\end{aligned} \tag{4.80}$$

Renormalized correlation functions with insertions of $\partial_\alpha S_\alpha(\mathbf{x})$, which are relevant for the Ward identity, can be expressed more explicitly by using that the operators $\mathbf{E}\cdot\partial_\beta\mathbf{h}$, $E_\alpha\partial_\beta u_\alpha$, $\mathbf{E}\cdot\mathbf{h}$, $E_\alpha u_\alpha$, proportional to equations of motion, generate contact terms [138, 139, 141] derived in Eqs. (4.27), (4.28), (4.29). Using Eqs. (4.72) and (4.74), and integrating over space, we obtain

$$\begin{aligned}\int \mathrm{d}^D x\ \partial_\alpha\tilde{G}^{(n,\ell)}_{S_\alpha(\mathbf{x})} = \Big[\frac{\partial}{\partial\ln\rho} + \beta_\lambda\frac{\partial}{\partial\tilde{\lambda}}\Big|_{M,\tilde{\mu}} + \beta_\mu\frac{\partial}{\partial\tilde{\mu}}\Big|_{M,\tilde{\lambda}} + \frac{n}{2}(\eta-\varepsilon) \\ + \ell(1+\eta-\varepsilon)\Big]\tilde{G}^{(n,\ell)}(\rho\mathbf{x}_1,..,\rho\mathbf{x}_n;\rho\mathbf{x}'_1,..,\rho\mathbf{x}'_\ell) = 0\end{aligned} \tag{4.81}$$

a relation equivalent to the RG flow equation (2.36).

For completeness, we also discuss the composite field $u_{\alpha\beta}$. By symmetries and power counting its renormalization has the form

$$u_{\alpha\beta} = Z_2[u_{\alpha\beta}] + \frac{1}{D}(Z_2' - Z_2)\delta_{\alpha\beta}[u_{\gamma\gamma}] \ , \tag{4.82}$$

where Z_2 and Z_2' are divergent coefficients. The factors Z_2 and Z_2', moreover,are determined to all orders by the following argument. Let us consider the stress field $\sigma_{\alpha\beta} = \lambda_0\delta_{\alpha\beta}u_{\gamma\gamma} + 2\mu_0 u_{\alpha\beta}$. This composite operator can be viewed as the conserved current associated with the shift symmetry $u_\alpha \to u_\alpha + B_\alpha$ and it has a conservation law $\partial_\beta\sigma_{\alpha\beta} = -E_\alpha$ which is identical, up to a sign, to the equations of motion of the u_α field. By a general property, the renormalization of the equation of motion operator is dual to that of the corresponding field: since u_α renormalizes as $u_\alpha = Z\tilde{u}_\alpha$, then ZE_α is a finite operator. It follows, as a result, that $Z(\partial_\beta\sigma_{\alpha\beta})$ is finite. However, this also implies that $Z\sigma_{\alpha\beta}$ is finite by itself, because any divergence in $Z\sigma_{\alpha\beta}$ would inevitably appear in the derivative. To see this more precisely, note that the infinite part $Z\sigma^{\rm div}_{\alpha\beta}$ of $Z\sigma_{\alpha\beta}$, if any, should be a linear combination of $u_{\alpha\beta}$ and $\delta_{\alpha\beta}u_{\gamma\gamma}$ satisfying the equation $\partial_\alpha(Z\sigma^{\rm div}_{\alpha\beta}) = 0$ identically. It can be checked that the only possibility is $Z\sigma^{\rm div}_{\alpha\beta} = 0$ and, therefore, that the full tensor $Z\sigma_{\alpha\beta}$ is finite. Using Eq. (4.82) and Eq. (2.34), we see that the combinations of renormalization constants

$$\frac{g_\mu Z_2}{Z} \ , \qquad \frac{(g_\lambda + 2g_\mu/D)}{Z}Z_2' \tag{4.83}$$

are free of poles in ε. This implies that we can choose

$$Z_2 = \frac{Z\tilde{\mu}}{g_\mu} \ , \qquad Z_2' = \frac{Z(D\tilde{\lambda} + 2\tilde{\mu})}{Dg_\lambda + 2g_\mu} \ . \tag{4.84}$$

The scaling dimensions of the scalar and traceless components of $u_{\alpha\beta}$ are then $D - 2 + \eta_2'$ and $D - 2 + \eta_2$, respectively, where

$$\eta_2' = \partial \ln Z_2'/\partial \ln M|_{\lambda_0,\mu_0} \ , \qquad \eta_2 = \partial \ln Z_2/\partial \ln M|_{\lambda_0,\mu_0} \ . \tag{4.85}$$

At the fixed point P_4 all components of $u_{\alpha\beta}$ scale with the same dimension $\Delta_{u_{\alpha\beta}} = 2 - \eta_*$.

4.B RENORMALIZATION OF NON-INVARIANT CURRENTS

Besides invariant operators, expansion of the trace $\theta_{\alpha\alpha}$ includes the vector fields $u_\alpha u_{\beta\beta}$ and $u_\beta u_{\alpha\beta}$, which break the shift symmetry $u_\alpha \to u_\alpha + B_\alpha$ and the linearized embedding-space rotational symmetry. This appendix shows that these vectors are non-renormalized, up to total derivatives.

As a first step, it is convenient to analyze the tensor $J_{\gamma,\alpha\beta} = u_\gamma \sigma_{\alpha\beta}$, where $\sigma_{\alpha\beta} = \lambda_0 \delta_{\alpha\beta} u_{\delta\delta} + 2\mu_0 u_{\alpha\beta}$ is the stress field, which is also the conserved current associated with the symmetry under $u_\alpha \to u_\alpha + B_\alpha$. A priori, the renormalization of $u_\gamma \sigma_{\alpha\beta}$ involves the mixing of all composite fields of dimension 3 symmetric under $\alpha \leftrightarrow \beta$ and invariant under $\mathbf{h} \to \mathbf{h} + \mathbf{B}$. (In dimensional regularization there is no mixing with operators of lower dimension). Renormalization is however simplified by the following considerations. Taking the derivative $\partial_\alpha J_{\gamma,\alpha\beta} = -E_\beta u_\gamma + \partial_\alpha u_\gamma \sigma_{\alpha\beta}$ gives the sum of two simple terms. The first, $-E_\beta(\mathbf{x}) u_\gamma(\mathbf{x})$, vanishes with equations of motion and acts, when inserted in a correlation function, as the generator of the infinitesimal field redefinition $u_\alpha(\mathbf{x}') \to u_\alpha(\mathbf{x}') + \epsilon \delta_{\alpha\beta} \delta(\mathbf{x} - \mathbf{x}') u_\gamma(\mathbf{x})$. This transformation, being linear, can be equivalently represented in terms of renormalized fields as $\tilde{u}_\alpha(\mathbf{x}') \to \tilde{u}_\alpha(\mathbf{x}') + \epsilon \delta_{\alpha\beta} \delta(\mathbf{x} - \mathbf{x}') \tilde{u}_\gamma(\mathbf{x}')$, a change of variables which preserves the finiteness of correlation functions. It follows that insertions of $-E_\beta u_\gamma$ in renormalized functions is finite, and does not require renormalization. It is, in fact, a general property that operators of the form $E_\phi \phi$ are not renormalized [138]. The second term in $\partial_\alpha J_{\gamma,\alpha\beta}$, $\partial_\alpha u_\gamma \sigma_{\alpha\beta}$, requires subtractions but, being invariant under shifts of the u_α field, it can only mix with composite fields which are symmetric under both $\mathbf{h} \to \mathbf{h} + \mathbf{B}$ and $u_\alpha \to u_\alpha + B_\alpha$.

We can thus conclude that the UV-divergent part $J^{\rm div}_{\gamma,\alpha\beta}$ of $J_{\gamma,\alpha\beta}$ must have the property that $\partial_\alpha J^{\rm div}_{\gamma,\alpha\beta}$ is invariant under shifts of all fields. This, however, implies in turn that $J^{\rm div}_{\gamma,\alpha\beta}$ must be shift-invariant by itself. To derive this result, let us denote as $\epsilon J^{\rm div}_{\mu,\gamma,\alpha\beta}$ the variation of $J^{\rm div}_{\gamma,\alpha\beta}$ under an infinitesimal uniform translation $u_\alpha \to u_\alpha + \epsilon \delta_{\alpha\mu}$. By power counting it must be a field of dimension 2 and, therefore, must have the form

$$J^{\rm div}_{\mu,\gamma,\alpha\beta} = a^{(1)}_{\rho\sigma,\mu,\gamma,\alpha\beta} M^\varepsilon u_\rho u_\sigma + a^{(2)}_{\rho,\sigma,\mu,\gamma,\alpha\beta} \partial_\rho u_\sigma + \frac{1}{2} a^{(3)}_{\rho\sigma,\mu,\gamma,\alpha\beta} (\partial_\rho \mathbf{h} \cdot \partial_\sigma \mathbf{h}) \ , \quad (4.86)$$

where $a^{(1)}$, $a^{(2)}$, and $a^{(3)}$ are invariant tensors (linear combinations of products of Kronecker symbols). At the same time, by the arguments above, it must satisfy the equation $\partial_\alpha J^{\rm div}_{\mu,\gamma,\alpha\beta} = 0$ identically. It can be checked that the only possibility is $J^{\rm div}_{\mu,\gamma,\alpha\beta} = 0$, which implies that $J^{\rm div}_{\gamma,\alpha\beta}$ is invariant under shifts.

The conclusion of this argument is that any counterterm entering the renormalization of $J_{\gamma,\alpha\beta}$ must be a tensor of dimension 3 invariant under translations of both the $\mathbf{h}$ and the u_α fields. These tensors have the schematic form $\partial\partial u$ and $\partial \mathbf{h} \cdot \partial\partial \mathbf{h}$ and, since

$$\partial_\mu \partial_\nu \mathbf{h} \cdot \partial_\rho \mathbf{h} = \frac{1}{2} \left[\partial_\nu (\partial_\mu \mathbf{h} \cdot \partial_\rho \mathbf{h}) + \partial_\mu (\partial_\nu \mathbf{h} \cdot \partial_\rho \mathbf{h}) - \partial_\rho (\partial_\mu \mathbf{h} \cdot \partial_\nu \mathbf{h}) \right] \ , \quad (4.87)$$

they can always be represented as total derivatives. Therefore, general counterterms needed for the renormalization of $J_{\gamma,\alpha\beta}$ have the form

$$\frac{1}{2} B_{\rho,\mu\nu,\gamma,\alpha\beta} \partial_\rho (\partial_\mu \mathbf{h} \cdot \partial_\nu \mathbf{h}) + C_{\rho\sigma,\mu,\gamma,\alpha\beta} \partial_\rho \partial_\sigma u_\mu \ , \quad (4.88)$$

where $B_{\rho,\mu\nu,\gamma,\alpha\beta}$ and $C_{\rho\sigma,\mu,\gamma,\alpha\beta}$ are invariant tensors with divergent coefficients. The renormalization of $J_{\gamma,\alpha\beta}$ in minimal subtraction can thus be written in the form

$$[J_{\gamma,\alpha\beta}] = J_{\gamma,\alpha\beta} + \frac{1}{2} B_{\rho,\mu\nu,\gamma,\alpha\beta} \partial_\rho (\partial_\mu \mathbf{h} \cdot \partial_\nu \mathbf{h}) + C_{\rho\sigma,\mu,\gamma,\alpha\beta} \partial_\rho \partial_\sigma u_\mu \ . \tag{4.89}$$

The final result for the renormalization of $J_{\gamma,\alpha\beta}$ has the following diagrammatic interpretation. Among 1PI correlation functions with insertion of $J_{\gamma,\alpha\beta} = u_\gamma \sigma_{\alpha\beta}$, there are two types of divergent Feynman diagrams: the undifferentiated u_γ field can be either connected to external legs or joined to loop lines (see Fig. 4.4). In all diagrams of the second type, like (c), (d), and (e) of Fig. 4.4, it is possible to factorize one power of the momentum of each external solid and wiggly line, as it follows directly from the structure of the interaction vertices. The corresponding divergences contribute to shift-invariant counterterms of the type $\partial\partial u$ and $\partial(\partial\mathbf{h}\cdot\partial\mathbf{h})$ in Eq. (4.89), but cannot generate renormalizations proportional to $J_{\gamma,\alpha\beta}$.

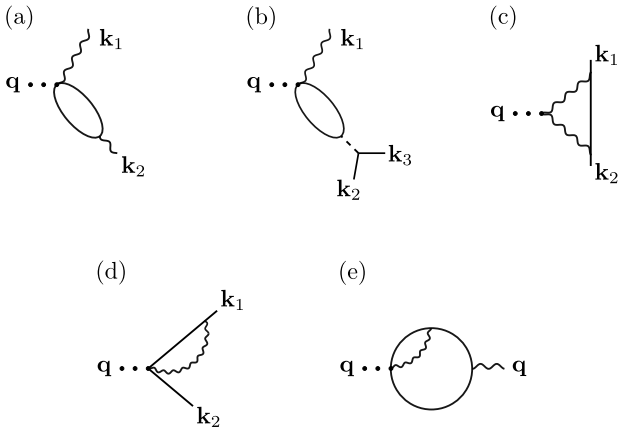

Figure 4.4: Some of the first divergent 1PI diagrams with insertion of $J_{\gamma,\alpha\beta}$. Dotted lines denote the operator insertion. In diagrams (a) and (b), the undifferentiated field u_γ is connected directly to external lines. In diagrams (c), (d), and (e), instead, it enters as a loop line.

Counterterms of the same form of $J_{\gamma,\alpha\beta}$ can only arise from diagrams of the first type, like (a) and (b) in Fig. 4.4, which contribute to correlations which are not shift-invariant. Since the undifferentiated u_γ field is contracted with external lines, the loop part in this class of diagrams is entirely determined by the insertion of $\sigma_{\alpha\beta}$, whose renormalization was studied in appendix 4.A. The arguments above show that the UV divergences of λ_0 and μ_0 are precisely cancelled to all orders by

these loop contributions, so that $J_{\gamma,\alpha\beta}$ is finite (up to counterterms introduced in Eq. (4.89)).

Taking two independent traces over the components of $J_{\gamma,\alpha\beta}$ we finally obtain relations for the renormalization of the vector fields $u_\alpha u_{\beta\beta}$ and $u_\beta u_{\alpha\beta}$. With a non-minimal renormalization choice, we can set

$$\begin{aligned} u_\alpha u_{\beta\beta} = {} & \frac{M^\varepsilon(D\tilde{\lambda}+2\tilde{\mu})}{D\lambda_0+2\mu_0}[u_\alpha u_{\beta\beta}] \\ & + b_1\partial_\alpha[\partial_\beta\mathbf{h}\cdot\partial_\beta\mathbf{h}] + b_2\partial_\beta[\partial_\alpha\mathbf{h}\cdot\partial_\beta\mathbf{h}] + b_3\partial^2[u_\alpha] + b_4\partial_\alpha\partial_\beta[u_\beta]\ , \end{aligned} \tag{4.90}$$

$$\begin{aligned} u_\beta u_{\alpha\beta} - \frac{1}{D}u_\alpha u_{\beta\beta} = {} & \frac{M^\varepsilon\tilde{\mu}}{\mu_0}\left\{[u_\beta u_{\alpha\beta}] - \frac{1}{D}[u_\alpha u_{\beta\beta}]\right\} \\ & + b_1'\partial_\alpha[\partial_\beta\mathbf{h}\cdot\partial_\beta\mathbf{h}] + b_2'\partial_\beta[\partial_\alpha\mathbf{h}\cdot\partial_\beta\mathbf{h}] + b_3'\partial^2[u_\alpha] + b_4'\partial_\alpha\partial_\beta[u_\beta]\ . \end{aligned} \tag{4.91}$$

4.C ENERGY-MOMENTUM TENSOR AND OPERATOR RENORMALIZATION IN THE GCI MODEL

Starting from the explicit expression of its Hamiltonian, Eq. (3.7), it can be shown that the GCI model admits the following symmetric energy-momentum tensor

$$\begin{aligned} \theta_{\alpha\beta} = {} & -\frac{1}{2}\delta_{\alpha\beta}(\partial^2\mathbf{h})^2 + 2\partial_\alpha\partial_\beta\mathbf{h}\cdot\partial^2\mathbf{h} - \partial_\alpha\mathbf{h}\cdot\partial_\beta\partial^2\mathbf{h} - \partial_\beta\mathbf{h}\cdot\partial_\alpha\partial^2\mathbf{h} \\ & + \frac{1}{D-1}\big[\delta_{\alpha\beta}\partial_\gamma\mathbf{h}\cdot\partial_\gamma\partial^2\mathbf{h} + \delta_{\alpha\beta}\partial_\gamma\partial_\delta\mathbf{h}\cdot\partial_\gamma\partial_\delta\mathbf{h} \\ & + (D-2)\partial_\gamma\mathbf{h}\cdot\partial_\alpha\partial_\beta\partial_\gamma\mathbf{h} - D\partial_\alpha\partial_\gamma\mathbf{h}\cdot\partial_\beta\partial_\gamma\mathbf{h}\big] \\ & - \frac{1}{2Y_0}\delta_{\alpha\beta}(\partial^2\chi)^2 + \frac{1}{Y_0}\big[2\partial_\alpha\partial_\beta\chi\partial^2\chi - \partial_\alpha\chi\partial_\beta\partial^2\chi - \partial_\beta\chi\partial_\alpha\partial^2\chi\big] \\ & + \frac{1}{(D-1)Y_0}\big[\delta_{\alpha\beta}\partial_\gamma\chi\partial_\gamma\partial^2\chi + \delta_{\alpha\beta}\partial_\gamma\partial_\delta\chi\partial_\gamma\partial_\delta\chi \\ & + (D-2)\partial_\gamma\chi\partial_\alpha\partial_\beta\partial_\gamma\chi - D\partial_\alpha\partial_\gamma\chi\partial_\beta\partial_\gamma\chi\big] \\ & - \frac{i}{2}\delta_{\alpha\beta}\big[(\partial_\gamma\mathbf{h}\cdot\partial_\delta\mathbf{h})\partial_\gamma\partial_\delta\chi - (\partial_\gamma\mathbf{h}\cdot\partial_\gamma\mathbf{h})\partial^2\chi\big] + i\big[(\partial_\beta\mathbf{h}\cdot\partial_\gamma\mathbf{h})\partial_\alpha\partial_\gamma\chi \\ & + (\partial_\alpha\mathbf{h}\cdot\partial_\gamma\mathbf{h})\partial_\beta\partial_\gamma\chi - (\partial_\alpha\mathbf{h}\cdot\partial_\beta\mathbf{h})\partial^2\chi - (\partial_\gamma\mathbf{h}\cdot\partial_\gamma\mathbf{h})\partial_\alpha\partial_\beta\chi\big] \\ & + \frac{i}{2}\partial_\gamma\big[(\partial_\alpha\mathbf{h}\cdot\partial_\beta\mathbf{h})\partial_\gamma\chi - (\partial_\alpha\mathbf{h}\cdot\partial_\gamma\mathbf{h})\partial_\beta\chi - (\partial_\beta\mathbf{h}\cdot\partial_\gamma\mathbf{h})\partial_\alpha\chi \\ & + (\delta_{\alpha\gamma}\partial_\beta\chi + \delta_{\beta\gamma}\partial_\alpha\chi - \delta_{\alpha\beta}\partial_\gamma\chi)(\partial_\delta\mathbf{h}\cdot\partial_\delta\mathbf{h})\big]\ , \end{aligned} \tag{4.92}$$

The identity for the trace, Eq. (4.41), can be derived from Eq. (4.92) by some algebraic steps and by the following results for the renormalization of the invariant operators $(\partial^2\mathbf{h})^2$ and $(\partial^2\chi)^2/Y_0$.

Within dimensional regularization, symmetries and power counting imply that the set of composite operators

$$\begin{aligned}
\mathcal{O}_1 &= \frac{1}{2}(\partial^2\mathbf{h})^2 - \frac{1}{Y_0}(\partial^2\chi)^2 \ , \qquad \mathcal{O}_2 = \frac{1}{2Y_0}(\partial^2\chi)^2 \ , \\
\mathcal{O}_3 &= \frac{1}{2Y_0}((\partial^2\chi)^2 - (\partial_\alpha\partial_\beta\chi\partial_\alpha\partial_\beta\chi)) \\
&= \frac{1}{2Y_0}\partial_\alpha\partial_\beta(\partial_\alpha\chi\partial_\beta\chi - \delta_{\alpha\beta}\partial_\gamma\chi\partial_\gamma\chi) \ , \\
\mathcal{O}_4 &= \frac{1}{Y_0}\partial^2\partial^2\chi \ , \\
\mathcal{O}_5 &= E = \frac{1}{Y_0}\partial^2\partial^2\chi + \frac{i}{2}((\partial^2\mathbf{h})^2 - (\partial_\alpha\partial_\beta\mathbf{h}\cdot\partial_\alpha\partial_\beta\mathbf{h}))
\end{aligned} \tag{4.93}$$

is closed under renormalization. The set (4.93), in fact, is a complete basis for all composite fields which are invariant under the symmetries of the GCI Hamiltonian (including the shifts $\mathbf{h} \to \mathbf{A} + \mathbf{B}_\alpha x_\alpha$, $\chi \to \chi + A + B_\alpha x_\alpha$) and which have operator dimension 4 in the ε-expansion. A residual mixing with the softer field $\mathcal{O}_6 = \partial^2\chi$, which has dimension 2, is removed by dimensional regularization.

The operator $\mathcal{O}_4$ is directly related to the elementary field χ and, therefore, has a simple multiplicative renormalization $\mathcal{O}_4 = ZZ_Y^{-1}[\mathcal{O}_4]$. Similarly $\mathcal{O}_5$, which is equal to the equation of motion of the χ field, renormalizes in a multiplicative way as $\mathcal{O}_5 = Z[\mathcal{O}_5]$. We also note that the last three operators in the set (4.93), $\mathcal{O}_3$, $\mathcal{O}_4$, and $\mathcal{O}_5$, are expressible as exact second derivatives of lower-dimensional fields. In particular, this implies that $[\mathcal{O}_3]$ is a linear combination of $\mathcal{O}_3$, $\mathcal{O}_4$, and $\mathcal{O}_5$, without a mixing with $\mathcal{O}_1$ and $\mathcal{O}_2$.

To study the renormalization of $\mathcal{O}_1$ we note that, when integrated over all space, it is equivalent to the variation of the Hamiltonian under the infinitesimal rescaling $\mathbf{h} \to (1+\epsilon/2)\mathbf{h}$, $\chi \to (1-\epsilon)\chi$. Therefore insertions of $\mathcal{O}_1$ at zero momentum have the only effect to generate a factor $(n/2-\ell)$ in front of correlation functions, where n is the number of external $\mathbf{h}$ fields and ℓ is the number of χ lines. An immediate consequence is that $\mathcal{O}_1$ is finite up to total-derivative operators which vanish at zero momentum. Since the only total-derivative fields which can enter as counterterms are $\mathcal{O}_3$, $\mathcal{O}_4$, and $\mathcal{O}_5$, we conclude that $\mathcal{O}_1$ can be renormalized to all orders as $\mathcal{O}_1 = [\mathcal{O}_1] + a_1[\mathcal{O}_3] + b_1[\mathcal{O}_4] + c_1[\mathcal{O}_5]$, where a_1, b_1, and c_1 are divergent coefficients.

The renormalization of $\mathcal{O}_2$ is constrained by the fact that the derivative of renormalized correlation functions with respect to Y is finite. Since, by Eq. (3.13), bare and renormalized correlation functions with n external $\mathbf{h}$ lines and ℓ external χ lines are related as $G^{(n,\ell)} = Z^{n/2-\ell}\tilde{G}^{(n,\ell)}$, we obtain that

$$-\left(\frac{n}{2}-\ell\right)\frac{\partial \ln Z}{\partial Y}\Big|_M \tilde{G}^{(n,\ell)} + Z^{\ell-n/2}\frac{\partial \ln Y_0}{\partial Y}\Big|_M \frac{\partial G^{(n,\ell)}}{\partial \ln Y_0} = \text{finite} \ . \tag{4.94}$$

The action of $\partial/\partial \ln Y_0$ on bare correlation functions generates insertion of $\mathcal{O}_2$ at zero momentum. The factor $(n/2+\ell)$, moreover, can be represented via the zero-momentum insertion of $\mathcal{O}_1$.

Using the relations

$$\frac{\partial \ln Z}{\partial Y}\Big|_M = \frac{\eta(Y)}{\beta(Y)} \ , \qquad \frac{\partial \ln Y_0}{\partial Y}\Big|_M = -\frac{\varepsilon}{\beta(Y)} \ , \tag{4.95}$$

we obtain that

$$\frac{\eta(Y)}{\beta(Y)}\mathcal{O}_1 + \frac{\varepsilon}{\beta(Y)}\mathcal{O}_2 \tag{4.96}$$

is finite up to total derivatives. It follows that the renormalization of $\mathcal{O}_2$ has the form (in the minimal subtraction scheme)

$$\mathcal{O}_2 = -\frac{1}{\varepsilon}\eta(Y)[\mathcal{O}_1] - \frac{\beta(Y)}{\varepsilon Y}[\mathcal{O}_2] + a_2[\mathcal{O}_3] + b_2[\mathcal{O}_4] + b_3[\mathcal{O}_5] \ , \tag{4.97}$$

where a_2, b_2, and c_2 are new divergent coefficients. Since in minimal subtraction $[\mathcal{O}_2] = [(\partial^2\chi)^2]/(2M^\varepsilon Y)$, we can rewrite this renormalization relation as

$$\begin{aligned} \frac{\varepsilon}{2Y_0}(\partial^2\chi)^2 = &-\eta(Y)[\mathcal{O}_1] - \frac{\beta(Y)}{2Y^2}M^{-\varepsilon}[(\partial^2\chi)^2] \\ &+ \varepsilon a_2[\mathcal{O}_3] + \varepsilon b_2[\mathcal{O}_4] + \varepsilon b_3[\mathcal{O}_5] \ . \end{aligned} \tag{4.98}$$

As a further consequence, we note that

$$\frac{\partial \tilde{G}^{(n,\ell)}}{\partial \ln Y}\Big|_M = \frac{1}{2M^\varepsilon Y}\int \mathrm{d}^D x \ \tilde{G}^{(n,\ell)}_{[(\partial^2\chi(\mathbf{x}))^2]} \ . \tag{4.99}$$

This relation can be used to prove the equivalence between dilatation Ward identities and the RG equations (3.16), in analogy with Ref. [138] and appendix 4.A.

5

QUANTUM MECHANICAL EFFECTS

We analyze the statistical mechanics of a free-standing quantum crystalline membrane within the framework of a systematic perturbative renormalization group (RG). A power-counting analysis shows that the leading singularities of correlation functions can be analyzed within an effective renormalizable model in which the kinetic energy of in-plane phonons and subleading geometrical nonlinearities in the expansion of the strain tensor are neglected. For membranes at zero temperature, governed by zero-point motion, the RG equations of the effective model provide a systematic derivation of logarithmic corrections to the bending rigidity and to the elastic Young modulus derived in earlier investigations. In the limit of a weakly applied external tension, the stress-strain relation at $T = 0$ is anomalous: the linear Hooke's law is replaced with a singular law exhibiting logarithmic corrections. For small, but finite temperatures, we use techniques of finite-size scaling to derive general relations between the zero-temperature RG flow and scaling laws of thermodynamic quantities such as the thermal expansion coefficient α, the entropy S, and the specific heat C. A combination of the scaling relations with an analysis of thermal fluctuations shows that, for small temperatures, the thermal expansion coefficient α is negative and logarithmically dependent on T, as predicted in an earlier work. Although the requirement $\lim_{T\to 0} \alpha = 0$, expected from the third law of thermodynamics is formally satisfied, α is predicted to exhibit such a slow variation to remain practically constant down to unaccessibly small temperatures.

This chapter has been published as:
Achille Mauri and Mikhail I. Katsnelson, "Perturbative renormalization and thermodynamics of quantum crystalline membranes", Phys. Rev. B **105**, 195434 (2022) (Editors' Suggestion); preprint: arXiv:2202.12842 (2022)

5.1 INTRODUCTION

The statistical mechanics of fluctuating elastic membranes has been investigated extensively over the last decades, in connection with a broad variety of physical systems, from biological layers to graphene and other atomically-thin two-dimensional materials. As it has long been realized, models of flexible surfaces subject to vanishing or small external tension exhibit a rich and striking physical behavior, controlled by an interplay between fluctuations and mechanical nonlinearities [1, 3, 6, 9–12, 17–21, 25, 26, 43, 44, 51, 62, 78]. A crucial prediction, in particular, is that for homogeneous free-standing membranes without an imposed stress, anharmonicities inherent in the geometrical definition of the elastic strain tensor are responsible for the stabilization of a macroscopically flat phase at finite temperatures [1, 6, 9, 10], and for a dramatic power-law renormalization of the effective scale-dependent bending rigidity and elastic constants. The presence of a quenched disorder, besides thermal fluctuations, has been predicted to induce an even richer physical behavior [1, 17, 25, 43, 44]. Renormalizations of elastic and thermodynamic properties by ripples have also been analyzed in experiments on graphene membranes [70, 72, 74, 75].

Over the last years, aiming at a more complete theory of fluctuations in graphene, several authors have revisited and extended the analysis by considering the effects of quantization [91, 162–164] and of the coupling between membrane phonons and Dirac electrons [54, 55, 165, 166]. The interaction between flexural and electronic degrees of freedom, in particular, has been predicted to generate mechanical instabilities leading to a spontaneous rippling of the membrane.

Despite the progress in investigations of the coupled membrane-electron problem, the theory of purely mechanical degrees of freedom in a flexible surface subject to both thermal and quantum fluctuations is already highly non-trivial. By a combination of elasticity theory and a one-loop momentum-shell renormalization group, Ref. [162, 163] showed that, for a homogeneous and unstressed membrane at absolute zero, mechanical nonlinearities give rise to logarithmic renormalizations of the wavevector-dependent bending stiffness and elastic constants, in sharp contrast with the much stronger power-law renormalizations induced by thermal fluctuations.

In Ref. [164], the theory of quantum flexible membranes was reanalyzed, and extended to the finite temperature case, within the framework of non-perturbative renormalization group (NPRG) techniques. For zero temperature, the weak coupling limit of the NPRG recovers results consistent with the momentum-shell predictions of Ref. [162, 163]. At non-zero temperature, the NPRG analysis allowed to smoothly interpolate a crossover between a short wavelength region of zero-point character, and a long-wavelength region, determined by thermal fluctuations. In more detail, the results of Ref. [164] predicted a RG flow exhibiting a first quantum region in

which anharmonicities are marginally irrelevant, followed, after a smooth crossover, by a classical region in which nonlinearities are relevant, destabilize the weak coupling approximation, and drive the system to the universal interacting fixed point describing classical thermally-fluctuating membranes [1, 10–12, 26, 51]. The corresponding correlation functions, in particular, behave in the long-wavelength limit according to the anomalous scaling law characteristic of classical membranes: in the limit of vanishing wavevector $\mathbf{k} \to 0$, the effective bending rigidity diverges as $\kappa(\mathbf{k}) \approx k^{-\eta_*}$ and the elastic Lamé constant vanish as $\lambda(\mathbf{k}), \mu(\mathbf{k}) \approx k^{2-2\eta_*}$. A similar picture was derived in Ref. [91], by combining a one-loop RG with a physical approximation: the replacement of the full anharmonic free energy with a Bose-Einstein function with renormalized phonon dispersions. Other field-theoretical analyses on quantum flexible membranes, such as the expansion for large embedding-space dimension and a generalization of the classical self-consistent screening approximation, were developed in Ref. [54], as a part of a wider analysis including the coupling between phonons and Dirac electrons. We finally note that, by different approaches, Refs. [167, 168], have predicted a dynamical behavior qualitatively in contrast with Refs. [91, 162–164]: that flexural phonon modes acquire a non-zero sound velocity and a linear dispersion relation $\omega(\mathbf{k}) \propto |\mathbf{k}|$.

In parallel with analytical approaches, fluctuations of a quantum graphene sheet have also been studied by numerical path-integral simulations based on realistic empirical potentials for interatomic interactions in carbon (see, for example, Ref. [36, 38]).

The objective of this work is to analyze the anharmonic effects in quantum membranes by systematic perturbative renormalization group methods. By a power-counting analysis, we construct an effective renormalizable model which we expect to capture the dominant singularities of physical quantities in the limit of low energies, momenta, temperatures and tensions. At $T = 0$, the model is renormalizable in the sense of power counting, although it exhibits anisotropic scaling between space and time, in analogy with other theories with "weighted power counting" [15, 100, 169–172]. The corresponding RG equations recover in a systematic framework the earlier results derived in Refs. [91, 162–164]. We also note that the model is mathematically equivalent to a theory of the decoupled lamellar phase of a three-dimensional stack of classical crystalline membranes analyzed in Ref. [11].

For finite temperatures, we use techniques well-known in the theory of finite size scaling and other finite-temperature field theories [15, 173]. In particular, we use the general property that ultraviolet divergences are temperature-independent and can be renormalized by T-independent counterterms [15, 173] to derive scaling laws for various thermodynamic quantities: the thermal expansion coefficient $\tilde{\alpha}$, the entropy $\tilde{S}$, and the specific heat $\tilde{C}$. By combining the scaling relations with an analysis of thermal fluctuations, we recover the result that, for a membrane

subject to zero external tension, $\tilde{\alpha}$ is negative and tends to zero in the limit $T \to 0$ as a logarithmic function of T, as predicted in Ref. [91].

The effective model and the method used to derive scaling equations are intrinsically focused on the behavior of thermodynamic quantities in the limit of small temperatures. Therefore, the theory developed here cannot capture the detailed T dependence of the thermal expansion coefficient at moderately high temperatures. In particular, the question whether $\tilde{\alpha}$ changes sign at a certain temperature [36, 168, 174, 175], is beyond the scope of this work. We note, however, that the behavior of out-of-plane fluctuations analyzed here contrasts with the prediction of a linear dispersion relation for flexural phonons, which was used in the analyses of Refs. [167, 168].

The coefficient of in-plane thermal expansion of graphene has been estimated by a number of experimental techniques, both for suspended samples and for samples bound to a substrate (see, for example, Refs. [74, 176–179] and references therein). Experimental results indicate usually a negative thermal expansion at not too large temperatures, although a positive expansion has been identified in Ref. [180] in the case of graphene on a Ir(111) substrate down to liquid helium temperatures.

It would be interesting to test experimentally the prediction of that $\tilde{\alpha}$ is nearly temperature-independent (the logarithmic functions of T change very slowly over broad temperature scales). This prediction applies only to membranes without a supporting substrate and without stress. For a nonzero applied tension, the low-temperature behavior of the thermal expansion coefficient was predicted to vanish in a faster way as $T \to 0$ in Ref. [91].

5.2 MODEL

To study fluctuations of a quantum membrane, we analyze throughout this work an effective low-energy model defined by the path integral

$$\mathcal{Z} = \int [\mathrm{d}\mathbf{h}(\mathbf{x},\tau)\mathrm{d}u_\alpha(\mathbf{x},\tau)]\mathrm{e}^{-S/\hbar} \tag{5.1}$$

and the imaginary-time action

$$\begin{aligned} S[\mathbf{h}(\mathbf{x},\tau),u_\alpha(\mathbf{x},\tau)] = \int_0^{\hbar/(k_\mathrm{B}\tilde{T})} \mathrm{d}\tau \int \mathrm{d}^2x \Big\{ \frac{\tilde{\rho}}{2}\dot{\mathbf{h}}^2 + \frac{\tilde{\kappa}}{2}(\partial^2\mathbf{h})^2 \\ + \frac{\tilde{\lambda}}{2}(u_{\alpha\alpha})^2 + \tilde{\mu}u_{\alpha\beta}u_{\alpha\beta} - \tilde{\sigma}\partial_\alpha u_\alpha \Big\} . \end{aligned} \tag{5.2}$$

The degrees of freedom $u_\alpha(\mathbf{x},\tau)$ and $\mathbf{h}(\mathbf{x},\tau)$ represent, respectively, in-plane and out-of-plane displacements of the mass points in the layer. The second line of the action represents the standard elastic energy [1, 6, 18] of a medium with bending

rigidity $\tilde{\kappa}$ and Lamé coefficients $\tilde{\lambda}$ and $\tilde{\mu}$, and is defined in terms of the strain tensor $u_{\alpha\beta} = (\partial_\alpha u_\beta + \partial_\beta u_\alpha + \partial_\alpha \mathbf{h} \cdot \partial_\beta \mathbf{h})/2$. The term $-\tilde{\sigma}\partial_\alpha u_\alpha$ describes an externally applied isotropic in-plane tension [18]. A positive $\tilde{\sigma} > 0$ drives a stretching of the membrane, while $\tilde{\sigma} < 0$ corresponds to a compressive stress, which tends to buckle the system out of plane. The first term in the action, $\tilde{\rho}\dot{\mathbf{h}}^2/2$, describes instead the kinetic energy of out-of-plane fluctuations, and is proportional to the areal mass density $\tilde{\rho}$ and to the square of the out-of-plane velocity $\dot{\mathbf{h}} = \partial \mathbf{h}(\mathbf{x}, \tau)/\partial\tau$. Although physically $\mathbf{h}$ is a scalar quantity, we consider in general $\mathbf{h}$ to be a vector with d_c components ($d_c = 1$ for physical membranes embedded in three-dimensional space).

To regularize ultraviolet divergences we implicitly assume a large-momentum cutoff Λ of the order of the inverse lattice spacing.

5.2.1 *Rescaled units*

By the change of variables $\tau \to (\tilde{\rho}/\tilde{\kappa})^{1/2}\tau$, $\mathbf{h} \to \hbar^{1/2}/(\tilde{\rho}\tilde{\kappa})^{1/4}\mathbf{h}$, $u_\alpha \to \hbar/(\tilde{\rho}\tilde{\kappa})^{1/2}u_\alpha$, the reduced action $\mathcal{S} = S/\hbar$ can be recast as

$$\mathcal{S} = \int_0^{1/T} \mathrm{d}\tau \int \mathrm{d}^2x \left\{ \frac{\dot{\mathbf{h}}^2}{2} + \frac{1}{2}(\partial^2 \mathbf{h})^2 + \frac{\lambda}{2}(u_{\alpha\alpha})^2 + \mu u_{\alpha\beta}u_{\alpha\beta} - \sigma \partial_\alpha u_\alpha \right\} , \quad (5.3)$$

where $u_{\alpha\beta} = (\partial_\alpha u_\beta + \partial_\beta u_\alpha + \partial_\alpha \mathbf{h} \cdot \partial_\beta \mathbf{h})/2$, $\lambda = \hbar\tilde{\lambda}/(\tilde{\rho}\tilde{\kappa}^3)^{1/2}$, $\mu = \hbar\tilde{\mu}/(\tilde{\rho}\tilde{\kappa}^3)^{1/2}$, $T = (\tilde{\rho}/\tilde{\kappa})^{1/2}k_\mathrm{B}\tilde{T}/\hbar$, and $\sigma = \tilde{\sigma}/\tilde{\kappa}$. After these rescalings, all quantities have a dimension in units of wavevector. The elastic parameters λ and μ, which play the role of coupling constants, are dimensionless, while the temperature T and the tension σ have the dimension of a wavevector squared.

Throughout the rest of this paper, we always use rescaled units, unless explicitly mentioned. Quantities in standard units of measurements are marked with tilde symbols. The in-plane strain $\tilde{v}$, the Gibbs free energy per unit area $\tilde{G} = -k_\mathrm{B}\tilde{T}A^{-1}\ln \mathcal{Z}$, the entropy density $\tilde{S} = -\partial\tilde{G}/\partial\tilde{T}$, the specific heat $\tilde{C} = \tilde{T}\mathrm{d}\tilde{S}/\mathrm{d}\tilde{T}$, and the thermal expansion coefficient $\tilde{\alpha} = 2\mathrm{d}\tilde{v}/\mathrm{d}\tilde{T}$, expressed in conventional units, are related to the corresponding rescaled quantities v, $\tilde{G} = -TA^{-1}\ln \mathcal{Z}$, $S = -\partial\tilde{G}/\partial T$, $C = T\mathrm{d}S/\mathrm{d}T$, $\alpha = 2\mathrm{d}v/\mathrm{d}T$ as

$$\begin{aligned} &\tilde{v} = \frac{\hbar v}{(\tilde{\rho}\tilde{\kappa})^{1/2}} , \qquad \tilde{G} = \frac{\hbar\tilde{\kappa}^{1/2}}{\tilde{\rho}^{1/2}}\tilde{G} , \qquad \tilde{S} = k_\mathrm{B}S \\ &\tilde{C} = k_\mathrm{B}C , \qquad \tilde{\alpha} = k_\mathrm{B}\alpha/\tilde{\kappa} . \end{aligned} \quad (5.4)$$

5.2.2 *Derivation of the effective model*

The effective action (5.2) can be derived from a more complete theory by a power counting argument. Focusing on the case of a vanishing external tension $\sigma = 0$, a

more complete model, which includes the kinetic energy of in-plane modes is given by the manifestly rotationally-invariant action [22, 85, 91, 164]

$$S[\mathbf{r}(\mathbf{x},\tau)] = \frac{1}{2}\int_0^{\frac{\hbar}{k_B T}} \mathrm{d}\tau \int \mathrm{d}^2x \left\{ \tilde{\rho}\dot{\mathbf{r}}^2 + \tilde{\kappa}(\partial^2\mathbf{r})^2 + \tilde{\lambda}(U_{\alpha\alpha})^2 + 2\tilde{\mu}U_{\alpha\beta}U_{\alpha\beta} \right\} , \quad (5.5)$$

where $\mathbf{r} \in \mathbb{R}^d$ denotes fluctuating coordinates in the d-dimensional ambient space and $U_{\alpha\beta} = (\partial_\alpha \mathbf{r}\cdot\partial_\beta\mathbf{r} - \delta_{\alpha\beta})/2$. This fully rotationally-invariant theory can be analyzed by parametrizing $\mathbf{r}(\mathbf{x},\tau) = (\xi\mathbf{x} + \mathbf{u}(\mathbf{x},\tau), \mathbf{h}(\mathbf{x},\tau))$, where $\mathbf{u}$ and $\mathbf{h}$ are in-plane and out-of-plane displacement fields, while ξ encodes the tendency of the membrane to shrink due to fluctuations [11, 18, 85, 91, 164]. At zero temperature, a loop expansion (formally an expansion in powers of $\hbar$ [15]) can be given by calculating order by order correlation functions and $\xi = 1 + c_1\hbar + c_2\hbar^2 + ...$ The non-interacting propagators of in-plane and out-of-plane modes, defining the basic elements in the corresponding diagrammating expansion, are, respectively

$$\begin{aligned} \bar{D}^{(0)}_{\alpha\beta}(\omega,\mathbf{k}) &= \frac{\hbar k_\alpha k_\beta}{(\tilde{\rho}\omega^2 + (\tilde{\lambda}+2\tilde{\mu})|\mathbf{k}|^2 + \tilde{\kappa}|\mathbf{k}|^4)k^2} + \frac{\hbar(k^2\delta_{\alpha\beta} - k_\alpha k_\beta)}{(\tilde{\rho}\omega^2 + \tilde{\mu}|\mathbf{k}|^2 + \tilde{\kappa}|\mathbf{k}|^4)k^2} , \\ \bar{G}^{(0)}_{ij}(\omega,\mathbf{k}) &= \frac{\hbar\delta_{ij}}{\tilde{\rho}\omega^2 + \tilde{\kappa}|\mathbf{k}|^4} . \end{aligned} \quad (5.6)$$

For small $\mathbf{k}$, $\bar{D}^{(0)}_{\alpha\beta}(\omega,\mathbf{k})$ has a pole for $\omega \sim |\mathbf{k}|$ reflecting the linear dispersion of acoustic phonons while $\bar{G}^{(0)}_{\alpha\beta}(\omega,\mathbf{k})$ has a pole for $\omega \sim k^2$, corresponding to the ultrasoft dispersion of flexural fluctuations at zero external tension. Due to the softer infrared behavior of flexural phonons, we can assume that poles of $\bar{G}^{(0)}$ generate the leading singularities at long wavelengths. In the region $\omega \sim k^2$, interactions can be analyzed within power counting by assigning dimension $[\mathbf{x}] = -1$ to the spacial coordinates and $[\tau] = -z = -2$ to the time coordinate [164] (see Refs. [100, 169–172] for discussions of of various field theories which lack Lorentz and Euclidean invariance and which exhibit "weigthed power counting", with different weigth for space and time coordinates). The behavior of propagators for $\mathbf{k} \to 0$, $\omega \to 0$, $\omega \sim k^2$ implies that the canonical dimensions of fields are, respectively, $[\mathbf{h}] = (2+z-4)/2 = 0$ and $[u_\alpha] = (2+z-2)/2 = 1$. An analysis of dimensions of operators then shows that the elastic parameters λ and μ are marginal, whereas the term $\tilde{\kappa}(\partial^2 u_\alpha)^2/2$, the nonlinear contribution $\partial_\alpha u_\gamma \partial_\beta u_\gamma$ to the strain tensor $U_{\alpha\beta} = ((\xi^2-1)\delta_{\alpha\beta} + \xi\partial_\alpha u_\beta + \xi\partial_\beta u_\alpha + \partial_\alpha\mathbf{h}\cdot\partial_\beta\mathbf{h} + \partial_\alpha u_\gamma\partial_\beta u_\gamma)/2$, and the in-plane kinetic energy $\tilde{\rho}\dot{u}_\alpha^2/2$ are all irrelevant in the sense of power counting. By dropping all power-counting irrelevant interactions, we arrive, after a change of variables $u_\alpha \to u_\alpha/\xi - (\xi^2-1)x_\alpha/(2\xi)$, to the effective model (5.2) with $\sigma = 0$.

Clearly, the effective model cannot describe the dynamics of in-plane phonons, which occurs at scales $\omega \sim |\mathbf{k}|$. Power counting indicates however that it should

capture in an exact way the leading singularities at long wavelengths of static correlation functions (diagrams with all external frequencies $\omega = 0$), and more generally, singularities of diagrams with external legs in the region $\omega \sim k^2$, relevant for the behavior of flexural phonons[1].

For simplicity, we will use the effective model (5.2) also to calculate thermodynamical properties of the membrane, such as the entropy and the average projected area, at finite temperature T and nonzero tension σ. We expect that the theory describes the leading singular behavior of thermodynamic quantities for small T and σ.

5.2.3 *Symmetries*

In full analogy with the theory of classical membranes, it can be checked that, when $\sigma = 0$, $\mathcal{S}$ is invariant under the "linearized rotations" [10, 11, 169]

$$\begin{aligned} \mathbf{h} &\to \mathbf{h} + \mathbf{A}_\alpha x_\alpha \ , \\ u_\alpha &\to u_\alpha - (\mathbf{A}_\alpha \cdot \mathbf{h}) - \frac{1}{2}(\mathbf{A}_\alpha \cdot \mathbf{A}_\beta) x_\beta \ , \end{aligned} \tag{5.7}$$

where $\mathbf{A}_\alpha$ is any fixed vector. This symmetry represents a linearized form of the original SO(d) invariance of the full theory, and reflects the fact that the layer is located in an isotropic ambient space (without external forces and with no externally-imposed in-plane tension). The associated Ward identities [10, 11, 169] play a crucial role in the dynamics and the renormalization of the model.

As a remark, we note that the linearized invariance (5.7) only emerges when all irrelevant terms are dropped from the action at the same time. If, instead, we had neglected the nonlinear contribution $\partial_\alpha u_\gamma \partial_\beta u_\gamma/2$ to the strain tensor but we had kept the kinetic energy of in-plane phonons $\tilde{\rho}\dot{u}_\alpha^2/2$, we would have arrived at a theory which lacks both the full rotational SO(d) symmetry and the linearized, effective rotational symmetry (5.7). In this case, renormalization would generate generic anisotropic interactions, including anisotropies which are relevant in the sense of power counting. This would then result in an artificial modification of the qualitative behavior of fluctuations. Although the crucial role of symmetries has been appreciated, several approaches in the earlier literature used actions or approximations which, in some steps of derivations, violate both the exact and the linearized SO(d) symmetries.

In particular, we note that the prediction of a contribution $\Sigma(0, \mathbf{k}) \propto k^2$ to the self-energy of flexural phonons at zero frequency, derived in Ref. [167], started from

1 We assume that the general power-counting principles for the effects of irrelevant interactions [15], which are usually derived in the framework of Euclidean-invariant theories, remain valid in the nonrelativistic model considered here. Specifically, we assume that the only effects of neglected irrelevant interactions at leading order for long wavelengths and low frequency is a renormalization of the value of the parameters $\tilde{\rho}$, $\tilde{\kappa}$, $\tilde{\lambda}$, and $\tilde{\mu}$, which become phenomenological quantities.

an action in which the nonlinear contribution to the strain tensor was neglected but the kinetic energy of in-plane phonons was retained. An explicit calculation using a full rotationally-invariant action [91] showed instead that self-energy corrections proportional to k^2 vanish in absence of external stress, consistently with the Ward identities [85]. The emergence of the linearized symmetry (5.7) ensures that the cancellation of terms proportional to k^2 is consistently captured by the effective model (5.3), as we verify below (see Sec. 5.6.1).

5.2.4 *Analogy with a model of lamellar phases*

After identification of the imaginary time τ with an additional space dimension z, the quantum action $\mathcal{S}$ turns out to be almost identical to the effective Hamiltonian

$$\begin{aligned} H = \int \mathrm{d}z \int \mathrm{d}^2x \Big\{ & \frac{B_0}{2}(\partial_z u_z)^2 + \frac{K_0}{2}(\partial_\perp^2 u_z)^2 \\ & + \frac{\mu_0^{\perp\perp}}{4}(\partial_\alpha u_\beta + \partial_\beta u_\alpha + \partial_\alpha u_z \partial_\beta u_z)^2 \\ & + \frac{\lambda_0^{\perp\perp}}{8}(2\partial_\alpha u_\alpha + \partial_\alpha u_z \partial_\alpha u_z)^2 + \\ & + \frac{1}{2}\lambda_0^{\perp z}(\partial_z u_z)(2\partial_\alpha u_\alpha + \partial_\alpha u_z \partial_\alpha u_z) \Big\} , \end{aligned} \tag{5.8}$$

which was analyzed by Guitter [169] as a model for a three-dimensional shearless stack of *classical* crystalline membranes. The identity between the two theories only emerges after irrelevant interactions are neglected in both models and under the assumption $\lambda_0^{\perp z} = 0$.

The theory of shearless stacks of membranes has been a subject of debate and some authors [181, 182] have proposed models which differ from Eq. (5.8) and thus contrast with the results of Ref. [169]. Establishing a detailed relation between lamellar phases and quantum membranes is beyond the scope of our work. We will verify, however, that the RG equations for the quantum membrane action recovers long-wavelength singularities identical to those predicted in Ref. [169].

5.3 INTEGRATION OVER IN-PLANE MODES

Since $\mathcal{S}$ is quadratic in u_α, the in-plane modes can be integrated out explicitly. To integrate out u_α it is essential to separate the strain tensor $u_{\alpha\beta}$ into uniform modes (with zero spacial momentum $\mathbf{k} = 0$) and non-uniform components (with spacial

Fourier components $\mathbf{k} \neq 0$). Integration over in-plane phonon modes $u_\alpha^{\mathbf{k}\neq 0}(\mathbf{x},\tau)$ with $\mathbf{k} \neq 0$ gives rise to an effective four-point vertex [54]

$$\mathcal{S}_{\rm int}^{\mathbf{k}\neq 0} = \frac{Y}{8}\int_0^{1/T} \mathrm{d}\tau \sum_{\mathbf{k}\neq 0} P^T_{\alpha\beta}(\mathbf{k}) P^T_{\gamma\delta}(\mathbf{k}) f_{\alpha\beta}(\mathbf{k},\tau) f_{\gamma\delta}(-\mathbf{k},\tau) \ , \tag{5.9}$$

where $f_{\alpha\beta}(\mathbf{k},\tau)$ is the spacial Fourier transform of the composite field $f_{\alpha\beta}(\mathbf{x},\tau) = (\partial_\alpha \mathbf{h}(\mathbf{x},\tau)\cdot\partial_\beta\mathbf{h}(\mathbf{x},\tau))$, $P^T_{\alpha\beta}(\mathbf{k}) = \delta_{\alpha\beta} - k_\alpha k_\beta/k^2$ is the projector transversal to the momentum transfer $\mathbf{k}$, and $Y = 4\mu(\lambda+\mu)/(\lambda+2\mu)$ is the (dimensionless) Young modulus. The interaction (5.9) represents physically an instantaneous long-range coupling between local Gaussian curvatures in the membrane, and is a direct quantum generalization of the usual effective interaction which emerges in classical theories [1, 6, 10, 18, 25, 85].

The analysis of zero modes differs depending on the ensemble considered (see Ref. [18] for an analysis of isometric and isotensional ensemble in the theory of classical membranes). Here, we find it convenient to use a fixed-stress, or "isotensional" ensemble [18], in which the external in-plane stress σ is kept fixed and the projected area is allowed to fluctuate. In this setting, we parametrize $u_\alpha(\mathbf{x},\tau) = v_{\alpha\beta}x_\beta + u_\alpha^{\mathbf{k}\neq 0}(\mathbf{x},\tau)$ and integrate over all values of both $u_\alpha^{\mathbf{k}\neq 0}(\mathbf{x},\tau)$ and $v_{\alpha\beta}$. After integration, we are lead to a contribution to the effective action

$$\int_0^{1/T}\mathrm{d}\tau \int \mathrm{d}^2x \left[\frac{\sigma}{2}(\partial_\alpha\mathbf{h}\cdot\partial_\alpha\mathbf{h}) - \frac{\sigma^2}{2(\lambda+\mu)}\right] + \mathcal{S}_{\rm int}^{\mathbf{k}=0} \ , \tag{5.10}$$

where

$$\begin{aligned}\mathcal{S}_{\rm int}^{\mathbf{k}=0} = A\int_0^{1/T}\mathrm{d}\tau \Bigg[&\frac{\lambda}{8}(f^0_{\alpha\alpha}(\tau) - \bar{f}^0_{\alpha\alpha})^2 \\ &+ \frac{\mu}{4}(f^0_{\alpha\beta}(\tau) - \bar{f}^0_{\alpha\beta})(f^0_{\alpha\beta}(\tau) - \bar{f}^0_{\alpha\beta})\Bigg] \ ,\end{aligned} \tag{5.11}$$

$f^0_{\alpha\beta}(\tau) = A^{-1}\int \mathrm{d}^2x(\partial_\alpha\mathbf{h}(\mathbf{x},\tau)\cdot\partial_\beta\mathbf{h}(\mathbf{x},\tau))$, and $\bar{f}^0_{\alpha\beta} = T\int_0^{1/T}\mathrm{d}\tau f^0_{\alpha\beta}(\tau)$. The average strain of the membrane in this ensemble is $\langle v_{\alpha\beta}\rangle = v\delta_{\alpha\beta}$, with $v = \sigma/(2(\lambda+\mu)) - \langle\partial_\alpha\mathbf{h}\cdot\partial_\alpha\mathbf{h}\rangle/4$ [17, 18, 85]. It is the sum of a Hookean contribution $\sigma/(2(\lambda+\mu))$, controlled by the bulk modulus $B = \lambda+\mu$, and a negative fluctuation term, proportional to $\langle\partial_\alpha\mathbf{h}\cdot\partial_\alpha\mathbf{h}\rangle$, which is nonvanishing also for $\sigma = 0$, and which represents the tendency of the projected in-plane area to contract due to statistical fluctuations of the layer in the out-of-plane direction.

The infinite-range interaction $\mathcal{S}_{\rm int}^{\mathbf{k}=0}$ is scaled by an overall factor A^{-1} and, by its definition, it vanishes when the Matsubara-frequency transfer between the

composite operators $f^0_{\alpha\beta}(\tau)$ is zero. These two facts together imply that, in the thermodynamic limit $A \to \infty$, $\mathcal{S}^{\mathbf{k}=0}_{\rm int}$ only contributes via diagrams of the type

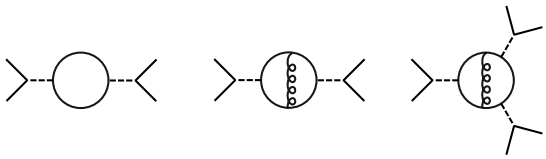

(5.12)

which (a) become disconnected when any zero-mode interaction line (represented by dashed lines) is cut and (b) have non-zero frequency transfer through all dashed lines. (The interaction $\mathcal{S}^{\mathbf{k}\neq 0}_{\rm int}$, denoted by wiggly lines can enter, instead, in arbitrary topology without suppressing the graphs). The diagrams (5.12), however, are only relevant for zero-mode correlation functions at finite frequency transfer and never enter as subgraphs of other correlation functions. For subsequent calculations in this work, we can thus safely neglect $\mathcal{S}^{\mathbf{k}=0}_{\rm int}$.

As a result, we can thus consider an effective theory for $\mathbf{h}$ fluctuations of the form:

$$\mathcal{S}_{\rm eff} = \int_0^{1/T} {\rm d}\tau \int {\rm d}^2x \left\{ \frac{\dot{\mathbf{h}}^2}{2} + \frac{1}{2}(\partial^2\mathbf{h})^2 + \frac{\sigma}{2}(\partial_\alpha \mathbf{h})^2 - \frac{\sigma^2}{2B} \right\} + \mathcal{S}^{\mathbf{k}\neq 0}_{\rm int} \ . \tag{5.13}$$

By a Hubbard-Stratonovich decoupling of the long-range interaction [183], the model can be expressed equivalently via the local action

$$\begin{aligned} \mathcal{S}_{\rm eff} = \int_0^{1/T} {\rm d}\tau \int {\rm d}^2x \Big\{ & \frac{\dot{\mathbf{h}}^2}{2} + \frac{1}{2}(\partial^2\mathbf{h})^2 + \frac{\sigma}{2}(\partial_\alpha \mathbf{h})^2 \\ & + \frac{1}{2Y}(\partial^2\chi)^2 + i\chi K - \frac{\sigma^2}{2B} \Big\} \ , \end{aligned} \tag{5.14}$$

where $\chi(\mathbf{x},\tau)$ is a mediator field and $K(\mathbf{x},\tau) = (\partial^2\mathbf{h}\cdot\partial^2\mathbf{h} - \partial_\alpha\partial_\beta\mathbf{h}\cdot\partial_\alpha\partial_\beta\mathbf{h})/2$ is, for small fluctuations, the local Gaussian curvature. The term $-\sigma^2/(2B)$ is a constant independent of the fluctuating fields $\mathbf{h}$, χ, and does not contribute to statistical averages. The only coupling constant in the model is thus the Young modulus Y.

By construction, the interaction-mediating field χ must be considered as a field with Fourier components only at nonzero momentum $\mathbf{k} \neq 0$. This implies that the tadpole graphs

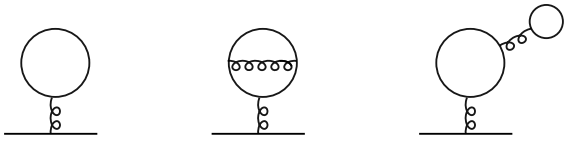

(5.15)

must be removed from the perturbative expansion, as in the theory of classical membranes [12].

5.4 RENORMALIZATION AND RG EQUATIONS AT ZERO TEMPERATURE

5.4.1 *RG for correlation functions*

At $T = 0$ the model is infinite in both spacial and temporal dimensions, and its renormalization can proceed in analogy with other bulk theories with weighted power counting [15, 100, 169–172]. In the representation (5.14), the basic elements defining diagrams in perturbation theory are the bare propagators of $\mathbf{h}$ and χ,

$$\begin{aligned} G^{(0)}_{ij}(\omega,\mathbf{k}) &= \quad\text{———}\quad = \frac{\delta_{ij}}{\omega^2 + k^4 + \sigma k^2} \ , \\ F^{(0)}(\omega,\mathbf{k}) &= \quad\text{ooooooo}\quad = \frac{Y}{k^4} \ , \end{aligned} \tag{5.16}$$

and the vertex

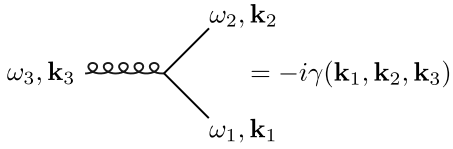

$$\begin{aligned} \gamma(\mathbf{k}_1,\mathbf{k}_2,\mathbf{k}_3) &= k_1^2 k_2^2 - (\mathbf{k}_1\cdot\mathbf{k}_2)^2 = k_2^2 k_3^2 - (\mathbf{k}_2\cdot\mathbf{k}_3)^2 \\ &= k_3^2 k_1^2 - (\mathbf{k}_3\cdot\mathbf{k}_1)^2 \ . \end{aligned} \tag{5.17}$$

The behavior of Feynman integrals under the rescaling $\mathbf{k} \to \lambda\mathbf{k}$, $\omega \to \lambda^z\omega = \lambda^2\omega$ shows that the weighted power-counting dimension [170] of a one-particle irreducible (1PI) diagram with I internal lines, V vertices, and L loops is $(2+z)L - 4I + 4V = 4(L - I + V) = 4$, independently of the order of perturbation theory. This ensures that the model is power-counting renormalizable. A potential danger for renormalizability [171] is that the propagator $F^{(0)}(\omega,\mathbf{k})$, being ω-independent, is not suppressed in the limit $\omega \to \infty$ at $\mathbf{k}$ fixed. However, this does not create difficulties, because it can be checked that in any diagram, all frequency integrals can be performed first and are convergent [2].

To complete the proof of renormalizability, it would be necessary to derive a generalization of the Weinberg theorem [184, 185], ensuring the equivalence between power-counting convergence and true convergence in multiloop diagrams. We will assume that this property remains valid in the model considered in this work.

2 A power-counting analysis restricted to the frequency-only part of the integrals shows that the ω integrations are all superficially convergent. An application of the Weinberg theorem ensures the finiteness of integrations [172].

The ultraviolet divergences of correlation functions can be removed by introducing an arbitrary subtraction scale M, a renormalized coupling $Y_{\rm R}$, and a renormalized action

$$\begin{aligned}\mathcal{S}^{(\rm R)}_{\rm eff} = \int {\rm d}\tau \int {\rm d}^2x \Big\{ \frac{\dot{\mathbf{h}}^2}{2} + \frac{Z}{2}(\partial^2\mathbf{h})^2 + \frac{\sigma}{2}(\partial_\alpha \mathbf{h})^2 \\ + \frac{1}{2K_Y}(\partial^2\chi)^2 + i\chi K - \frac{\sigma^2}{2B} \Big\} ,\end{aligned} \tag{5.18}$$

equipped with two logarithmically divergent counterterms Z and K_Y. This particularly simple form, with only two independent divergences, follows from the fact that the terms $\dot{\mathbf{h}}^2/2$, $\sigma(\partial_\alpha\mathbf{h})^2/2$, and the interaction $i\chi K$ are not renormalized. Indeed, due to the structure of the vertex (5.17), it is possible to factorize, from any 1PI diagram, two powers of the spacial momentum of each external leg. Therefore, the perturbative corrections to the self-energy of flexural fields cannot generate divergences proportional to ω^2 or to k^2, but only proportional to k^4, which contribute to the renormalization of Z. The possibility to factorize two powers of each external momentum also implies that loop corrections to the three-field vertex are superficially convergent, and thus the interaction $i\chi K$ does not require an independent counterterm. An identical mechanism occurs in the ε-expansion of classical membranes in dimension $D = 4 - \varepsilon$ [25, 183]. In principle, the one-point function $\langle \partial^2\chi \rangle$ constitutes a further independent divergence, but since χ is a field with components only at nonzero momentum $\mathbf{k} \neq 0$, this divergence is unphysical and has no effect on correlation functions.

Eq. (5.18) implies the following relations between bare and renormalized quantities

$$\begin{aligned}&\mathcal{S}_{\rm eff}[\mathbf{h},\chi,Y,\sigma] = \mathcal{S}^{(\rm R)}_{\rm eff}[\mathbf{h}_{\rm R},\chi_{\rm R},Y_{\rm R},\sigma_{\rm R}] + \text{constant} , \\ &\mathbf{h}(\mathbf{x},\tau) = Z^{1/4}\mathbf{h}_{\rm R}(\mathbf{x},\tau_{\rm R}) , \qquad \chi(\mathbf{x},\tau) = Z^{-1}\chi_{\rm R}(\mathbf{x},\tau_{\rm R}) , \\ &\tau = Z^{1/2}\tau_{\rm R} , \qquad \sigma = Z^{-1}\sigma_{\rm R} , \qquad Y = Z^{-3/2}K_Y\end{aligned} \tag{5.19}$$

and, according to standard techniques [15], the following RG equations for 1PI correlation functions in momentum space

$$\begin{aligned}\Big[\Lambda\frac{\partial}{\partial\Lambda} + \beta(Y)\frac{\partial}{\partial Y} - \frac{1}{2}(n - 4\ell + 2)\eta + \eta\sum_{i=1}^{n}\omega_i\frac{\partial}{\partial\omega_i} \\ + \eta\sum_{j=1}^{\ell}\omega'_j\frac{\partial}{\partial\omega'_j} + 2\eta\sigma\frac{\partial}{\partial\sigma}\Big]\Gamma^{(n,\ell)}_{i_1..i_n}(\omega_i,\mathbf{k}_i;\omega'_j,\mathbf{k}'_j) = 0 .\end{aligned} \tag{5.20}$$

In Eq. (5.20), Λ is the microscopic ultraviolet momentum cutoff and $\Gamma^{(n,\ell)}$ denotes the bare (unrenormalized) 1PI correlation function with n external $\mathbf{h}$ legs and ℓ

external χ legs. The RG flow function $\beta = \Lambda\partial Y/\partial\Lambda$ and the anomalous dimension $\eta = -\frac{1}{2}\Lambda\partial \ln Z/\partial\Lambda$ depend only on the bare dimensionless coupling Y.

By an explicit computation of the one-loop divergences in the self-energies of χ and of $\mathbf{h}$ for $\sigma = 0$ we find [54, 91, 162]

$$\Sigma^{(\mathbf{h})}_{ij}(\omega,\mathbf{k}) = \quad \sim \frac{3Y}{32\pi}\delta_{ij}k^4 \ln\Lambda \ , \qquad \Sigma^{(\chi)}(0,\mathbf{k}) = \quad \sim \frac{3d_c}{128\pi}k^4\ln\Lambda \ , \tag{5.21}$$

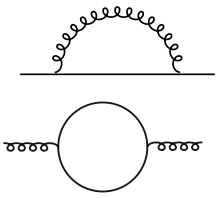

where $d_c = (d-2)$ is the number of components of the $\mathbf{h}$ field. Applying the RG equations to $G^{-1}_{ij}(\omega,\mathbf{k}) = \Gamma^{(2,0)}_{ij}(\omega,\mathbf{k}) = \omega^2 + k^4 + \sigma k^2 + \Sigma^{(\mathbf{h})}(\omega,\mathbf{k})$ and $F^{-1}(0,\mathbf{k}) = \Gamma^{(0,2)}(0,\mathbf{k}) = k^4/Y + \Sigma^{(\chi)}(0,\mathbf{k})$ shows that, at leading order,

$$\beta(Y) = 3\eta(Y)Y + \frac{3d_c}{128\pi}Y^2 \ , \qquad \eta(Y) = \frac{3}{64\pi}Y \ . \tag{5.22}$$

These RG functions imply that Y is marginally irrelevant: the theory is attracted to weak coupling at large length scales. Eqs. (5.22) are consistent, in a different scheme, with the earlier perturbative results of Refs. [91, 162] and also with the weak-coupling limit of the nonperturbative RG equations derived in Ref. [164].

5.4.2 *Gibbs free energy*

The Gibbs free energy per unit area at zero temperature, $\tilde{G}_0 = -A^{-1}\lim_{T\to 0}(T\ln\mathcal{Z})$, requires the introduction of additional counterterms to the field-independent part of the action. Since σ has power-counting dimension $[\sigma] = 2$, the required counterterms in the Lagrangian are a polynomial $a_0 + a_1\sigma + a_2\sigma^2/2$, where a_0 diverges as Λ^4, a_1 as Λ^2, and a_2 diverges logarithmically. By working within a massless scheme [15, 170], a_0, a_1, and a_2 can be chosen to be independent of the tension σ.

Taking into account these additional renormalizations, the renormalized action reads

$$\mathcal{S}^{(\mathrm{R})}_{\mathrm{eff}} = \int \mathrm{d}\tau \int \mathrm{d}^2x \Big\{ \frac{\dot{\mathbf{h}}^2}{2} + \frac{Z}{2}(\partial^2\mathbf{h})^2 + \frac{\sigma}{2}(\partial_\alpha\mathbf{h})^2 + \frac{1}{2K_Y}(\partial^2\chi)^2 + i\chi K + a_0 + a_1\sigma + \frac{1}{2}(a_2 - 1/B)\sigma^2 \Big\} \ . \tag{5.23}$$

To discuss RG equations it is convenient to separate $\tilde{G}_0 = V_{\mathrm{el}} + \Delta\tilde{G}_0$, where $V_{\mathrm{el}} = -\sigma^2/(2B)$ is the elastic Hookean contribution and $\Delta\tilde{G}_0$ is the fluctuation

part. The advantage of this separation is that $\Delta\tilde{G}_0$ depends only on the Young modulus Y and not on the bulk modulus B.

The fluctuation free energy $\Delta\tilde{G}_0^{(\mathrm{R})}$, calculated using the action (5.23), is finite for $\Lambda \to \infty$ at fixed Y_R and M. The physical free energy $\Delta\tilde{G}_0$, computed from the bare action (5.14) is related to $\Delta\tilde{G}_0^{(\mathrm{R})}$ by

$$Z^{1/2}\Delta\tilde{G}_0(Y, Z^{-1}\sigma, \Lambda) = \Delta\tilde{G}_0^{(\mathrm{R})}(Y_\mathrm{R}, \sigma, M) - a_0' - a_1\sigma - \frac{a_2}{2}\sigma^2 \ . \tag{5.24}$$

(a_0' differs from a_0 because it receives contributions from the path-integral measure during the change of variables $\mathbf{h} \to \mathbf{h}_\mathrm{R}$, $\chi \to \chi_\mathrm{R}$). The relation (5.24) and the finiteness of $\Delta\tilde{G}_0^{(\mathrm{R})}$ imply an inhomogeneous RG equation for the physical Gibbs free energy

$$\left[\Lambda\frac{\partial}{\partial\Lambda} + \beta(Y)\frac{\partial}{\partial Y} + 2\eta\sigma\frac{\partial}{\partial\sigma} - \eta\right]\Delta\tilde{G}_0(Y, \sigma, \Lambda) = b_0 + b_1\sigma + \frac{b_2}{2}\sigma^2 \ . \tag{5.25}$$

The constants b_0, b_1, and b_2 are independent of σ in the massless scheme and cannot depend on the arbitrary subtraction scale M. Thus they have the form $b_0 = \bar{b}_0(Y)\Lambda^4$, $b_1 = \bar{b}_1(Y)\Lambda^2$, and $b_2 = \bar{b}_2(Y)$.

5.5 RG FOR LOW-TEMPERATURE THERMODYNAMIC QUANTITIES

At finite temperatures, the continuum frequency ω is replaced by discrete bosonic Matsubara frequencies $\omega_n = 2\pi T n$. As a result, even for an infinitesimal T, the perturbative expansion at zero tension $\sigma = 0$ breaks down due to infrared (IR) divergences. The IR problems arise from the $\omega_n = 0$ component of the flexural propagator $G_{ij}^{(0)} = \delta_{ij}/(\omega_n^2 + k^4)$, which induces singularities when integrated over the two-dimensional spacial momenta. The physical origin of these divergences is the following: in the limit $\mathbf{k} \to 0$, the system behaves as a classical membrane [164]. For classical thermal fluctuations, anharmonic effects do not induce logarithmic corrections but, rather, power-law renormalizations [1, 6, 10–12, 22, 25]. The dramatic power-law singularities of the classical theory cannot be captured by a simple perturbative treatment, but require more detailed solutions, for example within the framework of the self-consistent screening approximation [25], the non-perturbative RG [26, 164], the large-d expansion [9, 22], or the ε-expansion [10, 19–21, 183].

Similar difficulties emerge in finite-size scaling problems and in other finite-temperature quantum field theories. A standard strategy to bypass the problem of IR singularities consists in integrating out modes with $n \neq 0$ and in deriving an effective field theory for modes with $n = 0$, to be solved by more exact methods [15].

The same strategy can be applied to the membrane action (5.14), with, however, a difference compared to the standard case: since the χ propagator $F^{(0)}(\omega, \mathbf{k}) = Y/k^4$

does not depend on the frequency ω, it is singular at small $\mathbf{k}$ not only at $\omega_n = 0$ but, in fact, for all Matsubara frequencies $\omega_n \neq 0$. As a result, subtracting the modes $\omega_n = 0$ does not introduce an IR cutoff to Feynman diagrams. This property is a consequence of the neglection of the kinetic energy of in-plane phonons. The singularity of $F^{(0)}(\omega, \mathbf{k})$, however, is neutralized by the factors k^2 attached to the vertices (5.17) and, therefore, the IR finiteness is still valid.

We can thus proceed as follows: we separate $\mathbf{h}(\mathbf{x}, \tau) = \mathbf{h}'(\mathbf{x}, \tau) + \mathbf{H}(\mathbf{x})$, where $\mathbf{H}(\mathbf{x}) = T \int_0^{1/T} \mathbf{h}(\mathbf{x}, \tau)$ is the mode with zero Matsubara frequency and $\mathbf{h}'(\mathbf{x}, \tau)$ the sum of all other modes with $\omega_n \neq 0$. We then integrate out $\mathbf{h}'(\mathbf{x}, \tau)$ and *all* degrees of freedom of $\chi(\mathbf{x}, \tau)$ (including the $\omega_n = 0$ mode of χ). This integration can be performed perturbatively without encountering IR divergences because in all $\mathbf{h}'$ propagators the finite frequency $\omega_n \neq 0$ provides an IR cutoff and in all χ propagators the singularity Y/k^4 of the propagator is compensated by a power k^4 coming from the vertex (5.17). Although the singularity of $F^{(0)}(\omega, \mathbf{k})$ does not introduce divergences, it still manifests itself in the fact that the effective theory for $\mathbf{H}(\mathbf{x})$ is highly non-local.

In order to disentangle modes which generate IR singularities from degrees of freedom which generate UV divergences, it is also convenient to separate $\mathbf{H}(\mathbf{x}) = \mathbf{H}_1(\mathbf{x}) + \mathbf{H}_2(\mathbf{x})$ into a slowly-varying field $\mathbf{H}_1(\mathbf{x})$, with momenta $|\mathbf{k}| < \Lambda_1$ and a fast field $\mathbf{H}_2(\mathbf{x})$ with momenta in the shell $\Lambda_1 < |\mathbf{k}| < \Lambda$, where Λ_1 is an arbitrary wavevector scale much smaller than Λ. Integrating out $\mathbf{h}'$, χ, and $\mathbf{H}_2$ can be done perturbatively and leaves us with an effective classical Hamiltonian

$$\mathcal{H}[\mathbf{H}_1(\mathbf{x}); Y, \sigma, T, \Lambda, \Lambda_1] = -T \ln \int [\mathrm{d}\mathbf{h}' \mathrm{d}\mathbf{H}_2 \mathrm{d}\chi] \mathrm{e}^{-\mathcal{S}[\mathbf{H}_1 + \mathbf{H}_2 + \mathbf{h}', \chi]} \,. \tag{5.26}$$

involving only slowly-varying long-wavelength modes.

A crucial observation in the theory of finite-size scaling and other finite-temperature field theories is that the counterterms which make the theory finite at $T = 0$ will also formally remove all ultraviolet divergences from observables at nonzero T [15, 173]. It is natural to assume that the same property remains valid for the membrane action. We can thus conclude that if we started from the action

$$\begin{aligned} \mathcal{S}_{\mathrm{eff}}^{(\mathrm{R})} = \int_0^{1/T} \mathrm{d}\tau \int \mathrm{d}^2 x \Big\{ & \frac{\dot{\mathbf{h}}^2}{2} + \frac{Z}{2} (\partial^2 \mathbf{h})^2 + \frac{\sigma}{2} (\partial_\alpha \mathbf{h})^2 \\ & + \frac{1}{2K_Y} (\partial^2 \chi)^2 + i\chi K + a_0 + a_1 \sigma + \frac{1}{2}(a_2 - 1/B)\sigma^2 \Big\} \,, \end{aligned} \tag{5.27}$$

equipped with the same zero-temperature counterterms Z, K_Y, a_0, a_1, and a_2 which appear in Eq. (5.23), after a perturbative integration over $\mathbf{h}'$, χ, and $\mathbf{H}_2$, and a final non-perturbative integration over $\mathbf{H}_1$ we would arrive at a renormalized Gibbs free energy per unit area $\tilde{G}^{(\mathrm{R})} = -A^{-1} T \ln \mathcal{Z}$ which remains finite for $\Lambda \to \infty$.

After separation of $\tilde{G} = V_{\rm el} + \Delta\tilde{G}$ into the Hookean part $-\sigma^2/(2B)$ and the fluctuation part $\Delta\tilde{G}$, the physical fluctuation free energy $\Delta\tilde{G}$, computed from the bare action (5.14) is related to the renormalized $\Delta\tilde{G}^{(\rm R)}$ by the equation

$$\begin{aligned}\Delta\tilde{G}^{(\rm R)}(Y_{\rm R},\sigma,T,M) = Z^{1/2}\Delta\tilde{G}(Y,Z^{-1}\sigma,Z^{-1/2}T,\Lambda) \\ + a_0' + a_1\sigma + \frac{a_2}{2}\sigma^2 \ .\end{aligned} \tag{5.28}$$

From Eq. (5.28) follows an inhomogeneous RG equation for the bare Gibbs free energy:

$$\begin{aligned}\left[\Lambda\frac{\partial}{\partial\Lambda} + \beta(Y)\frac{\partial}{\partial Y} + 2\eta\sigma\frac{\partial}{\partial\sigma} + \eta T\frac{\partial}{\partial T} - \eta\right]\Delta\tilde{G}(Y,\sigma,T,\Lambda) \\ = b_0 + b_1\sigma + \frac{b_2}{2}\sigma^2 \ .\end{aligned} \tag{5.29}$$

In Eq. (5.29), $\beta(Y)$, $\eta(Y)$, and the coefficients of the inhomogeneous part $b_0 = \bar{b}_0(Y)\Lambda^4$, $b_1 = \bar{b}_1(Y)\Lambda^2$, and $b_2 = \bar{b}_2(Y)$ are the same RG coefficients which appear in the zero-temperature equation (5.25) and, in particular, are temperature-independent.

As a remark, we note that the RG equations discussed above, as in any renormalizable theory [15], keep track of all terms which either diverge or remain finite when $\Lambda \to \infty$. Terms which vanish for large cutoff (for example a correction σ/Λ^2) are instead neglected. As a result, relations such as Eq. (5.29) are valid asymptotically when the cutoff Λ is much larger than other scales in the problem: $\Lambda \gg \sigma^{1/2}$, $\Lambda \gg T^{1/2}$. In standard units of measurement the condition $\Lambda \gg T^{1/2}$ implies that the temperature $\tilde{T}$ must be much smaller than the Debye temperature of flexural phonons $\tilde{T}_{\rm D} = \hbar\tilde{\kappa}^{1/2}\Lambda^2/(\tilde{\rho}^{1/2}k_{\rm B})$.

5.5.1 *RG equation for the effective classical Hamiltonian*

More generally, the effective classical Hamiltonian (5.26) must, by itself, satisfy a renormalization group equation

$$\begin{aligned}\left[\Lambda\frac{\partial}{\partial\Lambda} + \beta(Y)\frac{\partial}{\partial Y} + 2\eta\sigma\frac{\partial}{\partial\sigma} + \eta T\frac{\partial}{\partial T} - \frac{\eta}{2}\int {\rm d}^2x\ \mathbf{H}_1(\mathbf{x})\cdot\frac{\delta}{\delta\mathbf{H}_1(\mathbf{x})}\right. \\ \left. + \eta\right]\Delta\mathcal{H} = A\left(b_0 + b_1\sigma + \frac{b_2}{2}\sigma^2\right) \ ,\end{aligned} \tag{5.30}$$

where $\Delta\mathcal{H} = \mathcal{H} + A\sigma^2/(2B)$ is the fluctuation energy, with the Hookean contribution $AV_{\rm el} = -A\sigma^2/(2B)$ subtracted. Eq (5.30) expresses that the cutoff dependence of $\mathcal{H}$ is entirely carried by the zero-temperature counterterms Z, K_Y, a_0, a_1, a_2.

For the direct validity of Eq. (5.30), it is essential that all high-energy modes are integrated out, as in Eq. (5.26). If, for example, we did not integrate out the large-momentum modes $\mathbf{H}_2(\mathbf{x})$ with zero Matsubara frequency, we would have moved some of the UV infinities from the integrated modes to the degrees of freedom yet to be integrated. In this case, $\mathcal{H}$ would have included additional counterterms [173].

5.6 RESULTS

In this section, we derive explicit consequences of the RG relations for various statistical and thermodynamic quantities.

5.6.1 *Two-point correlation functions at $T = 0$, $\sigma = 0$, $\omega = 0$*

The interacting Green functions $G_{ij}(\omega, \mathbf{k})$ of the flexural field is the inverse of the 1PI function $\Gamma^{(2,0)}_{ij}(\omega, \mathbf{k})$. For $T = 0$, $\sigma = 0$, and $\omega = 0$, $G_{ij}(0, \mathbf{k}) = [\Gamma^{(2,0)}_{ij}(0, \mathbf{k})]^{-1}$ satisfies, as a particular case of Eq. (5.20), the RG equation

$$\left[\Lambda \frac{\partial}{\partial \Lambda} + \beta(Y) \frac{\partial}{\partial Y} - 2\eta\right] G^{-1}_{ij}(0, \mathbf{k}; Y, \Lambda) = 0 \; . \tag{5.31}$$

The renormalization group equations can be solved, in an usual way [15], by introducing a running coupling $y(\Lambda')$ and an amplitude renormalization $z(\Lambda')$ which, starting from the initial values $y(\Lambda) = Y$, $z(\Lambda) = 1$, evolve with the floating cutoff scale Λ' according to the flow equations

$$\begin{aligned} \Lambda' \frac{\mathrm{d}y(\Lambda')}{\mathrm{d}\Lambda'} &= \beta(y(\Lambda')) \; , \\ \Lambda' \frac{\mathrm{d} \ln z(\Lambda')}{\mathrm{d}\Lambda'} &= -2\eta(y(\Lambda')) \; . \end{aligned} \tag{5.32}$$

The one-loop RG flow gives

$$\begin{aligned} y(\Lambda') &= \frac{Y}{1 + \frac{3(d_c+6)Y}{128\pi} \ln \frac{\Lambda}{\Lambda'}} \; , \\ z(\Lambda') &= \left[1 + \frac{3(d_c+6)Y}{128\pi} \ln \frac{\Lambda}{\Lambda'}\right]^{\theta} = \left(\frac{Y}{y(\Lambda')}\right)^{\theta} \; , \end{aligned} \tag{5.33}$$

where $\theta = 4/(d_c + 6)$ is the quantum exponent.

To calculate $G_{ij}(0, \mathbf{k})$, we can integrate the RG flow down to a scale $\Lambda' \approx k$. Since $y(\Lambda')$ flows to small values as Λ' is reduced (it is marginally irrelevant), we can use perturbation theory and take the zero-order approximation $G^{-1}_{ij}(0, \mathbf{k}; y(\Lambda'), \Lambda') = k^4$. The scaling relation (5.31) then implies $G_{ij}(0, \mathbf{k}; Y, \Lambda) \approx \delta_{ij}/(z(k)k^4)$. By

similar arguments, we find that the two point function $F(0,\mathbf{k}) = \langle\chi(0,\mathbf{k})\chi(0,-\mathbf{k})\rangle$ of the auxiliary field χ scales as $F(0,\mathbf{k}) \approx z^{3/2}(k)y(k)/k^4$.

The scaling of $G_{ij}(0,\mathbf{k})$ shows that $z(k)$ plays the role of a bending-rigidity renormalization and $z^{3/2}(k)y(k)$ the role of an effective screened Young modulus. Returning to standard units, these results can thus be interpreted as a renormalization of the bending rigidity

$$\tilde{\kappa} \to \tilde{\kappa}_{\mathrm{r}}(k) = \left[1 + g_0 \ln\frac{\Lambda}{k}\right]^{\theta} \tilde{\kappa} \tag{5.34}$$

and of the elastic Young modulus $\tilde{Y} = 4\tilde{\mu}(\tilde{\lambda}+\tilde{\mu})/(\tilde{\lambda}+2\tilde{\mu})$

$$\tilde{Y} \to \tilde{Y}_{\mathrm{r}}(k) = \left[1 + g_0 \ln\frac{\Lambda}{k}\right]^{3\theta/2-1} \tilde{Y} \tag{5.35}$$

where

$$g_0 = \frac{3(d_c+6)Y}{128\pi} = \frac{3(d_c+6)\hbar\tilde{Y}}{128\pi(\tilde{\rho}\tilde{\kappa}^3)^{1/2}} \tag{5.36}$$

is the "quantum coupling constant" [91]. The bending rigidity gets stiffened by interactions and scales for $k \to 0$ as $[\ln(\Lambda/k)]^{\theta}$. The Young modulus $Y_{\mathrm{r}}(k)$, instead, is softened by fluctuations and behaves in the long-wavelength limit as $[\ln(\Lambda/k)]^{3\theta/2-1} = [\ln(\Lambda/k)]^{-d_c/(6+d_c)}$.

The same behavior has been predicted for quantum membranes in Refs. [91, 164]. An identical logarithmic singularity has also been found, for $d_c = 1$, by Ref. [169] in the context of lamellar stacks of membranes.

5.6.1.1 *Ultrasoft scaling of* $G^{-1}(0,\mathbf{k})$

From the result $G^{-1}_{ij}(0,\mathbf{k}) \approx k^4[\ln(\Lambda/k)]^{\theta}$ it follows, in particular, that the ultrasoft behavior $\lim_{\mathbf{k}\to 0} G^{-1}_{ij}(0,\mathbf{k})/k^2 = 0$ characteristic of unstressed membranes is preserved by anharmonic effects. This result is consistent with the general Ward identity $\lim_{\mathbf{k}\to 0} G^{-1}_{ij}(0,\mathbf{k})/k^2 = \sigma$, which is a consequence of rotational invariance [85] and which, here, can be traced to the linearized rotational symmetry (5.7) of the effective model (5.2).

We note, instead, that this limiting behavior contrasts with the derivations in Refs. [167, 168], which proposed that, even in an unstressed membrane, flexural phonons exhibit a finite acoustic sound velocity v and a linear dispersion relation $\omega = v|\mathbf{k}|$ for $\mathbf{k} \to 0$. Within the local elasticity model (without long-range interactions) the linear dispersion relation can only emerge when an external source, such as an in-plane stress, breaks the rotational symmetry explicitly. In the harmonic approximation, this follows from the fact that in a rotationally-invariant, unstressed membrane, a Lagrangian term proportional to $(\partial_\alpha \mathbf{h})^2/2$ cannot appear individually,

but only together with in-plane terms in an overall coupling $\sigma_A U_{\alpha\alpha}$ to the strain tensor $U_{\alpha\alpha} = (\partial_\alpha \mathbf{r} \cdot \partial_\alpha \mathbf{r} - 2)/2$. The contribution $\sigma_A U_{\alpha\alpha}$ represents a coupling to the change of the total area, rather than the in-plane area [186], and thus it is allowed without breaking the symmetry. However, $U_{\alpha\alpha}$ contains a term linear in $\partial_\alpha u_\alpha$ and, thus, shifts the equilibrium configuration at which the energy must be expanded. After expansion at the true energy minimum, the sound velocity term must disappear. Indeed, a term linear in $\sigma_A U_{\alpha\alpha}$ can always be fully removed from the action by a change of variables $\mathbf{r} \to \zeta \mathbf{r}$ [12], which is allowed for a membrane with free boundaries. After ζ is chosen in such way that terms linear in $\partial_\alpha u_\alpha$ disappear, the entire operator $U_{\alpha\alpha}$ drops from the action, showing that the inverse Green function behaves as $G_{ij}^{(0)-1}(0, \mathbf{k}) \propto k^4$. Beyond the harmonic approximation, the perturbative corrections can be assembled in the effective potential Γ, generating functional of one-particle irreducible correlation functions, which, by Ward identities, has the same symmetry of the action [15]. Because phonon excitations are gapless, the interacting Green function $G_{ij}^{-1}(0, \mathbf{k})$ can vanish slower than k^4 as a result of singular diagrammatic contributions which generate a non-analytic dependence on $\mathbf{k}$. However, the rotational symmetry forbids terms regular in $\mathbf{k}$ and proportional to k^2. For example, the first-order perturbative correction for classical membranes in two dimensions [3, 6] consists in a diagram suppressed by an overall factor k^4 but multiplied by a singular term $1/k^2$ arising from the loop integration. Although formally the contribution vanishes as k^2, its origin is different from a regular contribution directly proportional to k^2. Furthermore, the singular first-order term proportional to k^2 is, in fact, the first contribution to an infrared-divergent series which requires a resummation for example by the self-consistent screening approximation [24, 25], or the ε-expansion [10, 20, 183]. After resummation, the interacting correlation function for classical membranes can be shown to behave as $k^{4-\eta_*}$ where η_* is an universal exponent [10, 24, 25]. The value of η_* has been computed by several complementary techniques [10, 19–22, 24–26, 164, 183] (see also references in [183]) and, despite some scatter between different methods, is usually found to be approximately $\eta_* \simeq 0.8$. As a result, the full interacting Green function G^{-1} vanishes faster than k^2.

The same conclusions hold in presence of the linearized rotational invariance (5.7), which forces the action to depend on $(\partial_\alpha \mathbf{h})^2$ only via the linearized strain tensor $u_{\alpha\beta}$. (See Refs. [10, 11, 169] for a discussion of Ward identities). Terms linear in $u_{\alpha\alpha}$ can be fully removed by a change of variables $u_\alpha \to u_\alpha + \varepsilon x_\alpha$, a shift which is automatically performed when integrating over zero modes in the fixed-stress ensemble (see Sec. 5.3).

The prediction of a self-energy correction $\Sigma(\mathbf{k}) \approx k^2 \Lambda^2$, derived in Ref. [167], resulted from a theory in which the in-plane kinetic energy was kept but the strain tensor was approximated. This approximation breaks explicitly both the full and

the linearized rotational symmetry, leading to a result inconsistent with the Ward identities.

The quantum-mechanical average $\langle \hat{\mathbf{h}}(\mathbf{k})\hat{\mathbf{h}}(-\mathbf{k})\rangle$ is given by the integral over all frequencies $\int \mathrm{d}\omega/(2\pi)G(\omega,\mathbf{k})$. The scaling relations (5.20) and the one-loop approximation imply that $\langle \hat{\mathbf{h}}(\mathbf{k})\hat{\mathbf{h}}(-\mathbf{k})\rangle \approx 1/(z^{1/2}(k)k^2)$.

5.6.2 *Anomalous Hooke's law at $T = 0$*

The average strain of the membrane $\langle \partial_\alpha u_\beta\rangle = v\delta_{\alpha\beta}$ can be computed from the thermodynamic relation $v = -\frac{1}{2}(\partial\tilde{G}/\partial\sigma)$. Thus, it is the sum $v = \sigma/(2B) + \Delta v$ of the Hookean term and the fluctuation part $\Delta v = -\frac{1}{2}(\partial\Delta\tilde{G}/\partial\sigma) = -\langle(\partial_\alpha \mathbf{h})^2\rangle/4$. The RG equation (5.29) for the Gibbs free energy implies that, at zero temperature

$$\left[\Lambda\frac{\partial}{\partial\Lambda} + \beta(Y)\frac{\partial}{\partial Y} + 2\eta\sigma\frac{\partial}{\partial\sigma} + \eta\right]\Delta v = -\frac{1}{2}(\bar{b}_1(Y)\Lambda^2 + \bar{b}_2(Y)\sigma)\ . \tag{5.37}$$

The inhomogeneous coefficients $\bar{b}_1(Y)$ and $\bar{b}_2(Y)$ are non-zero already in the non-interacting model, because the Gibbs free energy at $T = 0$ (equivalent to the zero-point ground state energy) of free flexural phonons is

$$\begin{aligned}\Delta\tilde{G}_0 &= \frac{d_c}{2}\int\frac{\mathrm{d}^2k}{(2\pi)^2}\sqrt{k^4+\sigma k^2}\\ &= C_0 + \frac{d_c}{16\pi}\sigma\Lambda^2 - \frac{d_c}{32\pi}\sigma^2\ln\Lambda + \text{finite}\ ,\end{aligned} \tag{5.38}$$

and already contains divergences for $\Lambda\to\infty$. Matching Eq. (5.38) with the RG equation (5.25), we deduce $\bar{b}_1(Y) = d_c/(8\pi)+\mathrm{O}(Y)$ and $\bar{b}_2(Y) = -d_c/(16\pi)+\mathrm{O}(Y)$. Taking into account that the expansion of β and η start, respectively, at orders Y^2 and at order Y, it can be checked that the general solution of the RG equation (5.37) order by order in Y has the general structure

$$v = v_0 + \frac{\sigma}{2B} + \sum_{k=0}^{\infty}\sum_{\ell=0}^{k+1} a_{k\ell}\sigma Y^k\left(\ln(\Lambda^2/\sigma)\right)^\ell\ . \tag{5.39}$$

The first term, v_0, represents the average strain at zero imposed stress, and the second two terms describe the response to external tension.

By solving the RG equation (5.37) in the leading-logarithm approximation [15] (keeping only the most singular terms, with $\ell = k+1$), we find

$$v - v_0 = \frac{\sigma}{2B} + \frac{4\sigma}{3Y}\left[(z(\sigma^{\frac{1}{2}}))^{\frac{d_c}{4}} - 1\right]\ , \tag{5.40}$$

where $z(\sigma^{1/2})$ is the running amplitude defined in Eq. (5.33), evaluated at scale $\Lambda' = \sigma^{1/2}$.

Eq. (5.40) is consistent, at the leading logarithm level, with results obtained by other methods in Ref. [91, 169], and shows that, even at $T = 0$, the stress-strain relation is anomalous. Due to quantum fluctuations of flexural degrees of freedom, the macroscopic bulk modulus $B_{\rm eff} = \frac{1}{2}\partial\sigma/\partial v$ is not a constant, but a slowly-varying function of the applied tension:

$$\frac{1}{B_{\rm eff}(\sigma)} \approx \frac{1}{B} + \frac{8}{3Y}\left[\left(1 + \frac{3(d_c+6)Y}{256\pi}\ln\frac{\Lambda^2}{\sigma}\right)^{\frac{d_c}{d_c+6}} - 1\right] . \tag{5.41}$$

(In Eq. (5.41) we neglected a contribution from the derivative of $z(\sigma^{1/2})$, which does not contribute to the leading-logarithmic singularities). In the limit of zero tension $\sigma \to 0$, the bulk modulus vanishes as $B_{\rm eff}(\sigma) \approx [\ln(\Lambda^2/\sigma)]^{-d_c/(d_c+6)}$.

The physical origin of this singularity is the same which gives rise to the anomalous Hooke response in classical thermally-fluctuating membranes [11, 17, 72, 85]: for small σ the dominant effect of the applied tension is not a stretching of the interatomic distance, but rather a "flattening" of the distribution of out-of-plane flexural fluctuations. For parameters characteristic of two-dimensional materials, however, the singular behavior dominates over the regular one only at unphysically small values of the imposed tension (see Sec. 5.7). The singularity, in particular, is much weaker than the power-law-divergent anomalous Hooke's law characteristic of classical thermal fluctuations, derived in Refs. [11, 17, 85].

5.6.3 *Consequences of renormalizability on low-temperature thermodynamics*

Differentiating Eq. (5.29) with respect to the temperature T, annihilates the inhomogeneous terms $b_0 + b_1\sigma + b_2\sigma^2/2$, which are temperature-independent. As a result we find a homogeneous renormalization group equation for the entropy per unit area $S = -\partial\tilde{G}/\partial T|_\sigma$:

$$\left[\Lambda\frac{\partial}{\partial\Lambda} + \beta(Y)\frac{\partial}{\partial Y} + 2\eta\sigma\frac{\partial}{\partial\sigma} + \eta T\frac{\partial}{\partial T}\right]S = 0 , \tag{5.42}$$

valid in the limit of small tension $\sigma \ll \Lambda^2$ and small temperature $T \ll \Lambda^2$. By further differentiation with respect to T and to σ we find RG equations for the specific heat at constant tension $C = T\partial S/\partial T|_\sigma$ and for the thermal expansion coefficient $\alpha = 2\partial v/\partial T|_\sigma = \partial S/\partial\sigma|_T$:

$$\left[\Lambda\frac{\partial}{\partial\Lambda} + \beta(Y)\frac{\partial}{\partial Y} + 2\eta\sigma\frac{\partial}{\partial\sigma} + \eta T\frac{\partial}{\partial T}\right]C = 0 , \tag{5.43}$$

$$\left[\Lambda\frac{\partial}{\partial\Lambda} + \beta(Y)\frac{\partial}{\partial Y} + 2\eta\sigma\frac{\partial}{\partial\sigma} + \eta T\frac{\partial}{\partial T} + 2\eta\right]\alpha = 0 . \tag{5.44}$$

By using the standard method of characteristics [15], the solutions can be written as

$$\begin{aligned} S(Y,\sigma,T,\Lambda) &= S(y(\Lambda'),z^{-1}\sigma,z^{-1/2}T,\Lambda') \\ C(Y,\sigma,T,\Lambda) &= C(y(\Lambda'),z^{-1}\sigma,z^{-1/2}T,\Lambda') \\ \alpha(Y,\sigma,T,\Lambda) &= z^{-1}\alpha(y(\Lambda'),z^{-1}\sigma,z^{-1/2}T,\Lambda') \ , \end{aligned} \tag{5.45}$$

where $y(\Lambda')$ and $z = z(\Lambda')$ are the zero-temperature running couplings introduced in Sec. 5.6.1.

Some general consequences of the RG equations, however, become more manifest if the solutions are expressed in another well-known form [187]. By rewriting the definitions (5.32) of the flow of running couplings in the integral form

$$\ln\frac{\Lambda'}{\Lambda} = \varphi(y(\Lambda')) - \varphi(Y) \ , \qquad z(\Lambda') = \frac{\mathrm{e}^{f(y(\Lambda'))}}{\mathrm{e}^{f(Y)}} \ , \tag{5.46}$$

$$\varphi(x) = \int^x \frac{\mathrm{d}u}{\beta(u)} \ , \qquad f(x) = -2\int^x \mathrm{d}u\frac{\eta(u)}{\beta(u)} \ . \tag{5.47}$$

it can be checked that the dimensionless quantities

$$\begin{aligned} x_1 &= \ln\frac{\Lambda^2}{T} - \frac{1}{2}f(Y) - 2\varphi(Y) \ , \\ x_2 &= \frac{\sigma}{T}\mathrm{e}^{\frac{1}{2}f(Y)} \ , \end{aligned} \tag{5.48}$$

are RG-invariant (they do not change under the replacements $\Lambda \to \Lambda'$, $Y \to y(\Lambda')$, $T \to z^{-1/2}(\Lambda')T$, $\sigma \to z^{-1}(\Lambda')\sigma$).

Taking into account that α is dimensionless, while S and C have the dimension of an inverse area, the scaling relations can then be written in the form, equivalent to Eq. (5.45),

$$\begin{aligned} S(Y,\sigma,T,\Lambda) &= T\mathrm{e}^{\frac{1}{2}f(Y)}L(x_1,x_2) \ , \\ C(Y,\sigma,T,\Lambda) &= T\mathrm{e}^{\frac{1}{2}f(Y)}M(x_1,x_2) \ , \\ \alpha(Y,\sigma,T,\Lambda) &= \mathrm{e}^{f(Y)}N(x_1,x_2) \ , \end{aligned} \tag{5.49}$$

where L, M, and N are fixed functions of two parameters. The thermodynamic relations between S, C, and α imply

$$\begin{aligned} M(x_1,x_2) &= \left[1 - \frac{\partial}{\partial x_1} - x_2\frac{\partial}{\partial x_2}\right]L(x_1,x_2) \ , \\ N(x_1,x_2) &= \frac{\partial L(x_1,x_2)}{\partial x_2} \ . \end{aligned} \tag{5.50}$$

The detailed form of the functions L, M, and N is not fixed by the scaling relations, but requires a full solution of the problem, including an analysis of the long-wavelength degrees of freedom dominated by classical thermal fluctuations. However Eqs. (5.49), which are general consequences of the renormalizability of the zero-temperature theory, already have a predictive content, even without a full solution of the problem. They imply that, in the region $\sigma \ll \Lambda^2$, $T \ll \Lambda^2$ thermodynamic quantities depend on the microscopic material parameters Λ and Y only via overall scale factors independent of σ and T.

For example, the form of the thermal expansion coefficient at zero tension

$$\alpha = \mathrm{e}^{f(Y)} N(\ln(\Lambda^2/T) - f(Y)/2 - 2\varphi(Y), 0) \tag{5.51}$$

implies that, in a logarithmic plot of $\ln \alpha$ vs. $\ln T$, curves corresponding to different materials must have the same shape and differ only by rigid shifts along horizontal and vertical Cartesian axes.

These universality properties express, in the thermodynamical behavior, a standard consequence of renormalizability [187].

5.6.4 *Finite-temperature thermodynamics of an unstressed membrane: thermal expansion coefficient*

A more detailed prediction of the temperature dependence of thermodynamic quantities requires a complete theory of all degrees of freedom, from short-wavelength modes, frozen by quantization, to long-wavelength modes, controlled by thermal fluctuations.

To derive explicit expressions we use a combination of the scaling relations (5.45) with approximations analogue to those described in Ref. [91].

The theories of Refs. [91, 164] indicate that, for temperatures much smaller than the Debye temperature $\tilde{T}_{\mathrm{D}}$, correlation functions exhibit a double crossover between different regimes. For large momenta $|\mathbf{k}| \gg q_T$ flexural modes have fluctuations of zero-point character. In an intermediate window of length scales $q_{\mathrm{G}} \ll |\mathbf{k}| \ll q_T$ the system is expected to exhibit weakly-coupled harmonic fluctuations and a classical statistical distribution. Finally in the long-wavelength region $|\mathbf{k}| \ll q_{\mathrm{G}}$, fluctuations become strongly anharmonic and are controlled by the interacting fixed point characteristic of classical membranes [1, 10, 12, 18, 25, 26].

The crossover scale q_T separating zero-point from thermally activated regimes, can be estimated [91], as the wavelength at which the zero-temperature inverse Green function $G^{-1}_{ij}(0, \mathbf{k}) \approx z(k)k^4$ becomes of the order of T^2:

$$z(q_T) q_T^4 \simeq T^2 \ . \tag{5.52}$$

For a fully classical membrane with bending rigidity $\tilde{\kappa}_1$, Young modulus $\tilde{Y}_1$, and temperature $\tilde{T}_1$, the Ginzburg momentum q_{G} at which harmonic fluctuations

cross over to strongly-coupled nonlinear fluctuations is [1, 12, 18, 25, 85] $q_{\rm G} \simeq (3k_{\rm B}\tilde{T}_1\tilde{Y}_1/(16\pi\tilde{\kappa}_1^2))^{1/2}$. In the quantum problem it can be assumed that the same crossover criterion remains valid, with $\tilde{T}_1 = \tilde{T}$ and that $\tilde{\kappa}_1 = \tilde{\kappa}_{\rm r}(q_T)$, $\tilde{Y}_1 = \tilde{Y}_{\rm r}(q_T)$ are the renormalized parameters (5.34), (5.35), corrected by zero-point anharmonic effects, evaluated at the renormalization scale q_T [91]. In rescaled units, the corresponding crossover scale is

$$q_G^2 \simeq \frac{3Ty(q_T)}{16\pi(z(q_T))^{1/2}} \ . \tag{5.53}$$

With characteristic parameters of graphene (see Sec. 5.7), it can be verified that $(q_G/q_T)^2 = 3y(q_T)/16\pi$ is small, confirming the consistency of a region $q_{\rm G} \ll |\mathbf{k}| \ll q_T$.

By using Eq. (5.45), we can estimate the thermal expansion of the quantum membrane as

$$\alpha(Y,T,\Lambda) = (z(q_T))^{-1}\alpha(y(q_T), z(q_T)^{-1/2}T, q_T) \ . \tag{5.54}$$

In principle, the zero-temperature RG flow remains valid only as far as $\Lambda' \gg z^{-1/2}(\Lambda')T$, but, in a first approximation, it is justified to set directly $\Lambda' = q_T = z^{-1/2}(q_T)T$.

After the cutoff has been reduced from the microscopic scale to the thermal scale q_T, we can estimate α by neglecting quantum thermal effects and by identifying $\alpha(y(q_T), z^{-1/2}(q_T)T, q_T)$ with the thermal expansion coefficient of a classical membrane with the standard Hamiltonian [1, 6, 12, 91, 164]

$$\mathcal{H}_{\rm cl}[\mathbf{H}_1(\mathbf{x})] = \int {\rm d}^2x \left[\frac{\kappa_{\rm cl}}{2}(\partial^2\mathbf{H}_1)^2 + \frac{Y_{\rm cl}}{8}(P^T_{\alpha\beta}(-\partial^2)(\partial_\alpha\mathbf{H}_1\cdot\partial_\beta\mathbf{H}_1))^2 \right] . \tag{5.55}$$

In terms of the discussion of Sec. 5.5, this corresponds to approximating $\mathcal{H}[\mathbf{H}_1]$, the Hamiltonian for modes with zero Matsubara frequency, with Eq. (5.55), which is its tree-level approximation (without loop corrections).

In particular, we must consider a classical membrane with Young modulus $Y_{\rm cl} = y(q_T)$, temperature $T_{\rm cl} = z^{-1/2}(q_T)T$, bending rigidity $\kappa_{\rm cl} = 1$, and a large-momentum cutoff $\Lambda_{\rm cl} = q_T$.

Thermal fluctuations in classical statistical mechanics have been investigated extensively [1, 6, 12, 18, 19, 22, 25, 85, 183]. The momentum-dependent correlation function $G^{\rm (cl)}_{ij}(\mathbf{k}) = \langle h_i(\mathbf{k})h_j(-\mathbf{k})\rangle$ is predicted to behave as

$$G^{\rm (cl)}_{ij}(\mathbf{k}) = \delta_{ij}\begin{cases} \frac{T_{\rm cl}}{\kappa_{\rm cl}k^4} \ , & \text{for } q_{\rm G} \ll |\mathbf{k}| \ll \Lambda_{\rm cl} \\ \frac{T_{\rm cl}}{\kappa_{\rm cl}k^{4-\eta_*}q_{\rm G}^{\eta_*}} & \text{for } |\mathbf{k}| \ll q_{\rm G} \ , \end{cases} \tag{5.56}$$

where η_* is an universal exponent and $q_G = (3T_{\rm cl}Y_{\rm cl}/(16\pi\kappa_{\rm cl}^2))^{1/2}$.

Calculating directly the extension factor via the relation

$$\begin{aligned}\langle v_{\rm cl}\rangle &= -\frac{1}{4}\langle(\partial_\alpha \mathbf{h})^2\rangle = -\frac{1}{4}\int \frac{\mathrm{d}^2k}{(2\pi)^2} G_{ii}(\mathbf{k}) \\ &\simeq -\frac{d_c T_{\rm cl}}{8\pi\kappa_{\rm cl}}\left[\int_0^{q_{\rm G}} \frac{\mathrm{d}k}{q_{\rm G}^{\eta_*} k^{1-\eta_*}} + \int_{q_{\rm G}}^{\Lambda_{\rm cl}} \frac{\mathrm{d}k}{k}\right] = -\frac{d_c T_{\rm cl}}{8\pi\kappa_{\rm cl}}\left[\frac{1}{\eta_*} + \ln\frac{\Lambda_{\rm cl}}{q_{\rm G}}\right]\end{aligned} \tag{5.57}$$

and differentiating with respect to $T_{\rm cl}$ at $\Lambda_{\rm cl}$, $Y_{\rm cl}$ and $\kappa_{\rm cl}$ fixed we find the expression for the thermal expansion coefficient [188]

$$\alpha_{\rm cl} = 2\frac{\partial\langle v_{\rm cl}\rangle}{\partial T_{\rm cl}} = -\frac{d_c}{4\pi\kappa_{\rm cl}}\left[\frac{1}{\eta_*} - \frac{1}{2} + \ln\frac{\Lambda_{\rm cl}}{q_{\rm G}}\right] . \tag{5.58}$$

Identifying, in rescaled units, $\alpha = (z(q_T))^{-1}\alpha_{\rm cl}$, and setting the effective classical parameters to the renormalized values we then find an expression for the thermal expansion coefficient of quantum membranes

$$\alpha = -\frac{d_c}{4\pi z(q_T)}\left[\frac{1}{\eta_*} - \frac{1}{2} + \frac{1}{2}\ln\left(\frac{16\pi}{3y(q_T)}\right)\right] . \tag{5.59}$$

This expression, when $z(q_T)$ and $y(q_T)$ are replaced with the one-loop running couplings

$$y(q_T) = \frac{Y}{1 + \frac{3(d_c+6)Y}{128\pi}\ln\frac{\Lambda}{q_T}} , \quad z(q_T) = \left(\frac{Y}{y(q_T)}\right)^{\theta} , \tag{5.60}$$

coincides with the result derived in Ref. [91], up to a numerical factor.

The temperature dependence of α is entirely driven by the renormalization factors $y(q_T)$ and $z(q_T)$. As a result, the thermal expansion coefficient is a slow, logarithmic function of T. In the limit $T \to 0$, α tends to zero as

$$\alpha_T \approx -\frac{d_c}{8\pi}\frac{\ln(\ln(\Lambda^2/T))}{[(g_0/2)\ln(\Lambda^2/T)]^{\theta}} . \tag{5.61}$$

As a remark, we note that, despite being approximate, the solution (5.59) is automatically consistent with the general form (5.51), as it is true for any expression of the type $\alpha = (z(q_T))^{-1}F(y(q_T))$, constructed via running couplings.

The approximations which lead to Eq. (5.59) are very natural. We expect that the prediction of a nearly constant α at low temperature is exact and that Eq. (5.61) captures, up to a numerical factor, the correct behavior in the limit $T \to 0$.

5.6.5 *Renormalization and third law of thermodynamics*

The fact that α vanishes in the zero-temperature limit is formally consistent with the requirement $\lim_{T\to 0}\alpha(T) = 0$, which is expected in view of the Maxwell relation

$$\alpha = \left(\frac{\partial V}{\partial T}\right)_p = -\left(\frac{\partial S}{\partial p}\right)_T , \tag{5.62}$$

and the third law of thermodynamics $\lim_{T\to 0} S(T,p) = 0$ [36, 84, 167]. The logarithmic way in which the low temperature limit is realized at zero tension is, however, very unconventional [91]. In fact, the existence of an anomalous behavior can be already anticipated by dimensional analysis. The rescalings described in Sec. 5.2.1 show that, for $\sigma = 0$, the only dimensionful parameters in the theory (5.3) are the temperature T and the UV cutoff Λ. If there were no ultraviolet divergences, the fact that α is dimensionless would have implied that $\alpha = \phi(Y)$, a temperature-independent result which is manifestly inconsistent with the limit $\lim_{T\to 0} \alpha(T) = 0$. It is only the logarithmic correction due to UV divergences which introduces an explicit dependence on the UV cutoff scale Λ and allows for a variation of α at low temperatures. In presence of a nonzero tension σ, Ref. [91] predicted that the thermal expansion coefficient vanishes in a faster way for $T \to 0$.

5.7 APPLICATION TO GRAPHENE

To illustrate the results, we consider the case of a monolayer graphene, using parameters $\tilde{\rho} \simeq 7.6$ kg m^{-2}, $\tilde{\lambda} \simeq 3.4$ eV Å^{-2}, $\tilde{\mu} \simeq 9.3$ eV Å^{-2}, $\tilde{B} \simeq 12.7$ eVÅ^{-2}, $\tilde{Y} \simeq 21.4$ eV Å^{-2} [78], $\kappa \simeq 1.4$ eV [189]. Setting the codimension d_c to the physical value $d_c = 1$, we find that the bare value of the quantum coupling constant is small: $g_0 \simeq 0.02$. As a consequence, the one-loop approximations to the RG functions β and η are justified at all length scales of physical interest. The smallness of g_0 is related physically to the fact that the mass of nuclei is much larger than the mass of electrons [162, 163], and, thus, we expect it to be a general feature of most two-dimensional materials.

The ultraviolet cutoff Λ is of the order of the inverse interatomic distance $a \simeq 1.42$ Å. We choose to identify Λ with the "Debye radius" $\Lambda = (4\pi^2/3)^{1/4} a^{-1}$, defined by the condition that the phase space area $\pi\Lambda^2$ contains the same number of degrees of freedom of the hexagonal Brillouin zone of graphene. With this estimate, the Debye temperature is approximately $T_{\rm D} = \hbar(\tilde{\kappa}/\tilde{\rho})^{1/2}\Lambda^2/k_{\rm B} \simeq 750$ K.

The predictions discussed in Sec. 5.6 are illustrated in figures 5.1, 5.2, and 5.3. In all cases, the renormalizations induced by quantum-mechanical fluctuations induce a slow, logarithmic behavior of statistical and thermodynamic quantities.

In particular, we find that the thermal expansion coefficient $\tilde{\alpha}$ at low temperatures is nearly constant over broad ranges of low temperature, with an order of magnitude $\tilde{\alpha} \approx -k_{\rm B}/(4\pi\tilde{\kappa}) \approx -5 \times 10^{-6}$ K^{-1} up to a numerical factor of order unity, in agreement with a simple classical estimate [188]. The limit $\lim_{T\to 0} \alpha = 0$ is only approached logarithmically.

The prediction of a nearly constant $\tilde{\alpha}$ depends essentially on the fact that flexural phonon modes fluctuate in absence of an imposed stress and without binding forces (see Ref. [91] for an analysis on the role of tension and Refs. [179, 188] for discussions on the effects of a supporting substrate).

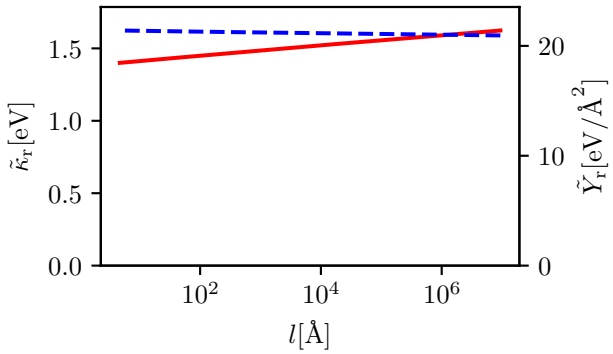

Figure 5.1: Effective wavevector-dependent bending rigidity (red solid line) and Young modulus (blue dashed line) as a function of wavelength $l = 2\pi/k$ for a graphene membrane at $T = 0$, as described by Eqs. (5.34) and (5.35). In the infinite-wavelength limit $\tilde{\kappa}_r(l)$ slowly diverges as $(\ln l)^{4/7}$ and $\tilde{Y}_r(l)$ slowly vanishes as $(\ln l)^{-1/7}$.

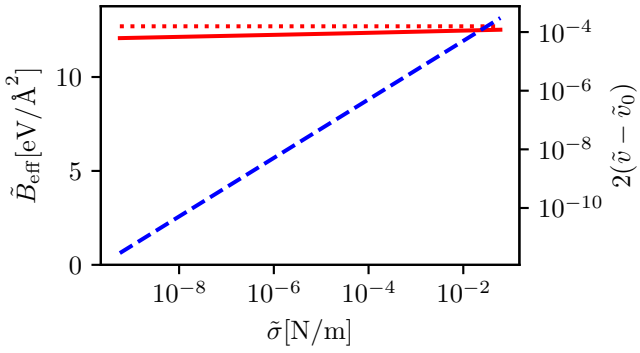

Figure 5.2: Anomalous Hooke's law for a graphene membrane at $T = 0$. The red solid line represents the macroscopic bulk modulus $\tilde{B}_{\rm eff} = \frac{1}{2}\partial\tilde{\sigma}/\partial\tilde{v}$ as a function of the applied tension $\tilde{\sigma}$, as described by Eq. (5.41). The red dotted line is constant as a function of the applied stress and identifies the microscopic bulk modulus $\tilde{B} \simeq 12.7$ eV Å^{-2} controlling the normal Hooke's law for a membrane constrained in two dimension (without quantum-mechanical out-of-plane fluctuations). The strain induced by tension is represented by blue dashed lines. The effective bulk modulus vanishes in the limit $\sigma \to 0$ as $\tilde{B}_{\rm eff}(\sigma) \approx (\ln(1/\sigma))^{-1/7}$. The singularity, however, is very slow.

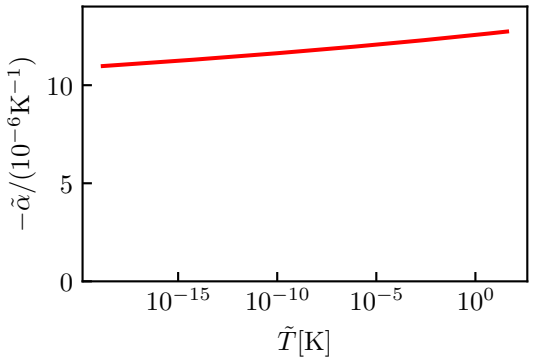

Figure 5.3: Negative thermal expansion coefficient for an unstressed graphene membrane as a function of temperature (red solid line). In the limit $T \to 0$, $\tilde{\alpha} \to 0$ as expected from the third law of thermodynamics, but the approach to zero is only logarithmic with $\tilde{T}$.

To conclude, we note that a more complete understanding of the thermodynamics of graphene samples requires a further analysis of the coupling between membrane fluctuations and Dirac electrons, which have been proposed to be at the origin of mechanical instabilities such as a spontaneous rippling [24, 54]. The role of electron fluctuations, however, is suppressed in insulating 2D materials such as hexagonal boron nitride.

5.8 SUMMARY AND CONCLUSIONS

To summarize, we have analyzed the theory of a fluctuating quantum mechanical membrane within the framework of perturbative renormalization group techniques. At zero temperature, the perturbative RG provides a systematic derivation of logarithmic singularities analyzed in earlier investigations by momentum-shell and by nonperturbative renormalization group techniques. In the limit of a weakly applied external tension $\tilde{\sigma}$, we recover the result that the stress-strain relation at $T = 0$ is singular: for $\tilde{\sigma} \to 0$, the strain behaves as $\tilde{\sigma}[\ln(1/\tilde{\sigma})]^{-1/7}$.

In the case of a small, but nonzero temperature, techniques of finite-size quantum field theory provide general scaling relations for thermodynamic quantities such as the entropy S, the specific heat C, and the thermal expansion coefficient α at vanishing or small external tension. By an approximate solution of the theory, we derive that the negative thermal expansion coefficient of an unstressed crystalline membrane vanishes for $T \to 0$ as a logarithmic function of the temperature.

ACKNOWLEDGMENTS

This work was supported by the Dutch Research Council (NWO) via the Spinoza Prize of Professor M.I. Katsnelson.

6

BILAYER GRAPHENE

We study thermal fluctuations of a free-standing bilayer graphene subject to vanishing external tension. Within a phenomenological theory, the system is described as a stack of two continuum crystalline membranes, characterized by finite elastic moduli and a nonzero bending rigidity. A nonlinear rotationally-invariant model guided by elasticity theory is developed to describe interlayer interactions. After neglection of in-plane phonon nonlinearities and anharmonic interactions involving interlayer shear and compression modes, an effective theory for soft flexural fluctuations of the bilayer is constructed. The resulting model, neglecting anisotropic interactions, has the same form of a well-known effective theory for out-of-plane fluctuations in a single-layer membrane, but with a strongly wave-vector dependent bare bending rigidity. Focusing on AB-stacked bilayer graphene, parameters governing interlayer interactions in the theory are derived by first-principles calculations. Statistical-mechanical properties of interacting flexural fluctuations are then calculated by a numerical iterative solution of field-theory integral equations within the self-consistent screening approximation (SCSA). The bare bending rigidity in the considered model exhibits a crossover between a long-wavelength regime governed by in-plane elastic stress and a short wavelength region controlled by monolayer curvature stiffness. Interactions between flexural fluctuations drive a further crossover between a harmonic and a strong-coupling regime, characterized by anomalous scale invariance. The overlap and interplay between these two crossover behaviors is analyzed at varying temperatures.

The main text of this chapter has been published as:
Achille Mauri, David Soriano, and Mikhail I. Katsnelson, "Thermal ripples in bilayer graphene", Phys. Rev. B **102**, 165421 (2020); preprint: arXiv:2007.00552 (2020)
The supplemental material to the publication has been synthesized and converted into an appendix (App. 6.B).

The statistical properties of thermally-fluctuating two-dimensional (2D) membranes have been the subject of extensive investigations [1, 3, 4]. Crystalline layers, characterized by fixed connectivity between constituent atoms and a subsequent elastic resistance to compression and shear, exhibit a particularly rich thermodynamical behavior, both in clean and disordered realizations [1, 3, 4, 6, 9–12, 23, 25, 26, 41, 42, 44, 51, 85]. In absence of substrates and without the action of an externally applied tension, fluctuations are only suppressed by elasticity and the bending rigidity of the layer. Although a naive application of the Mermin-Wagner theorem suggests the destruction of spontaneous order at any finite temperature, it has long been recognized that these freely-fluctuating elastic membranes exhibit an orientationally-ordered flat phase at low temperatures [6, 9]. As a result of strong nonlinear coupling between bending and shear deformations, thermal fluctuations in the flat phase present anomalous scale invariance characterized by universal non-integer exponents. In the long-wavelength limit, the scale-dependent effective compression and shear moduli are driven to zero as power laws of the wavevector q, while the effective bending rigidity diverges as $\kappa(q) \approx q^{-\eta}$ [10–12, 19, 25, 26, 183]. This anomalous infrared behavior sets in at a characteristic 'Ginzburg scale' $q_* \approx \sqrt{3TY/(16\pi\kappa^2)}$, where κ, Y and T are, respectively, the bare bending rigidity, Young modulus and temperature [3, 61]. For shorter wavelengths, $q > q_*$, within a membrane model based on continuum elasticity theory, fluctuation effects become negligible and the effective elastic moduli approach their bare values.

The first theoretical developments in the statistical mechanics of elastic membranes were driven by the physics of biological layers, polymerized membranes and other surfaces [1, 4, 56]. After the isolation of atomically-thin two-dimensional materials, the relevance of statistical mechanical predictions for these extreme membrane realizations has raised vast interest, in both theory [3, 25, 31, 41, 51, 61, 112] and experiments [69, 70, 72, 76, 190] (see also Refs. [65, 71, 73, 191, 192]).

In the case of atomically-thin 2D membranes, numerical simulations with realistic atomic interactions are accessible [31, 37, 38, 61, 112, 193, 194], which allows material-specific predictions of the fluctuation behavior. Furthermore, the physics of graphene and other 2D materials stimulated new questions as compared to previously considered membrane realizations.

By exfoliation of graphite, it is possible to controllably extract multilayer membranes composed of N stacked graphene sheets. As in the parent graphite structure, covalently-bonded carbon layers are tied by weaker van der Waals interactions. The large difference between the strengths of covalent and interlayer binding forces generates an intriguing mechanical and statistical behavior, which is attracting vast research interest [188, 195–199].

The properties of defect-free multilayers subject to small fluctuations, in the harmonic approximation, are already non-trivial. Mechanical properties are crucially determined by the coupling between interlayer shear deformation and out-of-plane,

bending, fluctuations. If layers are free to slide relative to each other at zero energy cost, we expect that the bending rigidity of the stack is controlled by the curvature stiffness of individual layers. We can thus assume that the bending rigidity is approximately $N\kappa$, where N is the number of layers and κ is the monolayer bare bending stiffness [188, 197–199]. By contrast, the presence of a nonzero interlayer shear modulus forces layers to compress or dilate in response to curvature. Assuming rigid binding between layers, the bending stiffness is then controlled by in-plane elastic moduli and it grows proportionally to $N(N^2-1)$ for $N \geq 2$ [200]. For large N, the limiting N^3 scaling of the bending stiffness [188, 197–200] is consistent with the continuum theory of thin elastic plates [3, 83, 188, 200]. In the case of graphene bilayer, the corresponding contribution to the bending rigidity can be written as $(B+\mu)l^2/2$, where B and μ are compression and shear moduli, and l is the interlayer distance [188].

A theory interpolating between these extreme regimes was developed, within a harmonic approximation, in Ref. [188]. As a modeling framework, the system was described as a stack of continuum two-dimensional elastic media. The energy functional describing coupling between layers was constructed by discretizing the continuum theory of a three-dimensional uniaxial solid. Within this model, coupled and decoupled fluctuation regimes are recovered as limiting cases for long and short wavelengths, connected by a crossover: coupling between flexural and interlayer shear deformations sets in for wave vectors smaller than characteristic scales determined by elastic stiffnesses and interlayer interactions [188].

Recent experimental measurements of the bending rigidity [195, 197, 199, 201, 202] present a large scatter and indicate smaller values compared to the theoretical prediction for the long-wavelength, rigidly coupled case. In the case of bilayer graphene, different experimental techniques lead to $\kappa = 35.5^{+20.0}_{-15.0}$ eV [201] and 3.35 ± 0.43 eV [202], significantly smaller than the elastic contribution $(B+\mu)l^2/2$, which corresponds to a rigidity of the order of 100 eV (theoretical predictions in Ref. [200] lead to $\kappa \simeq 160$ eV). For few-layer membranes with $N \geq 2$, Ref. [201] reported evidence that the overall bending rigidity scales as N^2. More recently, by analyzing pressurized bubbles in multilayer graphene, MoS_2, and hexhagonal BN, Ref. [197] reported values of κ intermediate between the uncoupled limit $N\kappa$ and the rigidly-coupled case, and interpreted the observed behavior as the result of interlayer slippage between atomic planes. Finally, Ref. [199] observed multilayer graphene membranes under varying bending angles. Values of the bending stiffness close to $N\kappa$ were observed for large angles, which was interpreted by a dislocation model of interlayer slippage.

Reported results for the interlayer shear modulus in multilayer graphene also exhibit a large dispersion, see e.g [195].

At finite temperatures, statistical properties of fluctuating stacks of crystalline membranes have been long investigated. A rich physics was predicted in early studies

motivated by lamellar phases of polymerized membranes. In particular, Ref. [203] predicted a sharp phase transition between a coupled state and a decoupled phase, in which algebraic decay of crystalline translational order makes interlayer shear coupling irrelevant. Ref. [169] elaborated on the properties of the decoupled state, within a nonlinear three-dimensional continuum theory and determined logarithmic renormalizations due to thermal fluctuations[1].

In the context of crystalline bilayer and multilayer graphene membranes, finite-temperature anharmonic lattice fluctuations were extensively addressed by numerical simulations (see, e.g. [193, 194, 204]).

In this work we study thermal fluctuations of ideal, defect-free bilayer graphene within a phenomenological, elasticity-like model. The theory of Ref. [188] is assumed as a starting point and generalized to include crucial nonlinearities which control anomalous scaling behavior. An interesting aspect introduced by finite temperatures stems from the interplay of different wavevector scales: characteristic scales marking the onset of coupling between flexural and interlayer shear, and Ginzburg scales q_* controlling the transition from harmonic to strongly nonlinear fluctuations. In order to obtain a global picture of correlation functions at arbitrary wavevector q, we derive a numerical solution of Dyson equations within the self-consistent screening approximation (SCSA) [23–25]. In the long wavelength limit, the universal power-law behavior predicted by membrane theory is recovered and the SCSA scaling exponent $\eta = 4/(1+\sqrt{15})$ is reproduced with high accuracy. The finite-wavelength solution, furthermore, gives access to crossovers in correlation functions and to non-universal properties specific to bilayer graphene. In order to develop material-specific predictions, we develop an *ab-initio* prediction of model parameters focusing on the case of AB-stacked bilayer graphene. The paper is organized as follows: in Sec. 6.1, after a brief discussion of theories for single-layer membranes, we introduce a phenomenological model which extends the theory of Ref. [188] with the inclusion of nonlinearities required by rotational invariance. Subsequently, the model is simplified by neglecting all nonlinearities but interactions of the collective out-of-plane displacement field. In 6.1.3, we derive an effective model for flexural fluctuations by successively integrating out all other fields. After neglection of anisotropic interactions, this model takes the form of a standard theory for crystalline membranes, with a strongly q-dependent bare bending rigidity. In Sec. 6.2 we discuss model parameters for AB-stacked bilayer graphene and describe first-principle calculations of the interlayer coupling moduli. In Sec. 6.3 correlation functions of the resulting model are calculated at arbitrary wavevector within the SCSA [23–25]; an iterative algorithm is used to determine numerical solutions of SCSA equations. Results are illustrated in Sec. 6.4. Finally, Sec. 6.5 discusses an extension to the theory in which nonlinearities in flexural fields of both layers are taken into account. Sec. 6.6 summarizes and concludes the paper.

1 See also Ref. [181].

6.1 MODEL

6.1.1 *Single layer*

This section briefly introduces existing models for two-dimensional crystalline membranes, extensively discussed in [1, 3, 4, 6, 9–12, 25, 41].

In a long-wavelength continuum limit, membrane configurations are specified by the coordinates $\mathbf{r}(\mathbf{x})$ in three-dimensional space of mass points in the 2D crystal, identified by an internal two-dimensional coordinate $\mathbf{x}$. After specification of an energy functional $H[\mathbf{r}(\mathbf{x})]$, the statistics of fluctuating configurations at a temperature T is governed by the Gibbs probability distribution

$$P[\mathbf{r}(\mathbf{x})] = \frac{1}{Z} \mathrm{e}^{-H_0[\mathbf{r}(\mathbf{x})]/T} \ , \tag{6.1}$$

where

$$Z = \int [\mathrm{d}\mathbf{r}(\mathbf{x})] \mathrm{e}^{-H_0[\mathbf{r}(\mathbf{x})]/T} \tag{6.2}$$

is the partition function, and $\int [\mathrm{d}\mathbf{r}(\mathbf{x})]$ denotes functional integration over the field $\mathbf{r}(\mathbf{x})$.

In the spirit of elasticity theory, a model for membranes with nonzero stiffness to curvature and strain is defined by the configuration energy [9, 11, 12]

$$H_0 = \int \mathrm{d}^2 x \left[\frac{\kappa}{2} \left(\partial^2 \mathbf{r} \right)^2 + \frac{\lambda}{2} \left(U_{\alpha\alpha} \right)^2 + \mu U_{\alpha\beta} U_{\alpha\beta} \right] \ , \tag{6.3}$$

where κ, λ, and μ are, respectively, the bending rigidity and Lamé elastic coefficients. The notation $\partial_\alpha = \partial / \partial x_\alpha$ indicates differentiation with respect to internal coordinates, and $U_{\alpha\beta} = \frac{1}{2} \left(\partial_\alpha \mathbf{r} \cdot \partial_\beta \mathbf{r} - \delta_{\alpha\beta} \right)$ is the strain tensor, proportional to the local deformation of the metric $g_{\alpha\beta} = \partial_\alpha \mathbf{r} \cdot \partial_\beta \mathbf{r}$ from the Euclidean metric $\delta_{\alpha\beta}$. In Eq. (6.3), mass points are labeled via their coordinates in a configuration of mechanical equilibrium: reference coordinates x_1, x_2 are chosen in such way that states of minimum energy are $\mathbf{r}(\mathbf{x}) = x_\alpha \mathbf{v}_\alpha + \mathbf{t} = x_1 \mathbf{v}_1 + x_2 \mathbf{v}_2 + \mathbf{t}$, where $\mathbf{v}_1$, $\mathbf{v}_2$ is any given pair of mutually orthogonal unit vectors and $\mathbf{t}$ is an arbitrary constant vector.

The energy functional (6.3) has been extensively discussed as a Landau-Ginzburg model for critical phenomena at the crumpling transition and also as a starting point to discuss scaling properties of the flat phase [1, 4, 9, 11, 26].

In the flat phase, it is convenient to parametrize $\mathbf{r}(\mathbf{x}) = (x_\alpha + u_\alpha(\mathbf{x}))\mathbf{v}_\alpha + h(\mathbf{x})\mathbf{n}$, where $\mathbf{n} = \mathbf{v}_1 \times \mathbf{v}_2$ denotes the normal to the membrane plane. Assuming that displacement fields and their gradients are small, such that $|\partial^2 u| \ll |\partial u|$ and $|\partial u| \ll 1$, Eq. (6.3) can be reduced by the replacements $U_{\alpha\beta} \to u_{\alpha\beta} = (\partial_\alpha u_\beta +$

$\partial_\beta u_\alpha + \partial_\alpha h \partial_\beta h)/2$, $(\partial^2 \mathbf{r})^2 \to (\partial^2 h)^2$, which leads to the standard approximate form[2] [1, 6, 10, 41]

$$\tilde{H}_0 = \int \mathrm{d}^2 x \left[\frac{\kappa}{2} (\partial^2 h)^2 + \frac{\lambda}{2} u_{\alpha\alpha}^2 + \mu u_{\alpha\beta}^2 \right] . \tag{6.4}$$

The neglected terms are expected to be unnecessary for an exact calculation of universal quantities such as scaling exponents. This is supported by a power-counting argument in the framework of a field-theoretic ε-expansion method [10]: after extension of the problem to D-dimensional membranes in a d-dimensional embedding space, neglected terms are irrelevant by power counting at the upper critical dimension $D = 4$. Eq. (6.4) thus plays the role of an effective theory [10, 11] suitable for calculation of scaling indices to all orders in an $\varepsilon = (4 - D)$-expansion.

In the transition from Eq. (6.3) to Eq. (6.4), neglected nonlinearities lead to an explicit breaking of rotational symmetry. However, as it is well known [4, 11], the underlying invariance is preserved in a deformed form: $\tilde{H}_0$ is invariant under the transformations

$$\begin{aligned} h(\mathbf{x}) &\to h(\mathbf{x}) + A_\alpha x_\alpha + B \ , \\ u_\alpha(\mathbf{x}) &\to u_\alpha(\mathbf{x}) - A_\alpha h(\mathbf{x}) - \frac{1}{2} A_\alpha A_\beta x_\beta + B'_\alpha \ , \end{aligned} \tag{6.5}$$

for arbitrary coordinate-independent A_α, B, and B'_α. This deformed symmetry and the subsequent Ward identities are crucial in the renormalization of the theory of membranes, and, most importantly, in the protection of the softness of flexural modes, which ensures the criticality of the theory without fine-tuning of parameters [4, 10, 11, 23, 25].

It is useful to compare Eqs. (6.3) and (6.4) with the Canham-Helfrich model for fluid membranes [1] and with the model for crystalline membranes developed in Ref. [10]. In Ref. [10], bending rigidity of the layer was introduced via an energy contribution of the form

$$\frac{\kappa}{2} \int \mathrm{d}^2 x (\partial_\alpha \mathbf{N})^2 = \frac{\kappa}{2} \int \mathrm{d}^2 x \mathbf{K}_\beta^\alpha \cdot \mathbf{K}_{\alpha\beta} \ , \tag{6.6}$$

where $\mathbf{N}$ is the local normal to the surface, $\mathbf{K}_{\alpha\beta}$ is the curvature tensor, and $\mathbf{K}_\beta^\alpha = g^{\alpha\gamma} \mathbf{K}_{\beta\gamma}$. Using that $\mathbf{K}_{\alpha\beta} = \mathbf{N}(\mathbf{N} \cdot \partial_\alpha \partial_\beta \mathbf{r})$ for two-dimensional surfaces (see e.g. Chap. 7 of Ref. [1]), Eq. (6.6) can be written as

$$\frac{\kappa}{2} \int \mathrm{d}^2 x g^{\beta\gamma} (\mathbf{N} \cdot \partial_\alpha \partial_\beta \mathbf{r})(\mathbf{N} \cdot \partial_\alpha \partial_\gamma \mathbf{r}) \ . \tag{6.7}$$

2 As discussed in Ref. [41], the comparison between curvature and elastic energies becomes nontrivial if the problem is analyzed in a large d-limit at fixed internal dimension $D = 2$.

Here $g^{\alpha\beta}$ denotes the inverse matrix of the metric tensor $g_{\alpha\beta} = \partial_\alpha \mathbf{r} \cdot \partial_\beta \mathbf{r}$. For small fluctuations, such that $g_{\alpha\beta} \simeq \delta_{\alpha\beta}$ and $\mathbf{N} \simeq \mathbf{n}$, the curvature energy reduces, at leading order, to

$$\frac{\kappa}{2} \int \mathrm{d}^2x \partial_\alpha \partial_\beta h \partial_\alpha \partial_\beta h = \frac{\kappa}{2} \int \mathrm{d}^2x \Big[(\partial^2 h)^2 + (\delta_{\alpha\beta}\partial^2 - \partial_\alpha \partial_\beta)(\partial_\alpha h \partial_\beta h) \Big] \ , \quad (6.8)$$

which, up to boundary terms, is equivalent to

$$\frac{\kappa}{2} \int \mathrm{d}^2x (\partial^2 h)^2 \ , \quad (6.9)$$

the curvature term in Eq. (6.4).

In the Canham-Helfrich model [1], the curvature stiffness for a fluid membrane with vanishing spontaneous curvature reads

$$\int \mathrm{d}^2x \sqrt{g} \Big[2\kappa_b H^2 + \kappa_G K \Big] \ , \quad (6.10)$$

where H and K are the mean and the Gaussian curvature, and $g = \det[g_{\alpha\beta}]$.

For 2D surfaces [1],

$$H = \frac{1}{2} K^\alpha_\alpha \quad \text{and} \quad K = \frac{1}{2} \Big[(K^\alpha_\alpha)^2 - K^\alpha_\beta K^\beta_\alpha \Big] \ , \quad (6.11)$$

where $K_{\alpha\beta} = \mathbf{N} \cdot \partial_\alpha \partial_\beta \mathbf{r}$, $K^\alpha_\beta = g^{\alpha\gamma} K_{\beta\gamma}$. The Canham-Helfrich energy functional (6.10) is reparametrization-invariant, expressing that the configuration energy is only sensitive to the geometrical shape of the surface in three-dimensional space and not on its internal coordinate system. As it was discussed in Ref. [10], in crystalline layers the crystal lattice singles out a natural parametrization of the membrane, and reparametrization-invariance is not a necessary requirement (see also Ref. [11] for a more general discussion in presence of non-flat internal metric).

For small fluctuations about a flat configuration, the mean and Gaussian curvatures reduce to

$$H \simeq \frac{1}{2} (\partial^2 h) \quad (6.12)$$

and

$$K \simeq \frac{1}{2} \big[(\partial^2 h)^2 - (\partial_\alpha \partial_\beta h)(\partial_\alpha \partial_\beta h) \big] = -\frac{1}{2} (\delta_{\alpha\beta}\partial^2 - \partial_\alpha \partial_\beta)(\partial_\alpha h \partial_\beta h) \ , \quad (6.13)$$

while $\sqrt{g} \simeq 1$. Integration over K then leads to a boundary term and a curvature energy density proportional to $(\partial^2 h)^2$ is recovered. More generally, the Gauss-Bonnet theorem implies that the integral $\int \mathrm{d}^2x \sqrt{g} K$ is topological invariant for closed surfaces, and the sum of boundary terms and a topological invariant for open surfaces.

In this work, curvature energy is considered to a leading order in the limit of small fluctuations about a flat configuration, and boundary terms arising from the surface integration of the leading-order Gaussian curvature, Eq. (6.13), are neglected.

We note, however, that the Gaussian curvature energy plays an important role in processes which involve a change of membrane topology [1] or finite-size membranes with a boundary. For example, a recent analysis of thermal fluctuations within the harmonic approximation [205], indicated an important role of Gaussian curvature energy in the statistics of fluctuating membranes with a free edge. Finally, we note that models with higher-order powers of curvature were considered in Ref. [206, 207], in relation with the problem of bolaamphiphilic vesicles.

As a concluding remark, we notice that the models discussed above assume locality of the configuration energy, and, therefore, do not include infinite-range forces such as van der Waals [208], dipole interactions [209] or the coupling with gapless electrons, discussed in connection with graphene in Refs. [54, 165].

6.1.2 *Bilayer*

We will model bilayer graphene as a stack of two coupled elastic membranes [188]. The corresponding energy functional can thus be written as

$$H = \sum_{i=1}^{2} H_i + H_c \ , \tag{6.14}$$

where

$$H_i = \int \mathrm{d}^2x \left[\frac{\kappa}{2} \left(\partial^2 \mathbf{r}_i \right)^2 + \frac{\lambda}{2} U_{i\alpha\alpha}^2 + \mu U_{i\alpha\beta}^2 \right] \tag{6.15}$$

are single-layer energies, and H_c represents coupling between membranes[3]. In Eq. (6.15), $\mathbf{r}_i$ and $U_{i\alpha\beta}$ denote the coordinates and the local deformation tensor of the i-th layer in the stack. As a model for interlayer interactions we assume a local coupling[4] truncated at the leading order in a gradient expansion. This corresponds to an energy functional of the form

$$H_c = \int \mathrm{d}^2x \, \mathcal{H}_c(\mathbf{x}) \tag{6.16}$$

with an energy density $\mathcal{H}_c(\mathbf{x})$ depending only on $\mathbf{r}_1(\mathbf{x})$ and $\mathbf{r}_2(\mathbf{x})$ and their leading-order gradients at $\mathbf{x}$. After introduction of sum and difference coordinates $\mathbf{r} =$

3 As in Sec. 6.1.1, the contributions of in-plane modes $(\partial^2 u_\alpha)^2$ to $(\partial^2 \mathbf{r})^2$ will eventually be neglected. The chosen curvature energy is thus equivalent, to leading order, to alternative expressions such as Eq. (6.6).

4 As discussed above, local interactions do not exhaust all possibilities due to the presence of infinite-range van der Waals interactions [208] and coupling with gapless electrons. Effects of non-local interactions are beyond the scope of this work, and will be neglected.

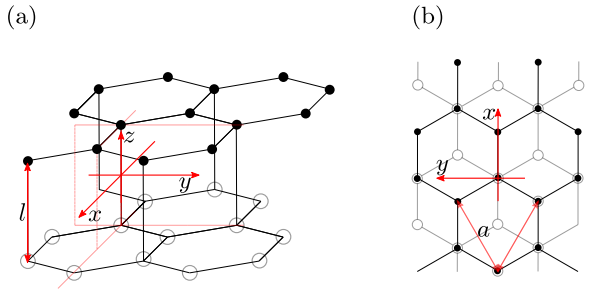

Figure 6.1: (a) Lattice structure of bilayer graphene in the Bernal (AB) stacking. (b) Top view of AB-stacked bilayer graphene.

$\frac{1}{2}(\mathbf{r}_1 + \mathbf{r}_2)$, $\mathbf{s} = \mathbf{r}_1 - \mathbf{r}_2$, invariance under translations in the three-dimensional ambient space implies that $\mathcal{H}_c$ cannot depend on $\mathbf{r}$, but only on its derivatives. In the leading order of a gradient expansion, we will thus assume that $\mathcal{H}_c(\mathbf{x})$ depends only on the local separation vector $\mathbf{s}$ and on the tangent vectors $\partial_\alpha \mathbf{r}$, neglecting dependence on higher derivatives such as $\partial_\alpha \mathbf{s}$ or $\partial^2 \mathbf{r}$. This level of approximation is analogous to the approach in Ref. [188], where the coupling energy is derived by discretization of a continuum three-dimensional elasticity theory. In the following, we will assume the developed elasticity-like theory as a model to describe finite-wavelength phenomena.

The most general form of $\mathcal{H}_c$ depending on $\mathbf{s}$ and $\partial_\alpha \mathbf{r}$ and consistent with rotational and inversion symmetries of the three-dimensional ambient space is a generic function of the scalar products

$$\partial_\alpha \mathbf{r} \cdot \partial_\beta \mathbf{r} \ , \qquad \mathbf{s} \cdot \partial_\alpha \mathbf{r} \ , \qquad s^2 \ . \tag{6.17}$$

In the configuration of mechanical equilibrium, neglecting a small uniform strain induced by interlayer coupling, $\mathbf{r}(\mathbf{x}) = x_\alpha \mathbf{v}_\alpha$ and the relative displacement between layers is $\mathbf{s}(\mathbf{x}) = l\mathbf{n}$, where l is the interlayer distance and $\mathbf{n} = \mathbf{v}_1 \times \mathbf{v}_2$. For small fluctuations, the coupling energy can thus be expanded in powers of the strain tensor $U_{\alpha\beta} = \frac{1}{2}\left(\partial_\alpha \mathbf{r} \cdot \partial_\beta \mathbf{r} - \delta_{\alpha\beta}\right)$, the field $\mathbf{s} \cdot \partial_\alpha \mathbf{r}$, which measures interlayer shear, and $s^2 - l^2$, which describes local dilations of the layer-to-layer distance.

Consistency with the dihedral D_{3d} symmetry of the AB-stacked bilayer graphene [210] (see Figs. 6.1a and 6.1b) selects, among general combinations of these terms, a subset of allowed invariant functions. Symmetry-consistent terms can be directly constructed by group theory arguments, or, equivalently, by adapting invariants from theory of three-dimensional elastic media. Identification of $\mathbf{s}/l = (\mathbf{r}_1 - \mathbf{r}_2)/l$ with a discrete version of $\partial_z \mathbf{r}$ in a corresponding three-dimensional theory, indicates that $\mathbf{s} \cdot \partial_\alpha \mathbf{r}/l$ and $(s^2 - l^2)/l^2$ have the same transformation properties of strain tensor components $U_{\alpha z} = \partial_\alpha \mathbf{r} \cdot \partial_z \mathbf{r}$ and $U_{zz} = \partial_z \mathbf{r} \cdot \partial_z \mathbf{r} - 1$, respectively. The

general elastic free-energy of uniaxial media with D_{3d} point group subject to uniform deformation reads[5] [83]

$$F = \frac{1}{2}\bar{C}_1(U_{\alpha\alpha})^2 + \bar{C}_2 U_{\alpha\beta}U_{\alpha\beta} + \frac{1}{2}C_1 U_{zz}^2 + \frac{1}{2}C_2 U_{\alpha z}^2 + C_3 U_{\alpha\alpha}U_{zz} + C_4\big[(U_{xx}-U_{yy})U_{xz} - 2U_{xy}U_{yz}\big] \ , \tag{6.18}$$

where Greek indices run over x and y components, and $\bar{C}_i$ and C_i are constants. In Eq. (6.18) and in the following, reference-space coordinates are interchangeably denoted as (x_1, x_2) or (x, y). Returning to the bilayer case, by drawing from analogous invariants in Eq. (6.18), we can write the functional H_c as

$$H_c = \int \mathrm{d}^2x \left[\frac{g_1}{8l^4}(s^2-l^2)^2 + \frac{g_2}{2l^2}(\mathbf{s}\cdot\partial_\alpha\mathbf{r})^2 + \frac{g_3}{4l^2}(s^2-l^2)U_{\alpha\alpha} + \frac{g_4}{2l}\big((\mathbf{s}\cdot\partial_x\mathbf{r})(U_{xx}-U_{yy}) - 2(\mathbf{s}\cdot\partial_y\mathbf{r})U_{xy}\big)\right] , \tag{6.19}$$

up to terms of quadratic order in the strains. Among functions of $\mathbf{s}$ and $\partial_\alpha\mathbf{r}$, other terms could be added to Eq. (6.19). One is an isotropic tension, $\sigma\int \mathrm{d}^2x\, U_{\alpha\alpha}$, reflecting uniform strain due to a small difference in lattice constants between monolayer and bilayer graphene. This tension can be eliminated by modifying the reference state about which strain is defined (see Refs. [12, 85, 91] for a discussion on thermally-induced uniform stretching). Such redefinition of the point of expansion implies a small shift in the elastic moduli. In addition, symmetry does not rule out a coupling of the form

$$\frac{\lambda'}{2}(U_{\alpha\alpha})^2 + \mu' U_{\alpha\beta}U_{\alpha\beta} \tag{6.20}$$

which contributes to the stretching elasticity of the bilayer as a whole. Due to the large difference in scale between covalent carbon-carbon interactions and interlayer van der Waals interactions, it is expected that λ' and μ' are much smaller than the monolayer Lamé moduli λ and μ. Similarly, it is expected that corrections to λ, μ and κ due to uniform strain are small. These effects are thus neglected in Eq. (6.19).

Collecting terms in Eq. (6.14), the model Hamiltonian for graphene bilayer thus reduces to:

$$H = H_1 + H_2 + \int \mathrm{d}^2x \left[\frac{g_1}{8l^4}\left(s^2-l^2\right)^2 + \frac{g_2}{2l^2}(\mathbf{s}\cdot\partial_\alpha\mathbf{r})^2 + \frac{g_3}{4l^2}\left(s^2-l^2\right)U_{\alpha\alpha} + \frac{g_4}{2l}\big((\mathbf{s}\cdot\partial_x\mathbf{r})(U_{xx}-U_{yy}) - 2(\mathbf{s}\cdot\partial_y\mathbf{r})U_{xy}\big)\right] . \tag{6.21}$$

5 In the case of ABA-stacked graphite, the symmetry group includes symmetry for $z \to -z$ and $c_{16} = 0$.

Within the harmonic approximation, after neglection of the anisotropic term in the last line, Eq. (6.21) reduces to the functional derived in Ref. [188].

In analogy with the standard crystalline membrane theory, it is convenient to parametrize the coordinate vectors $\mathbf{r}(\mathbf{x})$ and $\mathbf{s}(\mathbf{x})$ by separating in-plane and out-of-plane displacement fields: $\mathbf{r}(\mathbf{x}) = (x_\alpha + u_\alpha)\mathbf{v}_\alpha + h\mathbf{n}$ and $\mathbf{s}(\mathbf{x}) = \bar{u}_\alpha \mathbf{v}_\alpha + (l + \bar{h})\mathbf{n}$, where $\mathbf{u}, \bar{\mathbf{u}} \in \mathbb{R}^2$, $h, \bar{h} \in \mathbb{R}$. Fluctuations of relative coordinate $\bar{h}$ and the shear mode $\bar{u}_\alpha + l\partial_\alpha h$ are bounded by the couplings g_1 and g_2. For simplicity, similarly to the approach of Ref. [188], fluctuations of $\bar{h}$ and $\bar{u}_\alpha$ will thus be treated within a harmonic approximation. Furthermore, repeating standard approximations for single membranes [1, 6] we neglect the contribution $\kappa(\partial^2 u_\alpha)^2/2$ to the energy density and terms nonlinear in u_α in the strain tensor

$$U_{\alpha\beta} = \frac{1}{2}\left(\partial_\alpha \mathbf{r} \cdot \partial_\beta \mathbf{r} - \delta_{\alpha\beta}\right) = \frac{1}{2}(\partial_\alpha u_\beta + \partial_\beta u_\alpha + \partial_\alpha h \partial_\beta h + \partial_\alpha u_\gamma \partial_\beta u_\gamma) \ , \quad (6.22)$$

which is thus replaced with the approximate form $u_{\alpha\beta} = \frac{1}{2}(\partial_\alpha u_\beta + \partial_\beta u_\alpha + \partial_\alpha h \partial_\beta h)$.

After expansion of Eq. (6.21), these approximations lead to

$$\begin{aligned} \tilde{H} = \int \mathrm{d}^2 x \Big[& \kappa(\partial^2 h)^2 + \lambda(u_{\alpha\alpha})^2 + 2\mu u_{\alpha\beta} u_{\alpha\beta} \\ & + \frac{\kappa}{4}(\partial^2 \bar{h})^2 + \frac{\lambda}{4}(\partial_\alpha \bar{u}_\alpha)^2 + \frac{\mu}{8}(\partial_\beta \bar{u}_\alpha + \partial_\alpha \bar{u}_\beta)^2 \\ & + \frac{g_1}{2l^2}\bar{h}^2 + \frac{g_2}{2l^2}(\bar{u}_\alpha + l\partial_\alpha h)^2 + \frac{g_3}{2l}\bar{h} u_{\alpha\alpha} \\ & + \frac{g_4}{2l}\big((\bar{u}_x + l\partial_x h)(u_{xx} - u_{yy}) - 2(\bar{u}_y + l\partial_y h)u_{xy}\big) \Big] \ , \end{aligned} \quad (6.23)$$

which will be used as a starting point in Sec. 6.1.3.

Similarly to the standard theory of crystalline membranes [4, 11] (see Eq. (6.5)), this configuration energy possesses a continuous symmetry, which reflects the underlying invariance under rotations and translations in the embedding space: the Hamiltonian (6.23) is invariant under

$$\begin{aligned} & h(\mathbf{x}) \to h(\mathbf{x}) + A_\alpha x_\alpha + B \ , \\ & u_\alpha(\mathbf{x}) \to u_\alpha(\mathbf{x}) - A_\alpha h(\mathbf{x}) - \frac{1}{2} A_\alpha A_\beta x_\beta + B'_\alpha \ , \\ & \bar{h}(\mathbf{x}) \to \bar{h}(\mathbf{x}) \ , \qquad \bar{u}_\alpha \to \bar{u}_\alpha - l A_\alpha \ , \end{aligned} \quad (6.24)$$

for arbitrary A_α, B, B'_α. As in Eq. (6.5), transformations with $A_\alpha \neq 0$ represent linearized versions of rotations in three-dimensional space.

6.1.3 *Effective theory for flexural fluctuations*

Starting from the Gibbs probability distribution

$$P[h(\mathbf{x}), u_\alpha(\mathbf{x}), \bar{h}(\mathbf{x}), \bar{u}_\alpha(\mathbf{x})] = \frac{1}{Z}\mathrm{e}^{-\tilde{H}/T} \tag{6.25}$$

for fluctuations of the displacement fields $h(\mathbf{x})$, $u_\alpha(\mathbf{x})$, $\bar{h}(\mathbf{x})$, $\bar{u}_\alpha(\mathbf{x})$, we proceed to construct an effective theory describing the statistical properties of the flexural fluctuations $h(\mathbf{x})$ only, by systematically integrating out the remaining degrees of freedom. In Eq. (6.25), the Hamiltonian $\tilde{H}$ is assumed to be the approximate configuration energy of Eq. (6.23) and the normalization Z is given by the partition function

$$Z = \int [\mathrm{d}h\mathrm{d}u_\alpha \mathrm{d}\bar{h}\mathrm{d}\bar{u}_\alpha]\mathrm{e}^{-\tilde{H}[h,u_\alpha,\bar{h},\bar{u}_\alpha]/T} \ . \tag{6.26}$$

By explicit integration over relative fluctuations $\bar{h}$ and $\bar{u}_\alpha$, the effective Hamiltonian for fluctuations of u_α and h fields,

$$\tilde{H}'_{\mathrm{eff}}[h(\mathbf{x}), u_\alpha(\mathbf{x})] = -T \ln \left\{ \int [\mathrm{d}\bar{h}\mathrm{d}\bar{u}_\alpha]\mathrm{e}^{-\tilde{H}[h,u_\alpha,\bar{h},\bar{u}_\alpha]/T} \right\} , \tag{6.27}$$

is calculated as

$$\begin{aligned} \tilde{H}'_{\mathrm{eff}} = \int_{\mathbf{q}} \Big[& \frac{1}{2}\kappa_0(q) q^4 |h(\mathbf{q})|^2 + \frac{1}{2}\lambda_0(q)|u_{\alpha\alpha}(\mathbf{q})|^2 \\ & + \mu_0(q)|u_{\alpha\beta}(\mathbf{q})|^2 + \frac{g_4^2 l^2}{16 g_2^2}(\lambda+\mu) d_L(q) d_T(q) |A(\mathbf{q})|^2 \\ & - \frac{g_4 l^2}{4 g_2}(\lambda + 2\mu) d_L(q) q^2 h(\mathbf{q}) A^*(\mathbf{q}) \Big] \ . \end{aligned} \tag{6.28}$$

Details of the calculation are presented in appendix 6.A. In Eq. (6.28), $h(\mathbf{q})$ and $u_{\alpha\beta}(\mathbf{q})$ are Fourier components of $h(\mathbf{x})$ and $u_{\alpha\beta}(\mathbf{x})$, $A(\mathbf{q})$ is the Fourier transform of the anisotropic D_{3d}-invariant field

$$A(\mathbf{x}) = \partial_x u_{xx} - \partial_x u_{yy} - 2\partial_y u_{xy} \ , \tag{6.29}$$

$\int_{\mathbf{q}} = \int \mathrm{d}^2 q/(2\pi)^2$ denotes momentum integration, and $|u_{\alpha\beta}(\mathbf{q})|^2 = u_{\alpha\beta}(\mathbf{q}) u^*_{\alpha\beta}(\mathbf{q})$. Furthermore, we introduced the dimensionless functions

$$\begin{gathered} d_L(q) = \left[1 + \frac{(\lambda+2\mu) l^2 q^2}{2 g_2}\right]^{-1} , \qquad d_T(q) = \left[1 + \frac{\mu l^2 q^2}{2 g_2}\right]^{-1} , \\ \bar{d}(q) = \left[1 + \frac{\kappa l^2 q^4}{2 g_1}\right]^{-1} , \end{gathered} \tag{6.30}$$

and defined

$$\kappa_0(q) = 2\kappa + \frac{(\lambda+2\mu)l^2}{2} d_L(q) \ , \qquad \mu_0(q) = 2\mu - \frac{g_4^2}{4g_2} d_T(q) \ ,$$
$$\lambda_0(q) = 2\lambda - \frac{g_3^2}{4g_1}\bar{d}(q) + \frac{g_4^2}{4g_2} d_T(q) \ . \tag{6.31}$$

In the first three terms of Eq. (6.28) we recognize a Hamiltonian identical in form to the standard effective theory of crystalline membranes, Eq. (6.4), but with a q-dependent bending rigidity $\kappa_0(q)$ and Lamé coefficients $\lambda_0(q)$ and $\mu_0(q)$. The additional interaction involving $|A(\mathbf{q})|^2$ is a quadratic functional of the strain tensor and represents an anisotropic stiffness associated with gradients of the strain. Finally, the term proportional to $q^2 h(\mathbf{q}) A^*(\mathbf{q})$ introduces a coupling between the component $A(\mathbf{x})$ of the gradient of strain and the local curvature $\partial^2 h(\mathbf{x})$. In the following these last two interactions are neglected for simplicity.

The neglection of the first of these two terms is related to the assumption that the response of the bilayer to space-dependent strain is dominated by the sum of the stiffnesses of the two isolated layers at the scales of interest. With the same assumption, we approximate

$$\lambda_0(q) \simeq \lambda_0 = 2\lambda \ , \qquad \mu_0(q) \simeq \mu_0 = 2\mu \ , \tag{6.32}$$

neglecting the q-dependent contributions in Eq. (6.31). An estimate from the identification $g_3 = 2c_{13}l$, the experimental value $c_{13} = (0 \pm 3)$GPa for graphite [211, 212], and the parameters $l \simeq 3.25$Å, $g_1 \simeq 0.8$ eVÅ^{-2} (see Sec. 6.2) shows that the correction $-g_3^2/(4g_1)\bar{d}(q)$ is much smaller than 2λ and 2μ for any wavevector, which supports this approximation[6]. We assume that also terms $g_4^2/(4g_2)d_T(q)$ play a minor role.

With these approximations, we are lead to consider the effective Hamiltonian

$$\tilde{H}''_{\text{eff}} = \frac{1}{2}\int_{\mathbf{q}} \left[\kappa_0(q) q^4 |h(\mathbf{q})|^2 + \lambda_0 |u_{\alpha\alpha}(\mathbf{q})|^2 + 2\mu_0 |u_{\alpha\beta}(\mathbf{q})|^2\right] \ , \tag{6.33}$$

which is identical in form to the standard effective theory of crystalline membranes, Eq. (6.4), although the bending rigidity κ is replaced by the q-dependent $\kappa_0(q)$. The remaining integration over in-plane fields, therefore, proceeds in an usual way [1, 6, 12, 23, 25, 85] (see appendix 6.A). The resulting effective Hamiltonian for the flexural field $h(\mathbf{x})$ reads

$$\tilde{H}_{\text{eff}} = \frac{1}{2}\int_{\mathbf{q}} \kappa_0(q) q^4 |h(\mathbf{q})|^2 + \frac{1}{2}\int'_{\mathbf{q}} Y_0 \left|\frac{K(\mathbf{q})}{q^2}\right|^2 \ , \tag{6.34}$$

6 We note, however, that in Ref. [169] a perturbation analogue to a finite g_3 was identified as potentially important within the framework of three-dimensional continuum theories of stacks of membranes.

where

$$Y_0 = \frac{4\mu_0(\lambda_0+\mu_0)}{\lambda_0+2\mu_0} \tag{6.35}$$

and $K(\mathbf{q})$ is the Fourier transform of the composite field

$$K(\mathbf{x}) = -\frac{1}{2}(\delta_{\alpha\beta}\partial^2 - \partial_\alpha\partial_\beta)(\partial_\alpha h\partial_\beta h) = \frac{1}{2}\big[(\partial^2 h)^2 - (\partial_\alpha\partial_\beta h)(\partial_\alpha\partial_\beta h)\big] \ , \tag{6.36}$$

and the primed integral $\int'_{\mathbf{q}}$ is meant to run over the non-zero wavevector components, with the $\mathbf{q}=0$ contribution excluded [1, 12].

At leading order for small deformations, $K(\mathbf{x})$ coincides with the Gaussian curvature, Eq. (6.13), and Eq. (6.34) thus expresses a long-range curvature-curvature interaction. Physically, this nonlinearity encodes a frustration of out-of-plane fluctuations due to the elastic stiffness of the layer [1, 6]. Given an out-of-plane displacement field $h(\mathbf{x})$, it is not possible, in general, to choose the two displacement fields $u_x(\mathbf{x})$ and $u_y(\mathbf{x})$ in such way that the three components of the strain tensor $u_{xx}(\mathbf{x})$, $u_{yy}(\mathbf{x})$, $u_{xy}(\mathbf{x})$ vanish at all points. As Eq. (6.34) shows, regions with a finite Gaussian curvature inevitably induce a strain of order $\mathrm{O}(h^2)$ in the lattice, and involve an energy cost controlled by the elastic moduli [1, 6].

To conclude, we briefly discuss the neglected term proportional to

$$\int_{\mathbf{q}} d_L(q) q^2 h(\mathbf{q}) A^*(\mathbf{q}) \ . \tag{6.37}$$

After integration over in-plane fields, this term generates an anisotropic contribution to the q-dependent rigidity $\kappa_0(q)$ of the form

$$\delta\kappa_0(\mathbf{q}) = -\frac{g_4^2 l^4}{32 g_2^2}\frac{(\lambda+2\mu)^2}{\mu} d_L^2(q)\left[1 - \frac{\lambda+\mu}{\lambda+2\mu}\cos^2(3\theta)\right] q^2 \ , \tag{6.38}$$

where $\cos\theta = q_x/|\mathbf{q}|$. This contribution vanishes for $q\to 0$ and it is maximal for $q^2 \approx 2g_2/((\lambda+2\mu)l^2)$, where it is of the order of $g_4^2 l^2/(32 g_2)$. In addition, the term (6.37) generates a non-local interaction

$$i\frac{(\lambda+\mu)g_4 l^2}{2g_2}\int'_{\mathbf{q}} d_L(q) q_x (q_x^2 - 3q_y^2) h(\mathbf{q}) \frac{K^*(\mathbf{q})}{q^2} \ , \tag{6.39}$$

which couples the curvature tensor $\partial_\alpha\partial_\beta h$ to the approximate Gaussian curvature $K(\mathbf{x})$. Considerations of these effects is beyond the scope of this work. It is expected that the term (6.37) does not modify the exponent of the scaling behavior.

6.2 MODEL PARAMETERS FOR AB-STACKED BILAYER GRAPHENE

As discussed above, the bending rigidity κ and the Lamé coefficients λ and μ are approximated by their values for monolayer graphene, which is justified by the

weakness of van der Waals interactions in comparison with in-plane bonding. In the case of the in-plane Young modulus Y this approximation is consistent with experimental values illustrated in Ref. [195], which indicate for bilayer graphene a value of Y approximately equal to twice the corresponding monolayer modulus.

The elastic moduli and the bending stiffness of a monolayer graphene have been investigated extensively (see e.g. [195, 200, 213, 214]). Theoretical predictions and estimates of κ lead to values between 0.69 eV and approximately 2.4 eV [213–215].

By comparing results of atomistic Monte Carlo simulations and continuum membrane theory, the bare bending rigidity κ was predicted to present a significant temperature dependence [61]. This was attributed to anharmonic interactions between acoustic modes and other phonon branches, or, more generally, with degrees of freedom not captured by the membrane model. In Ref. [193], a similar result was obtained for bilayer graphene. In addition, by a similar fitting method Ref. [193] determined temperature-dependences of the interlayer compression modulus, analogue to g_1 in Eq. (6.23).

In the following, we neglect these temperature dependences and, similarly, effects of thermal expansion on the lattice constant a and the interlayer distance l. In further calculations, we adopt the values $\lambda \simeq 3.8$ eV Å^{-2} and $\mu \simeq 9.3$ eV Å^{-2}, which we deduced from the first-principle results of Ref. [111], and assume $\kappa = 1$ eV [31, 112].

To determine interlayer coupling parameters g_1 and g_2, we have performed density functional theory (DFT) calculations on AB-stacked bilayer graphene (see Figs. 6.1a and 6.1b). We use the plane-wave based code PWscf as implemented in the Quantum-Espresso *ab-initio* package [216]. A vacuum layer of more than 15 Å has been added in order to avoid perpendicular interaction between neighbouring cells. The quasi-Newton algorithm for ion relaxation is applied until the components of all forces are smaller than 10^{-5} Ry/bohr. The interlayer distance l and the lattice parameter a obtained after relaxation are shown in Table 6.1. For the self consistent calculations, we use a $36 \times 36 \times 1$ grid. The kinetic energy cutoff is set to 100 Ry. Projector augmented wave (PAW) pseudopotentials within the Perdew-Burke-Ernzerhoff (PBE) approximation [217] for the exchange-correlation functional are used for the C atoms. Van der Waals dipolar corrections are introduced during relaxation through the Grimme-D2 model [218].

To calculate the interlayer shear modulus g_2 and the out-of-plane compression modulus g_1, we apply deformations as shown in Fig. 6.2(a) and 6.2(b) respectively to the bilayer graphene unit cell. For simplicity, a frozen-ion approximation is assumed: during deformation, all atoms are displaced rigidly without allowing for a relaxation of the internal structure of the unit cell. After application of a sequence

	a	l	g_1	g_2	c_{33}	c_{44}
Bilayer	2.46	3.2515	0.80	0.11	-	-
Graphite	2.45	3.42±0.01	0.62(0.90)	0.096(0.10)	29(42)	4.5(4.8)

Table 6.1: Parameters for bilayer graphene obtained from first-principle calculations, compared with the elastic constants of AB-stacking graphite reported in Ref. [211]. In the elastic moduli of graphite, results in brackets were calculated considering van der Waals corrections [211]. The lattice constant a and interlayer distance l are expressed in Å, the couplings g_1 and g_2 in eV Å^{-2}, and the elastic moduli c_{33}, c_{44} in GPa. In the case of graphite, the values of g_1 and g_2 in the table are defined by the identifications $g_1 \equiv c_{33}l$, $g_2 \equiv c_{44}l$, where l is the graphite interlayer distance.

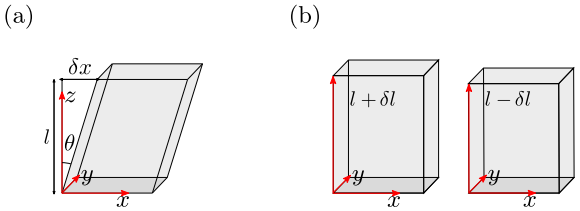

Figure 6.2: Scheme of (a) shear and (b) out-of-plane strains.

of relative shifts δx between carbon layers and variations δl of the layer-to-layer distance, the total energy per unit area E/A is fitted as:

$$\frac{E}{A} = \frac{E_0}{A} + \frac{g_1}{2}\frac{\delta l^2}{l^2} , \tag{6.40}$$

$$\frac{E}{A} = \frac{E_0}{A} + \frac{g_2}{2}\frac{\delta x^2}{l^2} . \tag{6.41}$$

The resulting values for g_1 and g_2 are illustrated in Table 6.1.

It is natural to compare the values of g_1 and g_2 with corresponding three-dimensional elastic moduli in graphite. A stack of membranes with interactions of the form (6.23) between nearest-neighbouring layers and vanishing interactions between non-neighbouring layers exhibits three-dimensional elastic moduli $c_{33} = g_1/l$ and $c_{44} = g_2/l$, where c_{33} and c_{44} are defined according to the Voigt notation:

$$\frac{E}{V} = \frac{1}{2}\sum_{i,j} c_{ij}\epsilon_i\epsilon_j ,$$
$$u_{\alpha\beta} = \begin{bmatrix} u_{xx} & u_{xy} & u_{xz} \\ u_{yx} & u_{yy} & u_{yz} \\ u_{zx} & u_{zy} & u_{zz} \end{bmatrix} = \begin{bmatrix} \epsilon_1 & \frac{\epsilon_6}{2} & \frac{\epsilon_5}{2} \\ \frac{\epsilon_6}{2} & \epsilon_2 & \frac{\epsilon_4}{2} \\ \frac{\epsilon_5}{2} & \frac{\epsilon_4}{2} & \epsilon_3 \end{bmatrix} , \tag{6.42}$$

where E/V is the energy density of the three-dimensional solid under uniform strain. In Table 6.1, our results for bilayer graphene are compared with *ab-initio*

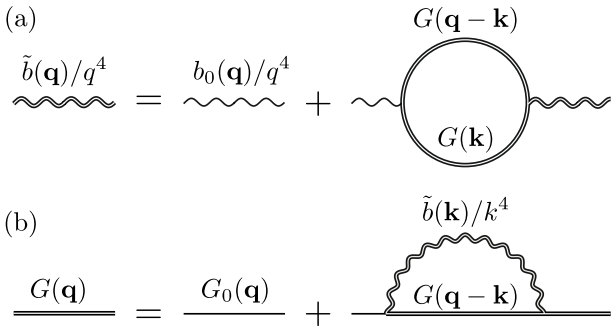

Figure 6.3: Graphical representation of the self-consistent screening approximation.

calculations for ideal AB-stacking graphite reported in Ref. [211]. The comparison indicates that values of g_1 and g_2 calculated in this work are of the same order of the corresponding graphite stiffnesses. We note, however, that the exact value of the shear modulus in multilayer graphene is still far from being understood. Reported values for the interlayer shear modulus exhibit a large dispersion (see e.g. [195, 202]). Raman measurements give values of the order of 4-5 GPa, while direct measurements using mechanical approaches give values of 0.36-0.49 GPa, increasing with the number of layers. This big discrepancy calls for a better understanding of interlayer dipolar or van der Waals interactions in layered materials, which is beyond the scope of this work. Experimental values of the interlayer shear modulus in graphite also exhibit a large scatter [195].

6.3 SELF-CONSISTENT SCREENING APPROXIMATION

Equilibrium correlation functions of the flexural field $h(\mathbf{x})$ at a temperature T can be calculated by functional integration from the effective Hamiltonian $\tilde{H}_{\text{eff}}$, Eq. (6.34). In this work, the two-point correlation function $G(\mathbf{q}) = \langle |h(\mathbf{q})|^2 \rangle$ is calculated within the self-consistent screening approximation [23–25].

In the considered model for bilayer graphene, the problem differs from conventional membrane theory only by the q-dependence of $\kappa_0(q)$. Therefore, SCSA equations can be written in a standard way [25], by adapting the conventional equations with the replacements $\kappa \to \kappa_0(q)$, $Y \to Y_0$.

The SCSA is defined diagrammatically in Fig. 6.3: by neglection of vertex corrections, Dyson equations are truncated to a closed set of integral equations for $G(\mathbf{q})$ and a screened-interaction propagator $D(\mathbf{q})$. For physical two-dimensional membranes in three-dimensional space, SCSA equations read [25]:

$$G^{-1}(\mathbf{q}) = G_0^{-1}(\mathbf{q}) + \Sigma(\mathbf{q}) \ , \qquad \tilde{b}^{-1}(\mathbf{q}) = b_0^{-1}(\mathbf{q}) + 3I(\mathbf{q}) \ , \tag{6.43}$$

where the self-energy $\Sigma(\mathbf{q})$ and the polarization bubble $I(\mathbf{q})$ are, respectively:

$$\Sigma(\mathbf{q}) = 2\int_{\mathbf{k}} \left[q^2k^2 - (\mathbf{q}\cdot\mathbf{k})^2\right]^2 \frac{\tilde{b}(\mathbf{k})}{k^4} G(\mathbf{q}-\mathbf{k}) \tag{6.44}$$

and

$$I(\mathbf{q}) = \frac{1}{3q^4}\int_{\mathbf{k}} \left[q^2k^2 - (\mathbf{q}\cdot\mathbf{k})^2\right]^2 G(\mathbf{q}-\mathbf{k})G(\mathbf{k}) \ . \tag{6.45}$$

For membranes described by Eq. (6.4), the zero-order propagators are

$$G_0^{-1}(\mathbf{q}) = \frac{\kappa q^4}{T} \ , \qquad b_0(\mathbf{q}) = \frac{Y}{2T} \ . \tag{6.46}$$

For bilayer graphene, after the approximations $\lambda_0(q) \simeq 2\lambda$ and $\mu_0(q) \simeq 2\mu$ (see Sec. 6.1.3), the zero-order flexural-field and interaction propagators for bilayer graphene read

$$G_0^{-1}(\mathbf{q}) = \frac{\kappa_0(q) q^4}{T} \ , \qquad b_0(\mathbf{q}) = \frac{Y_0}{2T} \ , \tag{6.47}$$

where, as in Eq. (6.31),

$$\kappa_0(q) = 2\kappa + \frac{(\lambda+2\mu)l^2}{2}\left[1 + \frac{(\lambda+2\mu)l^2q^2}{2g_2}\right]^{-1} \ . \tag{6.48}$$

In the long-wavelength limit, identification of power-law solutions of SCSA equations within the strong-coupling assumption $\Sigma(\mathbf{q}) \gg G_0^{-1}(\mathbf{q})$, $I(\mathbf{q}) \gg b_0^{-1}(\mathbf{q})$ yields analytical equations for the universal exponent η. After generalization to a theory of D-dimensional membranes embedded in a $(D+d_c)$-dimensional ambient space, the SCSA exponent $\eta(D,d_c)$ is exact to first order in $\varepsilon = 4-D$, to leading order in a $1/d_c$-expansion and for $d_c = 0$ [23, 25]. For the physical case $D=2$, $d_c=1$, the SCSA exponent $\eta = 4/(1+\sqrt{15}) \simeq 0.821$, shows a good agreement with complementary approaches such as numerical simulations and the nonperturbative renormalization group [26]. As compared with the SCSA, a second-order generalization which includes dressed diagrams with the topology of $\mathrm{O}(1/d_c^2)$ graphs in a large-d_c expansion, leads to quantitatively small corrections to universal quantities for $D=2$, $d_c=1$ [24], which supports the accuracy of the method. Recently, SCSA predictions have been compared with exact analytical calculations of η in second-order large-d_c [22] and ε-expansions [19, 183]. In Ref. [183], it was shown that the SCSA equations are exact at $\mathrm{O}(\varepsilon^2)$ within a non-standard dimensional continuation of the theory to arbitrary D. A more general two-loop theory was developed in Ref. [19], where a larger space of theories was considered. For models equivalent to the conventional dimensionally-continued membrane theory, the $\mathrm{O}(\varepsilon^2)$ was shown to deviate from the SCSA prediction.

In order to determine correlation functions at an arbitrary wavevector q, we solve SCSA equations numerically by an iterative algorithm. Starting from non-interacting propagators $G(\mathbf{q}) = G_0(\mathbf{q})$, $\tilde{b}(\mathbf{q}) = b_0(\mathbf{q})$, Eqs. (6.45) and (6.43) are used to determine the zero-order polarization bubble $I(\mathbf{q})$ and the first approximation to the screened interaction $\tilde{b}_1(\mathbf{q})$. The self-energy diagram in Fig. 6.3b is then calculated as a loop integral of $\tilde{b}_1(\mathbf{q})$ and $G_0(\mathbf{q})$, leading to a dressed Green's function $G_1(\mathbf{q})$. Iteration of the process generates a sequence of screened functions and dressed propagators

$$\begin{aligned} G_{n+1}^{-1}(\mathbf{q}) &= G_0^{-1}(\mathbf{q}) + \Sigma_n(\mathbf{q}) \ , \\ \tilde{b}_{n+1}^{-1}(\mathbf{q}) &= b_0^{-1}(\mathbf{q}) + 3I_n(\mathbf{q}) \ , \\ \Sigma_n(\mathbf{q}) &= 2\int_{\mathbf{k}} \left[q^2k^2 - (\mathbf{q}\cdot\mathbf{k})^2\right]^2 \frac{\tilde{b}_{n+1}(\mathbf{k})}{k^4} G_n(\mathbf{q}-\mathbf{k}) \ , \\ I_n(\mathbf{q}) &= \frac{1}{3q^4}\int_{\mathbf{k}} \left[q^2k^2 - (\mathbf{q}\cdot\mathbf{k})^2\right]^2 G_n(\mathbf{q}-\mathbf{k})G_n(\mathbf{k}) \ , \end{aligned} \tag{6.49}$$

which, after convergence, approach solutions to the SCSA equations. At each step in the iteration process, correlation functions are calculated on a grid of 50 wavevector points, evenly spaced in logarithmic scale and ranging between 10^{-7}Å^{-1} and 110Å^{-1}. Calculations with grids of 26 and 29 points are also performed to estimate the numerical accuracy (see appendix 6.B).

Twenty-five steps of the iteration algorithm are illustrated in Fig. 6.4. In order to calculate loop integrals, at each iteration $G(\mathbf{q})$ and $\tilde{b}(\mathbf{q})$ are interpolated by cubic splines[7] in logarithmic scale: $G(\mathbf{q})$ and $\tilde{b}(\mathbf{q})$ are interpolated as $G_n(\mathbf{q}) = A_1 \exp[f_1(\ln(q/B))]$, $\tilde{b}_n(\mathbf{q}) = A_2 \exp[f_2(\ln(q/B))]$, where f_1 and f_2 are cubic splines and A_1, A_2, B are constants. In the region $q < 10^{-7}\text{Å}^{-1}$, which is not covered by the wavevector grid, functions are extrapolated as pure power laws, $G_n \propto q^{-\eta(n)}$ and $\tilde{b}_n \propto q^{\eta_u(n)}$ with exponents and amplitudes matching the first two points in the grid.

In the calculation of integrals, we split two-dimensional wavevector integration into a sequence of one-dimensional integrals over k_y and k_x, the components of $\mathbf{k}$ respectively transverse and longitudinal to the external wavevector $\mathbf{q}$. In the computation, we use an adaptive algorithm for single-variable integration[8], and include k_y-integration in the function called by the outer k_x integral. Inner and outer integrals are evaluated within a relative accuracy 1.49×10^{-8} and 10^{-7} respectively.

7 Numerical interpolations were performed by the functions scipy.interpolate.PchipInterpolator, which implements a piecewise-cubic Hermite interpolating polynomial algorithm. For numerical integration we used the adaptive integration method implemented in scipy.integrate.quad. Both functions are distributed in the Scipy library (version 0.19.1).

8 See footnote 7.

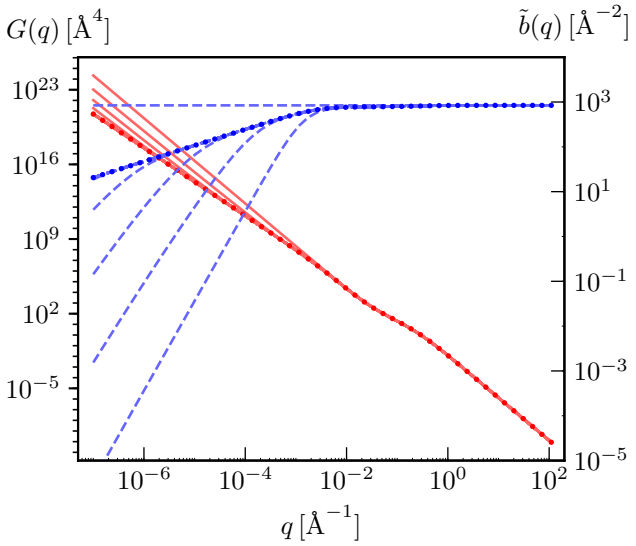

Figure 6.4: Sequence of correlation functions (red solid lines) and screened interactions (blue dashed lines) obtained by 25 iterations of the convergence algorithm. Data in the graph refer to a bilayer membrane with the parameters $\lambda = 3.8$ eV Å^{-2}, $\mu = 9.3$ eV Å^{-2}, $\kappa = 1$ eV, $l = 3.2515$ Å, $g_2 = 0.11$ eV Å^{-2} and $T = 300$ K. Correlation functions evaluated at the last iteration on the 50-point grid are shown by dots.

Although the self-energy and polarization bubble are convergent, a hard ultraviolet cutoff $\Lambda = 100\text{Å}^{-1}$ is imposed in explicit calculations. To estimate the numerical error due to the finite UV cutoff, we compared data sets calculated with $\Lambda = 100\text{Å}^{-1}$ and $\Lambda = 1000\text{Å}^{-1}$, which were obtained by calculating numerical solutions on wavevector grids consisting of 26 and 29 points respectively. Upon this change in UV cutoff, data sets for $G(q)$ and $\tilde{b}(q)$ deviate by less than 10^{-5} (see appendix 6.B).

In the numerical calculations, difficulties stem from the rapid variation of functions in regions of much smaller size than the integration domain and from the slow decay of integration tails at large k. To address these problems, integrals are performed piecewise. Specifically, the k_y integration domain is splitted into contiguous intervals with extrema $\{0, 10^{-1}q_1, q_1, 10q_1, q_2, 10q_2, 10^2q_2, 10^3q_2\}$, where $q_1 = \sqrt{q|\mathbf{q}-\mathbf{k}|}$ and $q_2 = \max[q, |\mathbf{q}-\mathbf{k}|]$. For any q and k_x and at any steps in the iteration process, characteristic scales q_1 and q_2 define roughly the width in k_y integration which contributes mostly to the integral value. The piecewise calculation defined above is then able to capture a small-scale peak in the integrand function and a long tail for $k_y \gg q_2$. In the subsequent k_x integrations, similarly, subintervals are chosen as $\{.., -10q, -q, 0, q, 10q, 10^2q..\}$.

After 25 iteration of the algorithm, the values of $G_n(\mathbf{q})$ and $\tilde{b}_n(\mathbf{q})$ at the grid of sampled wavevector points converge within a relative deviation smaller than 10^{-10}. The final results (see Sec. 6.4) reproduce the analytically-known SCSA exponent and amplitude ratio [23–25] closely: an estimate of the exponents η, η_u and the amplitudes z_1, z_2 of the scaling behavior

$$G^{-1}(\mathbf{q}) = z_1 q^{4-\eta} \ , \qquad \tilde{b}(\mathbf{q}) = z_2 q^{\eta_u} \ , \tag{6.50}$$

from the first two points of the wavevector grid gives values in the range $\eta = 0.8208515 \div 0.8208524$, $\eta_u = 0.35829478 \div 0.35829524$, and $z_1^2/z_2 = 0.1781321 \div 0.1781381$ for considered data sets for monolayer graphene at $T = 300$ K and bilayer graphene at different temperatures between 10 and 1500 K. These results are in close agreement with the analytical predictions $\eta = 4/(1+\sqrt{15}) \simeq 0.82085238$, $\eta_u = 2 - 2\eta \simeq 0.35829523$, and [24, 25]

$$\frac{z_1^2}{z_2} = \frac{3}{16\pi} \frac{\Gamma^2(1+\eta/2)\Gamma(1-\eta)}{\Gamma^2(2-\eta/2)\Gamma(2+\eta)} \simeq 0.17813212... \tag{6.51}$$

The individual amplitudes z_1 and z_2 and the crosssover behaviors at finite q are more sensitive to numerical error. A limitation to numerical accuracy derives from the need to interpolate $G(q)$ and $\tilde{b}(q)$ from a discrete set of data points. To estimate the order of the corresponding error, the numerical solution of SCSA equations was repeated after reduction to a broder grid, consisting of 26 wavevector points. Compared to data evaluated with the 50 q-point grid, interpolating functions exhibit a maximum relative deviation of the order of 2% in all considered sets of

data (see appendix 6.B for a more detailed analysis). The amplitudes z_1 and z_2 of the long-wavelength scaling regime exhibit a smaller discrepancy, of the order of 10^{-3}, upon change from the finer to the broader wavevector grid.

Numerical results indicate that the numerical values of the exponent and the amplitude ratio z_1^2/z_2 are much more accurate than the numerical precision in calculations of non-universal properties such as the amplitude and finite-wavelength dependences of $G(q)$ and $\tilde{b}(q)$. Qualitatively, universal properties are only sensitive to the region of small momenta, where $G(q)$ and $\tilde{b}(q)$ approach pure powers and the precision of numerical interpolation improves significantly.

6.4 RESULTS

The numerical algorithm described in Sec. 6.3 was used to determine solutions to the SCSA equations for graphene monolayer and bilayers at temperatures $T = 10$, 300, and 1500 K. Results are illustrated in Figs. 6.5, 6.6, 6.7, and 6.8, while numerical data are reported in appendix 6.B.

All reported results are derived within the framework of continuum models discussed in Sec. 6.1, which do not capture the effects of discreteness of the lattice. Figs. 6.5–6.8 illustrate correlation functions in the full wavevector range employed for the numerical calculation of the continuum-limit solution, $10^{-7}\text{Å}^{-1} < q < 10^{2}\text{Å}^{-1}$, although, on the lattice, only degrees of freedom with $q \lesssim 1\text{Å}^{-1}$ are physical.

The renormalized bending rigidity $\tilde{\kappa}(q) \equiv TG^{-1}(q)/q^4$, and the renormalized elastic modulus $\tilde{b}(q)$ [23, 25] for single-layer graphene at room temperature are illustrated by blue dashed lines in Fig. 6.5. As it is completely general within the framework of the elasticity model, Eq. (6.4), interaction effects are weak for $q \gtrsim q_*$, where $q_* = \sqrt{3TY/(16\pi\kappa^2)}$ [25, 61]. In the limit $q \gg q_*$, $\tilde{b}(q)$ and $\tilde{\kappa}(q)$ approach their bare values $Y/(2T)$ and κ, with negligible renormalizations. In constrast, for $q \lesssim q_*$ a strong coupling regime sets in. For $q \ll q_*$ the self-energy $\Sigma(q)$ and the polarization function $I(q)$ are much larger than the harmonic propagators $G_0^{-1}(q)$ and $b_0^{-1}(q)$; correlation functions scale as power laws [23–25]:

$$G^{-1}(\mathbf{q}) = z_1 q^{4-\eta} , \qquad \tilde{b}(\mathbf{q}) = z_2 q^{\eta_u} . \tag{6.52}$$

As mentioned above, numerical results are in close agreement with the scaling relation $\eta_u = 2 - 2\eta$, and the predictions, exact within SCSA, $\eta = 4/(1 + \sqrt{15})$ and $z_1^2/z_2 \simeq 0.17813212$ [23–25].

By a simple rescaling, the numerical solution obtained for monolayer graphene can be adapted to any membrane described by the elasticity model, Eq. (6.4). For any such membrane, the statistics of out-of-plane fluctuations is governed by a

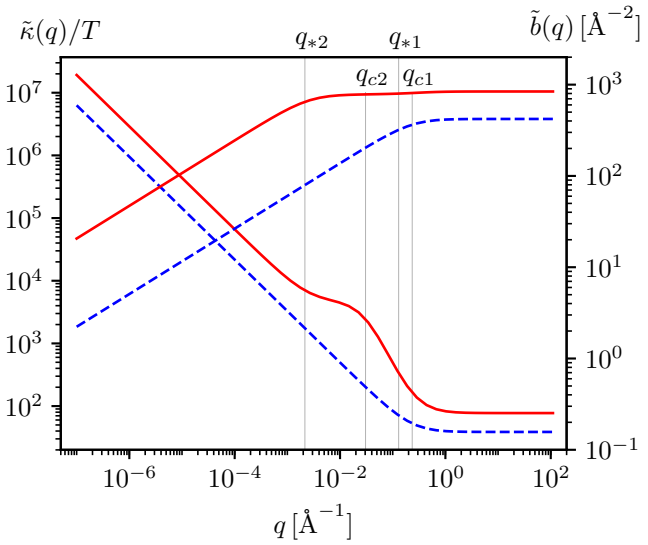

Figure 6.5: Renormalized bending rigidity $\tilde{\kappa}(q) = TG^{-1}(q)/q^4$ and renormalized elastic coefficient $\tilde{b}(q)$ for continuum models of monolayer (blue dashed lines) and bilayer graphene (red solid lines) at $T = 300$ K. For $q \to 0$, $\tilde{\kappa}(q)$ diverges for both curves as $q^{-\eta}$ and $\tilde{b}(q)$ approaches 0 as $q^{2-2\eta}$.

Hamiltonian of the form (6.34) with a wavevector-independent rigidity $\kappa_0(q) = \kappa$ and Young modulus $Y_0(q) = Y$. A scaling analysis then shows that

$$G(\mathbf{q}) = \frac{T}{\kappa q^4} g\left(\frac{q}{q_*}\right) \tag{6.53}$$

and

$$\tilde{b}(\mathbf{q}) = b_0 f\left(\frac{q}{q_*}\right) = \frac{Y}{2T} f\left(\frac{q}{q_*}\right) \ , \tag{6.54}$$

where $g(x)$ and $f(x)$ are independent of temperature and elastic parameters. In particular, the coefficient z_1 governing the amplitude of the scaling behavior has the form [219]

$$z_1 = \bar{z}_1 \frac{\kappa q_*^\eta}{T} \ , \tag{6.55}$$

where $\bar{z}_1$ is independent of T, κ, and Y. An estimate from the amplitude of G in monolayer graphene gives $\bar{z}_1 \simeq 1.177$ within SCSA. In the following, the scaling-analysis relations (6.53) and (6.54) are used to convert numerical data collected for monolayer graphene at $T = 300$ K to single membranes with arbitrary elastic parameters and temperature.

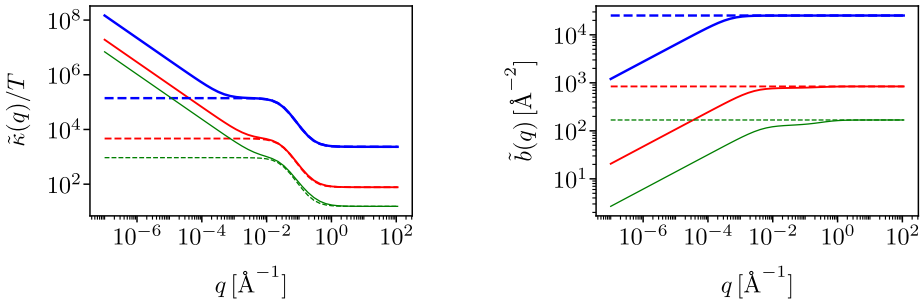

Figure 6.6: (a) Renormalized bending rigidity and (b) renormalized elastic modulus for bilayer graphene at $T = 10$ K (thick blue lines), 300 K (intermediate red lines), and 1500 K (thin green lines). Dashed lines illustrate the corresponding functions in the harmonic approximation.

As Figs. 6.5, 6.6 and 6.7 show, correlation functions in bilayer graphene exhibit a more intricate crossover behavior which extends from microscopic to mesoscopic scales. In contrast with the monolayer elasticity theory, the behavior of a bilayer is controlled by several length scales. The effective bare bending rigidity $\kappa_0(q)$, Eq. (6.48), approaches limiting values 2κ and $\bar{\kappa}_0 = 2\kappa + (\lambda + 2\mu)l^2/2$ for $q \gtrsim q_{1c}$ and for $q \lesssim q_{2c}$ respectively, where

$$q_{1c} = \sqrt{\frac{g_2}{2\kappa}} \simeq 0.2\text{Å}^{-1} \tag{6.56}$$

and

$$q_{2c} = \frac{1}{l}\sqrt{\frac{2g_2}{\lambda + 2\mu}} \simeq 3 \times 10^{-2}\text{Å}^{-1} \,. \tag{6.57}$$

A crossover in the mechanical behavior [188] takes place between these two scales: $q_{2c} < q < q_{1c}$. The strong q-dependence of $\kappa_0(q)$ has a crucial impact on the harmonic correlation functions. The effective rigidity $\tilde{\kappa}(q) = TG^{-1}(q)/q^4$ and elastic coefficient $\tilde{b}(q) = b_0$ in the harmonic approximation, which coincide with their bare value $\kappa_0(q)$ and $b_0(q) = b_0$, are illustrated by dashed lines in Fig. 6.6 and by grey dotted lines in Fig. 6.7.

At finite temperatures, for a single membrane, crossover from weak to strong coupling is marked by the Ginzburg scale $q_* = \sqrt{3TY/(16\pi\kappa^2)}$. In the case of bilayer graphene, two scales analogue to q_* can be anticipated:

$$q_{1*} = \sqrt{\frac{3T}{16\pi}\frac{(2Y)}{(2\kappa)^2}} = \frac{q_*}{\sqrt{2}} \tag{6.58}$$

and

$$q_{2*} = \sqrt{\frac{3T}{16\pi}\frac{(2Y)}{\bar{\kappa}_0^2}} \ . \tag{6.59}$$

While q_{1*} is close to the Ginzburg scale for a monolayer graphene, q_{2*} is smaller by two orders of magnitude due to the strong enhancement of $\bar{\kappa}_0 \gg 2\kappa$.

The inverse lattice spacing $1/a \simeq 1\text{Å}^{-1}$ defines a further scale for fluctuations of the atomic crystal, which marks a limit of validity for the continuum model employed here.

In order to study the interplay and overlap between these crossover effects, we analyzed fluctuations in bilayer graphene at temperatures $T = 10$, 300, and 1500 K. For small temperatures, the mechanical and the weak-strong coupling crossovers are disentangled. At $T = 10$ K both $q_{2*} \simeq 4 \times 10^{-4}\text{Å}^{-1}$ and $q_{1*} \simeq 2 \times 10^{-2}\text{Å}^{-1}$ are smaller than q_{1c}, and furthermore $q_{2*} \ll q_{2c}$. As it is confirmed by the numerical results, throughout the region $q_{2c} < q < q_{1c}$ thermal effects are negligible. Strong coupling behavior sets in only at $q < q_{2*} < q_{2c}$, a region where $\kappa_0(q)$ has already converged to its limiting value $\bar{\kappa}_0$. A more detailed analysis of the collected numerical data shows that for $q > 4 \times 10^{-3}\text{Å}^{-1}$, $\tilde{\kappa}(q) = TG^{-1}(q)/q^4$ and $\tilde{b}(q)$ differ from their harmonic aproximations $\kappa_0(q)$ and $b_0(q)$ by less than 3%. For $q < 4 \times 10^{-3}\text{Å}^{-1}$, instead, numerical data agree within 3% with correlation functions of a single membrane with Young modulus $2Y$ and rigidity $\bar{\kappa}_0$, which was obtained by rescaling monolayer graphene results via Eqs. (6.53) and (6.54). In particular, in the scaling region $q \ll q_{2*}$, the amplitude z_1' of the power-law behavior $G^{-1}(\mathbf{q}) = z_1' q^{4-\eta}$ differs from the corresponding single-membrane value

$$z_1 = \bar{z}_1 \frac{\bar{\kappa}_0 q_{2*}^\eta}{T} \simeq 1.177 \frac{\bar{\kappa}_0 q_{2*}^\eta}{T} \tag{6.60}$$

only by a deviation of the order of 10^{-3}.

Fig. 6.7 illustrates an explicit comparison between full correlation functions for bilayer graphene at $T = 10$ K, their harmonic approximation, and the corresponding functions for single membranes having Young modulus $2Y$ and bending rigidity 2κ and $\bar{\kappa}_0$. Ratios between corresponding functions are presented in Fig. 6.8.

At room temperature, the mechanical and the weak-strong coupling crossovers have a more sizeable overlap: the characteristic scale $q_{1*} \simeq 0.13\text{Å}^{-1}$ is of the same order of q_{1c}. As it can be seen in Fig. 6.8(b), the renormalized bending rigidity $\tilde{\kappa}(q)$ exhibits a larger deviation from the harmonic approximation at scales of the order of 10^{-1}Å^{-1}. However, the effect is relatively small. For $q \gtrsim 10^{-2}\text{Å}^{-1}$, $\tilde{\kappa}(q)$ and $\tilde{b}(q)$ differ from the corresponding functions in the harmonic approximation by less than 10%. In the long wavelength region $q \lesssim 10^{-2}\text{Å}^{-1}$, instead, $\tilde{\kappa}(q)$ and $\tilde{b}(q)$ agree within 9% with the renormalized rigidity $\tilde{\kappa}_1(q)$ and elastic modulus $\tilde{b}_1(q)$ of a single membrane with bare bending stiffness $\bar{\kappa}_0$ and Young modulus $2Y$. In particular, comparing amplitudes of the leading scaling behavior in the limit $q \to 0$

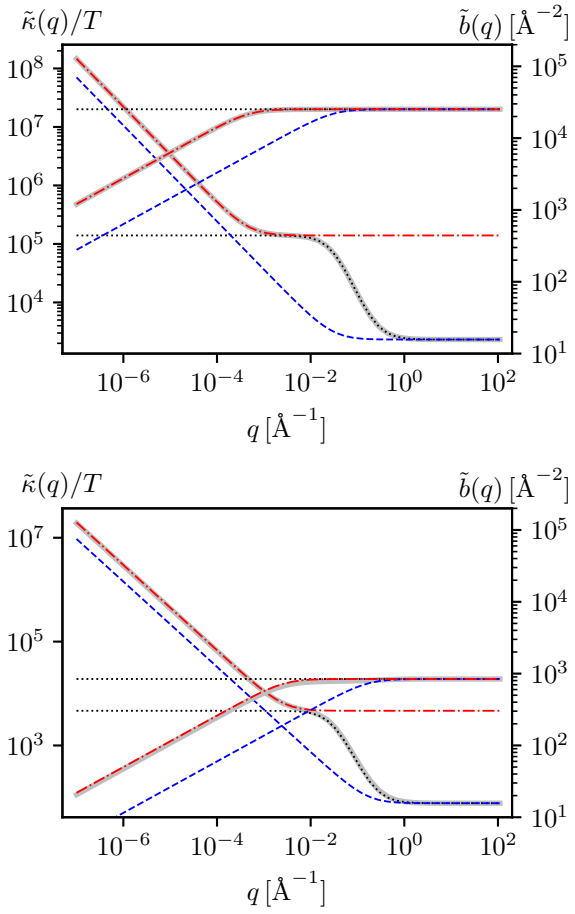

Figure 6.7: Renormalized bending rigidity and renormalized elastic modulus for bilayer graphene at T =10 K (top panel) and T = 300 K (bottom panel). Thick solid grey lines represent $\tilde{\kappa}(q)/T$ and $\tilde{b}(q)$ obtained by numerical solution of SCSA equations for bilayer graphene. The corresponding functions in the harmonic approximation $\kappa_0(q)$ and $b_0(q) = b_0 = Y_0/(2T)$ are illustrated as black dotted lines. The blue dashed curves show the SCSA correlation functions for a single membrane with Young modulus $2Y$ and bending rigidity 2κ, i.e., twice as large than in monolayer graphene. The correlation functions of a single membrane with Young modulus $2Y$ and the much larger bending rigidity $2\kappa + (\lambda + 2\mu)l^2/2$ is illustrated by red dash-dotted lines.

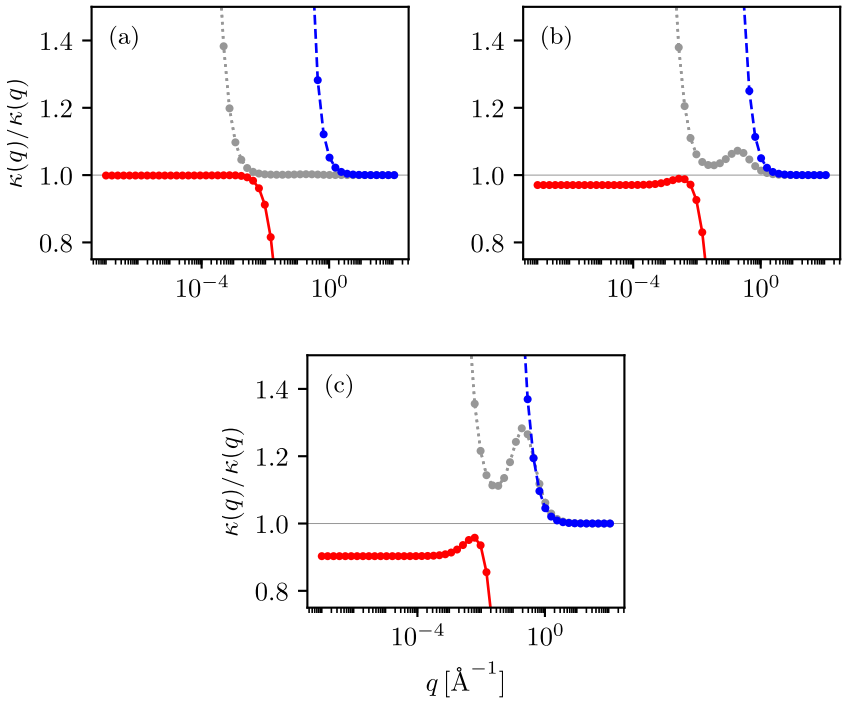

Figure 6.8: Ratio between the renormalized bending rigidity $\tilde{\kappa}(q)$ and the bare effective rigidity $\kappa_0(q)$ (grey dotted lines), the renormalized rigidity $\tilde{\kappa}_1(q)$ of a single-layer membrane with parameters $2Y$ and 2κ (blue dashed line), and the analogue function $\tilde{\kappa}_2(q)$ for parameters $2Y$ and $\bar{\kappa}_0$ (red solid line). Panels (a), (b), and (c) refer to data at T =10, 300, and 1500 K respectively. A horizontal line at 1 is drawn as guide to the eye.

shows that $\tilde{\kappa}(q)$ and $\tilde{b}(q)$ deviate from $\tilde{\kappa}_1(q)$ and $\tilde{b}_1(q)$ by approximately 3% and 6%, respectively[9]. An explicit comparison is illustrated graphically in Fig. 6.7.

The effects of thermal renormalizations are more pronounced at $T = 1500$ K, as Fig. 6.8(c) shows. Within the considered model, the amplitude of the long-wavelength power-law behavior $\tilde{\kappa}(q) = Tz_1''q^{-\eta}$ differs from the scaling limit of $\tilde{\kappa}_1(q)$, $\tilde{\kappa}_1(q) = \bar{z}_1\bar{\kappa}_0(q_{2*}/q)^{\eta}$, by approximately 10%.

In correspondence with crossover regions for $\tilde{\kappa}(q)$, the renormalized elastic coefficient $\tilde{b}(q)$ exhibits a flection (see Fig. 6.7). Since $b_0(q)$ is assumed to be wavevector-independent, this behavior reflects corresponding crossovers in the polarization function $I(q)$.

9 As discussed in Sec. 6.3, both for monolayer and bilayer graphene the ratio z_1^2/z_2 between amplitudes controlling the power-law behaviors $G^{-1}(q) = z_1q^{4-\eta}$ and $\tilde{b}(q) = z_2q^{\eta_u}$ is consistent with the universal value $z_1^2/z_2 = \frac{3}{16\pi}\frac{\Gamma^2(1+\eta/2)\Gamma(1-\eta)}{\Gamma^2(2-\eta/2)\Gamma(2+\eta)} \simeq 0.17813212...$

As a final remark, it should be noted that features in the reported results with q of the order of 1Å^{-1} and their contribution to the renormalization of the long-wavelength behavior can be sensitive to microscopic effects not captured by the continuum approximation employed here. Renormalizations beyond the continuum model are expected to grow with increasing temperature and to become important when strong nonlinear effects occur at microscopic scales.

6.5 INCLUSION OF INTERLAYER FLEXURAL NONLINEARITIES

In the model considered in this work, nonlinearities in $\bar{h} = h_1 - h_2$ and $\bar{u}_\alpha$ have been neglected. As a result of the harmonic approximation, however, Eq. (6.23) fails to recover the theory of two independent nonlinearly-fluctuating layers in the complementary limit $g_1, g_2, g_3, g_4 \to 0$. A minimal extension of the theory necessary to connect this limiting regime can be constructed by including nonlinearities in the interlayer flexural field $\bar{h}$, while neglecting anharmonicity in in-plane displacement fields. With this extension, an analogue of Eq. (6.23) reads:

$$\begin{aligned}\tilde{H} = \frac{1}{2}\int \mathrm{d}^2x \Big\{ & \kappa(\partial^2 h_1)^2 + \lambda(u_{1\alpha\alpha})^2 + 2\mu(u_{1\alpha\beta})^2 \\ & + \kappa(\partial^2 h_2)^2 + \lambda(u_{2\alpha\alpha})^2 + 2\mu(u_{2\alpha\beta})^2 \\ & + \frac{g_1}{l^2}\bar{h}^2 + \frac{g_2}{l^2}(\bar{u}_\alpha + (l+\bar{h})\partial_\alpha h)^2 + \frac{g_3}{2l}(u_{1\alpha\alpha} + u_{2\alpha\alpha}) \\ & + \frac{g_4}{l}[(\bar{u}_x + (l+\bar{h})\partial_x h)(u_{xx} - u_{yy}) - 2(\bar{u}_y + (l+\bar{h})\partial_y h)u_{xy}] \Big\} ,\end{aligned} \tag{6.61}$$

where $u_{i\alpha\beta} = \frac{1}{2}(\partial_\alpha u_{i\beta} + \partial_\beta u_{i\alpha} + \partial_\alpha h_i \partial_\beta h_i)$ are approximate strain tensors of the i-th layer. For $g_1, g_2, g_3, g_4 = 0$, Eq. (6.61) reduces to two copies of the well-known nonlinear effective theory for monolayer membranes [6, 10, 11, 41].

Developing a general theory for weakly coupled membranes with large interlayer-distance fluctuations is a complex problem. If the field $\bar{h}$ is regarded as critical, with a propagator scaling as q^{-4}, power counting indicates an infinite number of relevant and marginal perturbations (see e.g. [220] for a related analysis). Eq. (6.61), therefore, is not a general Hamiltonian but rather, a minimal extension which connects the harmonic theory to a nonlinear decoupled regime of the two membranes.

The theory defined by Eq. (6.4) is invariant under the transformations (see [4, 11])

$$\begin{aligned} h_1(\mathbf{x}) &\to h_1(\mathbf{x}) + A_\alpha x_\alpha + B \\ h_2(\mathbf{x}) &\to h_2(\mathbf{x}) + A_\alpha x_\alpha + B \\ u_{1\alpha}(\mathbf{x}) &\to u_{1\alpha}(\mathbf{x}) - A_\alpha \left(\frac{l}{2} + h_1(\mathbf{x}) \right) - \frac{1}{2} A_\alpha A_\beta x_\beta + B'_\alpha \\ u_{2\alpha}(\mathbf{x}) &\to u_{2\alpha}(\mathbf{x}) + A_\alpha \left(\frac{l}{2} - h_2(\mathbf{x}) \right) - \frac{1}{2} A_\alpha A_\beta x_\beta + B'_\alpha \ , \end{aligned} \tag{6.62}$$

which represent deformed versions of rotations in the embedding space, adapted to match the neglection of in-plane nonlinearities.

Qualitatively, in the case of bilayer graphene, anharmonic terms in $\bar{h}$ are expected to play a minor role.

6.6 SUMMARY AND CONCLUSIONS

In summary, this work analyzed the statistical mechanics of equilibrium thermal ripples in a tensionless sheet of suspended bilayer graphene. The individual graphene membranes forming the bilayer were described as continuum two-dimensional media with finite bending rigidity and elastic moduli. For the description of interlayer interactions a phenomenological model in the spirit of elasticity theory was constructed. Although the fluctuation energy is expanded to leading order for small deformations, anharmonicities emerge as a necessary consequence of rotational invariance, which forces the energy to be expressed in terms of nonlinear scalar strains.

For explicit calculations, the model was simplified by neglecting nonlinearities in the interlayer shear and compression modes, and by dropping anharmonic interactions of collective in-plane displacements. An effective theory describing the statistics of soft flexural fluctuations was then derived by Gaussian integration. The resulting model is controlled by bending rigidity and a long-range interactions between local Gaussian curvatures and it is identical in form to the analogue theory for a monolayer membrane. However, the bare bending rigidity $\kappa_0(q)$ exhibits a strong wavevector dependence at mesoscopic scales. Relevant phenomenological parameters governing the strength of interlayer interactions were derived in the case of AB-stacked bilayer graphene through *ab-initio* density functional theory calculations, by combining an exchange-correlation functional within the Perdew-Burke-Ernzerhoff approximation and van der Waals corrections in the Grimme-D2 model.

Due to the formal equivalence to a corresponding single-membrane theory, the statistical mechanics of fluctuations can be addressed by well-developed approaches. In this work, the field theory integral equations of motion were solved within the

self-consistent screening approximation. In order to access correlation functions at arbitrary wavevector q, SCSA equations were solved numerically by an iterative algorithm.

The numerical solutions recover with good accuracy analytical SCSA predictions for universal properties in the long-wavelength scaling behavior. At mesoscopic lengths, the calculated correlation functions exhibit a rich crossover behavior, driven by the harmonic coupling between bending and interlayer shear and by renormalizations due to nonlinear interactions.

In the final part of the paper, a minimal extension of the theory, including nonlinearities in the flexural fields of both layers was briefly discussed.

ACKNOWLEDGMENTS

The work of A. M. and M. I. K. was supported by the Dutch Research Council (NWO) via the Spinoza Prize. D. S. acknowledges financial support from the EU through the MSCA Project No. 796795 SOT-2DvdW. Part of this work was carried out on the Dutch national e-infrastructure with the support of SURF Cooperative.

APPENDIX 6

6.A DERIVATION OF THE EFFECTIVE THEORY FOR FLEXURAL FLUCTUATIONS

The statistical distribution for fluctuations of $h(\mathbf{x})$ and $u_\alpha(\mathbf{x})$ is obtained from the complete Gibbs distribution of the problem by integration over $\bar{h}(\mathbf{x})$ and $\bar{u}_\alpha(\mathbf{x})$:

$$P[h(\mathbf{x}), u_\alpha(\mathbf{x})] = \frac{1}{Z}\int [\mathrm{d}\bar{h}\mathrm{d}\bar{u}_\alpha]\mathrm{e}^{-\tilde{H}/T} \ . \tag{6.63}$$

This leads to an effective Hamiltonian

$$\tilde{H}'_{\mathrm{eff}} = -T\ln\Big\{\int [\mathrm{d}\bar{h}\mathrm{d}\bar{u}_\alpha]\mathrm{e}^{-\tilde{H}/T}\Big\} \ . \tag{6.64}$$

Since $\tilde{H}$, Eq. (6.23), is quadratic in $\bar{u}_\alpha(\mathbf{x})$ and $\bar{h}(\mathbf{x})$ functional integrations over $\bar{h}(\mathbf{x})$, $\bar{u}_\alpha(\mathbf{x})$, take the form of general Gaussian integrals

$$\begin{aligned} z[J_a] = \int [\mathrm{d}\varphi_a] \exp\Big\{ -\Big[\frac{1}{2}\int_{\mathbf{x}}\int_{\mathbf{x}'} B_{ab}(\mathbf{x},\mathbf{x}')\varphi_a(\mathbf{x})\varphi_b(\mathbf{x}') \\ + \int_{\mathbf{x}} J_a(\mathbf{x})\varphi_a(\mathbf{x})\Big]\Big\} \ , \end{aligned} \tag{6.65}$$

where $J_a(\mathbf{x})$ is a space-dependent source and $B_{ab}(\mathbf{x},\mathbf{x}') = B_{ba}(\mathbf{x}',\mathbf{x})$ is a symmetric, positive definite operator independent of $J_a(\mathbf{x})$. By explicit calculation, the Gaussian integral reads

$$z[J_a(\mathbf{x})] = \mathcal{Z} \exp\left[\frac{1}{2}\int_{\mathbf{x}}\int_{\mathbf{x}'} \Delta_{ab}(\mathbf{x},\mathbf{x}')J_a(\mathbf{x})J_b(\mathbf{x}')\right] , \tag{6.66}$$

where the propagator $\Delta_{ab}(\mathbf{x},\mathbf{x}')$ is the inverse of $B_{ab}(\mathbf{x},\mathbf{x}')$:

$$\int \mathrm{d}^2x'' B_{ac}(\mathbf{x},\mathbf{x}'')\Delta_{cb}(\mathbf{x}'',\mathbf{x}') = \delta_{ab}\delta(\mathbf{x}-\mathbf{x}') . \tag{6.67}$$

and the normalization $\mathcal{Z}$, formally given by

$$\mathcal{Z} = \int [\mathrm{d}\varphi_a] \mathrm{e}^{-\frac{1}{2}\int \mathrm{d}^2x \int \mathrm{d}^2x' B_{ab}(\mathbf{x},\mathbf{x}')\varphi_a(\mathbf{x})\varphi_b(\mathbf{x}')} , \tag{6.68}$$

is independent of the source $J_a(\mathbf{x})$.

To integrate over $\bar{u}_\alpha$, it is convenient to shift variables by the replacement $\bar{u}_\alpha \to \bar{u}_\alpha - l\partial_\alpha h$. With these shifted variables Eq. (6.23) reads, up to boundary terms,

$$\begin{aligned}\tilde{H} = \int \mathrm{d}^2x \Big[& \kappa(\partial^2 h)^2 + \lambda(u_{\alpha\alpha})^2 + 2\mu u_{\alpha\beta}u_{\alpha\beta} \\ & + \frac{\kappa}{4}(\partial^2\bar{h})^2 + \frac{\lambda}{4}(\partial_\alpha\bar{u}_\alpha)^2 + \frac{\mu}{8}(\partial_\alpha\bar{u}_\beta + \partial_\beta\bar{u}_\alpha)^2 \\ & + \frac{(\lambda+2\mu)l^2}{4}(\partial^2 h)^2 - \frac{(\lambda+2\mu)l}{2}(\partial_\alpha\bar{u}_\alpha)\partial^2 h \\ & + \frac{g_1}{2l^2}\bar{h}^2 + \frac{g_2}{2l^2}\bar{u}_\alpha^2 + \frac{g_3}{2l}\bar{h}u_{\alpha\alpha} + \frac{g_4}{2l}\bar{u}_\alpha A_\alpha \Big] ,\end{aligned} \tag{6.69}$$

where $A_x = u_{xx} - u_{yy}$ and $A_y = -2u_{xy}$. From the $\bar{u}_\alpha$-dependent terms, we read the inverse propagator

$$B_{\alpha\beta}(\mathbf{x},\mathbf{x}') = \frac{1}{T}\Big\{ -\frac{1}{2}\big[(\lambda+\mu)\partial_\alpha\partial_\beta + \mu\delta_{\alpha\beta}\partial^2\big] + \frac{g_2}{l^2}\delta_{\alpha\beta}\Big\}\delta(\mathbf{x}-\mathbf{x}') , \tag{6.70}$$

and the source

$$J_\alpha(\mathbf{x}) = \frac{1}{T}\Big[\frac{(\lambda+2\mu)l}{2}\partial_\alpha\partial^2 h + \frac{g_4}{2l}A_\alpha(\mathbf{x})\Big] . \tag{6.71}$$

The propagator $\Delta_{\alpha\beta}$, inverse of $B_{\alpha\beta}$, is then

$$\begin{aligned}\Delta_{\alpha\beta}(\mathbf{x},\mathbf{x}') &= T\int_{\mathbf{q}} \Big\{ \Big[\frac{P^L_{\alpha\beta}(\mathbf{q})}{g_2/l^2 + (\lambda+2\mu)q^2/2} + \frac{P^T_{\alpha\beta}(\mathbf{q})}{g_2/l^2 + \mu q^2/2}\Big] \mathrm{e}^{i\mathbf{q}\cdot(\mathbf{x}-\mathbf{x}')}\Big\} \\ &= \frac{T}{g_2/l^2}\int_{\mathbf{q}} \Big\{ \big[d_L(q)P^L_{\alpha\beta}(\mathbf{q}) + d_T(q)P^T_{\alpha\beta}(\mathbf{q})\big]\mathrm{e}^{i\mathbf{q}\cdot(\mathbf{x}-\mathbf{x}')}\Big\} ,\end{aligned} \tag{6.72}$$

where $P^L_{\alpha\beta}(\mathbf{q}) = q_\alpha q_\beta/q^2$ and $P^T_{\alpha\beta}(\mathbf{q}) = \delta_{\alpha\beta} - q_\alpha q_\beta/q^2$ are longitudinal and transverse projectors and $d_L(q)$ and $d_T(q)$ are dimensionless functions defined in Eq. (6.30). Using Eq. (6.66) we obtain, up to an unimportant normalization factor,

$$\begin{aligned}\int [\mathrm{d}\bar{u}_\alpha] \mathrm{e}^{-\tilde{H}/T} = \exp\Big\{ \frac{T}{2g_2/l^2} \int_{\mathbf{q}} \big[\big(d_L(q) P^L_{\alpha\beta}(\mathbf{q}) d_T(q) P^T_{\alpha\beta}(\mathbf{q}) \big) J_\alpha(\mathbf{q}) J^*_\beta(\mathbf{q}) \big] \\ - \frac{1}{T} \int \mathrm{d}^2x \Big[\kappa (\partial^2 h)^2 + \lambda (u_{\alpha\alpha})^2 + 2\mu u_{\alpha\beta} u_{\alpha\beta} \\ + \frac{(\lambda+2\mu) l^2}{4} (\partial^2 h)^2 + \frac{g_1}{2l^2} \bar{h}^2 + \frac{g_3}{2l} \bar{h} u_{\alpha\alpha} \Big] \Big\} ,\end{aligned} \tag{6.73}$$

where $J_\alpha(\mathbf{q})$ is the Fourier transform of $J_\alpha(\mathbf{x})$,

$$J_\alpha(\mathbf{q}) = \frac{1}{T} \Big[- i \frac{(\lambda+2\mu) l}{2} q_\alpha q^2 h(\mathbf{q}) + \frac{g_4}{2l} A_\alpha(\mathbf{q}) \Big] , \tag{6.74}$$

being $h(\mathbf{q})$ and $A_\alpha(\mathbf{q})$ the Fourier transforms of $h(\mathbf{x})$ and $A_\alpha(\mathbf{x})$ respectively. After introduction of $A(\mathbf{x}) = \partial_\alpha A_\alpha$ and the corresponding Fourier components $A(\mathbf{q}) = i q_\alpha A_\alpha(\mathbf{q})$, an explicit calculation of Eq. (6.73) gives:

$$\begin{aligned}\int [\mathrm{d}\bar{u}_\alpha] \mathrm{e}^{-\tilde{H}/T} = \exp \Big\{ - \frac{1}{T} \Big[\int_{\mathbf{q}} \Big(\frac{1}{2} \kappa_0(q) |h(\mathbf{q})|^2 + \mu_0(q) |u_{\alpha\beta}(\mathbf{q})|^2 \\ + \frac{g_4^2}{8g_2} d_T(\mathbf{q}) |u_{\alpha\alpha}(\mathbf{q})|^2 - \frac{g_4 l^2}{4g_2} (\lambda+2\mu) d_L(q) q^2 h(\mathbf{q}) A^*(\mathbf{q}) \\ + \frac{g_4^2 l^2}{16 g_2^2} (\lambda+\mu) d_L(q) d_T(q) |A(\mathbf{q})|^2 \Big) \\ + \int \mathrm{d}^2x \Big(\lambda (u_{\alpha\alpha})^2 + \frac{\kappa}{4} (\partial^2 \bar{h})^2 + \frac{g_1}{2l^2} \bar{h}^2 + \frac{g_3}{2l} \bar{h} u_{\alpha\alpha} \Big) \Big] \Big\} ,\end{aligned} \tag{6.75}$$

where $\kappa_0(q)$ and $\mu_0(q)$ are the q-dependent bending rigidity and shear modulus introduced in Eq. (6.31). In the derivation, it is useful to take advantage of the identity

$$A_\alpha(\mathbf{q}) A^*_\alpha(\mathbf{q}) = 2 |u_{\alpha\beta}(\mathbf{q})|^2 - |u_{\alpha\alpha}(\mathbf{q})|^2 . \tag{6.76}$$

As a next step, we can integrate out the $\bar{h}$ field. This generates an effective interaction between the sources $g_3 u_{\alpha\alpha}(\mathbf{x})/(2Tl)$, mediated by the propagator

$$\Delta(\mathbf{x}, \mathbf{x}') = T \int_{\mathbf{q}} \frac{\mathrm{e}^{i\mathbf{q}\cdot(\mathbf{x}-\mathbf{x}')}}{g_1/l^2 + \kappa q^4/2} = \frac{T}{g_1/l^2} \int_{\mathbf{q}} \bar{d}(q) \mathrm{e}^{i\mathbf{q}\cdot(\mathbf{x}-\mathbf{x}')} , \tag{6.77}$$

the inverse of

$$B(\mathbf{x}, \mathbf{x}') = \frac{1}{T} \Big[\frac{\kappa}{2} \partial^4 + \frac{g_1}{l^2} \Big] \delta(\mathbf{x} - \mathbf{x}') . \tag{6.78}$$

Using Eq. (6.66), we then obtain

$$\begin{aligned}\int [\mathrm{d}\bar{u}_\alpha \mathrm{d}\bar{h}] \mathrm{e}^{-\tilde{H}/T} = \exp\Big\{ -\frac{1}{T}\Big[\int_{\mathbf{q}} \Big(\frac{1}{2}\kappa_0(q)|h(\mathbf{q})|^2 + \mu_0(q)|u_{\alpha\beta}(\mathbf{q})|^2 \\ + \lambda|u_{\alpha\alpha}(\mathbf{q})|^2 + \frac{g_4^2}{8g_2} d_T(\mathbf{q})|u_{\alpha\alpha}(\mathbf{q})|^2 - \frac{g_3^2}{8g_1}\bar{d}(q)|u_{\alpha\alpha}(\mathbf{q})|^2 \\ - \frac{g_4 l^2}{4g_2}(\lambda+2\mu) d_L(q) q^2 h(\mathbf{q}) A^*(\mathbf{q}) \\ + \frac{g_4^2 l^2}{16 g_2^2}(\lambda+\mu) d_L(q) d_T(q) |A(\mathbf{q})|^2 \Big) \Big] \Big\} ,\end{aligned} \tag{6.79}$$

from which we recognize the effective Hamiltonian $\tilde{H}'_{\mathrm{eff}}[h(\mathbf{x}), u_\alpha(\mathbf{x})]$, Eq. (6.28) in the main text.

We finally wish to eliminate the in-plane displacement fields $u_\alpha(\mathbf{x})$. Neglecting, as in the main text, the interactions $\int_{\mathbf{q}} |A(\mathbf{q})|^2$ and $\int_{\mathbf{q}} q^2 h(\mathbf{q}) A^*(\mathbf{q})$, we are lead to the calculation of

$$\tilde{H}_{\mathrm{eff}}[h(\mathbf{x})] = -T \ln \Big\{ \int [\mathrm{d}u_\alpha] \exp\big[-\tilde{H}''_{\mathrm{eff}}/T \big] \Big\} , \tag{6.80}$$

with

$$\tilde{H}''_{\mathrm{eff}} = \frac{1}{2}\int_{\mathbf{q}} \Big[\kappa_0(q) q^4 |h(\mathbf{q})|^2 + \lambda_0(q)|u_{\alpha\alpha}(\mathbf{q})|^2 + 2\mu_0(q)|u_{\alpha\beta}(\mathbf{q})|^2 \Big] . \tag{6.81}$$

Although, eventually, we will assume q-independent Lamé coefficients $\lambda_0(q)$ and $\mu_0(q)$, it is not difficult to keep general q-dependent couplings in the course of the derivation.

Eq. (6.81) is identical in form with the standard configuration energy of a crystalline membrane, but with elastic and bending parameters replaced by the q-dependent functions defined in Eq. (6.31). Integration over u_α then proceeds in an usual way (see Chap. 6 of Ref. [1] and Refs. [12, 23, 25, 85]).

As a first step, it is important to separate the $\mathbf{q} = 0$ component of the strain tensor $u_{\alpha\beta}(\mathbf{x})$ [1] (see also Ref. [85] for an analysis of zero-modes in presence of external tension):

$$u_{\alpha\beta}(\mathbf{x}) = u^0_{\alpha\beta} + c^0_{\alpha\beta} + \frac{1}{2}\int'_{\mathbf{q}} (iq_\alpha u_\beta(\mathbf{q}) + iq_\beta u_\alpha(\mathbf{q}) + c_{\alpha\beta}(\mathbf{q})) \mathrm{e}^{i\mathbf{q}\cdot\mathbf{x}} . \tag{6.82}$$

Here

$$c_{\alpha\beta}(\mathbf{q}) = \int \mathrm{d}^2x \mathrm{e}^{-i\mathbf{q}\cdot\mathbf{x}} \partial_\alpha h(\mathbf{x}) \partial_\beta h(\mathbf{x}) \tag{6.83}$$

is the Fourier transform of the field $c_{\alpha\beta} = \partial_\alpha h \partial_\beta h$, $c^0_{\alpha\beta}$ is its $\mathbf{q} = 0$ component, and $u^0_{\alpha\beta}$ is the uniform component of $(\partial_\alpha u_\beta + \partial_\beta u_\alpha)/2$. The primed integral, $\int'_{\mathbf{q}}$, is intended to run over all nonzero wavevectors, with the $\mathbf{q} = 0$ term excluded.

In the functional integral, we can consider separate integrations over uniform and finite-wavelength components. After the translation of variables $u^0_{\alpha\beta} \to u^0_{\alpha\beta} - c^0_{\alpha\beta}$, the integral over uniform components factorizes and gives an irrelevant normalization constant, independent on the $h(\mathbf{x})$ field.

In order to perform the remaining integral over the $\mathbf{q} \neq 0$ components of u_α, it is convenient to decompose $c_{\alpha\beta}(\mathbf{q})$ in the form [1]

$$c_{\alpha\beta}(\mathbf{q}) = iq_\alpha\phi_\beta(\mathbf{q}) + iq_\beta\phi_\alpha(\mathbf{q}) + P^T_{\alpha\beta}(\mathbf{q})\omega(\mathbf{q}) \ , \tag{6.84}$$

where $\phi_\alpha(\mathbf{q})$ is a two-component vector and

$$\omega(\mathbf{q}) = P^T_{\alpha\beta}(\mathbf{q})c_{\alpha\beta}(\mathbf{q}) \ . \tag{6.85}$$

This decomposition is possible for any two-dimensional symmetric matrix. After the shift of integration variables $u_\alpha(\mathbf{x}) \to u_\alpha(\mathbf{x}) - \phi_\alpha(\mathbf{x})$, the Fourier components of the strain tensor become independent of $\phi_\alpha(\mathbf{q})$. An explicit calculation then leads to the effective Hamiltonian

$$H_{\rm eff} = \frac{1}{2}\int_{\mathbf{q}} \kappa_0(q)q^4|h(\mathbf{q})|^2 + \int'_{\mathbf{q}} \frac{Y_0(q)}{8}|\omega(\mathbf{q})|^2 \ , \tag{6.86}$$

with

$$Y_0(q) = \frac{4\mu_0(q)(\lambda_0(q)+\mu_0(q))}{\lambda_0(q)+2\mu_0(q)} \ . \tag{6.87}$$

Inspecting Eq. (6.85), we recognize that $\omega(\mathbf{q}) = 2K(\mathbf{q})/q^2$, where $K(\mathbf{q})$ is the Fourier transform of the approximate Gaussian curvature, Eq. (6.13). With the approximation $\lambda_0(q) \simeq 2\lambda$, $\mu_0(q) \simeq 2\mu$, $Y_0(q) = 4\mu_0(\lambda_0+\mu_0)/(\lambda_0+2\mu_0)$, we thus obtain Eq. (6.34) of the main text.

6.B NUMERICAL SOLUTION OF SCSA EQUATIONS

As discussed in the main text, a logarithmic wavevector grid consisting of 50 wavevector points ranging between 10^{-7} and 110Å^{-1} is used and integrations are performed by introducing a hard UV cutoff $\Lambda = 100\text{Å}^{-1}$. Data for bilayer graphene are calculated with an identical set of wavevector points, and by imposing the same cutoff $\Lambda = 100\text{Å}^{-1}$ in momentum integrations.

In order to estimate the numerical error due to discretization of the wavevector grid and the subsequent interpolation, correlation functions were recalculated using a broader wavevector grid consisting of 26 points[10]. To facilitate comparison, the q grid was chosen in such way that the first 25 points coincide with a subset of

10 All data sets have been made available as supplemental materials to the publication "Thermal ripples in bilayer graphene", Phys. Rev. B **102**, 165421 (2020). For more information on the numerical accuracy of the data, we refer the reader to the published article.

wavevector points used in the finer grid. A graphical comparison between data obtained with denser and broader grids is illustrated in Fig. 6.9.

Overall, the maximum relative deviation between data points (at the common q vectors) is of the order of 10^{-3}. The continuous interpolating functions have a larger discrepancy, but remain within a maximum overall deviation of the order of 2%. Fig. 6.10 compares data calculated with two different ultraviolet cutoffs $\Lambda_1 = 100$ Å^{-1} and $\Lambda_2 = 1000$ Å^{-1}. As the figure shows, results are stable with good accuracy.

The fact that all curves in Figs. (6.9) and (6.10) tend to constants for $q \to 0$ reflects that the leading numerical error for $q \to 0$ is a constant amplitude renormalization. This renormalization is accumulated at all length scales and thus is sensitive to numerical inaccuracies in the large-momentum region. The universal quantities (the exponents η, η_u, and the amplitude ratio z_1^2/z_2) are instead insensitive to the short-wavelength details, and depend only on the scaling region, where correlation functions are linear in logarithmic scale and interpolation error becomes negligible[10]. For example, the exponent η extracted from the numerical solutions for monolayer graphene remains stable within 3×10^{-11}.

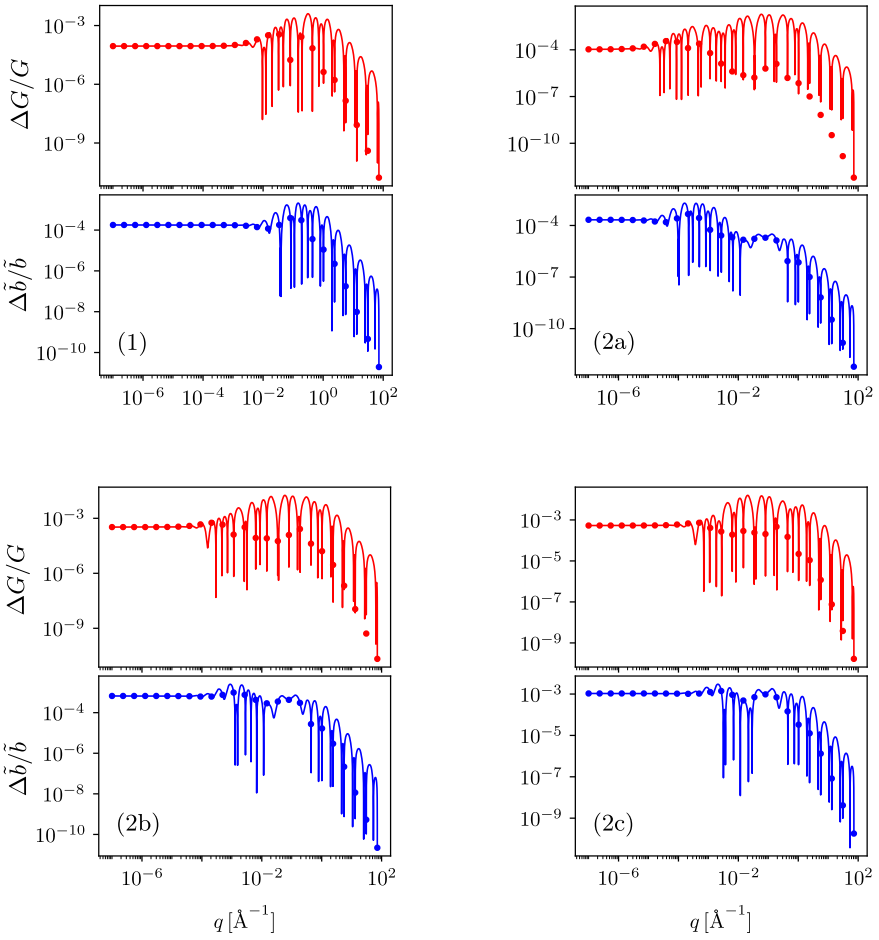

Figure 6.9: Comparison between data sets calculated with 50-point and 26-point wavevector grids for monolayer graphene at $T = 300$ K (1) and bilayer graphene at $T = 10$ K (2a), $T = 300$ K (2b), and $T = 1500$ K (2c). Top and bottom panels illustrate, respectively, the ratios $\Delta G/G = |G_1 - G_2|/|G_1|$ and $\Delta\tilde{b}/\tilde{b} = |\tilde{b}_1 - \tilde{b}_2|/|\tilde{b}_1|$, where G_1 and $\tilde{b}_1$ are calculated with a 50-point wavevector grid, while G_2 and $\tilde{b}_2$ are obtained with a broader 26-point grid. Dots illustrate the values of $\Delta G/G$ and $\Delta\tilde{b}/\tilde{b}$ at the points of the broader wavevector grid, which, by construction, coincide with a subset of q-points of the finer grid. The deviation between interpolating functions in the two data sets is illustrated by continuous lines.

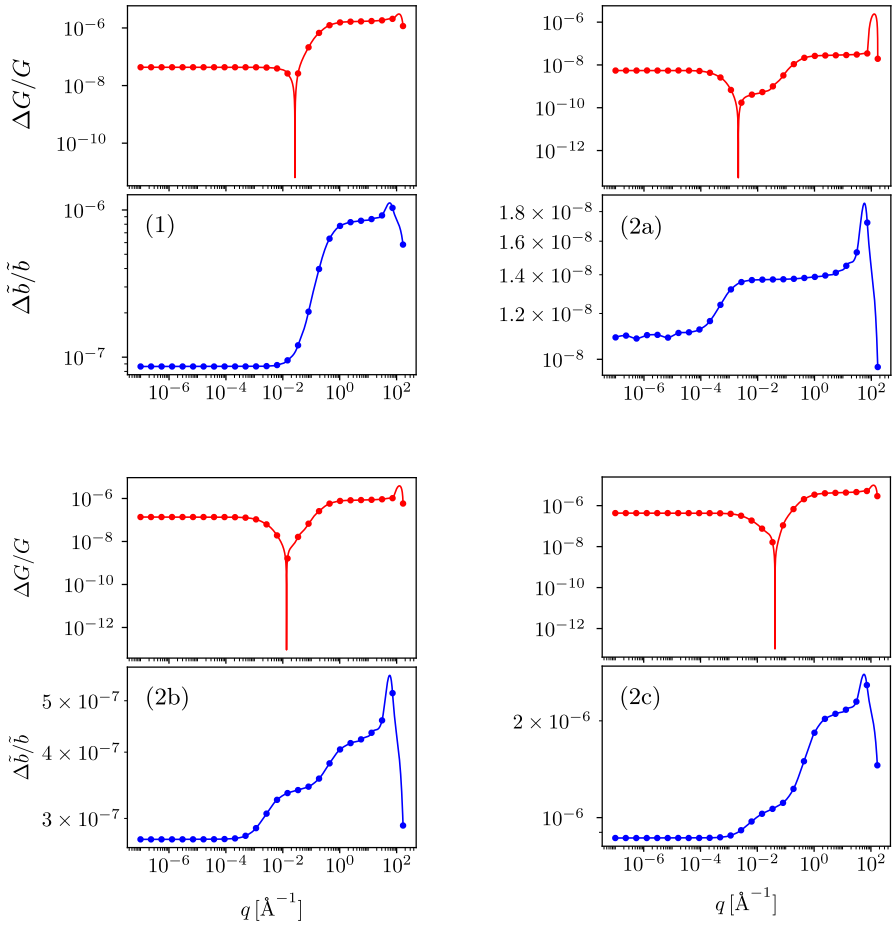

Figure 6.10: Comparison between data sets calculated with different UV cutoff $\Lambda_1 = 100$ and $\Lambda_2 = 1000$ Å^{-1}. Red and blue lines represent, respectively, the relative deviations $\Delta G/G = |G_1 - G_2|/G_1$ and $\Delta\tilde{b}/\tilde{b} = |\tilde{b}_1 - \tilde{b}_2|/b_1$ where G_1 and $\tilde{b}_1$ are computed with cutoff $\Lambda_1 = 100$Å^{-1} and G_2, $\tilde{b}_2$ with cutoff $\Lambda_2 = 1000$ Å^{-1}. The four panels show data for monolayer graphene at $T = 300$ K (1) and bilayer graphene at $T = 10$ K (2a), $T = 300$ K (2b), and $T = 1500$ K (2c).

BIBLIOGRAPHY

[1] D. R. Nelson, T. Piran, and S. Weinberg, eds., *Statistical mechanics of membranes and surfaces*, 2nd ed. (World Scientific, Singapore, 2004).

[2] D. R. Nelson, *Defects and geometry in condensed matter physics* (Cambridge University Press, 2002).

[3] M. I. Katsnelson, *The physics of graphene*, 2nd ed. (Cambridge University Press, Cambridge, 2020).

[4] M. J. Bowick and A. Travesset, Phys. Rep. **344**, 255 (2001).

[5] M. J. Bowick and L. Giomi, Advances in Physics **58**, 449 (2009).

[6] D. R. Nelson and L. Peliti, J. Physique **48**, 1085 (1987).

[7] N. D. Mermin and H. Wagner, Phys. Rev. Lett. **17**, 1133 (1966).

[8] B. I. Halperin, J. Stat. Phys. **175**, 521 (2018).

[9] F. David and E. Guitter, EPL **5**, 709 (1988).

[10] J. A. Aronovitz and T. C. Lubensky, Phys. Rev. Lett. **60**, 2634 (1988).

[11] E. Guitter, F. David, S. Leibler, and L. Peliti, J. Physique **50**, 1787 (1989).

[12] J. Aronovitz, L. Golubovic, and T. C. Lubensky, J. Physique **50**, 609 (1989).

[13] K. G. Wilson and J. Kogut, Phys. Rep. **12**, 75 (1974).

[14] S.-K. Ma, *Modern theory of critical phenomena*, Advanced Book Classics (Westview Press, 2000).

[15] J. Zinn-Justin, *Quantum field theory and critical phenomena*, 4th ed., Vol. 113, International series of monographs on physics (Oxford University Press, 2002).

[16] G. Parisi, *Statistical field theory*, Frontiers in Physics (Addison-Wesley, 1988).

[17] I. V. Gornyi, V. Y. Kachorovskii, and A. D. Mirlin, 2D Mater. **4**, 011003 (2017).

[18] S. Shankar and D. R. Nelson, Phys. Rev. E **104**, 054141 (2021).

[19] O. Coquand, D. Mouhanna, and S. Teber, Phys. Rev. E **101**, 062104 (2020).

[20] S. Metayer, D. Mouhanna, and S. Teber, Phys. Rev. E **105**, L012603 (2022).

[21] A. Pikelner, EPL **138**, 17002 (2022).

[22] D. R. Saykin, I. V. Gornyi, V. Y. Kachorovskii, and I. S. Burmistrov, Ann. Phys. **414**, 168108 (2020).

[23] P. Le Doussal and L. Radzihovsky, Phys. Rev. Lett. **69**, 1209 (1992).

[24] D. Gazit, Phys. Rev. E **80**, 041117 (2009).

[25] P. Le Doussal and L. Radzihovsky, Ann. Phys. **392**, 340 (2018).

[26] J.-P. Kownacki and D. Mouhanna, Phys. Rev. E **79**, 040101(R) (2009).

[27] N. Hasselmann and F. L. Braghin, Phys. Rev. E **83**, 031137 (2011).

[28] F. L. Braghin and N. Hasselmann, Phys. Rev. B **82**, 035407 (2010).

[29] G. Gompper and D. Kroll, Curr. Opin. Colloid Interface Sci. **2**, 373 (1997).

[30] G. Gompper and D. M. Kroll, J. Phys. Condens. Matter **9**, 8795 (1997).

[31] J. H. Los, M. I. Katsnelson, O. V. Yazyev, K. V. Zakharchenko, and A. Fasolino, Phys. Rev. B **80**, 121405(R) (2009).

[32] A. Tröster, Phys. Rev. B **87**, 104112 (2013).

[33] W. Gao and R. Huang, J. Mech. Phys. Solids **66**, 42 (2014).

[34] D. Wei and F. Wang, J. Chem. Phys. **141**, 144701 (2014).

[35] A. Tröster, Phys. Rev. E **91**, 022132 (2015).

[36] C. P. Herrero and R. Ramírez, J. Chem. Phys. **145**, 224701 (2016).

[37] J. H. Los, J. M. H. Kroes, K. Albe, R. M. Gordillo, M. I. Katsnelson, and A. Fasolino, Phys. Rev. B **96**, 184108 (2017).

[38] J. Hašík, E. Tosatti, and R. Martoňák, Phys. Rev. B **97**, 140301(R) (2018).

[39] D. R. Nelson and L. Radzihovsky, EPL **16**, 79 (1991).

[40] D. C. Morse and T. C. Lubensky, Phys. Rev. A **46**, 1751 (1992).

[41] I. V. Gornyi, V. Y. Kachorovskii, and A. D. Mirlin, Phys. Rev. B **92**, 155428 (2015).

[42] O. Coquand, K. Essafi, J.-P. Kownacki, and D. Mouhanna, Phys. Rev. E **97**, 030102(R) (2018).

[43] O. Coquand and D. Mouhanna, Phys. Rev. E **103**, L031001 (2021).

[44] D. R. Saykin, V. Y. Kachorovskii, and I. S. Burmistrov, Phys. Rev. Research **2**, 043099 (2020).

[45] A. Košmrlj and D. R. Nelson, Phys. Rev. E **88**, 012136 (2013).

[46] A. Košmrlj and D. R. Nelson, Phys. Rev. E **89**, 022126 (2014).

[47] S. Mori and M. Wadati, J. Phys. Soc. Jpn. **62**, 3864 (1993).

[48] F. F. Abraham and M. Kardar, Science **252**, 419 (1991).

[49] J. Toner, Phys. Rev. Lett. **62**, 905 (1989).

[50] K. Essafi, J.-P. Kownacki, and D. Mouhanna, Phys. Rev. Lett. **106**, 128102 (2011).

[51] A. Košmrlj and D. R. Nelson, Phys. Rev. B **93**, 125431 (2016).

[52] I. S. Burmistrov, I. V. Gornyi, V. Y. Kachorovskii, M. I. Katsnelson, J. H. Los, and A. D. Mirlin, Phys. Rev. B **97**, 125402 (2018).

[53] I. S. Burmistrov, V. Y. Kachorovskii, M. J. Klug, and J. Schmalian, Phys. Rev. Lett. **128**, 096101 (2022).

[54] F. Guinea, P. Le Doussal, and K. J. Wiese, Phys. Rev. B **89**, 125428 (2014).

[55] T. Cea, M. Ruiz-García, L. L. Bonilla, and F. Guinea, Phys. Rev. B **101**, 235428 (2020).

[56] F. S. Schmidt, K. Svoboda, N. Lei, I. B. Petsche, L. E. Berman, C. R. Safinya, and G. S. Grest, Science **259**, 952 (1993).

[57] T. Hwa, E. Kokufuta, and T. Tanaka, Phys. Rev. A **44**, R2235 (1991).

[58] X. Wen, C. W. Garland, T. Hwa, M. Kardar, E. Kokufuta, Y. Li, M. Orkisz, and T. Tanaka, Nature **355**, 426 (1992).

[59] M. S. Spector, E. Naranjo, S. Chiruvolu, and J. A. Zasadzinski, Phys. Rev. Lett. **73**, 2867 (1994).

[60] S. Chaieb, V. K. Natrajan, and A. A. El-rahman, Phys. Rev. Lett. **96**, 078101 (2006).

[61] M. I. Katsnelson and A. Fasolino, Acc. Chem. Res. **46**, 97 (2013).

[62] J. H. Los, A. Fasolino, and M. I. Katsnelson, npj 2D Materials and Applications **1**, 9 (2017).

[63] J. C. Meyer, A. K. Geim, M. I. Katsnelson, K. S. Novoselov, T. J. Booth, and S. Roth, Nature Lett. **446**, 60 (2007).

[64] A. Locatelli et al., ACS Nano **4**, 4879 (2010).

[65] C. S. Ruiz-Vargas, H. L. Zhuang, P. Y. Huang, A. M. van der Zande, S. Garg, P. L. McEuen, D. A. Muller, R. G. Hennig, and J. Park, Nano Lett. **11**, 2259 (2011).

[66] D. A. Krilenko, A. T. Dideykin, and G. Van Tendeloo, Phys. Rev. B **84**, 235417 (2011).

[67] P. Xu, M. Neek-Amal, S. D. Barber, J. K. Schoelz, M. L. Ackerman, P. M. Thibado, A. Sadeghi, and F. M. Peeters, Nature Commun. **5**, 3720 (2014).

[68] S. Deng and V. Berry, Mater. Today **19**, 197 (2016).

[69] R. J. T. Nicholl, H. J. Conley, N. V. Lavrik, I. Vlassiouk, Y. S. Puzyrev, V. P. Sreenivas, S. T. Pantelides, and K. I. Bolotin, Nat. Commun. **6**, 8789 (2015).

[70] M. K. Blees et al., Nature **524**, 204 (2015).

[71] A. Georgi, P. Nemes-Incze, B. Szafranek, D. Neumaier, V. Geringer, M. Liebmann, and M. Morgenstern, Phys. Rev. B **94**, 184302 (2016).

[72] R. J. T. Nicholl, N. V. Lavrik, I. Vlassiouk, B. R. Srijanto, and K. I. Bolotin, Phys. Rev. Lett. **118**, 266101 (2017).

[73] F. Colangelo, P. Pingue, V. Mišeikis, C. Coletti, F. Beltram, and S. Roddaro, 2D Mater. **6**, 025005 (2019).

[74] G. Lopez-Polin, C. Gomez-Navarro, and J. Gomez-Herrero, Nano Mater. Sci. **10**, 1 (2021).

[75] G. López-Polín, C. Gómez-Navarro, V. Parente, F. Guinea, M. I. Katsnelson, F. Pérez-Murano, and J. Gómez-Herrero, Nat. Phys. **11**, 26 (2015).

[76] G. López-Polín, M. Jaafar, F. Guinea, R. Roldán, C. Gómez-Navarro, and J. Gómez-Herrero, Carbon **124**, 42 (2017).

[77] G. López-Polín, M. Ortega, J. G. Vilhena, I. Alda, J. Gomez-Herrero, P. A. Serena, C. Gomez-Navarro, and R. Pérez, Carbon **116**, 670 (2017).

[78] J. H. Los, A. Fasolino, and M. I. Katsnelson, Phys. Rev. Lett. **116**, 015901 (2016).

[79] S. Rychkov, *EPFL lectures on conformal field theory in D≥3 dimensions*, Springer Briefs in Physics (Springer, 2017).

[80] D. Poland, S. Rychkov, and A. Vichi, Rev. Mod. Phys. **91**, 015002 (2019).

[81] D. J. Amit, *Field theory, the renormalization group and critical phenomena*, 2nd ed. (World Scientific, 1984).

[82] A. Z. Patashinskii and V. L. Pokrovskii, *Fluctuation theory of phase transitions* (Pergamon Press, 1980).

[83] L. D. Landau and E. M. Lifshitz, *Theory of elasticity* (Pergamon Press, Oxford, 1970).

[84] L. D. Landau and E. Lifshitz, *Statistical physics, part I* (Pergamon Press, Oxford, 1980).

[85] I. S. Burmistrov, V. Y. Kachorovskii, I. V. Gornyi, and A. D. Mirlin, Ann. Phys. **396**, 119 (2018).

[86] A. Polyakov, Nucl. Phys. B **268**, 406 (1986).

[87] B. Davidovitch, Y. Sun, and G. M. Grason, Proc. Natl. Acad. Sci. U.S.A **116**, 1483 (2019).

[88] O. Coquand, Phys. Rev. B **100**, 125406 (2019).

[89] I. M. Lifshitz, Zh. Eksp. Teor. Fiz. **22**, 475 (1952).

[90] I. Low and A. V. Manohar, Phys. Rev. Lett. **88**, 101602 (2002).

[91] I. S. Burmistrov, I. V. Gornyi, V. Y. Kachorovskii, M. I. Katsnelson, and A. D. Mirlin, Phys. Rev. B **94**, 195430 (2016).

[92] F. J. Wegner, J. Phys. C: Solid State Phys. **7**, 2098 (1974).

[93] P. W. Anderson, *Basic notions of condensed matter physics* (Addison Wesley, 1984).

[94] F. J. Wegner and A. Houghton, Phys. Rev. A **8**, 401 (1973).

[95] J. Berges, N. Tetradis, and C. Wetterich, Phys. Rep. **363**, 223 (2002).

[96] E. Guitter, F. David, S. Leibler, and L. Peliti, Phys. Rev. Lett. **61**, 2949 (1988).

[97] E. Cerda and L. Mahadevan, Phys. Rev. Lett. **90**, 074302 (2003).

[98] H. Diamant and T. A. Witten, Phys. Rev. Lett. **107**, 164302 (2011).

[99] P. Ares, Y. B. Wang, C. R. Woods, J. Dougherty, L. Fumagalli, F. Guinea, B. Davidovitch, and K. S. Novoselov, Proc. Nat. Acad. Sci. U.S.A. **118**, e2025870118 (2021).

[100] E. Brézin and J. Zinn-Justin, Phys. Rev. B **13**, 251 (1976).

[101] K. G. Wilson, Phys. Rev. Lett. **28**, 548 (1972).

[102] K. Sun, A. Souslov, X. Mao, and T. C. Lubensky, Proc. Natl. Acad. Sci. U.S.A **109**, 12369 (2012).

[103] V. Riva and J. Cardy, Phys. Lett. B **622**, 339 (2005).

[104] X. Xing, R. Mukhopadhyay, T. Lubensky, and L. Radzihovsky, Phys. Rev. E **68**, 021108 (2003).

[105] M. Moshe and J. Zinn-Justin, Phys. Rep. **385**, 69 (2003).

[106] A. J. Bray, Phys. Rev. Lett. **32**, 1413 (1974).

[107] K. Essafi, J.-P. Kownacki, and D. Mouhanna, Phys. Rev. E **89**, 042101 (2014).

[108] R. Cuerno, R. G. Caballero, A. Gordillo-Guerrero, P. Monroy, and J. J. Ruiz-Lorenzo, Phys. Rev. E **93**, 022111 (2016).

[109] J. Yu, M. I. Katsnelson, and S. Yuan, Phys. Rev. B **106**, 045418 (2022).

[110] R. Roldán, A. Fasolino, K. V. Zakharchenko, and M. I. Katsnelson, Phys. Rev. B **83**, 174104 (2011).

[111] X. Wei, B. Fragneaud, C. A. Marianetti, and J. W. Kysar, Phys. Rev. B **80**, 205407 (2009).

[112] A. Fasolino, J. H. Los, and M. I. Katsnelson, Nat. Mater. **6**, 858 (2007).

[113] A. Košmrlj and D. R. Nelson, Phys. Rev. X **7**, 011002 (2017).

[114] G. Goon, K. Hinterbichler, A. Joyce, and M. Trodden, J. High Energy Phys. **11**, 100 (2016).

[115] P. Di Francesco, P. Mathieu, and D. Sénéchal, *Conformal field theory* (Springer, 1997).

[116] Y. Nakayama, Phys. Rep. **569**, 1 (2015).

[117] A. B. Zamolodchikov, JETP Lett. **43**, 730 (1986).

[118] J. Polchinski, Nucl. Phys. B **303**, 226 (1988).

[119] J. Cardy, arXiv:0807.3472 (2008).

[120] I. Jack and H. Osborn, Nucl. Phys. B **343**, 647 (1990).

[121] M. A. Luty, J. Polchinski, and R. Rattazzi, J. High Energy Phys. **01**, 152 (2013).

[122] J.-F. Fortin, B. Grinstein, and A. Stergiou, J. High Energy Phys. **01**, 184 (2013).

[123] A. Dymarsky, Z. Komargodski, A. Schwimmer, and S. Theisen, J. High Energy Phys. **10**, 171 (2015).

[124] A. Dymarsky and A. Zhiboedov, J. Phys. A: Math. Theor. **48**, 41FT01 (2015).

[125] A. Dymarsky, K. Farnsworth, Z. Komargodski, M. A. Luty, and V. Prilepina, J. High Energy Phys. **02**, 099 (2016).

[126] Y. Nakayama, Phys. Rev. D **102**, 065018 (2020).

[127] C. M. Hull and P. K. Townsend, Nucl. Phys. B **274**, 349 (1986).

[128] G. Arutyunov, S. Frolov, B. Hoare, R. Roiban, and A. A. Tseytlin, Nucl. Phys. B **903**, 262 (2016).

[129] C. M. Ho and Y. Nakayama, J. High Energy Phys. **07**, 109 (2008).

[130] S. El-Showk, Y. Nakayama, and S. Rychkov, Nucl. Phys. B **848**, 578 (2011).

[131] Y. Nakayama, Phys. Rev. D **87**, 085005 (2013).

[132] Y. Nakayama, Phys. Rev. D **95**, 065016 (2017).

[133] Y. Oz, Eur. Phys. J. C **78**, 655 (2018).

[134] Y. Nakayama, Phys. Rev. D **95**, 046006 (2017).

[135] Y. Nakayama, Phys. Rev. D **95**, 066010 (2017).

[136] Y.-Z. Li, H. Lü, and H.-Y. Zhang, Eur. Phys. J. C **79**, 592 (2019).

[137] L. Schäfer, J. Phys. A: Math. Gen. **9**, 377 (1976).

[138] L. S. Brown, Ann. Phys. **126**, 135 (1980).

[139] M. F. Paulos, S. Rychkov, B. C. van Rees, and B. Zan, Nucl. Phys. B **902**, 246 (2016).

[140] B. Delamotte, M. Tissier, and N. Wschebor, Phys. Rev. E **93**, 012144 (2016).

[141] G. De Polsi, M. Tissier, and N. Wschebor, J. Stat. Phys. **177**, 1089 (2019).

[142] S. Meneses, J. Penedones, S. Rychkov, J. M. Viana Parente Lopes, and P. Yvernay, J. High Energy Phys. **04**, 115 (2019).

[143] J. A. Dietz and T. R. Morris, J. High Energy Phys. **07**, 64 (2013).

[144] Y. Nakayama, "Functional renormalization group approach to dipolar fixed point which is scale invariant but non-conformal," [Conference presentation. 10$^{\text{th}}$ International Conference on Exact Renormalization Group 2020].

[145] G. Parisi, Phys. Lett. B **39**, 643 (1972).

[146] E. Pajer and D. Stefanyszyn, J. High Energy Phys. **06**, 008 (2019).

[147] Y. Nakayama, Ann. Phys. **372**, 392 (2016).

[148] I. Giordanelli, N. Posé, M. Mendoza, and H. J. Herrmann, Sci. Rep. **6**, 22949 (2016).

[149] J. Cardy, Ann. Phys. **318**, 81 (2005).

[150] G. Parisi, J. Stat. Phys. **23**, 49 (1980).

[151] J. Cardy, *Scaling and renormalization in statistical physics*, Vol. 5, Cambridge Lecture Notes in Physics (Cambridge University Press, 1996).

[152] D. Dorigoni and S. Rychkov, arXiv:09210.1087, `10.48550/arXiv.0910.1087` (2009).

[153] J. Wess, Nuovo Cim. **18**, 1086 (1960).

[154] R. Jackiw and S.-Y. Pi, J. Phys. A: Math. Theor. **44**, 223001 (2011).

[155] C. Brust and K. Hinterbichler, J. High Energy Phys. **02**, 066 (2017).

[156] O. J. Rosten, Eur. Phys J. C **78**, 312 (2018).

[157] H. Osborn, Nucl. Phys. B **363**, 486 (1991).

[158] E. Brezin, J. C. Le Guillou, and J. Zinn-Justin, Phys. Rev. D **8**, 434 (1973).

[159] C. G. Callan, S. Coleman, and R. Jackiw, Ann. Phys. **59**, 42 (1970).

[160] F. Arici, D. Becker, C. Ripken, F. Saueressig, and W. D. van Sluijlekom, J. Math. Phys. **59**, 082302 (2018).

[161] T. Okui, Phys. Rev. D **99**, 061701(R) (2019).

[162] E. I. Kats and V. V. Lebedev, Phys. Rev. B **89**, 125433 (2014).

[163] E. I. Kats and V. V. Lebedev, Phys. Rev. B **94**, 079904(E) (2016).

[164] O. Coquand and D. Mouhanna, Phys. Rev. E **94**, 032125 (2016).

[165] D. Gazit, Phys. Rev. B **80**, 161406(R) (2009).

[166] P. San-Jose, J. González, and F. Guinea, Phys. Rev. Lett. **106**, 045502 (2011).

[167] B. Amorim, R. Roldán, E. Cappelluti, A. Fasolino, F. Guinea, and M. I. Katsnelson, Phys. Rev. B **89**, 224307 (2014).

[168] V. N. Bondarev, V. M. Adamyan, and V. V. Zavalniuk, Phys. Rev. B **97**, 035426 (2018).

[169] E. Guitter, J. Physique **51**, 2407 (1990).

[170] D. Anselmi and M. Halat, Phys. Rev. D **76**, 125011 (2007).

[171] D. Anselmi, J. High Energy Phys. **02**, 051 (2008).

[172] I. Arav, Y. Oz, and A. Raviv-Moshe, J. High Energy Phys. **11**, 064 (2019).

[173] J. Zinn-Justin, arXiv:hep-ph/0005272 (2000).

[174] K. V. Zakharchenko, M. I. Katsnelson, and A. Fasolino, Phys. Rev. Lett. **102**, 046808 (2009).

[175] J.-W. Jiang, B.-S. Wang, J.-S. Wang, and H. S. Park, J. Phys.: Condens. Matter **27**, 083001 (2015).

[176] W. Bao, F. Miao, Z. Chen, H. Zhang, W. Jang, C. Dames, and C. N. Lau, Nat. Nanotechnol. **4**, 562 (2009).

[177] V. Singh, S. Sengupta, H. S. Solanki, R. Dhall, A. Allain, S. Dhara, P. Pant, and M. M. Deshmukh, Nanotechnology **21**, 165204 (2010).

[178] D. Yoon, Y.-W. Son, and H. Cheong, Nano Lett. **11**, 3227 (2011).

[179] Q. Feng, D. Wei, Y. Su, Z. Zhou, F. Wang, and C. Tian, Small **17**, 2006146 (2021).

[180] F. Jean, T. Zhou, N. Blanc, R. Felici, J. Coraux, and G. Renaud, Phys. Rev. B **88**, 165406 (2013).

[181] Y. Hatwalne and S. Ramaswamy, arXiv:cond-mat/0009294 (2000).

[182] Y. Hatwalne, S. Ramaswamy, and J. Toner, Phys. Rev. Lett. **70**, 2090 (1993).

[183] A. Mauri and M. I. Katsnelson, Nucl. Phys. B **956**, 115040 (2020).

[184] S. Weinberg, Phys. Rev. **118**, 838 (1960).

[185] Y. Hahn and W. Zimmermann, Commun. Math. Phys. **10**, 330 (1968).

[186] R. Ramírez and C. P. Herrero, Phys. Rev. B **95**, 045423 (2017).

[187] M. Gell-Mann and F. Low, Phys. Rev. **95**, 1300 (1954).

[188] P. L. de Andres, F. Guinea, and M. I. Katsnelson, Phys. Rev. B **86**, 144103 (2012).

[189] D. Tisi, "Temperature dependence of phonons in graphene," MA thesis (2017).

[190] J. C. Meyer, A. K. Geim, M. I. Katsnelson, K. S. Novoselov, D. Obergfell, S. Roth, C. Girit, and A. Zettl, Solid State Commun. **143**, 101 (2007).

[191] M. Pozzo, D. Alfè, P. Lacovig, P. Hofmann, S. Lizzit, and A. Baraldi, Phys. Rev. Lett. **106**, 135501 (2011).

[192] J. K. Schoelz, P. Xu, V. Meunier, P. Kumar, M. Neek-Amal, P. M. Thibado, and F. M. Peeters, Phys. Rev. B **91**, 045413 (2015).

[193] K. V. Zakharchenko, J. H. Los, M. I. Katsnelson, and A. Fasolino, Phys. Rev. B **81**, 235439 (2010).

[194] C. P. Herrero and R. Ramírez, Phys. Rev. B **101**, 035405 (2020).

[195] C. Androulidakis, K. Zhang, M. Robertson, and S. Tawfick, 2D Mater. **5**, 032005 (2018).

[196] J. H. Kim, J. H. Jeong, N. Kim, R. Joshi, and G.-H. Lee, J. Phys. D: Appl. Phys. **52**, 083001 (2018).

[197] G. Wang, Z. Dai, J. Xiao, S. Z. Feng, C. Weng, L. Liu, Z. Xu, R. Huang, and Z. Zhang, Phys. Rev. Lett. **123**, 116101 (2019).

[198] F. Pan, G. Wang, L. Liu, Y. Chen, Z. Zhang, and X. Shi, J. Mech. Phys. Solids **122**, 340 (2019).

[199] E. Han, J. Yu, E. Annevelink, J. Son, D. A. Kang, K. Watanabe, T. Taniguchi, E. Ertekin, P. Y. Huang, and A. M. van der Zande, Nat. Mater. **19**, 305 (2020).

[200] D.-B. Zhang, E. Akatyeva, and T. Dumitrică, Phys. Rev. Lett. **106**, 255503 (2011).

[201] N. Lindahl, D. Midtvedt, J. Svensson, O. A. Nerushev, N. Lindvall, A. Isaacsson, and E. E. B. Campbell, Nano Lett. **12**, 3526 (2012).

[202] X. Chen, C. Yi, and C. Ke, Appl. Phys. Lett. **106**, 101907 (2015).

[203] J. Toner, Phys. Rev. Lett. **64**, 1741 (1990).

[204] A. K. Singh and R. G. Hennig, Phys. Rev. B **87**, 094112 (2013).

[205] M. Zelisko, F. Ahmadpoor, H. J. Gao, and P. Sharma, Phys. Rev. Lett. **119**, 068002 (2017).

[206] M. I. Katsnelson and A. Fasolino, J. Phys. Chem. B **110**, 30 (2006).

[207] O. V. Manyuhina, J. J. Hetzel, M. I. Katsnelson, and A. Fasolino, Eur. Phys. J. E **32**, 223 (2010).

[208] H. Kleinert, Phys. Lett. A **136**, 253 (1989).

[209] A. Mauri and M. I. Katsnelson, Ann. Phys. **412**, 168016 (2020).

[210] L. M. Malard, M. H. D. Guimarães, D. L. Mafra, M. S. C. Mazzoni, and A. Jorio, Phys. Rev. B **79**, 125426 (2009).

[211] G. Savini, Y. J. Dappe, S. Öberg, J. C. Charlier, M. I. Katsnelson, and A. Fasolino, Carbon **49**, 62 (2011).

[212] A. Bosak, M. Krisch, M. Mohr, J. Maultzsch, and C. Thomsen, Phys. Rev. B **75**, 153408 (2007).

[213] E. Cadelano, S. Giordano, and L. Colombo, Phys. Rev. B **81**, 144105 (2010).

[214] L. J. Karssemeijer and A. Fasolino, Surf. Sci. **605**, 1611 (2011).

[215] K. H. Michel, S. Costamagna, and F. M. Peeters, Phys. Rev. B **91**, 134302 (2015).

[216] P. Giannozzi, S. Baroni, N. Bonini, M. Calandra, R. Car, C. Cavazzoni, D. Ceresoli, G. L. Chiarotti, M. Cococcioni, and I. Dabo, J. Phys. Condens. Matter **21**, 395502 (2009).

[217] J. P. Perdew, K. Burke, and M. Ernzerhof, Phys. Rev. Lett. **77**, 3865 (1996).

[218] S. Grimme, J. Comput. Chem. **27**, 1787 (2006).

[219] M. I. Katsnelson, Phys. Rev. B **82**, 205433 (2010).

[220] K. J. Wiese, Phys. Lett. B **387**, 57 (1996).

RESEARCH DATA MANAGEMENT

This thesis research has been carried out in accordance with the research data management policy of the Institute for Molecules and Materials (IMM) of Radboud University, the Netherlands.[11]

The following datasets have been produced during this research:

- **Chapter 6**: numerical solutions of SCSA equations for monolayer and bilayer graphene. The corresponding data sets are available as supplemental material attached to the publication: Achille Mauri, David Soriano, and Mikhail I. Katsnelson, "Thermal ripples in bilayer graphene", Phys. Rev. B **102**, 165421 (2020), doi:10.1103/PhysRevB.102.165421. Data can also be accessed at arXiv:2007.00552 (2020), doi:10.48550/arXiv.2007.00552.

  Scripts used to generate numerical results have been archived at the IMM manuscript server and can be requested to the Data Officer of the department of Theory of Condensed Matter, IMM, Radboud University.

11 https://www.ru.nl/rdm/vm/policy-documents/policy-imm/

SUMMARY

This thesis analyzes the effects of thermal fluctuations on the elasticity and the thermodynamic behavior of two-dimensional solids. The main focus is on 2D solids which are free-standing (not supported by a substrate) and which are subject to vanishing or small external tension.

The interplay between thermal fluctuations and nonlinear interactions in free standing layers has been the subject of vast investigations, from biological systems to 2D materials such as graphene. As it has long been realized, it leads to a complex problem, at the boundary between elasticity theory, geometry and critical phenomena. Similarly to a system at the critical temperature of a second-order phase transition, the phonon modes of a membrane subject to zero tension is predicted to be governed by a scale-invariant field theory, described by an *interacting* fixed point of the renormalization group. The corresponding anomalous scale invariance implies striking power-law renormalizations of elastic parameters and non-Hookean elastic properties, dominated by the response of statistical fluctuations.

The research contributions derived during this work are presented in the last four chapters of this thesis (Chap. 3-6). The analyses in Chap. 3 and Chap. 4 focus on the problem of a continuum elastic medium subject to thermal fluctuations, in the framework of classical statistical mechanics. Chapter 3 illustrates a calculation of scaling indices up to order ε^2 within an ε-expansion, based on a systematic field-theoretical renormalization group method and a non-conventional continuation of the elasticity theory from the physical dimensionality $D = 2$ to general $D = 4-\varepsilon$. Chapter 4 studies whether the scale invariance of phonon fluctuations extends to a larger conformal invariance. By an analysis of the energy-momentum tensor to all orders in the ε-expansion it is argued that the model is only scale invariant and not conformal. The same conclusion holds for elasticity theory in $D = 4 - \varepsilon$ and for the non-conventional continuation of the theory introduced in chapter 3. The two continuations lead to two different fixed points which are both scale invariant but nonconformal. This result can be useful in the search for general connections between scale and conformal symmetries, a subject of recent investigations in quantum field theory and statistical mechanics.

Chapter 5 explores the low-temperature behavior of free standing membranes, where quantum mechanical effects are important. A method based on perturbative renormalization group equations and finite-size scaling techniques is used in order to revisit some predictions derived in earlier investigations. In particular, the method provides a new derivation of the striking logarithmic temperature dependence of

the thermal expansion coefficient, which was deduced in the earlier analysis of Ref. [91] by a different method.

Chapter 6 develops a theory of thermal fluctuations and anharmonic effects in a fluctuating bilayer graphene. The theory is combined with numerical calculations in order to derive a prediction of fluctuation amplitudes at various temperatures.

The thesis starts with two opening chapters (Chap. 1 and Chap. 2), which introduce the subject and make the reading self-contained.

SAMENVATTING

In deze thesis bekijken we het effect van thermische fluctuaties op de elasticiteit en op het thermodynamische gedrag van twee dimensionale (2D) vaste stoffen. De focus ligt hierbij op vrijstaande 2D materialen (niet ondersteund door een substraat) waar geen, of hele kleine externe spanningen op staan. Het samenspel tussen thermische fluctuaties en niet-lineaire interacties in vrijstaande 2D lagen is het onderwerp van uitgebreid onderzoek, van zowel biologische systemen tot 2D materialen als grafeen. Zoals al lang bekend, leidt het tot een complexe problemen op de grens tussen elasticiteitstheorie, geometrie en kritische fenomenen. Net als bij een systeem met een tweede-orde faseovergang op de kritieke temperatuur, is het voorspelt dat fononen in een membraan, zonder mechanische spanning, beheerst worden door een schaalinvariante veldentheorie, beschreven door een interactief dekpunt van de renormalisatie groep. De overeenkomstige afwijkende schaalinvariantie impliceert een opvallende renormalisatie van machtsfunctie van de elastische parameter en niet-Hookeaanse elastische eigenschappen, gedomineerd door de reactie van statistische fluctuaties. De resultaten van dit onderzoek staan beschreven in de laatste vier hoofdstukken van deze thesis (Hfst. 3-6). De analyse in Hfst. 3 en Hfst. 4 focust op het probleem van continue elastische media onderhevig aan thermische fluctuaties, op de manier van klassieke statistische mechanica. Hoofdstuk 3 beschrijft de berekening van het schalen van indices tot de tweede orde ε^2, binnen een ε expansie, gebaseerd op een systematische veldentheoretische renormalisatie groep methode en een onconventionele voortzetting van de elasticiteitsleer van fysische dimensies in $D = 2$ naar $D = 4 - \varepsilon$. Hoofdstuk 4 bestudeert of de schaalinvariantie van fonoonfluctuaties uitgebreid kan worden naar een bredere conformistische invariantie. Uit een analyse van de energie-impuls tensor tot alle orders in de ε expansie, kan er geconcludeerd worden dat het model alleen schaal invariant is en niet conformistisch. Dezelfde conclusie kan worden getrokken voor de elasticiteitsleer in $D = 4 - \varepsilon$ en voor de onconventionele voortzetting van de theorie geïntroduceerd in Hfst. 3. De twee voortzettingen leiden tot twee verschillende dekpunten welke schaalinvariant zijn maar niet conformistisch. Deze resultaten kunnen nuttig zijn in de zoektocht naar generieke overeenkomsten tussen schaal en conformistische symmetrieën, welke het onderwerp zijn van verschillende onderzoeken in kwantumveldentheorie en statistische mechanica. Hoofdstuk 5 onderzoekt het lage temperatuur gedrag van vrijstaande membranen, waarbij de kwantummechanische effecten belangrijk zijn. Er wordt gebruik gemaakt van een methode gebaseerd op een storingsrekening van renormalisatie groep vergelijkingen en eindige schaal technieken, om hiermee terug te kijken op voorspellingen gemaakt in eerdere analyses. De methode geeft vooral

een nieuwe afleiding van de opvallende logaritmische temperatuur afhankelijkheid van de thermische expansie coëfficiënt, welke ook op een andere manier gevonden is in eerder onderzoek door Ref. [91]. In Hfst 6 wordt een theorie ontwikkeld voor de thermische fluctuaties van niet harmonische effecten in fluctuerend dubbellaags grafeen. De theorie wordt gecombineerd met numerieke berekeningen, om een voorspelling te doen van de fluctuatie-amplitude voor verschillende temperaturen. De eerste twee hoofdstukken van deze thesis worden gewijd aan het geven van een introductie en om het onderwerp op zichzelf staande te maken.

PUBLICATIONS

Publications on which this thesis is based

1. Achille Mauri and Mikhail I. Katsnelson, "Perturbative renormalization and thermodynamics of quantum crystalline membranes", Phys. Rev. B **105**, 195434 (2022) (Editors' Suggestion); preprint: arXiv:2202.12842 (2022)

2. Achille Mauri and Mikhail I. Katsnelson, "Scale without conformal invariance in membrane theory", Nucl. Phys. B **969**, 115482 (2021); preprint: arXiv:2104.06859 (2021)

3. Achille Mauri, David Soriano, and Mikhail I. Katsnelson, "Thermal ripples in bilayer graphene", Phys. Rev. B **102**, 165421 (2020); preprint: arXiv:2007.00552 (2020)

4. Achille Mauri and Mikhail I. Katsnelson, "Scaling behavior of crystalline membranes: an ε-expansion approach", Nucl. Phys. B **956**, 115040 (2020); preprint: arXiv:2003.04043 (2020)

Other publications

1. Achille Mauri and Mikhail I. Katsnelson, "Thermal fluctuations in crystalline membranes with long-range dipole-dipole interactions", Ann. Phys. **412**, 168016 (2020); preprint: arXiv:1901.05879 (2019)

2. A. N. Rudenko, A. V. Lugovskoi, A. Mauri, Guodong Yu, Shengjun Yuan, and M. I. Katsnelson, "Interplay between in-plane and flexural phonons in electronic transport of two-dimensional semiconductors", Phys. Rev. B **100**, 075417 (2019); preprint: arXiv:1902.09152 (2019)

3. Achille Mauri and Marco Polini, "Dielectric function and plasmons of doped three-dimensional Luttinger semimetals", Phys. Rev. B **100**, 165115 (2019); preprint: arXiv:1904.10825 (2019)

ACKNOWLEDGMENTS

This thesis represents the last step of a PhD journey at the department of Theory of Condensed Matter (TCM) of Radboud University. Working within the TCM group, for over four years, has been for me a very important experience and has crucially shaped my scientific growth. Therefore, I wish to express my deep gratitude to the many people who were involved and who accompanied me in this path.

First of all, I want to thank my supervisor, Mikhail Katsnelson. Misha, the many opportunities which I had by working at TCM have been unvaluable for me and I cannot overstate how much I learnt from the many discussions and works with you. I hope that I will be able to take with me a bit of your creativity, openness, and broad knowledge. I am also very grateful for much availability and support in infinitely many occasions.

I would also like to thank Mikhail Titov. Misha, the numerous conversations with you have been very stimulating and have greatly broadened my view on condensed matter physics. I am also thankful for your constant availability to share your experience and suggestions.

I am grateful to Annalisa Fasolino for inspiring discussions in the beginning stage of my PhD, and later, for her interest on the development of my research projects during her visits to Nijmegen.

During my PhD, I had the chance to collaborate with Alexander Rudenko, Andrey Lugovskoi, Guodong Yu, Shengjun Yuan, and David Soriano. Thank you for having shared the efforts in the interesting works together! I learnt much by working with you and I feel privileged for the opportunity of our collaboration.

My understanding of the physics of membranes has been deepened by many interesting discussions with Jan Los. I also want to thank Andrey Bagrov, for stimulating conversations on quantum field theory. Being able to knock at the door of Malte Rösner has been very helpful. Malte, thanks for the nice discussions on solid state physics and the numerous suggestions on preparing articles, posters, and seminars.

The support of Belinda Eijgenraam has really helped me much. Belinda, thank you for your generous help! And also for organizing many lunches, days out, games, Sinterklaas celebrations, which were always very fun and made me feel warmly welcomed from the very first day at the university.

A big thank also goes to many colleagues and friends. Robert, it has been great to share the office with you and to conclude long days at the university with conversations, jokes, dinners, walks (very long ones, why didn't we use a bike?). Koen, I always enjoyed your jokes in italian. I also want to thank you for your wise

pieces of advice, which many times have been a precious help. Ivan, thanks for conversations on physics and life, often ending up in very fun jokes. You are also a very creative screenwriter and movie director! Andrei, your style as a movie director is different from that of Ivan, but not less impressive! Askar, it has been great to play music with you and Misha Baglai in the "pasta factory"! Bektur, Mika, Fabio, you have been very nice officemates! I have many memories of moments spent together with Edo, Marion, Lennert, Peiliang, Manuel, Zhenya, Yunhua, Tom, Jin, Qi, Yann, Tjacco, Danis, Zewen, Xiaotian, Weiqing, Swagata, Hylke, Guus, Erik. Thank you all. These years in Nijmegen have been really great!

Finally, I want to thank my parents Gianvittorio and Nicoletta and my brother Carlo. Without your support this thesis would not have been possible. Thank you for all your help during these years!

Achille Mauri

CURRICULUM VITAE

Achille Mauri was born in Milan, Italy, on 22 March 1994. Between 2007 and 2012, he attended the scientific high school at Istituto di Istruzione Superiore Statale Severi-Correnti in Milan. Between 2012 and 2017 he studied physics at the University of Pisa and at Scuola Normale Superiore. In 2015, he obtained a Bachelor Degree of Physics at University of Pisa with a thesis on "Hyperfine splitting of rubidium energy levels", supervised by Prof. Alberto Di Lieto and Prof. Giampiero Paffuti. In 2017, he obtained the Master Degree of Physics at University of Pisa, defending a thesis titled "Many-body effects in three-dimensional Luttinger semimetals", supervised by Prof. Marco Polini. At the end of university studies, he received the 'Diploma di Licenza' from Scuola Normale Superiore.

Between February 2018 and February 2022, Achille Mauri has worked as a PhD student at the department of Theory of Condensed Matter of Radboud University, under the supervision of Prof. dr. Mikhail I. Katsnelson. He is currently working as a researcher in the same department.